



HAL
open science

Coherent transport of waves in random media: from mesoscopic correlations to Anderson localization

Nicolas Cherroret

► **To cite this version:**

Nicolas Cherroret. Coherent transport of waves in random media: from mesoscopic correlations to Anderson localization. Condensed Matter [cond-mat]. Université Joseph-Fourier - Grenoble I, 2009. English. NNT: . tel-00424792

HAL Id: tel-00424792

<https://theses.hal.science/tel-00424792>

Submitted on 17 Oct 2009

HAL is a multi-disciplinary open access archive for the deposit and dissemination of scientific research documents, whether they are published or not. The documents may come from teaching and research institutions in France or abroad, or from public or private research centers.

L'archive ouverte pluridisciplinaire **HAL**, est destinée au dépôt et à la diffusion de documents scientifiques de niveau recherche, publiés ou non, émanant des établissements d'enseignement et de recherche français ou étrangers, des laboratoires publics ou privés.

THÈSE

pour obtenir le grade de

DOCTEUR DE L'UNIVERSITÉ JOSEPH FOURIER – GRENOBLE I

Présentée par

Nicolas CHERRORET

Transport cohérent en milieu aléatoire:
des corrélations mésoscopiques à la localisation d'Anderson

Préparée au

LABORATOIRE DE PHYSIQUE ET DE MODÉLISATION DES MILIEUX
CONDENSÉS

sous la direction de
Sergey E. SKIPETROV

Soutenue le 1^{er} octobre 2009 devant la commission d'examen

M. Dominique DELANDE	Rapporteur
M. Georg MARET	Examineur
M. Laurent SANCHEZ-PALENCIA	Examineur
M. Sergey E. SKIPETROV	Examineur
M. Bart VAN TIGGELEN	Président du jury
M. Peter WÖLFLE	Rapporteur

À mon grand-père

Il est un moment à chaque aube où
la lumière est comme en suspens
[. . .] La création retient son souffle.

DOUGLAS ADAMS

Remerciements

En ce mois de juillet 2006, alors que je scrutais pour la énième fois le site des propositions de thèse de l’université de Grenoble après une expérience mitigée de fin de Master, je suis tombé sur ces quelques mots qui m’avaient jusqu’alors échappé: “étude de la localisation d’Anderson”. Une thématique étudiée au Laboratoire de Physique et de Modélisation des Milieux Condensés. Un coup de fil et une rapide visite plus tard, j’avais décidé ce que je souhaitais pour les trois prochaines années. Finir sur une décision si affirmée après tant d’errements ne pouvait être possible qu’après une discussion avec mon futur directeur de thèse, Sergey Skipetrov. Je lui en suis profondément reconnaissant. La suite des événements est simple à résumer: une thèse passée dans les meilleurs conditions possibles sous son encadrement. Sa disponibilité, sa bonne humeur et son professionnalisme ont été simplement exceptionnels. Je le remercie sincèrement pour tout cela.

J’adresse tout mes remerciements à Dominique Delande et Peter Wölfle pour avoir accepté le rôle de rapporteur de mon travail de thèse, ainsi que pour leurs commentaires concernant le manuscrit. Je remercie également vivement Georg Maret et Laurent Sanchez-Palencia d’avoir participé à mon jury de thèse.

Je remercie chaleureusement tous les membres permanents du LPMMC pour l’ambiance très agréable qu’ils contribuent tous à créer. Venir travailler dans un tel environnement a toujours été pour moi un réel plaisir. Je remercie tout particulièrement le grand chef de (l’ex-) équipe onde, Bart van Tiggelen, qui ne fut jamais très loin au cours de ces trois années, regardant de temps à autre ma thèse d’un oeil avisé par dessus l’épaule de Sergey. Je souhaite également témoigner toute ma reconnaissance à Françoise Berthoud, pour ses très nombreux conseils et encouragements. Avoir réussi à guérir une ancienne allergie pour tout ce qui touche de près ou de loin le monde du développement n’était pas une mince affaire! Je remercie aussi Jean-Daniel, l’homme auquel aucun problème informatique ne résiste, pour sa gentillesse et sa disponibilité, ainsi que Michèle, Laurence et Emmanuelle du côté du secrétariat.

Durant cette thèse, j’ai eu la chance de passer quelques mois à l’université de

Konstanz en Allemagne, aux côtés d'un groupe d'expérimentateurs. A ce titre, je remercie le collègue franco-allemand ainsi que le International Research Training Group (Soft Condensed Matter Physics of Model Systems) de m'avoir donné l'opportunité de cet échange. Je sais gré au professeur Georg Maret ainsi qu'à Christof Aegerter pour m'avoir accueilli dans leur groupe. Grosses Dankeschön an alle Studenten des Fachbereichs Physik für ihre Freundlichkeit. Ich vergesse nicht Sabine Lucas, ohne die die Schreibearbeit ein Alptraum gewesen wäre!

J'adresse mes vifs remerciements aux deux autres Nicolas qui ont partagé avec moi ces trois années de thèse, et bien plus que cela, leur amitié. Je leur souhaite bon courage et toute la réussite possible pour la suite. Je n'oublie pas bien sûr mes deux autres co-bureau, Giulia et Sébastien, qui ont encore quelque temps à tirer au labo. Impossible de résumer tous les bons moments passés avec eux, au labo ou en dehors. Je les remercie chaleureusement pour tous ces instants. Merci également aux post-docs, Gianluca, Andrey, Xiaolong et Vitalie, ainsi qu'à tous les stagiaires et autres thésards qui se sont succédés aux cours de ces trois années.

Puisque la vraie vie commence évidemment en dehors du labo, je me dois de dire quelques mots à tous mes chers amis grenoblois (et aussi à certains qui ont trahi leur ville...). Ces mots ne valent certes pas une bonne conversation au Druid's, mais ont le mérite d'être ici flanqués d'un certain solennel. Merci à David et Vincent pour ces retrouvailles hebdomadaires dans la taverne la plus tranquille de Gre... Merci à Matthieu, Elo, et à Seb et Flo les deux montagnards pour toutes ces agréables soirées passées à savourer différentes gastronomies tout en discutant de nos vies respectives... J'ai une pensée aussi pour Manu et Philippe, qui ne furent pour moi jamais très loin lors de ces repas.

Je n'oublie pas bien sûr Amaury et ses acolytes, que je ne peux citer tous ici... Les moments passés avec vous ont toujours été un bouffée d'oxygène... Passer de la secte des thésards à celle des ingés et autres archis fut toujours une agréable conversion!

Je remercie enfin mes parents et toute ma famille qui m'ont accompagné pendant cette thèse.

Enfin, toute ma tendresse va à Delphine, qui fut toujours présente tout au long de ces trois ans, malgré l'éloignement. Je remercie l'appui de notre pont aérien, organisé par deux compagnies qui ont eu l'idée lumineuse de venir se concurrencer sur Bordeaux Grenoble. Pourriez-vous le faire aussi sur Bordeaux Strasbourg s'ils vous plaît?

Grenoble, octobre 2009

Nicolas Cherroret

Abstract

This thesis is devoted to the study of coherent effects that arise when a wave propagates in a strongly disordered medium. We address several aspects of their dynamics, with special interest in mesoscopic correlations and Anderson localization.

First, we demonstrate a generalized form of the self-consistent theory of Anderson localization, adapted to the description of finite open media. This theory introduces a diffusion coefficient that depends on position. The importance of this property is highlighted through the investigation of the phenomenon of transverse confinement of waves in disordered media. The theory is also confronted to predictions of the scaling theory of localization.

The second part of the thesis focuses on the dynamics of intensity speckle patterns that arises from the propagation of short pulses in a disordered waveguide. We study the two-point intensity correlation function associated with the speckle pattern. This function contains the information about the universal conductance fluctuations, well known in mesoscopic conductors. In the dynamic situation, conductance fluctuations acquire a time dependence, are enhanced at long times and lose their universal nature. These results are confirmed by a microwave experiment.

In a last part, we investigate the physics of matter-wave speckle patterns, resulting from the expansion of a Bose-Einstein condensate in a random potential. They are found to exhibit long-range correlations that grow with time, and can take negative values. We interpret these results in terms of a random displacement of the center of mass of the condensate. The role of atomic interactions during the expansion of the condensate is discussed.

Cette thèse est consacrée à l'étude des effets cohérents qui apparaissent lorsqu'une onde se propage dans un milieu fortement désordonné. Différents aspects de leur dynamique sont traités, et un intérêt particulier est accordé aux corrélations mésoscopiques et à la localisation d'Anderson.

Dans un premier temps, nous démontrons une version généralisée de la théorie auto-cohérente de la localisation d'Anderson, adaptée à la description des milieux finis et ouverts. Cette théorie introduit un coefficient de diffusion dépendant de la position. L'importance de cette propriété est soulignée à travers l'étude du phénomène de confinement transverse des ondes dans les milieux désordonnés. La théorie est également confrontée aux prédictions de la théorie d'échelle de la localisation.

La deuxième partie de la thèse explore la dynamique des figures de tavelures résultant de la propagation d'impulsions courtes dans un guide d'ondes désordonné. Nous étudions la fonction de corrélation à deux points de l'intensité associée à la figure de tavelures. Cette fonction contient l'information sur les fluctuations universelles de conductance, bien connues dans les conducteurs mésoscopiques. Dans le cas dynamique, les fluctuations de conductance acquièrent une dépendance temporelle, augmentent avec le temps et perdent leur caractère universel. Ces résultats sont confirmés par une expérience menée à l'aide de micro-ondes.

Pour finir, nous étudions la physique des figures de tavelures résultant de l'expansion d'un condensat de Bose-Einstein dans un potentiel aléatoire. De telles figures présentent des corrélations de longue portée qui augmentent avec le temps, et peuvent éventuellement prendre des valeurs négatives. Ces résultats sont interprétés en termes d'un déplacement aléatoire du centre de masse du condensat. Le rôle des interactions atomiques lors de l'expansion du condensat est discuté.

Contents

1	General introduction	1
1.1	Elastic scattering in random media	1
1.1.1	Random media	1
1.1.2	Single scattering	3
1.2	Multiple scattering in random media	4
1.2.1	Mean free path	4
1.2.2	Characteristic lengths	5
1.2.3	Regimes of propagation	6
1.3	Outline of the thesis	7
I	Anderson localization in finite media	9
2	Anderson localization: an overview	11
2.1	Basic definitions	12
2.1.1	Fundamental definitions	12
2.1.2	Practical criteria	13
2.2	Quantum and classical waves	16
2.2.1	Electronic conductors	16
2.2.2	Localization of classical waves	17
2.3	Experimental quest for Anderson localization	19
2.3.1	End of 20 th century: first attempts...	19
2.3.2	A 21 st century rich in experiments	19
2.4	Theoretical approaches	23
2.4.1	The scaling theory	23
2.4.2	The self-consistent theory	24
2.4.3	Other approaches	27
2.5	Conclusion	28

3	Microscopic approach to Anderson localization in finite media	31
3.1	Theoretical framework	33
3.1.1	Intensity Green's function	33
3.1.2	Assumptions	34
3.2	Interference effects in finite media	35
3.2.1	Diagrammatic approach	35
3.2.2	Classical diffusion equation	36
3.2.3	Interference effects and reciprocity principle	37
3.3	Derivation of self-consistent equations	39
3.4	Energy conservation and boundary conditions	41
3.4.1	Energy conservation	41
3.4.2	Boundary conditions	42
3.5	Conclusion	43
4	Application of the self-consistent theory: transverse confinement	45
4.1	Spatially-resolved transmission coefficient of a slab	46
4.2	Transverse confinement of continuous waves	48
4.2.1	Width of the transmission profile	48
4.2.2	Results	49
4.2.3	Reflection	52
4.2.4	Role of absorption	52
4.3	Transverse confinement with short pulses	53
4.3.1	Width of dynamic transmission profile	54
4.3.2	Results and discussion	54
4.4	Conclusion	57
5	Self-consistent versus scaling theory	59
5.1	The scaling theory of localization	60
5.1.1	Scaling function	60
5.1.2	Regimes of disorder and dimensionality	61
5.1.3	Critical exponent	62
5.2	Stationary transport properties of a slab	63
5.2.1	Total transmission	63
5.2.2	Comparison with the scaling theory	65
5.3	Scaling function and the self-consistent theory	65
5.3.1	Scaling function	65
5.3.2	Critical exponent	66
5.4	Conclusion	68
II	Dynamics of intensity speckle patterns	69
6	Intensity correlations in waveguides	71
6.1	Intensity correlation function	72

6.1.1	Description of intensity speckle patterns in terms of multiple scattering paths	72
6.1.2	Intensity correlation function	73
6.2	Intensity correlations in waveguides	73
6.2.1	Framework	73
6.2.2	Average intensity	75
6.2.3	Perturbative approach	76
6.2.4	The \mathcal{C}_2 correlation	78
6.2.5	The \mathcal{C}_3 correlation	79
6.2.6	Physical interpretation	79
6.3	Experimental measurement of intensity correlations in waveguides . .	80
6.3.1	Direct measurements	80
6.3.2	Polarization-resolved measurements	81
6.4	Conclusion	82
7	Dynamics of intensity speckle patterns	83
7.1	Average intensity and intensity correlation function	84
7.1.1	Framework	84
7.1.2	Field correlation function	85
7.1.3	Average intensity	86
7.1.4	Time-dependent intensity correlation function	87
7.2	Dynamic \mathcal{C}_1 and \mathcal{C}_2 correlation functions	87
7.2.1	The \mathcal{C}_1 correlation function	87
7.2.2	The \mathcal{C}_2 correlation function	88
7.3	The \mathcal{C}_3 correlation function	89
7.3.1	Calculation of \mathcal{C}_3	89
7.3.2	Experimental measurement of \mathcal{C}_3	91
7.3.3	Role of absorption	95
7.3.4	Limitation of long times	96
7.4	Conclusion	96

III Bose-Einstein condensates expanding in random potentials **99**

8	Bose-Einstein condensates and disorder	101
8.1	Bose-Einstein condensates	103
8.1.1	Quantum gases: elementary considerations	103
8.1.2	Nonuniform and weakly interacting Bose-Einstein condensates	103
8.2	Bose-Einstein condensate expanding in a random potential: a toy model	105
8.3	Release of the condensate from the trap	106
8.3.1	Thomas-Fermi regime	107
8.3.2	Opening of the trap. Scaling	108
8.3.3	Momentum distribution at long times	109

8.4	Conclusion	109
9	Matter-wave speckle patterns	111
9.1	Preliminaries	112
9.1.1	Gross-Pitaevskii equation	112
9.1.2	Random potential	113
9.1.3	Quasi one-dimensional geometry	114
9.2	Density speckle and average density profile	115
9.2.1	Density speckle pattern	115
9.2.2	Average density profile of a BEC expanding in a quasi one-dimensional waveguide	116
9.2.3	Validity of the analysis	118
9.3	\mathcal{C}_1 and \mathcal{C}_2 correlation functions	119
9.3.1	Diagrammatic approach	119
9.3.2	Short-range \mathcal{C}_1 correlation	119
9.3.3	Long-range \mathcal{C}_2 correlation	120
9.4	Conclusion	125
10	Study of interactions	127
10.1	Perturbative treatment	128
10.2	Expansion in the absence of interactions	129
10.2.1	Diffusive expansion	130
10.2.2	Anderson localization	131
10.3	Nonlinear correction to the atomic density	133
10.3.1	Mean free path	133
10.3.2	Diffusion coefficient	134
10.4	Conclusion	137
A	Derivation of self-consistent equations	141
B	Average intensity and field correlation in a disordered waveguide	147
B.1	Intensity Green's function	147
B.2	Correlation of Green's functions	149
C	Gross-Pitaevskii equation	151
C.1	Energy functional	151
C.2	Gross-Pitaevskii equation	152
D	Density profile of a Bose-Einstein condensate	155
E	Nonlinear correction to the atomic density	159

List of symbols

Mathematical symbols

$*$	complex conjugate
\dagger	Hermitian adjoint
$\hat{\cdot}$	quantum operator
0^+	positive infinitesimal number
0^-	negative infinitesimal number
$\nabla_{\mathbf{r}}$	gradient operator applying to vector \mathbf{r}
$\Delta_{\mathbf{r}}$	Laplace operator applying to vector \mathbf{r}
Re	real part
Im	imaginary part
\mathcal{H}	Heaviside step function
δ_{ij}	Kronecker symbol
δ	functional derivation
$\delta(t), \delta(\mathbf{r})$	Dirac delta function
\mathcal{O}	asymptotic comparison
$\mathbb{1}$	identity matrix
$\overline{(\dots)}, \langle \dots \rangle$	ensemble average

Physical variables

α	dimensionless function defined in Sec. 2.4.2.3
$\beta(g)$	universal scaling function
$\beta(t)$	dimensionless function defined in Eq. (8.16)
χ	anticommuting Grassmann variable
$\chi(q_{\perp})$	$=\sqrt{1/\xi^2 + q_{\perp}^2}$
$\delta\epsilon(\mathbf{r})$	local dielectric constant
$\delta\psi_{\epsilon}$	small correction to ψ_{ϵ} due to interactions
δ_{ξ}	$=1/(\nu_0\xi^3)$
ΔE	average level spacing
δE	width of an eigenstate
δ_g	relative conductance difference in the vicinity of the Anderson transition
δI	fluctuation of intensity
Δn	first-order correction to the atomic density due to atomic interactions
δn	fluctuation of the atomic density
ΔR	distance between vectors \mathbf{r} and \mathbf{r}'
Δr	distance between vectors \mathbf{R} and \mathbf{R}'
$\bar{\epsilon}$	average dielectric constant
$\epsilon, \epsilon_j (j = 1, 2 \dots)$	atomic energy
ϵ_c	critical atomic energy of the Anderson transition
ϵ_k	energy of an atom of momentum k
$\epsilon(\mathbf{r})$	local dielectric constant
ζ	dimensionless longitudinal coordinate
Γ	complete vertex of a multiple scattering sequence
Γ_C	sum of maximally-crossed diagrams
Γ_D	sum of ladder diagrams
γ	dimensionless function defined in Sec. 2.4.2.3
Θ	N-particle wave function
θ	scattering angle
λ	wavelength
$\lambda(t)$	dimensionless function defined in Eq. (8.16)

λ_T	thermal de Broglie wavelength
μ	chemical potential
$\mu(\mathbf{r})$	relative fluctuation of the dielectric constant
ν	critical exponent of the Anderson transition
ν_0	density of states
ξ	localization length
ξ_μ	localization length of an atom of energy μ
$\boldsymbol{\rho}$	transverse part of vector \mathbf{r}
ρ	modulus of vector $\boldsymbol{\rho}$
σ	conductivity
σ	width of transverse intensity profile
$\frac{d\sigma}{d\Omega}$	differential scattering cross-section
σ_∞	long-time limit of σ
$\sigma_{\text{diff}}, \sigma_{\text{loc}}, \sigma_{\text{ME}}$	width of transverse intensity profile in the diffusive, localized regime and at the mobility edge, respectively.
σ_s	total scattering cross-section
σ_R	correlation length of the random potential
τ	mean free time
τ	time normalized by the Thouless time
τ_p	pulse duration normalized by the Thouless time
ν	dimensionless function defined in Sec. 2.4.2.3
Φ	grand canonical energy
Φ_n	eigenfunction of the Helmholtz equation in a waveguide
ϕ	atomic wave function
ϕ_0	wave function of the condensate at initial time of expansion
Ψ	classical scalar wave
Ψ	superfield
Ψ_0	field of a Gaussian pulse
Ψ_E	wave function of an electron of energy E
Ψ_i	partial wave
ψ	wave function of the condensate in real space
ψ_0	wave function of the condensate inside the trap
ψ_ϵ	wave function of the condensate in Fourier space
$\psi_{n,\{V\}}$	eigenfunctions of an Hamiltonian with disordered potential V

Ω	in Chapter 2, solid angle. Then, frequency difference
$\omega, \omega_i (i = 1, 2\dots)$	frequency
ω_0	carrier frequency
A	waveguide cross-section
$A_i (i = 1\dots 5)$	constants of the order of one
A_n	$= 1/[A\Phi_n(z_R)]$
a	size of a scatterer (in particular, radius of a Mie sphere)
a_0	extent of a trapped condensate without interactions
a_s	scattering length
B_n	$= k_n^2 D_B$
$B(\mathbf{q})$	Fourier transform of the correlation function of the random potential
b	dimensionless scaling parameter
C	intensity Green's function (propagator)
C_D	intensity Green's function in the absence of macroscopic interferences (diffusion propagator)
C_ϵ	diffusion propagator of an atom of energy ϵ
\mathcal{C}	intensity correlation function
$\mathcal{C}_1, \mathcal{C}_2, \mathcal{C}_3$	first-, second- and third-order contribution to the intensity correlation function
$\mathcal{C}_3^{(1)}, \mathcal{C}_3^{(2)}, \mathcal{C}_3^{(3)}, \mathcal{C}_3^{(4)}$	constitutive diagrams of \mathcal{C}_3
$C_{n,\{V\}}$	prefactor eigenfunctions of an Hamiltonian with disordered potential V
c	wave velocity
const	any constant
D	diffusion coefficient
D_ϵ	Boltzmann diffusion coefficient of an atom of energy ϵ
D_B	Boltzmann diffusion coefficient
D_{eff}	effective diffusion coefficient including interaction effects
d	dimensionality ($= 1, 2, 3$)
d	waveguide diameter
dS	surface element
$d\mathbf{S}$	vector normal to the surface element dS

E	electronic energy
\mathcal{E}	energy functional
E_{return}	energy returning to the source where it was emitted
E_c	critical electronic energy of the Anderson transition
e	electron charge
$\mathbf{e}_a, \mathbf{e}_b, \mathbf{e}_{a'}, \mathbf{e}_{b'}$	unit polarization vectors
$F(x)$	$= \text{sinc}^2(kx) \exp(-x/\ell)$
$f_1(m, n, p, q)$	function of the integers m, n, p and q , defined in Eq. (7.20)
$f_n(t)$	function $\propto \mathcal{H}(t) \exp(-n^2 t/t_D)$, with n an integer
$f(x)$	$= \text{sinc}(kx) \exp[-x/(2\ell)]$
G	amplitude Green's function; also, electronic conductance
G_ϵ	amplitude Green's function of an atom of energy ϵ
g	dimensionless conductance
g_0	interaction parameter
g_c	critical conductance
\hat{H}	Hamiltonian
\hat{H}_0	kinetic part of the Hamiltonian \hat{H}
H	Hikami box
$H^{(A)}, H^{(B)}, H^{(C)}$	constitutive diagrams of the Hikami box
h	Planck constant
\hbar	reduced Planck constant
I	intensity
i, j	integers
\mathbf{J}	total energy flux
J	interaction diagram
J_+	energy flux in the positive direction of axis z
K	kernel of the intensity correlation function
k	wave number; also, atomic momentum
k_μ	momentum of an atom of energy μ
k_B	Boltzmann constant
k_n	$= n\pi/L$, with n an integer
L	typical size of a disordered medium (thickness for a slab, length for a waveguide)
L_ϕ	coherence length
L_a	macroscopic absorption length
L_c	$= \ell \delta_g^{-\nu}$

ℓ	scattering mean free path
$\ell^{(1)}$	correction to the scattering mean free path due to interactions
ℓ_a	absorption length
ℓ_B	transport mean free path
m	atomic mass
m_1, m_2	refractive index contrasts
m_e	electron mass
m, n, p, q, r, s	integers
N	total number of atoms in a condensate
N	number of transverse modes in a waveguide
\mathbf{n}	unit vector
n_{diff}	long-time limit of the atomic density from diffusion theory
n_{loc}	long-time limit of the atomic density from localization theory
$n(\mathbf{r}, t)$	atomic density at position \mathbf{r} and time t
n_s	number density of scatterers
p_0	dimensionless interaction parameter
\hat{p}_i	momentum operator of atom i
$p(t)$	probability of crossing
\mathbf{q}	momentum
\mathbf{q}_\perp	transverse momentum
q_{max}	upper momentum cutoff
q_{min}	lower momentum cutoff
R	reflection coefficient
\mathbf{R}, \mathbf{R}'	source points in a waveguide
R_0	extent of a trapped condensate with interactions
r	internal reflection coefficient
r	modulus of vector \mathbf{r}
\bar{r}, \bar{r}'	reflection matrices
$\mathbf{r}, \mathbf{r}', \mathbf{r}_i$ ($i = 1, 2, \dots$)	position vectors
$\mathbf{r}_{n,\{V\}}$	site of a localized eigenfunction
S	commuting Grassmann variable
S	surface

S_{mnpq}	function of the integers m , n , p and q defined in Eq. (7.19)
$\bar{\mathcal{S}}$	action operator
\mathcal{S}	mean action
\bar{S}	scattering matrix
s	curvilinear abscissa
T	transmission coefficient; also, temperature
\mathcal{T}	dimensionless function defined in Sec. 2.4.2.3
t, t'	time
\bar{t}, \bar{t}'	transmission matrices
t_1	time beyond which the scattering mean free path is not affected by interactions
t_2	limit of long times for nonlinear corrections to the atomic density
t_a	absorption time
t_{arrival}	time at which the atomic density is maximum
T_c	condensation temperature
t_D	Thouless time
t_H	Heisenberg time
T_i ($i = 1 \dots N$)	eigenvalues of the transmission matrix
t_{loc}	time beyond which localization effects start affecting the expansion of a condensate in a random potential
T_{mnpq}	function of the integers m , n , p and q defined in Eq. (7.21)
t_p	pulse duration
\hat{U}	two-particle interaction potential
U_0	amplitude of the two-particle interaction potential
\mathbf{u}	unit vector
V	random/disordered potential; also, control volume
$\{V\}$	one realization of the random potential V
V_{\perp}	confining potential
V_{ω}	harmonic (trap) potential of frequency ω
V_{ext}	any external potential
v_{ϵ}	velocity of an atom of energy ϵ
v_{μ}	velocity of an atom of energy μ
v_R	amplitude of the random potential

W_ρ	width of transverse intensity profile
X	interference loop diagram
z	longitudinal part of vector \mathbf{r}
\tilde{z}	$\min(z, L - z)$
z'	longitudinal part of vector \mathbf{r}'
z_0	extrapolation length
$\langle z^2 \rangle$	mean-square size of a Bose-Einstein condensate
$\langle z_{\text{CM}}^2 \rangle$	mean-square amplitude of the center of mass of a Bose-Einstein condensate expanding in a random potential
z_c	free parameter of the diffusion coefficient at the mobility edge
z_M	$\max(z, z_R)$
z_m	$\min(z, z_R)$
z_R	longitudinal part of vector \mathbf{R}

CHAPTER 1

General introduction

Contents

1.1	Elastic scattering in random media	1
1.1.1	Random media	1
1.1.2	Single scattering	3
1.2	Multiple scattering in random media	4
1.2.1	Mean free path	4
1.2.2	Characteristic lengths	5
1.2.3	Regimes of propagation	6
1.3	Outline of the thesis	7

WHETHER one looks up at the sky, listens to music or receives a call on mobile phone, waves are ubiquitous in our everyday life. In particular, in the field of communications, waves have taken such an important place that knowledge of the mechanisms governing their propagation in more or less complex media has become essential. This thesis deals with propagation of waves in such media. In the present introduction, we outline some aspects of the physics of waves in random media, and provide the basic ingredients necessary for its proper understanding.

1.1 Elastic scattering in random media

1.1.1 Random media

Most of the media in which a wave is likely to propagate are “random”, or “disordered”. This term refers to a strong spatial heterogeneity of a particular parameter

of the medium, which may affect the propagation of the wave. Whereas for acoustic or seismic waves this parameter is the density of matter, for electromagnetic waves it is the refractive index. In this thesis, we are mostly interested in media made of many “impurities”, or scatterers, embedded in a material of different nature ¹. This covers a large variety of situations: molecules in the atmosphere, defects in a solid or proteins in a glass of milk, etc. The interaction of a wave with a scatterer is called a scattering event, or scattering process.



Figure 1.1: An example of random medium. Unlike most natural mountain lakes which are crystal clear, the lac blanc in the Belledonne Massif is “turbid”. The milky aspect of its water is due to “glacial flour”, particles of rock in suspension, carried by the glacial torrents and produced by the abrasion exerted by the glacier on the surrounding rocks.

The study of physics of waves in random media led to several, often unexpected, applications. For instance, diffusing wave spectroscopy offers a possibility to probe a medium by analyzing the properties of waves scattered by it. It was first developed for optical waves by G. Maret and P. E. Wolf [1], and later extended by J. H. Page *et al.* to acoustic waves [2]. One can also take advantage of the time-reversibility of acoustic waves to destroy tumors [3]: the field and phase of a wave scattered by a tumor in the skull are recorded, and then sent back, after time-reversal and amplification. The time-reversed wave follows exactly the same path in the medium, but in reverse, and finally focuses back on the tumor. Finally, the study of random media with gain paved the way towards the so-called random lasers, where the feedback mechanism is due to the scattering of waves and not to an external cavity [4].

¹A different situation —a matter-wave propagating in a random potential— will be considered in Part III.

1.1.2 Single scattering

In this thesis, we only consider the case where the interaction of the wave with a scatterer is elastic. This means that no energy is transferred to, or from the wave, the scattering event only modifying the direction of propagation. The “scattering power” of a given scatterer is measured by its scattering cross-section $\sigma_s = \int d\Omega (d\sigma/d\Omega)$, which has the dimensionality of a surface. $d\sigma/d\Omega$ is the differential scattering cross-section, a ratio between the wave flux scattered in a unit solid angle in the direction Ω and the incident wave flux per unit surface.

Three different types of scattering processes can be identified. First, when the wavelength λ is much larger than the typical size a of the scatterer, one speaks of Rayleigh scattering [5]. The main characteristic of this process is that for scalar waves, the angular distribution of scattered wave is isotropic (in other words, the differential scattering cross-section does not depend on the scattering angle). For Rayleigh scattering, σ_s is proportional to the inverse fourth power of the wavelength. For sunlight in the atmosphere for instance, the consequence is that Rayleigh scattering on molecules or aerosols is much more efficient in the blue part of the visible spectrum than in the red part. This leads to the blue color of the sky.

The opposite case $\lambda \ll a$ corresponds to the limit of geometrical optics. Propagation is described in terms of rays and governed by the so-called Snell’s law. In this regime, the scattering cross-section is twice the geometrical cross-section of the scatterer ($\sigma_s = 2\pi a^2$ for a sphere of radius a) [6].

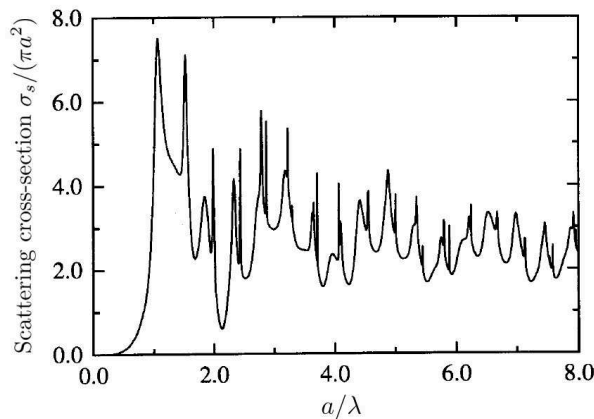


Figure 1.2: Plot of the scattering cross-section $\sigma_s/(\pi a^2)$ as a function of a/λ , for a sphere of radius a and of refractive index 2.8 in free space. At small values of a/λ , one recovers Rayleigh scattering, whereas at large values of a/λ , σ_s tends to $2\pi a^2$. In between, the scattering cross-section exhibits Mie resonances. Source: D. S. Wiersma, Ph.D. thesis, Amsterdam (1995).

Finally, the situation where the size of the scatterer is of the order of the wavelength is known as Mie scattering. This is the scattering process involved in thin clouds, where light is scattered by water droplets. The problem of scattering of a

wave by a sphere of size $\sim \lambda$ (called a Mie sphere) was first studied by Mie in 1908 [7]. Mie scattering is not isotropic (*i.e.*, the differential scattering cross-section depends on the scattering angle): Mie spheres scatter stronger in the forward direction. Another important property of this type of scattering process is that the scattering cross-section exhibits resonances for particular wavelengths (Fig. 1.2). This indicates that certain wavelengths are favored during the scattering process. Mie resonances are advantageously exploited in experiments to increase the “scattering power” of a random medium.

1.2 Multiple scattering in random media

1.2.1 Mean free path

When propagating in a random medium, a wave is likely to undergo several scattering events. This process is called multiple scattering, in contrast to single scattering, where the wave is only scattered once. It was first studied by O. D. Khvolson [8] and A. Schuster [9] a century ago. They developed the theory of radiative transfer. Since then, the latter has been used as a tool in astrophysics to describe the propagation of starlight through interstellar clouds or planetary atmospheres, and accede, in particular, to the spectral properties of stars. S. Chandrasekhar [10] and H. C. van de Hulst significantly contributed to these problems [11].

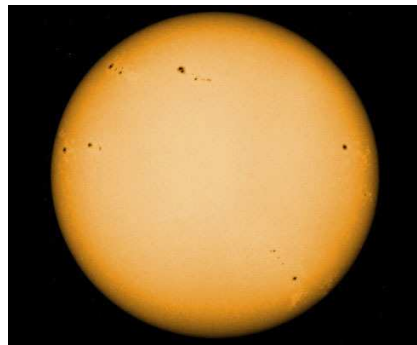


Figure 1.3: The theory of radiative transfer is used, for example, to accede to the temperature distribution inside the photosphere of the Sun from measurements of its intensity profile. Source: lecture of J. Gispert, LIF.

When studying the propagation of a wave in a random medium, the most fundamental length scale is the scattering mean free path ℓ , which is the average distance between two consecutive scattering events. Its value can vary considerably, depending on the nature of the wave and of the medium. For light, it can range from several meters in a very foggy atmosphere, to a fraction of micrometer in strongly scattering semiconductors powders. For electrons in metals, the mean free path is generally of the order of tens of nanometers. Finally, propagation of seismic waves in the crust can exhibit mean free paths of several tens of kilometers. For a dilute

ensemble of discrete scatterers, the mean free path is given by

$$\ell = \frac{1}{n_s \sigma_s}, \quad (1.1)$$

where σ_s is the scattering cross-section of individual scatterer, and n_s the number density of scatterers.

1.2.2 Characteristic lengths

Despite the apparent complexity of random media, relatively few characteristic lengths emerge from a quantitative description of transport of waves. In addition to the mean free path ℓ and the wavelength λ , we can list the following important length scales:

- The transport mean free path ℓ_B is the typical distance after which the wave loses the memory of its initial direction². The difference between ℓ and ℓ_B is depicted in the left panel of Fig. 1.4. For an ensemble of individual scatterers, each of which scattering more in the forward direction, ℓ_B is larger than ℓ . If θ denotes the angle between the wave vectors before and after the scattering event, ℓ_B is given by

$$\ell_B = \frac{\ell}{\int d\Omega (1 - \cos \theta) \frac{1}{\sigma_s} \frac{d\sigma(\theta)}{d\Omega}}. \quad (1.2)$$

- The absorption length ℓ_a is defined for classical waves (light, sound, microwaves, etc.). This is the distance over which the amplitude of the wave is strongly attenuated due to the presence of absorption inside the medium. It is related to the absorption time t_a through $\ell_a = ct_a$.
- The macroscopic absorption length L_a is the average distance between the start and end points of a random walk of length ℓ_a . It is obtained from the absorption length through the relation $L_a = \sqrt{\ell_B \ell_a / 3}$. The difference between ℓ_a and L_a is depicted in the right panel of Fig. 1.4.
- The coherence length L_ϕ is the typical distance up to which the phase coherence of a wave is preserved. For light from a He-Ne laser, for instance, $L_\phi \sim 0.3$ m is very large. For electrons in metals, the strong coupling between electrons and their environment makes the electronic coherence length very small (typically, $L_\phi \lesssim$ a few μm).

²The transport mean free path is also denoted ℓ^* . In this thesis, however, we prefer the notation ℓ_B (with B for Boltzmann), which refers to the transport mean free path in the absence of macroscopic interferences.

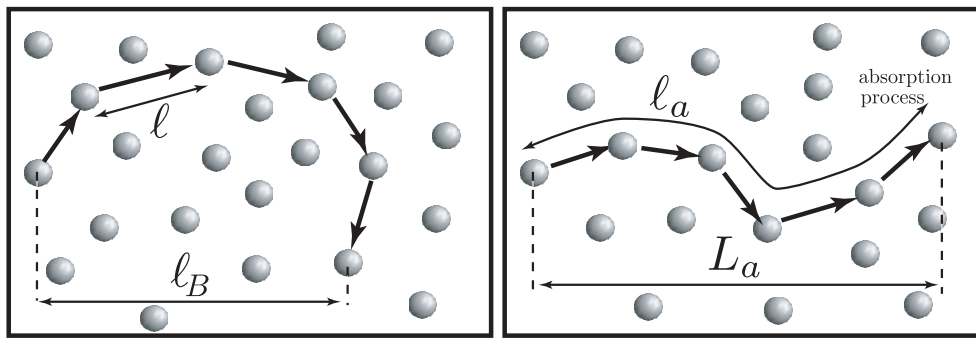


Figure 1.4: Difference between ℓ and ℓ_B (left) and between ℓ_a and L_a (right).

1.2.3 Regimes of propagation

Properties of transport of waves in a random medium can vary drastically depending on how the different characteristic lengths are ordered with respect to each other. Roughly, in a random medium of size L , we can distinguish the following regimes of propagation:

1. $L < \ell$: ballistic regime. In this regime, waves do not “see” the disorder. They propagate ballistically and do not undergo any scattering. Single scattering (*i.e.*, scattering on one impurity only) occurs when L becomes of the order of the mean free path.
2. $L \gg \ell$: multiple scattering regime. Waves are scattered many times from impurities of the disordered medium. A random medium where multiple scattering takes place looks opaque, and the direction of propagation of waves changes continuously. The difference between multiple scattering and single scattering is illustrated in Fig. 1.5.

Within the regime of multiple scattering $L \gg \ell$, different situations can occur. First, when $\lambda \ll \ell$, scattering events are very spaced and disorder is said to be “weak”. As a consequence, multiply scattered waves do not interfere with each other: transport is said to be *incoherent* and can be described by a random walk of step ℓ , governed by a diffusion equation for the wave intensity. When ℓ approaches λ , on the contrary, transport becomes *coherent*. Interference processes between multiply scattered waves start to set in and give rise to new effects that are not described by a diffusion process. Finally, when $\ell \lesssim \lambda$, disorder is “strong”, which may lead to the phenomenon of Anderson localization for which transport of waves comes to a halt³. Note that the appearance of coherent effects in transport requires the phase coherence of the wave. Therefore, such effects can be observed only when the coherence length L_ϕ is large enough. As far as classical waves are concerned, absorption only affects the amplitude of the wave, but does not break its phase coherence.

³More precise conditions for Anderson localization to take place will be given in Chapter 2.



Figure 1.5: Fans of light in a misty atmosphere. Sunlight undergoes a single scattering process on the edges of a thick cloud, which produces fans of light. These fans appear dark due to the shadow of the cloud on the misty air. Inside the cloud, the number of water droplets is very large, such that sunlight undergoes multiple scattering. This explains why the cloud appears dark. Source: Hans Häckel, *Farbatlas Wetterphänomene*, ©Ulmer Eugen Verlag (1999).

1.3 Outline of the thesis

This thesis presents a collection of studies on the coherent transport of waves in random media. We focus on interference effects that take place when a wave propagates in a sufficiently disordered material, and therefore go beyond diffusion theory. Whereas the fundamental concepts at the origin of coherent transport are the same for all waves, the *effects* of coherent transport can show up in different ways, depending on the wave properties. This contributes to the great richness of wave physics in the presence of disorder. In this thesis, we are mainly interested in two different types of waves, electromagnetic (classical) and matter waves. However, due to the universality of the underlying physics, many of the results presented in this work turn out to be general and not specific to a particular type of wave.

The first part of the thesis is devoted to the phenomenon of Anderson localization, which is the extreme manifestation of coherent transport in random media. Anderson localization is highly non trivial and has attracted the interest of physicists for the last five decades. We first review it and then demonstrate a recent microscopic theory of this phenomenon, adapted to the study of finite open media, starting from first principles. Making use of this theory, we study a new manifestation of Anderson localization, the confinement of a wave in the plane perpendicular to the direction of propagation.

In the second part, we analyze statistical properties of light transmitted through a random medium, neglecting Anderson localization. More specifically, we consider propagation of a short pulse through a disordered waveguide. Due to the randomness of the medium, the intensity of the wave exhibits a complicated interference pattern made of bright and dark spots, called a speckle pattern. Although appar-

ently random, such patterns exhibit long-range correlations due to the coherence of the underlying wave process. Since the medium is, in this case, excited by a time-dependent radiation, the speckle pattern *a priori* depends on time, and so do its correlations. We analyze this time dependence theoretically. We also present microwave measurements of these correlations, carried out by our colleagues at the University of Texas (San Antonio), and compare them to our theoretical analysis.

Finally, in the third part of the thesis, we study coherent transport of a very particular type of wave: a Bose-Einstein condensate, a matter wave made of an ensemble of atoms in the same quantum state, obtained at very low temperatures. We show that the speckle pattern, known for classical waves, has a counterpart for matter waves. We detail the statistical properties of these “matter-wave speckle patterns”, and analyze their time dependence. In the last chapter, we discuss the effects of weak atomic interactions on the expansion of a Bose-Einstein condensate in a random potential.

Part I

Anderson localization in finite media

Anderson localization: an overview

Contents

2.1	Basic definitions	12
2.1.1	Fundamental definitions	12
2.1.2	Practical criteria	13
2.2	Quantum and classical waves	16
2.2.1	Electronic conductors	16
2.2.2	Localization of classical waves	17
2.3	Experimental quest for Anderson localization	19
2.3.1	End of 20 th century: first attempts...	19
2.3.2	A 21 st century rich in experiments	19
2.4	Theoretical approaches	23
2.4.1	The scaling theory	23
2.4.2	The self-consistent theory	24
2.4.3	Other approaches	27
2.5	Conclusion	28

IN 1958, P. W. Anderson established that electronic diffusion could vanish in a sufficiently random potential, in the absence of electron-electron interactions [12]. He introduced a seminal model describing hopping of an electron from one site of an atomic lattice to another. In this “tight-binding model”, the disorder appeared as a random site energy. The basic idea of Anderson was to study the probability for the electron to stay on a given site, in order to show that depending on the “amount of disorder” electronic states could be either extended over the whole lattice (zero

probability), or localized on a site of the lattice (non-zero probability)¹. However, it was not until the late 1970's and the early 1980's that Anderson localization was really linked to wave physics and explained on that basis. It was then shown that the phenomenon was not specific for electrons but could take place for any coherent wave in a random potential. Since then, many theories of localization, more or less sophisticated, have emerged.

From the experimental point of view, the quest for Anderson localization has concerned many types of waves, with in the last twenty years a special interest for electromagnetic waves and, since recently, for matter waves. As far as electromagnetic waves are concerned, Anderson localization still remains a very elusive phenomenon. It has been searched for by generations of Ph.D. students, and today only a handful of experiments are convincing to demonstrate it. On the other hand, the study of localization using matter waves is very promising but is still in its early stages.

In this chapter we remind the necessary theoretical basis for the proper understanding of the phenomenon of Anderson localization². We also give a short review of recent experiments on the subject.

2.1 Basic definitions

It is difficult to provide a unique and unambiguous definition of Anderson localization of waves, applicable to any type of wave and any kind of random media. Many definitions are rather criteria that depend on the particular system that one considers. Anderson localization is often studied in different contexts, at different levels of complexity and through different physical observables. The probably simplest definition is due to Anderson himself: the “absence of diffusion” or “suppression of transport”. The definition of Anderson can, however, be hazardous in the sense that there exist other phenomena that can suppress diffusion, as well as transport can be subdiffusive. The purpose of this section is to attempt to characterize this phenomenon a bit more precisely. In Sec. 2.1.1 we consider fundamental properties of Anderson localization, whereas in Sec. 2.1.2 we discuss more practical criteria that one can use to determine whether a given sample exhibits localization or not.

2.1.1 Fundamental definitions

Strictly speaking, Anderson localization is defined in the infinite medium. The phenomenon also shows up in finite media but in a slightly different way. This situation will be extensively discussed later on. Here we first give fundamental definitions, keeping in mind that we consider the infinite disordered medium.

The most rigorous definition of Anderson localization is given by mathematicians [15]. Let us consider the Hamiltonian $\hat{H} = \hat{H}_0 + V$, where \hat{H}_0 is the kinetic part and V

¹The Anderson model is detailed, for instance, in the book of P. Sheng [13].

²More details can be found for instance in Ref. [14].

is a disordered (random) potential whose realizations are denoted $\{V\}$. We denote $\psi_{n,\{V\}}(\mathbf{r})$ the eigenfunctions of \hat{H} . The subscript n numbers the eigenfunctions whereas the subscript $\{V\}$ indicates that the eigenfunctions depend on the particular realization of the random potential. Anderson localization is said to take place when for all n and almost all realizations $\{V\}$, there exist sites $\mathbf{r}_{n,\{V\}}$ and constants $C_{n,\{V\}}$ for which

$$|\psi_{n,\{V\}}(\mathbf{r})| \leq C_{n,\{V\}} \exp\left(-\frac{|\mathbf{r} - \mathbf{r}_{n,\{V\}}|}{2\xi}\right), \quad (2.1)$$

where ξ is independent of the realization of disorder, and is called the localization length. As intuition suggests, Eq. (2.1) describes nothing but exponential localization of eigenfunctions in some region of space due to the presence of a random potential.

Eq. (2.1) has the following simple consequence for the transport of a wave packet with center of mass at \mathbf{r} propagating in a disordered material: its mean-square displacement $\langle \mathbf{r}^2 \rangle$ obeys

$$\langle \mathbf{r}^2 \rangle < \text{const}, \quad (2.2)$$

where $\langle \dots \rangle$ denotes averaging over realizations of the disordered potential V . This property is quite intuitive: the propagation of a wave packet in a disordered material in the regime of Anderson localization is halted after a certain time. In any dimension d , Eq. (2.2) implies that the diffusion coefficient of the wave packet is zero:

$$D = \frac{1}{2d} \lim_{t \rightarrow \infty} \frac{\langle \mathbf{r}^2 \rangle}{t} = 0, \quad (2.3)$$

where t denotes time. Eq. (2.3) is a very widespread definition of localization in physics. Incidentally, this turns out to be the definition given by Anderson himself in his original paper: the absence of diffusion means that the diffusion coefficient is zero. Eqs. (2.2) and (2.3) strongly contrast with the often encountered situation of waves propagating by diffusion in a disordered medium [16, 17]. In this case, properties (2.2) and (2.3) become

$$\langle \mathbf{r}^2 \rangle \propto t \text{ and } D = \text{const}. \quad (2.4)$$

Note that, strictly speaking, the definitions (2.1), (2.2) and (2.3) are not equivalent. As a matter of fact, the definition (2.1) is much stronger than the two others, and can be seen as the most fundamental definition of Anderson localization.

2.1.2 Practical criteria

In order to achieve Eqs. (2.1)-(2.3), one has to fulfill particular conditions that appear as practical criteria for Anderson localization. In this section, we discuss two of these criteria. They are very useful because they involve physical observables commonly measured in experiments, unlike the definition (2.1) of localization which applies directly to the wave function. The latter is inaccessible in experiments (the case of Bose-Einstein condensates in random potentials is an exception, see Sec. 2.3

and part III). In addition, these criteria are important from the historical point of view, because they paved the way for general theories of Anderson localization.

2.1.2.1 Ioffe-Regel criterion. Role of dimensionality

One of the oldest criteria for Anderson localization was introduced in a work of A. F. Ioffe and A. R. Regel in 1960 [18]. This criterion is valid for the infinite medium and is based on the wave picture of Anderson localization, outlined in the introduction of this thesis: Anderson localization occurs when interference effects between multiple scattered waves become plethoric inside the disordered material. A wave of wavelength λ and wave number $k = 2\pi/\lambda$, propagating in a disordered medium, is scattered from an impurity, then propagates freely without loss of energy before being scattered a second time, and so forth. This simple picture is valid as long as the typical distance between two consecutive scattering events — the scattering mean free path ℓ — much exceeds the wavelength. By contrast, when ℓ is of the order of λ , this scenario breaks down because interference effects may occur *during* the scattering process. Therefore, one expects localization to take place when $k\ell \lesssim \text{const}$, where $\text{const} \sim 1$. This condition is today referred to as the “Ioffe-Regel criterion”. It depicts Anderson localization as a phase transition separating a regime where waves are extended over large scales and propagate by diffusion ($k \gg 1/\ell$, “extended” or “diffusive” regime) from a regime where waves are localized in small regions of space ($k \ll 1/\ell$, “localized” regime). The transition region between these two regimes is usually referred to as the “critical regime” or “mobility edge”³.

At first sight, the above reasoning might be valid in any dimension. This however turns out to be wrong. As a matter of fact, a transition only exists in three dimensions. In contrast, in dimensions one and two waves are always localized whatever the value of $k\ell$! This property of localization was first noticed in the Anderson’s original paper, and then quantitatively explained by the scaling theory of localization. We shall come back to this point in more details in Sec. 2.4.1 and Chapter 5. In any case, the Ioffe-Regel criterion can be generalized to any dimension d in the following way:

$$k\ell \lesssim (k\ell)_c, \text{ where } (k\ell)_c = \begin{cases} \text{const} \sim 1, & d = 3 \\ \infty, & d = 1, 2. \end{cases} \quad (2.5)$$

The Ioffe-Regel criterion can be derived from several microscopic theories. In Sec. 2.4 we shall give an example of such a derivation from the self-consistent theory of localization.

2.1.2.2 Case of finite systems: Thouless criterion

Rigorously, the Ioffe-Regel criterion is only applicable to the infinite medium. In practice, however, all physical systems are finite. In addition, in order to observe

³As far as quantum waves are concerned, the kinetic energy E is generally preferred to the wave number k and the Ioffe-Regel criterion reads $E \lesssim E_c$.

localization by means of transport measurements, it is necessary to open the system.

The study of localization in finite open systems was initiated by Thouless in 1974 [19], and then reached a decisive stage with the scaling theory of localization (Sec. 2.4.1 and Chapter 5)⁴.

The idea of Thouless is that the eigenstates of a finite open system of size L achieve finite life times $\hbar/\delta E$ due to the leakage through the boundaries. In the extended regime, δE equals the ‘‘Thouless energy’’ $\hbar D(E)/L^2$, where $D(E)$ is the diffusion coefficient at energy E , and eigenstates are extended over the whole volume. According to Thouless, the properties of transport change drastically depending on how this energy compares to the average level spacing $\Delta E = 1/[\nu_0(E)L^d]$, where $\nu_0(E)$ is the density of states at energy E and d is the dimensionality of the system. The dimensionless ‘‘Thouless number’’ then naturally emerges as

$$g = \frac{\delta E}{\Delta E} = \hbar \nu_0(E) D(E) L^{d-2}. \quad (2.6)$$

When $g > 1$, the ‘‘width of eigenstates’’ δE is larger than the level spacing ΔE . This is the extended regime where states overlap. On the other hand, when $g < 1$, eigenstates are well resolved. They do not overlap and cannot support transport: this is the localized regime. Both situations are depicted in Fig. 2.1. In a finite

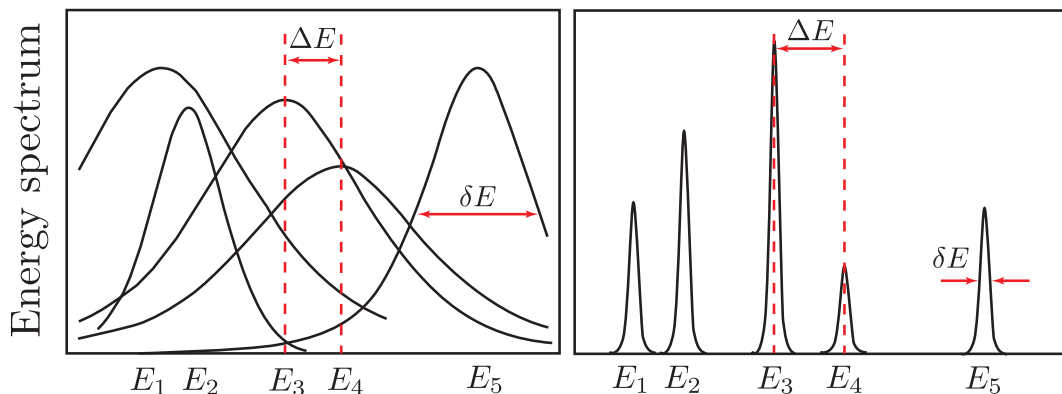


Figure 2.1: Sketch of typical energy spectra of a disordered system. In the extended regime (left) the width δE of eigenstates is large as compared to the level spacing ΔE . In the localized regime (right), $\delta E < \Delta E$ and eigenstates are well resolved.

open medium, a criterion for Anderson localization is then

$$g < g_c \simeq 1. \quad (2.7)$$

From Eq. (2.6), one sees that the Thouless number coincides with the Drude conductance G of a metal, but for a factor e^2/h . This is the reason why g is also called

⁴To be consistent with literature, we shall use the terminology of quantum mechanics, *i.e.* speak about ‘‘eigenstates’’ (instead of ‘‘eigenmodes’’ for classical waves) and use the energy E (instead of the frequency ω of the wave). The discussion is, however, valid for classical waves as well.

dimensionless conductance. However, it is important to note that the second equality of Eq. (2.6) is only true in the extended regime. Indeed, in the localized regime transport is inhibited and one expects the conductance to decay exponentially with L . We shall largely come back to this point in Chapter 5.

2.2 Quantum and classical waves

From the fundamental point of view, Anderson localization is an interference, wave phenomenon. Viewed in this light, Anderson localization is not specific to a particular type of wave. In this sense it can be qualified as universal. As a matter of fact, during the last half a century, a very large number of works concerned localization of both classical and quantum waves. In the literature, quantum waves usually refer to electrons, phonons or cold atoms (in the latter case one also speaks of matter waves), whereas classical waves refer to light, sound, microwaves or elastic waves. With quantum waves, the wave nature is of *quantum* origin and propagation is based on the Schrödinger equation, whereas with classical waves, laws of *classical* wave physics govern wave propagation.

Although Anderson localization exists for both families of waves, in the last quarter of the 20th century, experiments focused more on localization of classical waves, especially light and microwaves, rather than on localization of electrons. Since 2000, localization of cold atoms has been in the spotlight. Our purpose here is not to detail the particular case of a given type of wave, but rather to emphasize the main differences between electrons and electromagnetic waves which are of great importance from the historical point of view. The important case of matter waves will be discussed in detail in Part III of this thesis.

2.2.1 Electronic conductors

For electrons propagating in a disordered metal, Schrödinger equation reads

$$\frac{-\hbar^2}{2m_e} \nabla_{\mathbf{r}}^2 \Psi_E(\mathbf{r}) + V(\mathbf{r}) \Psi_E(\mathbf{r}) = \epsilon \Psi_E(\mathbf{r}), \quad (2.8)$$

where $\Psi_E(\mathbf{r})$ is the wave function of an electron of mass m_e and energy E . V is a potential which includes disorder and possibly other effects such as interactions with phonons or other electrons. In the simplest situation where one neglects such effects, V is just the local scattering potential generated by atomic impurities embedded in the conductor. Anderson localization of electrons then shows up through an exponentially small conductivity σ ⁵:

$$\sigma \sim \exp\left(-\frac{L}{\xi}\right) \xrightarrow{L \gg \xi} 0, \quad (2.9)$$

⁵This property will be demonstrated in Chapter 5.

where L is the size of the sample and ξ is the localization length. Anderson localization is therefore a synonym of zero conductivity. It can be observed as a metal-insulator transition that takes place when the density of impurities in the sample is increased. Furthermore, in principle, localization of electrons can be readily achieved by making the energy sufficiently small as compared to the scattering potential. In other words, the Ioffe-Regel criterion can be fulfilled by decreasing the energy E .

Unfortunately, in practice it is impossible to observe zero conductivity due to the strong coupling of electrons with their environment (electronic interactions, coupling with phonons, etc.). As a matter of fact, in disordered conductors at low temperatures, interactions of electrons with phonons induce finite conductivity σ^6 , given by the celebrated Mott's formula [20]

$$\sigma \propto \exp\left(\frac{-\delta_\xi}{k_B T}\right)^{1/(d+1)}, \quad (2.10)$$

where k_B is the Boltzmann constant, T is temperature, $\delta_\xi = 1/(\nu_0 \xi^3)$ with ν_0 the density of states per unit volume. This underlines the main problem of electronic systems: Anderson localization is inextricably linked to coupling of electrons with their environment. In addition, its experimental study requires samples of very small size (typically, a few μm) and low temperatures (due to small coherence lengths of electrons).

2.2.2 Localization of classical waves

The first ideas concerning Anderson localization of classical waves emerged from the works of S. John [21] and P. W. Anderson [22]. Since then, the experimental quest for Anderson localization of classical and, especially, electromagnetic waves has attracted a lot of interest. This is partly due to the weakly interacting character of photons, allowing one to focus exclusively on the effect of disorder, which is impossible with electrons. Besides, advances in the laser technology make available lasers with very large optical coherence lengths (of the order of several meters). Therefore, localization of classical waves may *a priori* be observed in macroscopic samples and at room temperatures. Unfortunately, the situation is not as idyllic as it seems, because localization is very difficult to achieve with electromagnetic waves, for reasons that we detail now. Let us consider an electromagnetic wave ψ of frequency ω propagating in a random medium⁷. The disorder is described by fluctuations $\delta\epsilon(\mathbf{r})$ of the local dielectric constant $\epsilon(\mathbf{r}) = \bar{\epsilon} + \delta\epsilon(\mathbf{r})$, where $\bar{\epsilon}$ is the average of $\epsilon(\mathbf{r})$. The counterpart of Eq. (2.8) for classical waves is the Helmholtz wave equation

$$-\nabla_{\mathbf{r}}^2 \psi(\mathbf{r}) - k^2 \mu(\mathbf{r}) \psi(\mathbf{r}) = k^2 \psi(\mathbf{r}), \quad (2.11)$$

⁶Interactions with phonons allow electrons to “hop” between localized states. This is the “variable-range hopping theory”.

⁷We neglect the vector nature of electromagnetic waves from here on.

where $k = \sqrt{\epsilon}\omega/c$ is the wave number and c the free-space velocity of the wave. We have introduced the relative fluctuation of the dielectric constant $\mu(\mathbf{r}) = \delta\epsilon(\mathbf{r})/\bar{\epsilon}$. A glance at Eq. (2.11) allows us to understand why Anderson localization of electromagnetic waves is so elusive: the disordered potential, analog to V for electrons, is here $-\hbar^2 k^2 \mu(\mathbf{r}) / (2m_e) \propto \omega^2$. A decrease of ω^2 (which is the analog of electronic energy ϵ in Eq. (2.8)) therefore affects the potential which decreases in the same way! Simply lowering the frequency is therefore insufficient to localize electromagnetic waves. This problem was discussed by S. John in 1984 [21], who suggested that, despite this complication, Anderson localization of light could still be observable. His idea was the following. As discussed in the introduction of this thesis, when an electromagnetic wave propagates in a disordered medium, one can distinguish three regimes of single scattering. When the wavelength $\lambda = 2\pi/k$ much exceeds the typical size a of scatterers, the scattering cross-section $\sigma_s \propto 1/\lambda^4$ (Rayleigh scattering). In the opposite limit $\lambda \ll a$, σ_s approaches the value $2\pi a^2$ given by geometrical optics. In the intermediate region $a \sim \lambda$ (Mie scattering), σ_s may possibly be very large due to Mie resonances. The typical wavelength dependence of the mean free path $\ell = 1/(n_s \sigma_s)$ is depicted in Fig. 2.2 for two different values m_1 and $m_2 > m_1$ of the refractive index contrast between the scatterers and their environment. One

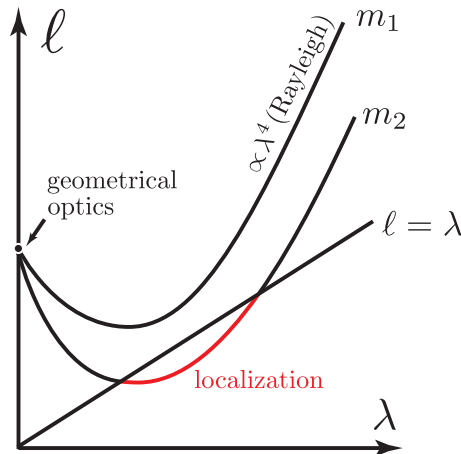


Figure 2.2: Schematic wavelength dependence of the scattering mean free path, for two values m_1 and m_2 of the refractive index contrast between the scatterers and their environment ($m_2 > m_1$). In the long-wavelength limit $\ell \propto \lambda^4$ (Rayleigh scattering). The short-wavelength limit corresponds to geometrical optics. In the intermediate regime (Mie scattering) there may exist a range of wavelengths for which the Ioffe-Regel criterion $\ell \lesssim \lambda$ is fulfilled and Anderson localization takes place.

sees that in the regime of Mie scattering and for a sufficiently high refractive index contrast, the mean free path can become small enough so that the localization condition (Ioffe-Regel criterion) $\ell \lesssim \lambda$ is fulfilled. Note that this discussion *suggests* that localization may show up for light but it is not a proof of its existence.

2.3 Experimental quest for Anderson localization

2.3.1 End of 20th century: first attempts...

The experimental search for localization falls within the broader field of coherent effects in transport of waves. The first experimental achievements related to Anderson localization date back to 1987, with, notably, the measurements of the conductivity at low temperatures demonstrating the Mott formula (2.10) [23]. Later, several articles dealt with corrections to the conductivity due to the effects of weak localization, a precursor of localization that takes place at weaker disorder [24]. However, as discussed in the previous section, since in metals localization is inextricably linked to the coupling of electrons with their environment, experimentalists turned very early to the study of classical waves. The first experimental step towards localization of such waves was the observation of a precursor effect, the coherent backscattering of waves, which consists in an enhancement of the reflected intensity in the direction opposite to the direction of irradiation. Experimental observation of the coherent backscattering effect requires strong disorder, but not as strong as for the observation of Anderson localization⁸. It was achieved in 1985 by two different groups: P. E. Wolf and G. Maret in Grenoble [25], and M. P. Albada and A. Lagendijk in Amsterdam [26].

The number of (often unfruitful) attempts to observe three-dimensional Anderson localization (*i.e.*, when a phase transition exists) is large and it would be futile to try to mention them all. In the 1990's, observation of Anderson localization of light was claimed in several works ([27, 28, 29] to cite a few). These works concluded on localization based on the observation of exponential decay of stationary transmission with sample thickness. This property of localization is the counterpart of the exponentially small conductivity in electronic systems (see Sec. 2.2.1) and will be discussed in detail in Chapter 5. However, conclusions of these works have been questioned because of the possibility for the decay observed to come from a residual (weak) absorption [30].

Later in 2000, observation of Anderson localization of microwaves was claimed by A. A. Chabanov *et al.* [31], based on the analysis of the statistical distribution of intensity of microwaves transmitted through a disordered medium. In this experiment, the samples were not three-dimensional but rather quasi one-dimensional waveguides. Thus, at the end of the 20th century an unequivocal proof of Anderson transition in three dimensions was still lacking.

2.3.2 A 21st century rich in experiments

At the beginning of the 21st century, several works provided clear observations of Anderson localization of different types of waves. Rather than citing them all, we focus here on a small set of experiments which, to the opinion of the author, were decisive stages in the experimental quest for Anderson localization. Interestingly,

⁸The coherent backscattering effect is related to weak localization.

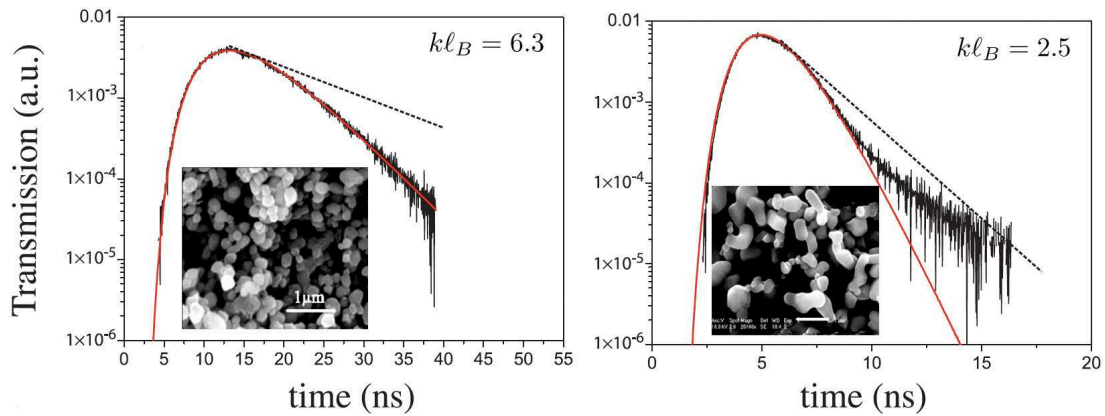


Figure 2.3: Profiles of time-dependent transmission of a short pulse, from Ref. [32]. The black curves are experimental data and the red curves are fits by diffusion theory. The difference between the red curves and the dashed black lines indicates the weight of absorption. Left profile: transmission in the regime of diffusion. The long-time tail of transmission exhibits a typical exponential decay. Right profile: transmission in the regime of Anderson localization. The tail exhibits a nonexponential decay and cannot be fitted by diffusion theory.

these works were realized in the last three years and two of them in 2008. This testifies to the experimental difficulty of localizing waves, and also proves that the subject is more lively than ever.

2.3.2.1 Localization of light...

A decisive observation of three-dimensional localization of light was achieved in 2006 by the team of G. Maret at the University of Konstanz [32]. In their experiment, the authors study the time-resolved profile of short pulses transmitted through a three-dimensional disordered medium. Samples are slabs of thickness of the order of a millimeter and of width much exceeding the thickness, made of compressed powders of submicron-sized TiO_2 particles. Compared to the steady-state case, the main benefit of such a *dynamic* experiment is that absorption and localization have different effects on the transmission profile. The two phenomena can then be distinguished unambiguously, in contrast to previous experiments [27, 28, 29]. In Fig. 2.3 we report the two main measurements of Ref. [32]. The left plot corresponds to a weakly disordered sample. The disorder parameter kl_B is large and light propagates by diffusion through the sample, which gives the exponential decay of the long-time tail of the transmission profile (black curve). In this case, the experimental results are well explained by diffusion theory (red curve). On the contrary, in the right plot the sample is much more disordered and transmission exhibits a nonexponential decay. In the presence of absorption, the diffusive exponential decay is preserved and only speeds up. Therefore, absorption cannot account for the observed nonexponential tail.

On the theoretical side, a power-law decay of the tail of dynamic transmission profiles was predicted by S. E. Skipetrov and B. A. van Tiggelen [33], which seems to corroborate the experimental observation. It should be noted that the experiment carried out in Konstanz is a real feat because samples with mean free paths of the order of 200 nm were necessary in order to observe localization of light.

2.3.2.2 ... sound...

Very recently, three-dimensional Anderson localization of sound was reported by the team of J. H. Page at the University of Manitoba in Canada [34]. Here the experimental demonstration is based on yet another consequence of localization called transverse confinement. The study of this phenomenon is the subject of Chapter 4. Here we only give the main elements necessary for the understanding of the experiment. For sound, length scales are larger than for light. In Ref. [34],

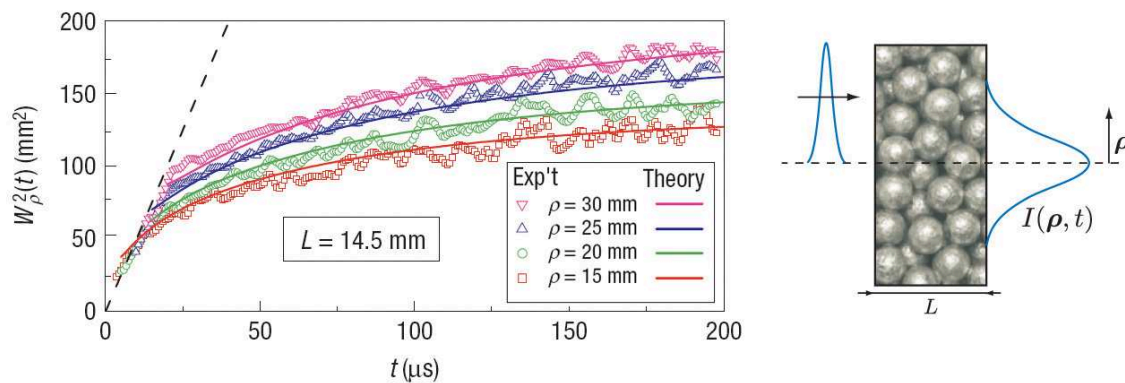


Figure 2.4: Right: sketch of the ultrasonic experiment. A short, focused pulse is sent into the disordered sample, and the transmitted intensity $I(\boldsymbol{\rho}, t)$ is measured at different transverse points $\boldsymbol{\rho}$ and different times t . Left: spot width $W_\rho^2(t)$ deduced from Eq. (2.12) and measurements of $I(\boldsymbol{\rho}, t)$, as a function of time and for different $\rho = |\boldsymbol{\rho}|$. The dashed line indicates the diffusive behavior $W_\rho^2(t) = 4D_B t$. Experimental curves are fitted by the self-consistent theory of localization.

disordered samples are ~ 20 mm thick slabs made of aluminium beads of diameter ~ 4 mm brazed together. Pulsed ultrasonic beams are focused on one side of the sample and the transmitted intensity is measured on the other side with hydrophones. The main difference with Maret's experiment is that here the spatial profile of the output spot is followed as a function of time. This is depicted in the drawing of Fig 2.4. The incoming pulse is focused at the transverse position $\boldsymbol{\rho} = \mathbf{0}$ on the input surface and the output transverse intensity profile $I(\boldsymbol{\rho}, t)$ is measured as a function of time for different $\rho = |\boldsymbol{\rho}|$. Very generally, one has

$$\frac{I(\boldsymbol{\rho}, t)}{I(\mathbf{0}, t)} = \exp \left[\frac{-\rho^2}{W_\rho^2(t)} \right], \quad (2.12)$$

where the “spot width” $W_\rho^2(t)$ is a function that is deduced from measured values of $I(\boldsymbol{\rho}, t)$. In the extended regime, sound propagates by diffusion and $W_\rho^2(t) = 4D_B t$, in agreement with Eq. (2.4). The transverse intensity profile is therefore Gaussian and its width grows linearly with time. On the other hand, if waves are localized, this profile departs from a Gaussian. $W_\rho^2(t)$ is expected to depend on ρ and to increase slower (if at all) with time. Typical dependencies $W_\rho^2(t)$, obtained in strongly disordered samples, with mean free paths of the order of 0.5 mm, are shown in Fig. 2.4. They demonstrate a saturation of $W_\rho^2(t)$ at long times, for any transverse position ρ . This behavior is very different from that expected in the extended regime, shown by a dashed line in the figure. This saturation at long times is called *transverse confinement*. Physically, this effect reflects the halt of spreading of the wave pulse along the transverse direction due to Anderson localization, in the sense of property (2.2). The self-consistent theory of localization reproduces very well the experimental results (solid lines in the figure).

2.3.2.3 ... and Bose-Einstein condensates.

The interest of physicists for Anderson localization of Bose-Einstein condensates is recent but very intense, as testifies the number of high quality papers, published on the subject in the last few years. Here the idea is to produce a Bose-Einstein condensate and let it expand in a random potential. As compared to experiments with classical waves, in experiments with condensates the propagating wave is replaced by the condensate and the disordered medium is replaced by a random potential which is produced artificially by means of optical techniques. Part III of the thesis is devoted to these systems.

There are several excellent articles reporting experiments on Bose-Einstein condensates expanding in random potentials. We choose here to discuss a recent experiment carried out by the french group of A. Aspect in Orsay [35], which has the benefit to be a “direct” observation of Anderson localization in the sense of definition (2.1). The expansion of the condensate in the random potential is depicted in the left panel of Fig. 2.5. A confining potential (depicted by the pink tube in Fig. 2.5) forces the condensate to expand only along one direction. The halt of expansion is observed at long times. This is shown in the inset of the right panel of Fig. 2.5. The points are the mean size of the condensate, which is proportional to time in the absence of random potential (green points) and saturates at long time in the presence of random potential (red points). This saturation is consistent with Anderson localization according to definition (2.2). However, the most striking effect is shown in the main plot of Fig. 2.5, which is a direct observation of the localization of the condensate in space. One clearly observes the exponential decay of the tails of the condensate density (wave function squared), in agreement with definition (2.1).

Today, experiments on three-dimensional localization of Bose-Einstein condensates have not been reported yet. However, in a very recent paper from the team of D. Delande in Paris, a three-dimensional localization in systems of cold Cesium atoms was reported [36]. Here it is not a question of propagation of a wave but of

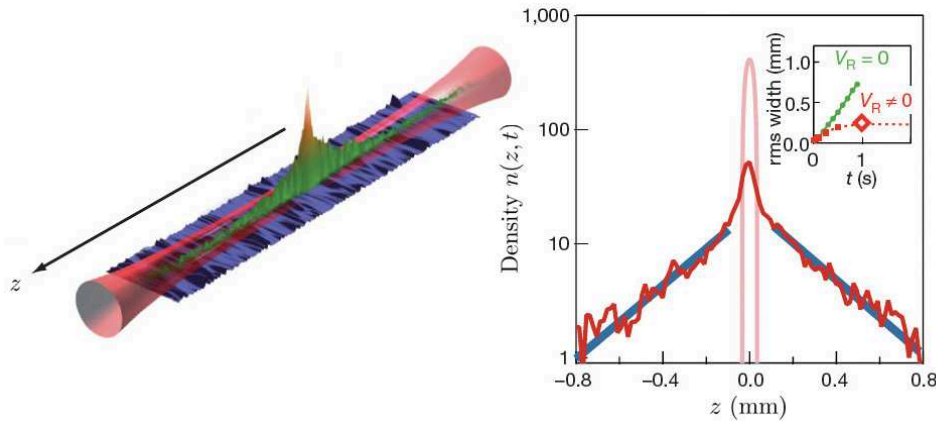


Figure 2.5: Left: sketch of the experiment. A Bose-Einstein condensate expands in a random potential shown in blue. The expansion is restricted to the z direction. The pink tube depicts longitudinal confinement. Right: direct measurement of the condensate density at a given (long) time, as a function of z . Tails exhibit exponential decay, typical for localization. The inset shows the mean size of the condensate in the absence (green points) and in the presence (red points) of random potential.

an experimental realization of a theoretical model called the quasi-periodic kicked rotor. Roughly speaking, this model describes the behavior, in momentum space, of a quantum pendulum which is periodically “kicked” with a force whose amplitude is modulated in time. Although this model seems very far from typical problems of disordered systems, it was proven to be an analog of the three-dimensional Anderson model [37]. In the experiment of Ref. [36], the role of the kicked pendulum is played by atoms exposed to a pulsed standing electromagnetic wave, and localization is directly observed from the measurement of the distribution of atomic momenta.

2.4 Theoretical approaches

In this section, we briefly review some of the main theories that allow a description of the phenomenon of Anderson localization, namely, the scaling theory, the self-consistent theory, the random matrix theory and the supersymmetric nonlinear σ -model. For the two latter we give a very short description since they will not be used in the following. We also give only the main lines of the scaling theory which is described in more detail in Chapter 5.

2.4.1 The scaling theory

One of the most prominent theoretical achievements after the paper of Anderson is certainly the scaling theory of localization. It was put forward by E. Abrahams, P. W. Anderson, D. C. Licciardello and T. V. Ramakrishnan in 1979 [38]. This theory

will be largely detailed in Chapter 5 and we simply give here the main lines.

The scaling theory extends the ideas of Thouless (see Sec. 2.7) and postulates that the dimensionless conductance is the only parameter needed for describing transport in a disordered medium of finite size. In this sense, the scaling theory is sometimes called one-parameter scaling theory. From this assumption and considerations similar to those of renormalization group theory, one can define a “scaling function” $\beta(g)$ which is universal, in the sense that it is independent of the microscopic properties of the sample (and only depends on g). The main purpose of scaling theory is the study of this β function, which provides a unified description of transport from the extended regime to the localized regime, in any dimension.

The scaling theory is very elegant and provides a description of the Anderson transition based on simple arguments. In addition, the fact that in dimensions one and two, states are localized whatever the degree of disorder, whereas in three dimensions there exists a phase transition separating extended from localized states (see the discussion of Sec. 2.1.2.1), emerges naturally from the theory. However, the scaling theory has a number of shortcomings. It is phenomenological and does not explain some fine features of Anderson localization (an example will be given in Chapter 4). Besides, the scaling theory fails to describe the *statistical* properties of transport in disordered media, as, for instance, the statistical distribution of conductance fluctuations.

2.4.2 The self-consistent theory

In this section we present the main features of the so-called self-consistent theory which was one of the first microscopic description of Anderson localization in the infinite medium. A complete derivation of a generalized version of this theory will be provided in the next chapter. Here we focus on its physical content.

2.4.2.1 Intuitive approach

From the microscopic point of view, the idea at the origin of the self-consistent theory of localization is that when a wave is emitted from some point inside a disordered medium, more energy comes back to the source than expected if waves behaved like classical particles. To be a bit more quantitative, it is valuable to look at this energy in more detail. In the framework of diffusion theory, the density of wave energy at a point \mathbf{r} and at time t of a wave packet emitted at time t' from a point \mathbf{r}' is given by the “intensity Green’s function” or “propagator” $C(\mathbf{r}, \mathbf{r}', t - t')$ (this quantity will be defined rigorously in Chapter 3), which in the extended regime, obeys the diffusion equation

$$(\partial_t - D_B \nabla_{\mathbf{r}}^2) C(\mathbf{r}, \mathbf{r}', t - t') = \delta(\mathbf{r} - \mathbf{r}') \delta(t - t'), \quad (2.13)$$

with $D_B = c\ell/3$ the diffusion coefficient [16]. Note that in the case of quantum particles, Eq. (2.13) holds as well, but the terminology is slightly different: C is called probability of quantum diffusion, and can be interpreted as a probability density of finding the particle in the vicinity of point \mathbf{r} at time t , provided that the

particle was at \mathbf{r}' at time t' . For simplicity let us assume that $t' = 0$. The energy density at the source at time t is then $C(\mathbf{r}, \mathbf{r}, t)$. In dimension d , the solution of diffusion equation (2.13) is given by

$$C(\mathbf{r}, \mathbf{r}', t) = \frac{1}{(4\pi D_B t)^{d/2}} \exp\left(-\frac{|\mathbf{r} - \mathbf{r}'|^2}{4D_B t}\right). \quad (2.14)$$

In a semi-classical picture, a ray propagating during a small time interval dt can be seen as a tube of diameter λ^{d-1} and of length cdt . The amount of energy returning to the source is then

$$E_{\text{return}} \simeq \int_0^\infty dt c \lambda^{d-1} C(\mathbf{r}, \mathbf{r}, t). \quad (2.15)$$

There is an ultraviolet divergence in the integral of Eq. (2.15). This reflects the breakdown of diffusion theory at very short times, when waves propagate ballistically. A way to overcome this problem is to introduce the mean free time ℓ/c as the lower limit of integration. Making use of $C(\mathbf{r}, \mathbf{r}, t) = 1/(4\pi D_B t)^{d/2}$, we readily obtain

$$E_{\text{return}} \sim \begin{cases} \frac{1}{(k\ell)^2}, & d = 3 \\ \infty, & d = 1, 2. \end{cases} \quad (2.16)$$

Eq. (2.16) is quite remarkable. For $d = 1$ and $d = 2$, diffusion theory predicts that an infinite amount of energy returns back to the point where the wave packet was initially emitted. This divergence signals the breakdown of diffusion theory whatever $k\ell$, which is not surprising because we have seen that in dimensions one and two localization always takes place. In three dimensions, Eq. (2.16) requires $k\ell > 1$ to make sense because for $k\ell \lesssim 1$ constructive interferences become significant, and the diffusive approach breaks down. As a matter of fact, we have just derived the Ioffe-Regel criterion discussed in Sec. 2.1.2.1.

2.4.2.2 Self-consistent equations

The self-consistent theory is one of the first microscopic theories of Anderson localization. It was proposed in the 1980's by D. Vollhardt and P. Wölfle [39]. By means of diagrammatic calculations, they derived a transport equation similar to the usual diffusion equation (2.13) but with the ‘‘classical’’ diffusion coefficient D_B replaced by a renormalized D , including interference effects at the origin of Anderson localization. The main consequence is that Eq. (2.13) is replaced by a system of *self-consistent* equations which read (in Fourier space)

$$\begin{cases} [-i\Omega - D(\Omega)\nabla_{\mathbf{r}}^2] C(\mathbf{r}, \mathbf{r}', \Omega) = \delta(\mathbf{r} - \mathbf{r}') & \text{(a)} \\ \frac{1}{D(\Omega)} = \frac{1}{D_B} + \frac{3}{\pi c \nu_0 \ell} \int \frac{d^d \mathbf{q}}{(2\pi)^3} \frac{1}{-i\Omega + Dq^2} & \text{(b)} \end{cases} \quad (2.17)$$

where ν_0 is the density of states. The integral of Eq. (2.17b) is nothing but $C(\mathbf{r}, \mathbf{r}, \Omega)$. This confirms the central role played by the return probability which directly drives

the renormalization of the diffusion coefficient. Notice that Eqs. (2.17) provide a unified description of both the extended and the localized regimes in space of any dimensionality.

2.4.2.3 Main results of the self-consistent theory

It is interesting to check whether the fundamental properties of transport in the regime of Anderson localization given in Sec. 2.1.1 (Eqs. (2.2) and (2.3)) follow from the self-consistent theory. For this purpose, we consider a wave packet initially located at position \mathbf{r}' , and study its propagation at long times. To fix the ideas, we consider the case of a three-dimensional medium. Eq. (2.17b) can be written as

$$\frac{D(\Omega)}{D_B} = 1 - \frac{\gamma}{2\pi^2} \int_0^\infty dq - \frac{i\Omega}{D(\Omega)} \frac{\gamma}{2\pi^2} \int_0^\infty \frac{dq}{-i\Omega/D(\Omega) + q^2}, \quad (2.18)$$

where we have introduced $\gamma = 3/(\pi c \nu_0 \ell)$. The ultraviolet divergence of the first integral arises from the breakdown of multiple scattering theory at short length scales, where waves propagate ballistically. It can be regularized by introducing an upper momentum cutoff $q_{\max} \sim 1/\ell$. This leads to

$$\frac{D(\Omega)}{D_B} = 1 - \frac{\gamma q_{\max}}{2\pi^2} + \frac{\gamma}{4\pi} \sqrt{\frac{-i\Omega}{D(\Omega)}}. \quad (2.19)$$

We now introduce the dimensionless variables $v = (1 - \gamma q_{\max}/2\pi^2)/(-i\Omega\tau)^{1/3}$, $\mathcal{T}(\Omega) = [D(\Omega)/D_B]/(-i\Omega\tau)^{1/3}$ and $\alpha = \gamma^2/(16\pi^2\tau D_B)$, where $\tau = \ell/c$ is the mean free time. Eq. (2.19) then reads

$$\mathcal{T}(\Omega)^3 - 2v\mathcal{T}(\Omega)^2 + v^2\mathcal{T}(\Omega) - \alpha^2 = 0. \quad (2.20)$$

The case $k\ell \gg 1$ corresponds to the extended regime ($\gamma \rightarrow 0$). For $k\ell \gg 1$, $\alpha \ll 1$ and, consequently, Eq. (2.20) can be rewritten as $\mathcal{T}(\mathcal{T} - v)^2 = 0$. The non-zero solution of this equation is $\mathcal{T} = v$. This yields

$$D(\Omega) = D_B \left[1 - \frac{1}{(k\ell)^2} \right]. \quad (2.21)$$

The regime $k\ell > 1$ is sometimes called “weak localization regime” because interference effects renormalize D by a small amount $\sim 1/(k\ell)^2$. Far in the extended regime, $k\ell \gg 1$ and $D = D_B$, in agreement with Eq. (2.4) expected for diffusion. In this regime, the energy density of the wave packet, the solution of Eq. (2.17a), is given by Eq. (2.14). The mean-square displacement $\langle \mathbf{r}^2 \rangle_{\text{diff}}$ of the wave packet in the extended regime follows straightforwardly:

$$\langle \mathbf{r}^2 \rangle_{\text{diff}} = 6D_B t, \quad (2.22)$$

which is again in agreement with Eq. (2.4).

Let us now consider the localized regime $k\ell < 1$ in the limit $|k\ell - 1| \ll 1$. In the low frequency limit $\Omega\tau \ll 1$, $|v| \gg 1$ and therefore Eq. (2.20) reduces to $\mathcal{T}(\Omega) = \alpha^2/v^2$, which yields

$$D(\Omega) = -i\Omega\xi^2, \quad (2.23)$$

where we have defined the length scale $\xi = 3\ell/[2(1 - k\ell)]$. In the limit $\Omega \rightarrow 0$, the diffusion coefficient vanishes, in agreement with the definition (2.3) of Anderson localization. In the localized regime, the energy density of the wave packet at long times then reads

$$C(\mathbf{r}, \mathbf{r}', t \rightarrow \infty) = \frac{1}{4\pi|\mathbf{r} - \mathbf{r}'|\xi^2} \exp\left(-\frac{|\mathbf{r} - \mathbf{r}'|}{\xi}\right). \quad (2.24)$$

From Eq. (2.24), we see that ξ gives the typical extent of the wave packet at long times in the localized regime: ξ is the localization length which has been introduced in Eq. (2.1)⁹. Finally, in the localized regime, the mean-square displacement of the wave packet is given by

$$\langle \mathbf{r}^2 \rangle_{\text{loc}} = 6\xi^2, \quad (2.25)$$

which is nothing but the property (2.2), with $\text{const} \sim \xi$.

2.4.3 Other approaches

Beyond the self-consistent theory, at least two other approaches allow to describe quantum transport in disordered media: the random matrix theory and the supersymmetric nonlinear σ -model. We briefly describe them in this section.

Random matrix theory was developed in the 1960's, under the impulse of E. P. Wigner and F. J. Dyson. The original motivation was then provided by the problem of energy level statistics in heavy nuclei. Since then, the theory has been extended to many other fields and, notably, to mesoscopic wave transport in disordered media. For a very complete review of random matrix theory we refer to the paper by C. W. J. Beenakker [40]. The idea of random matrix theory of quantum transport is to describe open disordered media through the statistical properties of the scattering matrix $\bar{\bar{S}}$ of a disordered system with N propagating modes:

$$\bar{\bar{S}} = \begin{pmatrix} \bar{\bar{r}} & \bar{\bar{t}}' \\ \bar{\bar{t}} & \bar{\bar{r}}' \end{pmatrix} \quad (2.26)$$

The scattering matrix allows to describe the amplitude of waves reflected from and transmitted through disordered media by the reflection matrices $\bar{\bar{r}}$ and $\bar{\bar{r}}'$ (reflection from left to left and from right to right) and transmission matrices $\bar{\bar{t}}$ and $\bar{\bar{t}}'$ (transmission from left to right and from right to left). The transport is then characterized by the statistics of eigenvalues of $\bar{\bar{S}}$. Because of current conservation, $\bar{\bar{S}}$ is unitary and, as a consequence, the four Hermitian matrices $\bar{\bar{t}}\bar{\bar{t}}^\dagger$, $\bar{\bar{t}}'\bar{\bar{t}}'^\dagger$, $\mathbb{1} - \bar{\bar{r}}\bar{\bar{r}}^\dagger$, and

⁹Notice that the localization length diverges at the mobility edge $k\ell = 1$. This property is characteristic of phase transitions and will be discussed in more detail in Chapter 5.

$\mathbb{1} - \bar{r}'\bar{r}'^\dagger$ have the same set of eigenvalues T_1, T_2, \dots, T_N . This set is sufficient to characterize transport in the disordered medium. From very few assumptions, O. N. Dorokhov [41] and independently P. A. Mello, P. Pereyra, and N. Kumar [42] were able to derive an equation describing the evolution of the distribution function of T_1, T_2, \dots, T_N with the size L of a disordered system. This equation is known as the DMPK equation, and it turns out to be a very powerful tool to describe transport in disordered media. It was successfully applied to explain the phenomenon of universal conductance fluctuations (see Chapter 6) or the statistics of conductance fluctuations in disordered wires.

A major advantage of random matrix theory is that it is nonperturbative and thus provides a unified description of both extended and localized regimes of wave propagation. Besides, it was recently generalized to include dynamics [43]. A major shortcoming of random matrix theory is that it is, by construction, restricted to one-dimensional and quasi one-dimensional systems.

Another very sophisticated theory of quantum transport in disordered media is the field theory. The idea of this theory is to replace the path integrals of the diagrammatic approach by integrations over complex fields. In its modern form, the field theory exploits properties of Grassmann algebra to describe interactions between these fields. The resulting model is known as the supersymmetric nonlinear σ -model (for reviews see for instance [44, 45]). In this model, the Green's function G of Schrödinger equation (2.8) is written as a functional integral over a two-component field $\Psi^T = (S, \chi)$ of commuting (S) and anticommuting (χ) Grassmann variables:

$$G(\mathbf{r}, \mathbf{r}', \epsilon) = i\hbar \int D\Psi S(\mathbf{r})S^*(\mathbf{r}') \exp \left[i\hbar \int d\mathbf{R} \Psi^\dagger(\mathbf{R})(\hat{H} - \epsilon + i0^+)\Psi(\mathbf{R}) \right]. \quad (2.27)$$

From this functional formulation, one expresses the intensity Green's function as an integral over fields Ψ which can be evaluated by means of the saddle point method.

The field theory is nonperturbative and can be applied to study disordered systems in any dimension¹⁰. This makes it a very powerful tool to study the Anderson transition. Unfortunately, it is highly technical and does not always give the necessary physical insight to guide experiments.

2.5 Conclusion

In this chapter we reviewed the main definitions and properties of Anderson localization, as well as the main theoretical approaches available to describe it. Our purpose was more to provide a theoretical basement for the remainder of this thesis, rather than to give an exhaustive review of localization. In the following, we shall

¹⁰At first sight, the field theory seems very far from the random matrix theory or usual diagrammatic treatments. They are, however, well related. For instance, results of the diagrammatic theory can be derived from the field theory [40], and it was shown that the supersymmetric nonlinear σ -model is equivalent to the random matrix theory in the limit of $N, L/\ell \rightarrow \infty$ with $N\ell/L = \text{const}$ [44].

encounter several times some of the criteria discussed in Sec. 2.1, for various systems studied in this thesis.

From here on, we shall exclusively make use of the self-consistent theory to describe Anderson localization. Strictly speaking however, in the form presented in this chapter, the self-consistent theory is only valid in the infinite medium. It is therefore required to generalize it to open media of finite size. This will be done in the next chapter by means of a position-dependent diffusion coefficient. The self-consistent theory generalized in this way is extremely suitable to provide quantitative descriptions of realistic experimental situations. For instance, it allows account for different types of source (short pulses, focused beams, plane waves etc.) and for samples of various shapes. Incidentally, the experiments discussed in Secs. 2.3.2.1 and 2.3.2.2 can be successfully explained in the framework of this theory.

Microscopic approach to Anderson localization in finite media

Contents

3.1	Theoretical framework	33
3.1.1	Intensity Green's function	33
3.1.2	Assumptions	34
3.2	Interference effects in finite media	35
3.2.1	Diagrammatic approach	35
3.2.2	Classical diffusion equation	36
3.2.3	Interference effects and reciprocity principle	37
3.3	Derivation of self-consistent equations	39
3.4	Energy conservation and boundary conditions	41
3.4.1	Energy conservation	41
3.4.2	Boundary conditions	42
3.5	Conclusion	43

THROUGHOUT this thesis, Anderson localization will be treated by means of the self-consistent theory of D. Vollhardt and P. Wölfle. In the previous chapter, we stressed that in its original form (Eqs. (2.17)), the self-consistent theory is, in principle, only valid for the infinite medium. However, in any physical experiment samples are finite. Moreover, in the particular case of transport experiments, they are necessarily *open* to the external world. For instance, localization experiments generally require exciting the disordered sample in some way and then measuring transmitted or reflected field or intensity. It is therefore important to adapt Eqs. (2.17) to the case of finite disordered media, Of course this problem is not new.

Already in its original form, the self-consistent theory was used to study localization in finite systems: the simplest way to account for finite-size effects is to introduce the system size L as a lower cut-off $\sim 1/L$ in the integral over momentum in Eq. (2.17b). Such an approach can be more or less successful in making qualitative predictions in the spirit of the scaling theory of localization (see Chapter 5), but it becomes insufficient when one is interested in fine details of multiple wave scattering close to the mobility edge and in the localized regime. In 2000, van Tiggelen *et al.* proposed a natural generalization of self-consistent theory to media of finite size by introducing a *position-dependent* diffusion coefficient D [46]:

$$\begin{cases} (-i\Omega - \nabla_{\mathbf{r}} \cdot D(\mathbf{r}, \Omega) \nabla_{\mathbf{r}}) C(\mathbf{r}, \mathbf{r}', \Omega) = \delta(\mathbf{r} - \mathbf{r}') & \text{(a)} \\ \frac{1}{D(\mathbf{r}, \Omega)} = \frac{1}{D_B} + \frac{6\pi}{k^2 \ell} C(\mathbf{r}, \mathbf{r}, \Omega). & \text{(b)} \end{cases} \quad (3.1)$$

The fundamental difference between Eqs. (2.17) and (3.1) is that the return probability $C(\mathbf{r}, \mathbf{r}, \Omega)$ in Eq. (3.1b) explicitly depends on \mathbf{r} , and hence D depends on position too.

One can question the physical meaning of the diffusion coefficient depending on position. A simple picture can be obtained in the stationary case $\Omega \rightarrow 0$. In the infinite medium, the diffusion coefficient $D(\Omega \rightarrow 0)$ is zero, as we saw in Sec. 2.4.2.3. In a finite medium, the diffusion coefficient is also expected to vanish in the bulk where there is no difference with the infinite medium, but close to boundaries the situation may be different. Indeed, in the vicinity of a boundary, the amount of energy coming back to the point where it was initially emitted (given by $C(\mathbf{r}, \mathbf{r}, \Omega)$) is less than in the infinite medium because of the increased probability for the wave to leave the medium through the boundary. Therefore, in a finite medium it seems natural that transport may drastically differ depending on whether one looks at regions near boundaries or deep in the bulk. This leads to a position-dependent renormalized diffusion coefficient D , the renormalization being less important near the boundaries of the disordered medium.

The generalized self-consistent theory was recently used to study the dynamics of Anderson localization in quasi one-dimensional [47, 48] and three-dimensional [33] random media. Meanwhile, the generalized self-consistent equations (3.1) have never been derived microscopically. Such a derivation is highly desirable for at least two reasons. First, recent results indicate that the position dependence of D is crucial for the internal consistency of the theory itself and that some of the important features of Anderson localization cannot be reproduced without fully taking it into account (an example of such a situation will be discussed in Chapter 4). Second, the very fact that D should be position-dependent can be questioned in favor of momentum [49] or time [50] dependencies studied in the past, unless the position dependence of D is given a microscopic justification. This calls for a rigorous derivation of self-consistent equations in a medium of finite size, showing the emergence of position-dependent D from microscopic equations of wave propagation and clarifying the physics behind it.

The purpose of this chapter is to present a mathematical derivation of the self-consistent equations of localization (3.1) in a finite medium of size L much exceeding the two main “microscopic” length scales of the problem: the wavelength λ and the mean free path ℓ . To fix the ideas, in this chapter we make use of the terminology of classical waves, but the results can be readily extended to the transport of quantum particles (*e.g.*, an electron or an atom at low temperatures) described by the Schrödinger equation with a disordered potential.

The chapter is organized as follows. In Sec. 3.1, we introduce notations and define precisely the concept of intensity Green’s function that appeared already in the previous chapter. Then, the main “building block” of our derivation — an “interference loop” that we insert inside ladder diagrams to account for interference effects in the intensity Green’s function — is calculated in Sec. 3.2. In Sec. 3.3, we sum an infinite series of diagrams for the intensity Green’s function and obtain the self-consistent equations of localization. Sec. 4.3 is devoted to the treatment of boundary conditions and a discussion of energy conservation. Finally, we summarize our main results and discuss their implications in Sec. 3.5. Technical details of calculations are collected in Appendix A.

3.1 Theoretical framework

3.1.1 Intensity Green’s function

We consider propagation of a scalar, monochromatic wave of circular frequency ω in a three-dimensional disordered medium of finite size. Propagation of waves in such a medium is governed by the Helmholtz equation:

$$[\Delta_{\mathbf{r}} + k^2(1 + \mu(\mathbf{r}))]G(\mathbf{r}, \mathbf{r}', \omega) = \delta(\mathbf{r} - \mathbf{r}'), \quad (3.2)$$

where $G(\mathbf{r}, \mathbf{r}', \omega)$ is the amplitude Green’s function. G is the wave field at point \mathbf{r} and frequency ω due to a point source located at point \mathbf{r}' . $\mu(\mathbf{r}) = \delta\epsilon(\mathbf{r})/\bar{\epsilon}$ is the relative fluctuation of the dielectric constant $\epsilon(\mathbf{r}) = \bar{\epsilon} + \delta\epsilon(\mathbf{r})$, $\bar{\epsilon}$ is the average dielectric constant, $k = \sqrt{\bar{\epsilon}}\omega/c$ is the wave number, and c is the speed of wave in a homogeneous medium with $\epsilon = 1$ (vacuum). We assume that $\mu(\mathbf{r})$ obeys the white-noise Gaussian statistics [16]:

$$k^4 \overline{\mu(\mathbf{r})\mu(\mathbf{r}')} = \frac{4\pi}{\ell} \delta(\mathbf{r} - \mathbf{r}'), \quad (3.3)$$

where the overline denotes averaging over realizations of disorder and ℓ is the scattering mean free path. We now assume weak disorder:

$$k\ell \gg 1. \quad (3.4)$$

This inequality was already introduced in the previous chapter and defines the extended regime of wave propagation. Under the assumption of weak disorder, the

average amplitude Green's function can be calculated. We do not detail this calculation which is standard and can be found, for instance, in the book of E. Akkermans and G. Montambaux [16]. The result is

$$\overline{G}(\mathbf{r}, \mathbf{r}', \omega) = -\frac{1}{4\pi |\mathbf{r} - \mathbf{r}'|} \exp\left(ik |\mathbf{r} - \mathbf{r}'| - \frac{|\mathbf{r} - \mathbf{r}'|}{2\ell}\right). \quad (3.5)$$

Eq. (3.5) indicates that a wave propagating in a disordered medium is strongly attenuated over distances of the order of the mean free path. Strictly speaking, this result is valid only in the infinite medium. However, it holds in a medium of finite size as well, provided that the points \mathbf{r} and \mathbf{r}' are at least one mean free path from the boundaries. Let us now introduce the average intensity Green's function (or propagator):

$$C(\mathbf{r}, \mathbf{r}', \Omega) = \frac{4\pi}{c} \overline{G(\mathbf{r}, \mathbf{r}', \omega_1) G^*(\mathbf{r}, \mathbf{r}', \omega_2)}, \quad (3.6)$$

where $\omega_1 = \omega_0 + \Omega/2$, $\omega_2 = \omega_0 - \Omega/2$, and we omit the dependence of C on the carrier frequency ω_0 . We assume the latter to be fixed in the remainder of this chapter. Physically, let us remind that the inverse Fourier transform $C(\mathbf{r}, \mathbf{r}', t - t')$ of Eq. (3.6) describes the density of wave energy at \mathbf{r} at time t due to a short pulse emitted at time t' by a point source at \mathbf{r}' .

3.1.2 Assumptions

The analysis of the intensity Green's function C is generally complicated and relatively simple results can be obtained only under certain assumptions that we detail below and that will be adopted from here on.

1. Weak disorder (Eq. (3.4)). This condition has already been used above for the derivation of the average amplitude Green's function. However, as seen from the previous chapter, the description of Anderson localization requires to go towards the limit $k\ell \lesssim 1$. This will be done in Sec. 3.3 by means of a self-consistency principle.
2. Intensity is measured at large distances \mathbf{r} from the source point \mathbf{r}' (*i.e.*, $|\mathbf{r} - \mathbf{r}'| \gg \ell$), and slow dynamics $\Omega \ll \omega_0, c/\ell$. This means that we consider only slow spatial variations of C and neglect any effects that might be due to its variations on the scale of the order of wave period $\sim 1/\omega_0$ or mean free time ℓ/c^1 [16].
3. Time-reversal invariance. This assumption is fundamental for the derivation of the self-consistent equations of localization. It indicates that transport properties remain unchanged when t is changed to $-t$.

¹One speaks of hydrodynamic assumption.

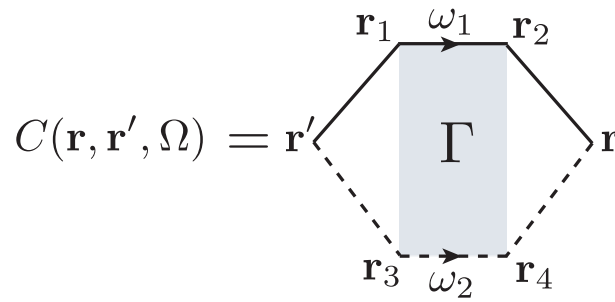


Figure 3.1: General diagrammatic form of the intensity Green's function $C(\mathbf{r}, \mathbf{r}', \Omega)$, which is the average of the product of two amplitude Green's functions G and G^* of frequencies ω_1 and ω_2 , respectively. Solid and dashed lines denote \overline{G} and $\overline{G^*}$, respectively. The gray rectangle Γ denotes the multiple scattering sequence followed by G and G^* between points \mathbf{r}_1 and \mathbf{r}_2 and \mathbf{r}_3 and \mathbf{r}_4 , respectively. \mathbf{r}' is the source point and \mathbf{r} the observation point.

3.2 Interference effects in finite media

3.2.1 Diagrammatic approach

The original derivation of self-consistent equations (2.17) by D. Vollhardt and P. Wölfle [39] heavily relies on the translational invariance of the medium *on average* and, therefore, cannot be straightforwardly extended to a medium of finite size that lacks translational invariance even after ensemble averaging.

The starting point of our derivation is the diagram for the intensity Green's function (Fig. 3.1). The physical process depicted by this diagram is the following. The wave is emitted from the point \mathbf{r}' . The first scattering events for the amplitude Green's functions G and G^* occur at points \mathbf{r}_1 and \mathbf{r}_3 , respectively. Between points \mathbf{r}_1 and \mathbf{r}_2 , G undergoes a multiple scattering process — symbolized by the gray rectangle Γ in Fig. 3.1— as well as G^* between \mathbf{r}_3 and \mathbf{r}_4 . The intensity is finally measured at \mathbf{r} . The diagram of Fig. 3.1 can be written as²

$$\begin{aligned}
 C(\mathbf{r}, \mathbf{r}', \Omega) &= \frac{4\pi}{c} \overline{G(\mathbf{r}, \mathbf{r}', \omega_1)} \times \overline{G^*(\mathbf{r}, \mathbf{r}', \omega_2)} \\
 &+ \frac{4\pi}{c} \int d\mathbf{r}_1 d\mathbf{r}_2 d\mathbf{r}_3 d\mathbf{r}_4 \overline{G(\mathbf{r}_1, \mathbf{r}', \omega_1)} \times \overline{G^*(\mathbf{r}_3, \mathbf{r}', \omega_2)} \\
 &\times \Gamma(\mathbf{r}_1, \mathbf{r}_2, \mathbf{r}_3, \mathbf{r}_4, \Omega) \overline{G(\mathbf{r}, \mathbf{r}_2, \omega_1)} \times \overline{G^*(\mathbf{r}, \mathbf{r}_4, \omega_2)}, \quad (3.7)
 \end{aligned}$$

where $\Gamma(\mathbf{r}_1, \mathbf{r}_2, \mathbf{r}_3, \mathbf{r}_4, \Omega)$ is called a vertex function and is depicted by the gray rectangle in Fig. 3.1 (as for C , we have omitted the dependence of Γ on the carrier frequency). In principle, this function includes all possible combinations of multiple scattering paths followed by G and G^* in the disordered medium. The first term

²To lighten the notation, in this chapter we use $d\mathbf{x}$ instead of $d^3\mathbf{x}$ to denote three-dimensional integration over a vector \mathbf{x} .

$(4\pi/c)\overline{G} \times \overline{G}^*$ on the right-hand side of Eq. (3.7) is exponentially small at large distances $|\mathbf{r} - \mathbf{r}'| \gg \ell$ (see Eq. (3.5)). It will be neglected in the following.

3.2.2 Classical diffusion equation

In the regime of weak disorder, defined by $k\ell \gg 1$, $\Gamma(\mathbf{r}_1, \mathbf{r}_2, \mathbf{r}_3, \mathbf{r}_4, \Omega) \simeq \delta(\mathbf{r}_1 - \mathbf{r}_3)\delta(\mathbf{r}_2 - \mathbf{r}_4)\Gamma_D(\mathbf{r}_1, \mathbf{r}_2, \Omega)$ with Γ_D a sum of ladder diagrams [13, 16, 39] shown in Fig. 3.2a. These diagrams describe a sum of multiple scattering processes in which G and G^* follow *exactly* the same sequence of scattering events (each scattering event is depicted by a cross in Fig. 3.2a).

We denote C given by Eq. (3.7) with Γ_D substituted for Γ by C_D . At large distances $|\mathbf{r} - \mathbf{r}'| \gg \ell$ and in the limit of small Ω , one derives the diffusion equation (2.13) for the intensity Green's function C (this derivation can be found, for instance, in Ref. [16]):

$$(-i\Omega - D_B\Delta_{\mathbf{r}})C_D(\mathbf{r}, \mathbf{r}', \Omega) = \delta(\mathbf{r} - \mathbf{r}'), \quad (3.8)$$

where, we remind, $D_B = c\ell/3$ is the Boltzmann diffusion coefficient. This equation holds in the infinite medium as well as in finite media, provided that it is supplemented with appropriate boundary conditions in the latter case. Eq. (3.8) ignores interference effects and treats the wave as a classical particle that propagates through a disordered medium by diffusion. In this regime, transport is said to be incoherent.

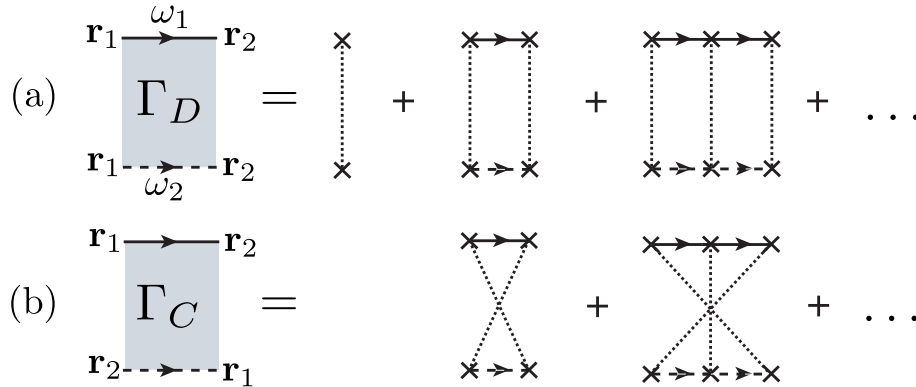


Figure 3.2: (a) Sum of ladder diagrams $\Gamma_D(\mathbf{r}_1, \mathbf{r}_2, \Omega)$ and (b) sum of maximally-crossed diagrams $\Gamma_C(\mathbf{r}_1, \mathbf{r}_2, \Omega)$. Solid and dashed lines denote \overline{G} and \overline{G}^* , respectively. The dotted line symbolizes the correlation function of disorder $k^4\mu(\mathbf{r})\mu(\mathbf{r}')$ given by Eq. (3.3). Crosses denote scattering events. Integrations over positions of all internal scattering events are assumed. In all diagrams of this chapter, \overline{G} and \overline{G}^* should be evaluated at frequencies $\omega_1 = \omega_0 + \Omega/2$ and $\omega_2 = \omega_0 - \Omega/2$, respectively. We show this explicitly in the panel (a) of this figure only.

3.2.3 Interference effects and reciprocity principle

We now come to the study of corrections to ladder diagrams, and therefore consider interference (or “coherent”) effects in transport. For this purpose, we first introduce a sum of maximally-crossed diagrams $\Gamma_C(\mathbf{r}_1, \mathbf{r}_2, \Omega)$ shown in Fig. 3.2b. If we do not consider the first term on the right-hand side of Fig. 3.2a, we can formally obtain Γ_C from Γ_D by rotating the bottom propagation line of the diagram of Fig. 3.2a by 180° in the plane perpendicular to the plane of the figure. The time-reversal invariance (see Sec. 3.1.2) then implies $\Gamma_C(\mathbf{r}_1, \mathbf{r}_2, \Omega) = \Gamma_D(\mathbf{r}_1, \mathbf{r}_2, \Omega)$ if $|\mathbf{r}_1 - \mathbf{r}_2|$ exceeds the correlation length of disorder (*i.e.*, if $\mathbf{r}_1 \neq \mathbf{r}_2$ for the white-noise disorder that we consider here) because the first term of Fig. 3.2a can be neglected in this case.

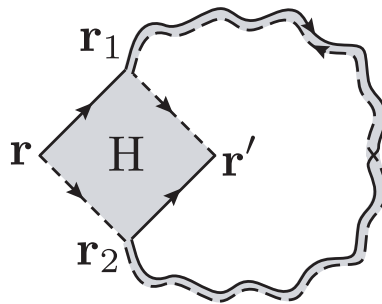


Figure 3.3: The diagram $X(\mathbf{r}, \mathbf{r}', \Omega)$ that we use to introduce interference effects in the calculation of intensity Green’s function. This diagram is made of a four-point Hikami box $H(\mathbf{r}, \mathbf{r}_1, \mathbf{r}', \mathbf{r}_2)$ (detailed in Appendix A.1) and of the sum of maximally-crossed diagrams $\Gamma_C(\mathbf{r}_1, \mathbf{r}_2, \Omega)$ shown by the wavy loop connecting \mathbf{r}_1 and \mathbf{r}_2 .

To account for interference effects during propagation, we consider a loop-shaped diagram $X(\mathbf{r}, \mathbf{r}', \Omega)$ shown in Fig. 3.3. This diagram is the building block of coherent transport. We shall see that it describes the fundamental interference process that leads to Anderson localization. This diagram represents the self-crossing of two fields propagating in a disordered medium, and is made of a square diagram known as a four-point Hikami box $H(\mathbf{r}, \mathbf{r}_1, \mathbf{r}', \mathbf{r}_2)$ [51, 52] and of a sum of maximally-crossed diagrams $\Gamma_C(\mathbf{r}_1, \mathbf{r}_2, \Omega)$. The diagram H is detailed in Appendix A.1. The diagram X can be written as

$$X(\mathbf{r}, \mathbf{r}', \Omega) = \int d\mathbf{r}_1 d\mathbf{r}_2 H(\mathbf{r}, \mathbf{r}_1, \mathbf{r}', \mathbf{r}_2) \Gamma_D(\mathbf{r}_1, \mathbf{r}_2, \Omega), \quad (3.9)$$

where we replaced $\Gamma_C(\mathbf{r}_1, \mathbf{r}_2, \Omega)$ by $\Gamma_D(\mathbf{r}_1, \mathbf{r}_2, \Omega)$ by making use of time-reversal invariance.

Because H is a local object having non-zero value only when all the four points \mathbf{r} , \mathbf{r}_1 , \mathbf{r}' and \mathbf{r}_2 are within a distance of order ℓ from each other, we can expand Γ_D in series around \mathbf{r} , assuming that its spatial variations are small at the scale of ℓ :

$$\begin{aligned} \Gamma_D(\mathbf{r}_1, \mathbf{r}_2, \Omega) \simeq & \left\{ 1 + (\mathbf{r}_1 - \mathbf{r}) \cdot \nabla_{\mathbf{r}_1} + (\mathbf{r}_2 - \mathbf{r}) \cdot \nabla_{\mathbf{r}_2} \right. \\ & \left. + \frac{1}{2} [(\mathbf{r}_1 - \mathbf{r}) \cdot \nabla_{\mathbf{r}_1}]^2 + \frac{1}{2} [(\mathbf{r}_2 - \mathbf{r}) \cdot \nabla_{\mathbf{r}_2}]^2 + \dots \right\} \Gamma_D(\mathbf{r}_1 = \mathbf{r}, \mathbf{r}_2 = \mathbf{r}, \Omega). \end{aligned} \quad (3.10)$$

We truncate this expansion to the first order in the remainder of our derivation. We now make use of a fundamental ingredient of transport theory: the reciprocity principle. This principle states that one can interchange detector and source without changing the result. In particular, the reciprocity principle is valid for the intensity as well as for the field. In our case we apply it to the field, which gives $\Gamma_D(\mathbf{r}_1, \mathbf{r}_2, \Omega) = \Gamma_D(\mathbf{r}_2, \mathbf{r}_1, \Omega)$. This allows us to rewrite Eq. (3.10) as

$$\Gamma_D(\mathbf{r}_1, \mathbf{r}_2, \Omega) \simeq \left[1 + \frac{1}{2}(\mathbf{r}_1 + \mathbf{r}_2 - 2\mathbf{r}) \cdot \nabla_{\mathbf{r}} \right] \Gamma_D(\mathbf{r}, \mathbf{r}, \Omega). \quad (3.11)$$

Substituting this into Eq. (3.9) we obtain

$$X(\mathbf{r}, \mathbf{r}', \Omega) = \left[H(\mathbf{r}, \mathbf{r}') + \frac{1}{2} \mathbf{H}_f(\mathbf{r}, \mathbf{r}') \cdot \nabla_{\mathbf{r}} \right] \Gamma_D(\mathbf{r}, \mathbf{r}, \Omega), \quad (3.12)$$

with

$$H(\mathbf{r}, \mathbf{r}') = \int d\mathbf{r}_1 d\mathbf{r}_2 H(\mathbf{r}, \mathbf{r}_1, \mathbf{r}', \mathbf{r}_2) \quad (3.13)$$

and

$$\mathbf{H}_f(\mathbf{r}, \mathbf{r}') = \int d\mathbf{r}_1 d\mathbf{r}_2 (\mathbf{r}_1 + \mathbf{r}_2 - 2\mathbf{r}) H(\mathbf{r}, \mathbf{r}_1, \mathbf{r}', \mathbf{r}_2). \quad (3.14)$$

The first term on the right-hand side of Eq. (3.12) is present, be the medium finite or not. The second term on the right-hand side is non-zero only in a finite medium because then $\Gamma_D(\mathbf{r}, \mathbf{r}, \Omega)$ depends on \mathbf{r} due to broken translational invariance! It will be seen from the following that this term is of fundamental importance for the derivation of self-consistent equations of localization in a finite medium. A calculation detailed in Appendix A.2 gives

$$\mathbf{H}_f(\mathbf{r}, \mathbf{r}') = -(\mathbf{r} - \mathbf{r}') H(\mathbf{r}, \mathbf{r}'). \quad (3.15)$$

Substituting Eq. (3.15) into Eq. (3.12) we obtain

$$X(\mathbf{r}, \mathbf{r}', \Omega) = H(\mathbf{r}, \mathbf{r}') \left[1 - \frac{1}{2}(\mathbf{r} - \mathbf{r}') \cdot \nabla_{\mathbf{r}} \right] \Gamma_D(\mathbf{r}, \mathbf{r}, \Omega). \quad (3.16)$$

For convenience of calculations, we introduce the difference variable $\Delta\mathbf{r} = \mathbf{r} - \mathbf{r}'$, such that a given function f of \mathbf{r} and \mathbf{r}' becomes a function \tilde{f} of \mathbf{r} and $\Delta\mathbf{r}$. In particular, $H(\mathbf{r}, \mathbf{r}')$ becomes $\tilde{H}(\Delta\mathbf{r})$ and does not depend on \mathbf{r} . Using the new set of variables \mathbf{r} and $\Delta\mathbf{r}$, we have $\Gamma_D(\mathbf{r}, \mathbf{r}, \Omega) = \tilde{\Gamma}_D(\mathbf{r}, \Delta\mathbf{r} = \mathbf{0}, \Omega)$. Equation (3.16) becomes

$$\tilde{X}(\mathbf{r}, \Delta\mathbf{r}, \Omega) = \tilde{H}(\Delta\mathbf{r}) \left[1 - \frac{1}{2}\Delta\mathbf{r} \cdot \nabla_{\mathbf{r}} \right] \tilde{\Gamma}_D(\mathbf{r}, \mathbf{0}, \Omega). \quad (3.17)$$

We now take the Fourier transform of Eq. (3.17) with respect to $\Delta\mathbf{r}$ and consider the limit $\mathbf{q} \rightarrow \mathbf{0}$. The Fourier transform $\tilde{H}(\mathbf{q})$ of $\tilde{H}(\Delta\mathbf{r})$ is equal to $D_B \ell^4 q^2 / 8\pi c k^2$ in this limit (see Appendix A.1). We then obtain

$$\tilde{X}(\mathbf{r}, \mathbf{q}, \Omega) = \frac{-\ell^4 D_B}{8\pi c k^2} [(i\mathbf{q})^2 + (i\mathbf{q}) \cdot \nabla_{\mathbf{r}}] \tilde{\Gamma}_D(\mathbf{r}, \mathbf{0}, \Omega). \quad (3.18)$$

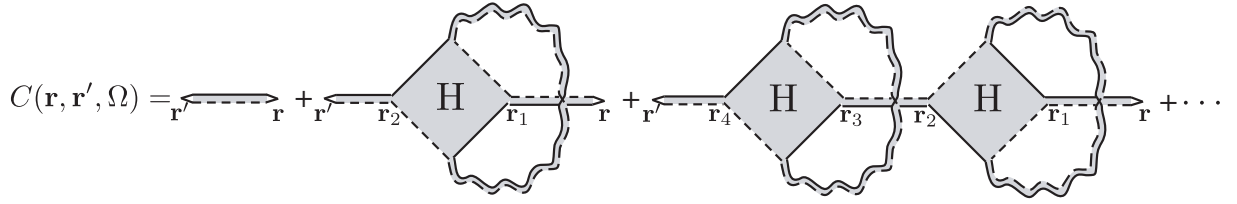


Figure 3.4: An infinite series of diagrams contributing to the intensity Green's function. The first term is the sum of ladder diagrams. The second term is the sum of ladder diagrams with a single interference loop denoted by wavy lines and equal to an infinite sum of maximally-crossed diagrams. Next terms contain 2, 3, etc. consecutive interference loops. The ladder and the maximally-crossed diagrams are joined together by a Hikami box detailed in Appendix A.1. The analytic representation of this diagrammatic series is given by Eq. (3.21).

An approximate expression for $\tilde{X}(\mathbf{r}, \Delta\mathbf{r}, \Omega)$ can then be obtained by the inverse Fourier transform of Eq. (3.18) with respect to \mathbf{q} (see Appendix A.3):

$$\tilde{X}(\mathbf{r}, \Delta\mathbf{r}, \Omega) = \frac{-\ell^4 D_B}{8\pi c k^2} \{ [\Delta_{\Delta\mathbf{r}} \delta(\Delta\mathbf{r})] + [\nabla_{\Delta\mathbf{r}} \delta(\Delta\mathbf{r})] \cdot \nabla_{\mathbf{r}} \} \tilde{\Gamma}_D(\mathbf{r}, \mathbf{0}, \Omega). \quad (3.19)$$

Because $\nabla_{\Delta\mathbf{r}} \delta(\Delta\mathbf{r}) = \nabla_{\mathbf{r}} \delta(\mathbf{r} - \mathbf{r}')$ and $\Delta_{\Delta\mathbf{r}} \delta(\Delta\mathbf{r}) = \Delta_{\mathbf{r}} \delta(\mathbf{r} - \mathbf{r}')$, Eq. (3.19) can be rewritten in terms of the original variables \mathbf{r} and \mathbf{r}' as

$$X(\mathbf{r}, \mathbf{r}', \Omega) = \frac{-\ell^4 D_B}{8\pi c k^2} \nabla_{\mathbf{r}} \cdot [\Gamma_D(\mathbf{r}, \mathbf{r}, \Omega) \nabla_{\mathbf{r}}] \delta(\mathbf{r} - \mathbf{r}'). \quad (3.20)$$

3.3 Derivation of self-consistent equations

We now use the diagram X of Fig. 3.3 analyzed in the previous section to include interference effects in the calculation of intensity Green's function $C(\mathbf{r}, \mathbf{r}', \Omega)$. To this end, we insert the “interference loop” X in the sum of ladder diagrams for C_D and account for the possibility of having multiple consecutive interference loops. This leads to an infinite series of diagrams shown in Fig. 3.4. This series can be written analytically as

$$\begin{aligned} C(\mathbf{r}, \mathbf{r}', \Omega) &= C_D(\mathbf{r}, \mathbf{r}', \Omega) + \frac{4\pi c}{\ell^2} \int C_D(\mathbf{r}, \mathbf{r}_1, \Omega) X(\mathbf{r}_1, \mathbf{r}_2, \Omega) C_D(\mathbf{r}_2, \mathbf{r}', \Omega) d\mathbf{r}_1 d\mathbf{r}_2 \\ &+ \left(\frac{4\pi c}{\ell^2} \right)^2 \int C_D(\mathbf{r}, \mathbf{r}_1, \Omega) X(\mathbf{r}_1, \mathbf{r}_2, \Omega) C_D(\mathbf{r}_2, \mathbf{r}_3, \Omega) \\ &\times X(\mathbf{r}_3, \mathbf{r}_4, \Omega) C_D(\mathbf{r}_4, \mathbf{r}', \Omega) d\mathbf{r}_1 d\mathbf{r}_2 d\mathbf{r}_3 d\mathbf{r}_4 + \dots \end{aligned} \quad (3.21)$$

We now apply the operator $-i\Omega - D_B \Delta_{\mathbf{r}}$ to Eq. (3.21) and use Eq. (3.8) for C_D and Eq. (3.20) for $X(\mathbf{r}, \mathbf{r}')$. This yields (see the detailed calculation in Appendix A.3):

$$[-i\Omega - D_B \Delta_{\mathbf{r}}] C(\mathbf{r}, \mathbf{r}', \Omega) = \delta(\mathbf{r} - \mathbf{r}') - \frac{\ell^2 D_B}{2k^2} \nabla_{\mathbf{r}} \cdot [\Gamma_D(\mathbf{r}, \mathbf{r}, \Omega) \nabla_{\mathbf{r}} C(\mathbf{r}, \mathbf{r}', \Omega)], \quad (3.22)$$

or

$$\left[-i\Omega - \nabla_{\mathbf{r}} \cdot \left(D_B - \frac{\ell^2 D_B}{2k^2} \Gamma_D(\mathbf{r}, \mathbf{r}, \Omega) \right) \nabla_{\mathbf{r}} \right] C(\mathbf{r}, \mathbf{r}', \Omega) = \delta(\mathbf{r} - \mathbf{r}'). \quad (3.23)$$

In addition, we demonstrate in Appendix A.4 that

$$\Gamma_D(\mathbf{r}, \mathbf{r}, \Omega) = (4\pi c/\ell^2) C_D(\mathbf{r}, \mathbf{r}, \Omega). \quad (3.24)$$

This allows us to define a renormalized, position-dependent diffusion coefficient

$$D(\mathbf{r}, \Omega) = D_B - \frac{2\pi c}{k^2} D_B C_D(\mathbf{r}, \mathbf{r}, \Omega). \quad (3.25)$$

and rewrite Eq. (3.23) as

$$[-i\Omega - \nabla_{\mathbf{r}} \cdot D(\mathbf{r}, \Omega) \nabla_{\mathbf{r}}] C(\mathbf{r}, \mathbf{r}', \Omega) = \delta(\mathbf{r} - \mathbf{r}'). \quad (3.26)$$

The last step consists in applying the self-consistency principle, first introduced in the original paper by D. Vollhardt and P. Wölfle [39]. This can be done by using $D(\mathbf{r}, \Omega)$ instead of D_B when calculating the second term on the right-hand side of Eq. (3.25). Diagrammatically, this procedure is equivalent to inserting “secondary loops” in the loops shown by wavy lines in Fig. 3.4 and then inserting the same loops in these secondary loops, etc., thus obtaining a sum of diagrams with an infinite sequence of loops inserted one inside the other. Physically, this simply means that the same, self-consistent diffusion coefficient $D(\mathbf{r}, \Omega)$ should be used when we calculate the intensity Green’s function C and the sum of maximally-crossed diagrams Γ_C . More specifically, we have to perform the following replacements:

1. We replace D_B by D in $H(\mathbf{r}, \mathbf{r}')$ in Eq. (3.16), or equivalently in $H(\mathbf{q})$, such that D_B is replaced by D in the second term on the right-hand side of Eq. (3.25).
2. We replace D_B by D in Γ_D in Eq. (3.16), which amounts to replace C_D by C in the second term on the right-hand side of Eq. (3.25).

Equation (3.25) then becomes $D(\mathbf{r}, \Omega) = D_B - (2\pi c/k^2) D(\mathbf{r}, \Omega) C(\mathbf{r}, \mathbf{r}, \Omega)$ or

$$\frac{1}{D(\mathbf{r}, \Omega)} = \frac{1}{D_B} + \frac{6\pi}{k^2 \ell} C(\mathbf{r}, \mathbf{r}, \Omega). \quad (3.27)$$

This completes the derivation of self-consistent equations of localization — Eqs. (3.26) and (3.27) — in a medium of finite size.

The solution of the diffusion equation (3.26) in three dimensions diverges when $\mathbf{r}' \rightarrow \mathbf{r}$: $C(\mathbf{r}, \mathbf{r}', \Omega) \propto 1/|\mathbf{r} - \mathbf{r}'|$. This unphysical divergence poses potential problems in Eq. (3.27) that contains $C(\mathbf{r}, \mathbf{r}, \Omega)$. One possibility to regularize this divergence is to represent $C(\mathbf{r}, \mathbf{r}', \Omega)$ as a Fourier transform of $C(\mathbf{r}, \mathbf{q}, \Omega)$, where \mathbf{q} is a variable conjugated to $\Delta\mathbf{r} = \mathbf{r} - \mathbf{r}'$, and then cut off the integration over \mathbf{q} at some $q_{max} \sim 1/\ell$,

in the same way as we have done in Chapter 2 for the self-consistent equations in the infinite medium. The exact proportionality constant between q_{max} and $1/\ell$ will determine the exact position of the mobility edge $k\ell \sim 1$. It is also possible to cut off only the integration over $\mathbf{q}_\perp = (q_x, q_y)$, leaving the integration over q_z unrestricted. Such a two-dimensional cutoff is easier to implement for the particular geometry of a disordered slab perpendicular to the z axis (this procedure will be applied in Chapter 4). As could be expected, the main qualitative features of final results are largely insensitive to the details of the large- q cutoff, although quantitative details can vary slightly.

3.4 Energy conservation and boundary conditions

3.4.1 Energy conservation

It is important to note that although we have obtained Eq. (3.26) by summing only the diagrams of certain type and neglecting many other diagrams, this equation satisfies the conservation of energy *exactly*. Indeed, let us take its inverse Fourier transform with respect to Ω :

$$\frac{\partial C(\mathbf{r}, \mathbf{r}', t)}{\partial t} - \int \frac{d\Omega}{2\pi} \nabla_{\mathbf{r}} \cdot D(\mathbf{r}, \Omega) \nabla_{\mathbf{r}} C(\mathbf{r}, \mathbf{r}', \Omega) e^{-i\Omega t} = \delta(\mathbf{r} - \mathbf{r}') \delta(t). \quad (3.28)$$

The flux of energy is given by Fick's law:

$$\mathbf{J}(\mathbf{r}, \mathbf{r}', t) = - \int \frac{d\Omega}{2\pi} D(\mathbf{r}, \Omega) \nabla_{\mathbf{r}} C(\mathbf{r}, \mathbf{r}', \Omega) e^{-i\Omega t}. \quad (3.29)$$

By integrating Eq. (3.28) over a control volume V contained inside the disordered medium and enclosed by a surface S , we obtain

$$\int_V \frac{\partial C(\mathbf{r}, \mathbf{r}', t)}{\partial t} d\mathbf{r} = - \int_V \nabla_{\mathbf{r}} \cdot \mathbf{J}(\mathbf{r}, \mathbf{r}', t) d\mathbf{r} + \delta(t) \int_V \delta(\mathbf{r} - \mathbf{r}') d\mathbf{r}. \quad (3.30)$$

We now apply the Gauss-Ostrogradsky theorem to the first term on the right-hand side of Eq. (3.30) and assume that the source point \mathbf{r}' is contained inside V :

$$\frac{d}{dt} \int_V C(\mathbf{r}, \mathbf{r}', t) d\mathbf{r} = - \oint_S \mathbf{J}(\mathbf{r}, \mathbf{r}', t) \cdot d\mathbf{S} + \delta(t). \quad (3.31)$$

Here $d\mathbf{S}$ is a vector normal to the surface element dS and directed outwards the volume V .

Equation (3.31) is a conservation equation. It states that the variation of wave energy in the volume V is given by a balance of energy emitted by the source (the second term on the right-hand side) and energy leaving the volume through its surface S (the first term on the right-hand side).

3.4.2 Boundary conditions

The proper account for boundary conditions is very important in finite media. This subject has been largely discussed in [13, 16, 53] and we invite the interested reader to consult these articles for more details. Although inside a disordered medium the energy flux $\mathbf{J}(\mathbf{r}, \mathbf{r}', t)$ can have arbitrary magnitude and direction consistent with the diffusion equation (3.26) and Fick's law, additional factors come into play at the surface of the medium. More specifically, for an open disordered medium of convex shape surrounded by the free space, no energy flux enters the medium from outside, provided that all sources are located inside the medium. This simple principle allows a derivation of boundary conditions for the intensity Green's function at the surface of disordered medium. Following X. J. Zhu *et al.* [53], we consider a disordered medium occupying the half-space $z > 0$ ("semi-infinite medium"). Let us first define the *specific* intensity $I(\mathbf{u}, \mathbf{r}, \mathbf{r}', \Omega)$, as the intensity at point \mathbf{r} , propagating in the direction of a unit vector \mathbf{u} and produced by a source located in \mathbf{r}' . One generally assumes that the specific intensity is weakly anisotropic, that is weakly depends on \mathbf{u} . Under this assumption we can make an expansion of I in spherical harmonics and truncate it at the first order:

$$\begin{aligned} I(\mathbf{u}, \mathbf{r}, \mathbf{r}', \Omega) &\simeq C(\mathbf{r}, \mathbf{r}', \Omega) + \frac{3}{c} \mathbf{J}(\mathbf{r}, \mathbf{r}', \Omega) \cdot \mathbf{u} \\ &= C(\mathbf{r}, \mathbf{r}', \Omega) - \frac{3}{c} D(\mathbf{r}, \Omega) \nabla_{\mathbf{r}} C(\mathbf{r}, \mathbf{r}', \Omega) \cdot \mathbf{u}, \end{aligned} \quad (3.32)$$

where Fick's law was used to obtain the second line. The total flux of wave energy crossing some plane $z = \text{const}$ at point \mathbf{r} in the positive direction of axis z is

$$J_+(\mathbf{r}, \mathbf{r}', \Omega) = \frac{c}{4\pi} \int_0^{2\pi} d\phi \int_0^{\pi/2} d\theta \sin \theta u_z I(\mathbf{u}, \mathbf{r}, \mathbf{r}', \Omega), \quad (3.33)$$

where $u_z = \cos \theta$ is the z component of \mathbf{u} . We then substitute Eq. (3.32) into Eq. (3.33) and perform integrations over θ and ϕ . This yields

$$J_+(\mathbf{r}, \mathbf{r}', \Omega) = \frac{C(\mathbf{r}, \mathbf{r}', \Omega)c}{4} - \frac{D(\mathbf{r}, \Omega)}{2} \frac{\partial C(\mathbf{r}, \mathbf{r}', \Omega)}{\partial z}. \quad (3.34)$$

By requiring $J_+(\mathbf{r}, \mathbf{r}', \Omega) = 0$ at the surface $z = 0$ of the medium, we obtain the following boundary condition:

$$C(\mathbf{r}, \mathbf{r}', \Omega)|_{z=0} - \frac{2}{c} D(\mathbf{r}, \Omega)|_{z=0} \left. \frac{\partial C(\mathbf{r}, \mathbf{r}', \Omega)}{\partial z} \right|_{z=0} = 0. \quad (3.35)$$

For a medium of more complex but still convex shape, the above derivation can be repeated locally in the vicinity of each point of the medium surface S , assumed to be locally flat. This yields

$$C(\mathbf{r}, \mathbf{r}', \Omega) - \frac{2\ell}{3} \frac{D(\mathbf{r}, \Omega)}{D_B} [\mathbf{n}(\mathbf{r}) \cdot \nabla_{\mathbf{r}}] C(\mathbf{r}, \mathbf{r}', \Omega) = 0, \quad (3.36)$$

where $\mathbf{n}(\mathbf{r})$ is a unit inward normal to the surface S at the point $\mathbf{r} \in S$. This equation is the boundary condition for the intensity Green's function at an open boundary. It can possibly be generalized to include internal reflections of waves at the boundary by replacing $2\ell/3$ by a larger “extrapolation length” z_0 .

3.5 Conclusion

In this chapter, we derived the self-consistent equations of Anderson localization — Eqs. (3.26) and (3.27) — starting from the first principles. Mathematically, this was achieved by dressing the ladder propagator with “interference loops” made of maximally-crossed diagrams. Each loop was inserted into the ladder with the help of a Hikami-box diagram. The self-consistent equations were then obtained by applying the self-consistency principle.

The essential difference of our derivation compared to the derivation of self-consistent equations in the infinite medium is the position dependence of the sum of ladder diagrams $\Gamma_D(\mathbf{r}, \mathbf{r}', \Omega)$ with coinciding end points $\mathbf{r} = \mathbf{r}'$. This position dependence leads to the appearance of an additional term, proportional to $\nabla_{\mathbf{r}}\Gamma_D(\mathbf{r}, \mathbf{r}, \Omega)$, in a series expansion of $\Gamma_D(\mathbf{r}_1, \mathbf{r}_2, \Omega)$ around an arbitrary point \mathbf{r} . As a consequence, one has to keep an additional term in the expression of Hikami box employed to connect ladder and maximally-crossed diagrams in our approach. It is this term that finally allows us to derive self-consistent equations of localization in a medium of finite size.

Although the condition $k\ell \gg 1$ was explicitly used to derive Eqs. (3.26) and (3.27), one can still hope that, similarly to self-consistent equations in the infinite medium, they could yield reasonable results in the vicinity of mobility edge and in the localized regime. According to recent works (concerning, for instance, the coherent backscattering effect in the localized regime [46] or the transmission of short pulses through waveguides [47] and three-dimensional slabs [33]), this indeed seems to be the case. However, one should understand that even though the general form of these equations might be largely universal in both diffusive and localized regimes, the numerical prefactor $6\pi/k^2\ell$ in front of the second term in the self-consistent equation for $D(\mathbf{r}, \Omega)$, Eq. (3.27), should not be taken too seriously because it originates from the calculation of complicated diagrams that was carried out in the limit $k\ell \gg 1$ only. When the result is extrapolated to $k\ell \lesssim 1$, this prefactor could vary and, in general, its dependence on $k\ell$ is likely to be more complex than just $1/(k\ell)^2$. In addition, the self-consistent theory neglects interference processes insensitive to the breakdown of time-reversal invariance by, *e.g.*, a strong magnetic field. The inclusion of such processes in the theoretical description would at least change the prefactor in Eq. (3.27). In Refs. [47, 33], for example, a larger prefactor was used in Eq. (3.27) to study the vicinity of the localization transition. This was justified by a comparison of some of the final results with those of the supersymmetric nonlinear σ -model [45]. Such a comparison indicates that the prefactor $6\pi/k^2\ell$ in Eq. (3.27) has to be multiplied by 2 to obtain an exact correspondence between the

two theoretical approaches. To be consistent with this previous work, we shall also use a larger prefactor ($12\pi/(k^2\ell)$ instead of $6\pi/(k^2\ell)$) when using Eq. (3.27) in the remainder of this thesis.

Finally, we signal that very recently, a derivation of Eqs. (3.26) and (3.27) in the particular case of the semi-infinite medium was proposed by C. Tian [54], in the framework of the supersymmetric nonlinear σ -model.

Application of the self-consistent theory: transverse
confinement

Contents

4.1	Spatially-resolved transmission coefficient of a slab . . .	46
4.2	Transverse confinement of continuous waves	48
4.2.1	Width of the transmission profile	48
4.2.2	Results	49
4.2.3	Reflection	52
4.2.4	Role of absorption	52
4.3	Transverse confinement with short pulses	53
4.3.1	Width of dynamic transmission profile	54
4.3.2	Results and discussion	54
4.4	Conclusion	57

THE difficulty of producing highly disordered samples as well as the possible confusion between localization of waves and other phenomena that slow down the transport require the knowledge of unambiguous experimental signatures of Anderson localization. Such signatures can be found in the thickness dependence of the average transmission coefficient of a random sample (see Sec. 2.3.1 and Chapter 5), in the shape of the coherent backscattering cone [28, 29], in the statistical distribution of transmitted intensity [31], or in the time-of-flight profiles of transmitted waves [57, 47, 32, 48] (see Chapter 2 for the discussion of experiment [32]). In the recent experiment of H. Hu *et al.* [34] that we detailed in Sec. 2.3.2.2, it was suggested

that Anderson localization could be demonstrated by looking at the transverse distribution of transmission of ultrasonic pulses through a three-dimensional disordered medium. Localization then showed up through the transverse confinement of the transmission profile¹. In this chapter we present a systematic theoretical study of this effect. This provides a guide for future experiments to exploit this interesting new phenomenon to access localization of various types of waves (light, sound, etc.).

The ideal theoretical background for studying transverse confinement of waves is the self-consistent theory of localization adapted to finite media, presented in Chapter 3. We recall below the self-consistent equations of localization in a finite medium:

$$\begin{cases} [-i\Omega - \nabla_{\mathbf{r}} \cdot D(\mathbf{r}, \Omega) \nabla_{\mathbf{r}}] C(\mathbf{r}, \mathbf{r}', \Omega) = \delta(\mathbf{r} - \mathbf{r}') & \text{(a)} \\ \frac{1}{D(\mathbf{r}, \Omega)} = \frac{1}{D_B} + \frac{12\pi}{k^2 \ell} C(\mathbf{r}, \mathbf{r}, \Omega). & \text{(b)} \end{cases} \quad (4.1)$$

In this chapter, we use Eqs. (4.1) to study the transverse confinement of both a continuous monochromatic beam and a short pulse focused to a point at the surface of a disordered slab. We investigate three regimes of propagation: Anderson localization, extended (diffusive) regime and mobility edge. We also discuss the role of absorption.

4.1 Spatially-resolved transmission coefficient of a slab

In this chapter, we focus on the transmission of a wave through a disordered slab confined between the planes $z = 0$ and $z = L$. This geometry is quite popular in experiments and can be readily taken into account in the self-consistent theory of localization. For this purpose, we decompose the couple of vectors \mathbf{r}, \mathbf{r}' of Eq. (4.1a) into a transverse part $\boldsymbol{\rho}$, which is the projection of the vector $\mathbf{r} - \mathbf{r}'$ onto the xy plane, and a longitudinal part (z, z') . Note that this decomposition relies on the translational invariance of ensemble-averaged quantities in the xy plane. In the remainder of the chapter, we assume that the incoming wave is focused at some point of the surface $z = 0$ of the slab. A point-like source is assumed to be located at a point $\mathbf{r}' = (\mathbf{0}, z' = \ell)$, about a mean free path from the surface $z = 0$ (this point lies in the plane in which the incident wave is converted into a diffusive one). This is summarized in Fig. 4.1. We can now express the intensity Green's function of Eq. (4.1a) as

$$C(\mathbf{r}, \mathbf{r}', \Omega) = C(\boldsymbol{\rho}, z, z', \Omega). \quad (4.2)$$

¹The phenomenon of transverse confinement described here should not be confused with transverse localization that takes place in a medium that is translationally invariant along the direction z of beam propagation and disordered in the perpendicular xy plane. Transverse localization was predicted theoretically by H. de Raedt *et al.* [55] and observed experimentally by T. Schwarz *et al.* [56].

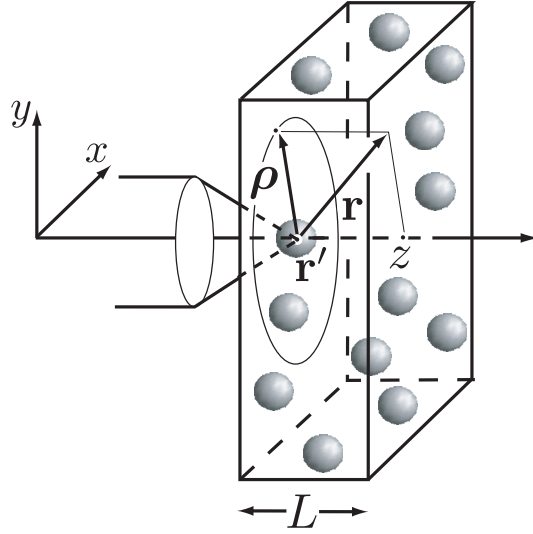


Figure 4.1: A disordered slab of thickness L (in the longitudinal direction z) and infinite in the xy plane is irradiated by an incoming wave focused at some point of the surface $z = 0$. In the first approximation, we can assume that the source of waves is point-like and located at a point $\mathbf{r}' = (\mathbf{0}, z' = \ell)$, about one mean free path from the focalization point. Intensity is measured in a point \mathbf{r} . We define $\boldsymbol{\rho}$ as the projection of the vector $\mathbf{r} - \mathbf{r}'$ onto the xy plane. z is the longitudinal coordinate of vector \mathbf{r} and z' that of \mathbf{r}' .

We denote by \mathbf{q}_\perp the momentum associated with $\boldsymbol{\rho}$ in Fourier space. Then, due to the translational invariance of the return probability $C(\mathbf{r}, \mathbf{r}, \Omega)$ in the xy plane, $D(\mathbf{r}, \Omega) = D(z, \Omega)$ and Eqs. (4.1) become

$$\left\{ \begin{array}{l} \left[-i\Omega - \frac{d}{dz}D(z, \Omega)\frac{d}{dz} + D(z, \Omega)q_\perp^2 \right] C(\mathbf{q}_\perp, z, z', \Omega) = \delta(z - z') \quad (\text{a}) \\ \frac{1}{D(z, \Omega)} = \frac{1}{D_B} + \frac{12\pi}{k^2\ell} \int \frac{d^2\mathbf{q}_\perp}{(2\pi)^2} C(\mathbf{q}_\perp, z, z, \Omega). \quad (\text{b}) \end{array} \right. \quad (4.3)$$

As explained in Sec. 3.3, we regularize the ultraviolet divergence of the integral of Eq. (4.3b) by introducing a two-dimensional momentum cutoff q_{\max} . The latter is chosen so that the mobility edge occurs at $k\ell = 1$ in the infinite medium. This leads to $q_{\max} = 1/(3\ell)$ [33]. Eqs. (4.3) have to be solved with the proper boundary conditions for C (see Sec. 3.4.2), which read for the slab $C \mp z_0[D(z, \Omega)/D_B]\partial_z C = 0$ at $z = 0$ and $z = L$, where $z_0 = 2\ell/3$ is the extrapolation length (for the sake of simplicity, we neglect internal reflections).

In this chapter, a physical quantity of interest is the spatially-resolved transmission coefficient at frequency Ω , defined as

$$T(\boldsymbol{\rho}, \Omega) = -D(z = L, \Omega) \left. \frac{\partial C(\boldsymbol{\rho}, z, z', \Omega)}{\partial z} \right|_{z=L}. \quad (4.4)$$

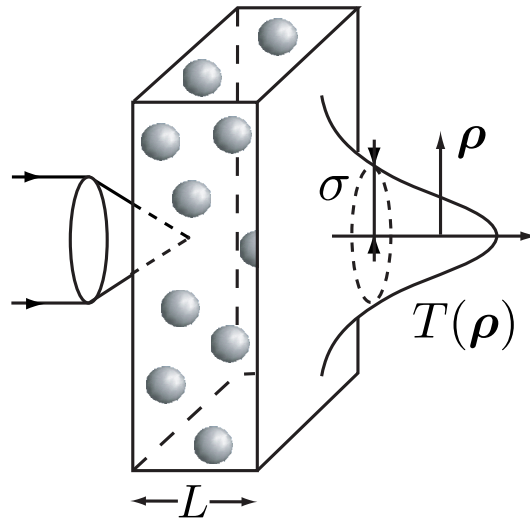


Figure 4.2: A continuous beam is focused on the surface of a three-dimensional disordered slab of thickness L . The bell-shaped average position-dependent transmission coefficient $T(\boldsymbol{\rho})$ has a width σ that depends on the strength of disorder in the medium.

In the remainder of the chapter, we solve Eqs. (4.3) in two different cases. First, we set $\Omega = 0$, which corresponds to a continuous focused beam. Second, we consider the general situation $\Omega \neq 0$, which is necessary to describe transmission of short pulses.

4.2 Transverse confinement of continuous waves

4.2.1 Width of the transmission profile

In this section, we consider the case of a disordered slab irradiated by a continuous wave. We thus set $\Omega = 0$ in Eqs. (4.3) and consider the bell-shaped profile of transmission $T(\boldsymbol{\rho}) = T(\boldsymbol{\rho}, 0)$ at the face $z = L$ of the slab (Fig. 4.2). A way to characterize the transmission profile $T(\boldsymbol{\rho})$ in the different regimes of wave propagation — weak disorder (diffusion, $k\ell \gg 1$), strong disorder (localization, $k\ell < 1$) and the critical regime (mobility edge, $k\ell = 1$) — is to look at the thickness dependence of its mean-square width σ^2 . The latter is defined as

$$\sigma^2 = \frac{\int d^2\boldsymbol{\rho} \rho^2 T(\boldsymbol{\rho})}{\int d^2\boldsymbol{\rho} T(\boldsymbol{\rho})}, \quad (4.5)$$

which for the slab can be rewritten as

$$\sigma^2 = \frac{-\frac{1}{q_\perp} \frac{\partial}{\partial q_\perp} \left[q_\perp \frac{\partial T(\mathbf{q}_\perp)}{\partial q_\perp} \right] \Big|_{q_\perp=0}}{T(\mathbf{q}_\perp) \Big|_{q_\perp=0}}, \quad (4.6)$$

where we have introduced the Fourier transform $T(\mathbf{q}_\perp) = -D(z = L, \Omega = 0) \times \partial C(\mathbf{q}_\perp, z, z' = \ell, \Omega = 0) / \partial z \Big|_{z=L}$ of $T(\boldsymbol{\rho})$ and $q_\perp = |\mathbf{q}_\perp|$.

In the following, we assume the large thickness limit $L \gg \ell$. As a consequence, $L \gg z_0$ and boundary conditions take the approximate form $C = 0$ at $z = 0$ and $z = L$ (Dirichlet boundary conditions).

4.2.2 Results

4.2.2.1 Diffusive regime

In the limit of weak disorder ($k\ell \gg 1$), the position dependence of D can be neglected and one can set $D(z, 0) = D_B[1 - (k\ell)^{-2}]$, where D_B is the Boltzmann diffusion coefficient (this is Eq. (2.21)). In this case, Eqs. (4.3) can be readily solved and we find the following expression for the transmission coefficient:

$$T(\mathbf{q}_\perp) = \frac{\sinh(q_\perp \ell)}{\sinh(q_\perp L)}. \quad (4.7)$$

From Eq. (4.6), we calculate the mean-square width σ^2 in the limit $L \gg \ell$:

$$\sigma_{\text{dif}}^2 \simeq \frac{2L^2}{3}. \quad (4.8)$$

The linear increase of σ with the slab thickness is typical for diffusion.

4.2.2.2 Localized regime

In the regime of Anderson localization ($k\ell < 1$), equations (4.3) should be solved in a self-consistent way. Because the exact analytical solution does not exist, we make the following ansatz: $D(z, 0) \simeq D(0, 0) \exp(-2\tilde{z}/\xi)$ with $\tilde{z} = \min(z, L - z)$ and $\xi = 3\ell/[2(1 - k\ell)]$ the localization length in the limit $|k\ell - 1| \ll 1$. This ansatz is inspired by the observation that this $D(z, 0)$ represents an asymptotically exact solution in a semi-infinite medium for $z \gg \xi$ [46]. Then, the analytical solution of Eqs. (4.3) reads

$$T(\mathbf{q}_\perp) = \frac{\exp(\ell/\xi) \xi \chi(q_\perp) \sinh[\ell \chi(q_\perp)]}{-1 + \cosh[\ell \chi(q_\perp)] + \xi \chi(q_\perp) \sinh[L \chi(q_\perp)]}, \quad (4.9)$$

where $\chi(q_\perp) = \sqrt{1/\xi^2 + q_\perp^2}$. A simple expression for σ^2 can then be obtained in the limit $\ell \ll \xi \ll L$, *i.e.* far inside the localized regime:

$$\sigma_{\text{loc}}^2 \simeq 2L\xi. \quad (4.10)$$

In the localized regime, σ increases as a square root of L , in contrast to the diffusive regime. Note that one might have naively expected $\sigma_{\text{loc}}^2 \propto \xi^2$ in the localized regime. The subtle point is that the transmission T is evaluated as a function of the transverse position ρ on the output surface of the slab and not as a function of the radial distance from the source. The fact that L appears in Eq. (4.10) is therefore simply a geometrical effect. Eq. (4.10) relates σ to the localization length ξ , which offers an elegant way of measuring the latter experimentally.

4.2.2.3 Mobility edge

At the mobility edge ($k\ell = 1$), an approximate expression for D is $D(z, 0) \simeq D(0, 0)/(1 + \tilde{z}/z_c)$. Just like in the case of strong disorder, this approximation for D is inspired by the solution for the semi-infinite medium and deviates from the numerical solution in the central part of the slab only. $D(0, 0)$ and z_c depend on the exact value of z_0 in the boundary conditions. For the simplified boundary conditions discussed above (Dirichlet), one has $D(0, 0) = D_B$ and $z_c \simeq 3\ell$ [46]. We then obtain

$$T(\mathbf{q}_\perp) = \frac{\ell + z_c}{q_\perp z_c (2z_c + L)} \frac{\eta_1(q_\perp)}{\eta_2(q_\perp)\eta_3(q_\perp)}, \quad (4.11)$$

where

$$\begin{aligned} \eta_1(q_\perp) &= I_1(q_\perp z_c) K_1[q_\perp(\ell + z_c)] - K_1(q_\perp z_c) I_1[q_\perp(\ell + z_c)], \\ \eta_2(q_\perp) &= I_1(q_\perp z_c) K_0[q_\perp(z_c + L/2)] + K_1(q_\perp z_c) I_0[q_\perp(z_c + L/2)] \text{ and} \\ \eta_3(q_\perp) &= I_1(q_\perp z_c) K_1[q_\perp(z_c + L/2)] - K_1(q_\perp z_c) I_1[q_\perp(z_c + L/2)]. \end{aligned}$$

Here I_j and K_j ($j = 1, 2$) denote the modified Bessel functions of the first and second kind, respectively. In the large thickness limit $L \gg \ell, z_c$, the corresponding value of σ^2 is

$$\sigma_{\text{ME}}^2 = \frac{3L^2}{8}. \quad (4.12)$$

At the mobility edge, the mean-square size has therefore the same thickness dependence as in the diffusive regime, which was not expected *a priori*. The smaller prefactor 3/8 is important because it indicates that the transverse confinement is stronger than for $k\ell \gg 1$.

4.2.2.4 Comparison to numerical solution and discussion

We summarize the analytical results (4.8), (4.10) and (4.12) in Table 4.1. Because these results are derived using approximate ansatz for $D(z, 0)$, a comparison with exact numerical solutions is required to justify their validity. To this end, we solved the self-consistent equations of localization (4.3) numerically, without any *a priori* model for the diffusion coefficient. The resulting mean-square widths σ^2 are shown as functions of slab thickness L in Fig. 4.3 (symbols) in the three regimes of wave

$k\ell$	$D(z, 0)$	σ^2
$k\ell \gg 1$ (diffusion)	$D_B \left[1 - \frac{1}{(k\ell)^2} \right]$	$\frac{2}{3}L^2 - \mathcal{O}(\ell^2)$
$k\ell = 1$ (mobility edge)	$\frac{D_B}{1 + \tilde{z}/z_c}$	$\frac{3}{8}L^2 + \mathcal{O}(Lz_c)$
$k\ell < 1$ (localization)	$D_B e^{-2\tilde{z}/\xi}$	$2L\xi + \mathcal{O}(\xi^2)$

Table 4.1: Summary of analytical results for the position-dependent diffusion coefficient $D(z, 0)$ and its associated mean-square width σ^2 of the position-resolved transmission coefficient $T(\boldsymbol{\rho})$ describing transmission of a tightly focused monochromatic beam through a disordered slab of thickness $L \gg \ell$. ℓ is the mean free path, k is the wave number, $z_c \simeq 3\ell$, ξ is the localization length, and $\tilde{z} = \min(z, L - z)$. We assume $z_c \ll L$ for $k\ell = 1$ and $\ell \ll \xi \ll L$ for $k\ell < 1$.

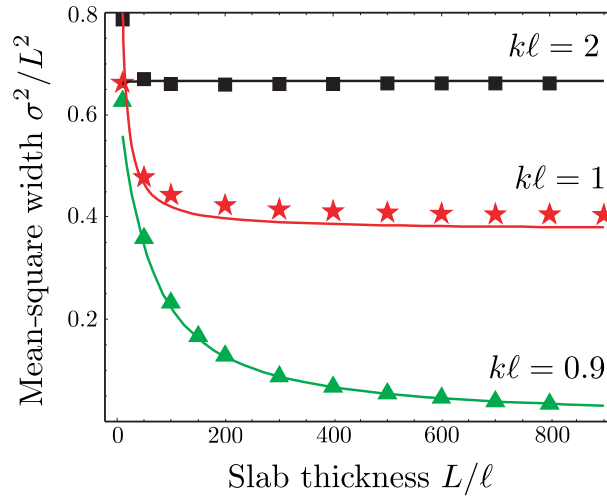


Figure 4.3: Comparison of approximate analytical (lines) and exact numerical (symbols) results for the mean-square width σ^2 of the spatially resolved stationary transmission coefficient $T(\boldsymbol{\rho})$ of a slab.

propagation. The agreement between analytical (solid lines) and numerical results is satisfactory, confirming the validity of our analytical analysis.

An important comment is in order. It is remarkable that in the diffusive regime ($kl \gg 1$), $\sigma^2 = 2L^2/3$ does *not* depend on D and even a very small, but finite and spatially uniform diffusion coefficient would lead to the same result for σ^2 as a large D . This emphasizes the importance of the position dependence of $D(z, 0)$ in the localized regime $kl < 1$ and at the mobility edge $kl = 1$. Note that this is the first time that the position dependence of D is absolutely *vital* to obtain a result that is different from the universal diffusive outcome. Scale-dependent but spatially uniform diffusion coefficients $D \propto 1/L$ and $D \propto \exp(-L/\xi)$ put forward by the scaling theory explain the scaling of the total transmission coefficient at the mobility edge and in the localized regime (see Chapter 5). However, being uniform in space, these expressions for D result in exactly the same mean-square width of the transmitted beam as $D = D_B$: $\sigma^2 = 2L^2/3$. It is therefore the position dependence of D that accounts for the different expressions for σ^2 that we find in the three regimes of wave propagation.

4.2.3 Reflection

For the sake of completeness, we briefly discuss the spatially-resolved *reflection* coefficient

$$R(\boldsymbol{\rho}) = D(z=0) \left. \frac{\partial C(\boldsymbol{\rho}, z, z' = \ell, \Omega = 0)}{\partial z} \right|_{z=0}. \quad (4.13)$$

The mean-square width of the reflection profile can be calculated similarly to that of the transmission, *i.e.* from Eq. (4.6) with $R(\mathbf{q}_\perp)$ replacing $T(\mathbf{q}_\perp)$. In the diffusive regime $kl \gg 1$, we obtain

$$R(\mathbf{q}_\perp) = \frac{\sinh[q_\perp(L - \ell)]}{\sinh(q_\perp L)}, \quad (4.14)$$

whereas in the localized regime

$$R(\mathbf{q}_\perp) = \exp(\ell/\xi) \frac{\sinh[(L - \ell)\chi(q_\perp)] - \cosh[\ell\chi(q_\perp)] + \xi\chi(q_\perp) \cosh[(L - \ell)\chi(q_\perp)]}{-1 + \cosh[\ell\chi(q_\perp)] + \xi\chi(q_\perp) \sinh[L\chi(q_\perp)]}, \quad (4.15)$$

where $\chi(q_\perp) = \sqrt{1/\xi^2 + q_\perp^2}$. We do not give here $R(\mathbf{q}_\perp)$ at the mobility edge because it is very cumbersome and does not bring any supplementary information. Results for the mean-square width σ of the reflection profile in the limit of thick slabs are summarized in Table 4.2. It is worthwhile to note that in the limit of $L \rightarrow \infty$ (semi-infinite medium), σ remains finite only in the localized regime.

4.2.4 Role of absorption

Absorption was a serious obstacle for unambiguous interpretation of a number of experiments on Anderson localization (see the discussion in Sec. 2.3.1). It is therefore important to study its role in the context of transverse confinement of waves

$k\ell$	σ^2
$k\ell \gg 1$ (diffusion)	$\frac{4L\ell}{3} - \mathcal{O}(\ell^2)$
$k\ell = 1$ (mobility edge)	$2\ell(\ell + 2z_c) \ln(L/\ell) + \mathcal{O}(z_c^2)$
$k\ell < 1$ (localization)	$2\xi\ell + \mathcal{O}(L\ell e^{-L/\xi})$

Table 4.2: Summary of analytical results for the mean-square width σ^2 of the position-resolved reflection coefficient $R(\boldsymbol{\rho})$ describing reflection of a tightly focused monochromatic beam from a disordered slab of thickness $L \gg \ell$. We assume $z_c \ll L$ for $k\ell = 1$ and $\ell \ll \xi \ll L$ for $k\ell < 1$.

in three dimensions. In the diffusive regime, it can be readily estimated by simply replacing q_\perp by $\sqrt{q_\perp^2 + 1/L_a^2}$ in Eqs. (4.7) and (4.14). L_a is the macroscopic absorption length, defined in the introduction of the thesis. Taking absorption into account leads to the following expressions for the position-resolved transmission and reflection coefficients in the diffusive regime ($k\ell \gg 1$):

$$\sigma^2 = 2L_a \left[L \coth\left(\frac{L}{L_a}\right) - \ell \coth\left(\frac{\ell}{L_a}\right) \right] \quad (4.16)$$

for transmission and

$$\sigma^2 = 2L_a \left[L \coth\left(\frac{L}{L_a}\right) - (L - \ell) \coth\left(\frac{L - \ell}{L_a}\right) \right] \quad (4.17)$$

for reflection. These equations can be simplified in the limits of weak ($L_a \gg L$) and strong ($L_a \ll L$) absorption. The mean-square width is shown in Table 4.3 at the leading order in L/L_a (for $L_a \gg L$) or L_a/L (for $L_a \ll L$). If L_a much exceeds the sample thickness L , σ^2 only acquires small corrections (Table 4.3). However, in the opposite case of $L_a \ll L$ we obtain $\sigma^2 \simeq 2LL_a$ in transmission and $\sigma^2 \simeq 2\ell L_a$ in reflection, *i.e.* absorption plays *exactly* the same role as localization and the resulting equations for σ^2 coincide with those obtained in the localized regime, with ξ replaced by L_a . This indicates that a study of stationary transverse confinement does not allow to distinguish localization from absorption.

4.3 Transverse confinement with short pulses

A way to overcome complications due to absorption was suggested by recent works [57, 32, 48, 47]. The idea is to study the *dynamics* of wave propagation rather than

σ^2	Transmission	Reflection
$L_a \gg L$	$\frac{2L^2}{3} - \frac{2L^2}{45} \left(\frac{L}{L_a}\right)^2$	$\frac{4L\ell}{3} - \frac{8L\ell}{45} \left(\frac{L}{L_a}\right)^2$
$L_a \ll L$	$2LL_a$	$2\ell L_a$

Table 4.3: σ^2 for transmission and reflection coefficients in the diffusive regime, taking into account absorption, in the limits of $L_a \gg L$ and $L_a \ll L$, respectively, at the leading order in L/L_a or L_a/L .

the stationary transport. We adopt this idea here too and replace the continuous incident beam in the experiment depicted in Fig. 4.2 by a short pulse. As a consequence, the width σ^2 of the transmission profile now acquires a time dependence. In this section, the slab thickness L is fixed and we study σ as a function of time.

4.3.1 Width of dynamic transmission profile

To describe time-dependent transmission of a short pulse through a disordered slab, we need a solution of Eqs. (4.3) for $\Omega \neq 0$. $\sigma(t)$ is then defined as

$$\sigma^2(t) = \frac{\int d^2\boldsymbol{\rho} \rho^2 T(\boldsymbol{\rho}, t)}{\int d^2\boldsymbol{\rho} T(\boldsymbol{\rho}, t)}. \quad (4.18)$$

By introducing $T(\mathbf{q}_\perp, \Omega)$ as the Fourier transform of $T(\boldsymbol{\rho}, t)$ with respect to time and position, Eq. (4.18) can be rewritten as

$$\sigma^2(t) = -\frac{\int_{-\infty}^{\infty} d\Omega e^{-i\Omega t} \frac{1}{q_\perp} \frac{\partial}{\partial q_\perp} \left[q_\perp \frac{\partial T(\mathbf{q}_\perp, \Omega)}{\partial q_\perp} \right] \Big|_{q_\perp=0}}{\int_{-\infty}^{\infty} d\Omega e^{-i\Omega t} T(\mathbf{q}_\perp, \Omega) \Big|_{q_\perp=0}}. \quad (4.19)$$

As compared to the stationary case $\Omega = 0$, the analysis is now considerably more involved because no simple analytic approximation exists for $D(z, \Omega)$ at arbitrary $\Omega \neq 0$.

4.3.2 Results and discussion

One way to compute σ^2 is to solve the self-consistent equations of localization (4.3) numerically. The results are presented in the main plot of Fig. 4.4 under the form of time dependencies of $\sigma^2(t)$, in the three regimes of propagation and for a fixed slab thickness L . $k\ell \gg 1$ corresponds to diffusion (continuous black curve) and $k\ell = 1$ to the mobility edge (red curve). In the localized regime we choose L/ξ rather than

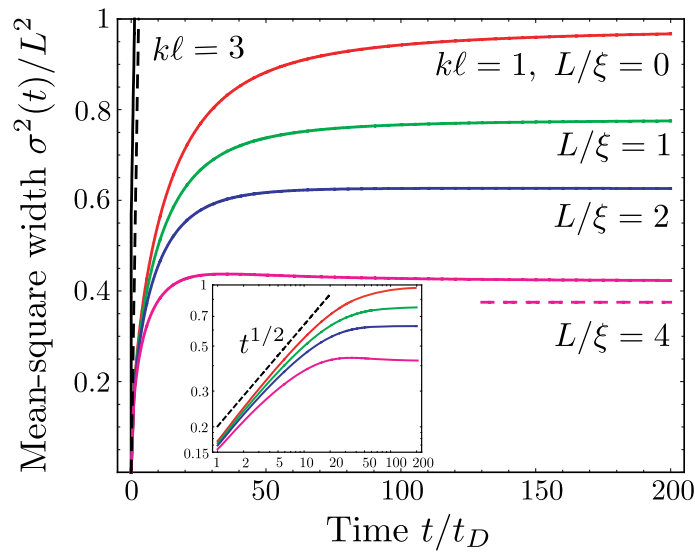


Figure 4.4: Numerically calculated mean-square width $\sigma^2(t)$ of the time-dependent transmission coefficient $T(\boldsymbol{\rho}, t)$ of a disordered slab in the diffusive regime ($k\ell = 3$), at the mobility edge ($k\ell = 1$), and in the localized regime ($L/\xi = 1, 2, 4$). The dashed lines show $\sigma^2(t) = 4D_B[1 - (k\ell)^{-2}]t$ for $k\ell = 3$ and $\sigma_\infty^2 = 2L\xi(1 - \xi/L)$ for $L/\xi = 4$. The thickness of the slab is $L = 100\ell$. Time is given in units of $t_D = L^2/(\pi^2 D_B)$. The inset shows the same results in the log-log scale, the dashed line is $\sigma^2(t) \propto t^{1/2}$.

$k\ell$ as a parameter measuring the strength of disorder (continuous green, blue and pink curves)². The time dependence of $\sigma^2(t)$ is analyzed below.

4.3.2.1 Long-time behavior

First, in the diffusive regime $k\ell > 1$ one readily obtains $\sigma^2(t) \simeq 4Dt$, where $D \simeq D_B[1 - (k\ell)^{-2}]$ (this is the only regime where an analytical result can be found for σ). For $k\ell = 3$ this result is shown in Fig. 4.4 by a dashed line which is indeed very close to the result of the numerical calculation (solid black line). The difference between diffusive and localized regimes at long times is manifest in Fig. 4.4. The rise of $\sigma^2(t)$ with time is unbounded for $k\ell > 1$, whereas $\sigma^2(t)$ saturates at a finite value σ_∞^2 for $k\ell < 1$ (solid green, blue and pink curves). The latter result can be understood from the following approximate calculation which, however, turns out to be quite adequate. Instead of using the self-consistent equation for $D(\mathbf{r}, \Omega)$, let us simply set $D(z, \Omega) = -i\Omega\xi^2$, which is the solution of self-consistent model in the infinite medium in the limit $\Omega \rightarrow 0$ (see Eq. (2.23)). A straightforward calculation then yields $\sigma_\infty^2 = 2L\xi(1 - \xi/L)$ up to the first order in $\xi/L \ll 1$. This equation, shown by a dashed horizontal line in Fig. 4.4, falls fairly close to the numerical result

²There is no preference here between the parameters L/ξ and $k\ell$ because L is fixed and ξ is directly related to $k\ell$ through the relation $\xi \simeq 3\ell/[2(1 - k\ell)]$.

at $L/\xi = 4$, allowing us to conjecture that it might be a good estimate of σ_∞^2 in the limit of $L \gg \xi$.

Our calculation suggests that the saturation of $\sigma^2(t)$ at a constant level takes place not only in the localized regime, but also at the mobility edge (solid red curve). We find the asymptotic value of $\sigma(t)$ to be $\sigma_\infty \approx L$ (see Fig. 4.4).

4.3.2.2 Short-time behavior

To study the time dependence of $\sigma^2(t)$ at the mobility edge and in the localized regime at moderate times, we replot the curves of the main plot, except the one corresponding to $k\ell = 3$, in the inset of Fig. 4.4 in a log-log scale. We clearly see that the initial growth of $\sigma^2(t)$ with t is power-law: $\sigma^2(t) \propto t^\alpha$ with $\alpha \simeq 0.5$. It is remarkable that this power-law growth is observed not only in the localized regime but at the mobility edge $k\ell = 1$ as well. To understand the power exponent $\alpha \simeq 0.5$, let us consider a point source of waves located inside a random medium of size $L \gg \ell$, very far from its boundaries. Neglecting the position dependence of D , we obtain the return probability by Fourier transforming Eq. (2.17a):

$$C(\mathbf{r}, \mathbf{r}, \Omega) = \frac{1}{2\pi^2} \int_{q_{\min}}^{q_{\max}} \frac{dq q^2}{-i\Omega + D(\Omega)q^2}, \quad (4.20)$$

where $q_{\min} \sim 1/L$ accounts for the finite size of the medium and $q_{\max} \sim 1/\ell$ ensures convergence of the integral. Inserting this expression into Eq. (2.17) and solving for $D(\Omega)$ at $k\ell = 1$, we find $D(\Omega) \propto (-i\Omega)^{1/3}$ for $\Omega \gg D_B/L^2$ and $D(\Omega) \propto (-i\Omega)^{1/2}$ for $\Omega \ll D_B/L^2$. The typical mean-square radius $\langle \mathbf{r}^2 \rangle$ of the profile of intensity due to a point source in three dimensions is then $\langle \mathbf{r}^2 \rangle \propto t^{2/3}$ for $t \ll L^2/D_B$ and $\langle \mathbf{r}^2 \rangle \propto t^{1/2}$ for $t \gg L^2/D_B$. If we now assume that $\langle \mathbf{r}^2 \rangle$ and $\sigma^2(t) = \langle \boldsymbol{\rho}^2 \rangle$ in transmission through a slab behave in a similar way, we obtain a qualitative explanation for the power-law scaling $\sigma^2(t) \propto t^{1/2}$ that we observe in Fig. 4.4 at $t > t_D$. However, this simple argument does not explain saturation of $\sigma^2(t)$ at a constant level at larger times.

Another interesting and unexpected feature of $\sigma^2(t)$ that we find sufficiently deep in the localized regime is its nonmonotonicity with time: the curve corresponding to $L/\xi = 4$ in Fig. 4.4 has a weakly pronounced but clearly visible maximum at $t/t_D \simeq 30$. Even though this nonmonotonicity is predicted by the self-consistent theory (we checked that the maximum is present at least for $L/\ell = 50$ –200 and $L/\xi = 3$ –6), it remains to be seen whether it is an artifact of the model or a real physical phenomenon.

4.3.2.3 Absorption

It is worthwhile to stress that the time-dependent $\sigma^2(t)$ is not sensitive to absorption. Indeed, absorption would show up through the same exponential factor $\exp(-t/t_a)$, with t_a the absorption time, in the numerator and the denominator of Eq. (4.18). This factor would then cancel out. Therefore, all curves of Fig. 4.4 remain exactly

the same in an absorbing medium. This provides a solution to the long-standing issue of distinguishing localization from absorption [28, 30, 29, 31], as was recently demonstrated in the experiment discussed in Sec. 2.3.2.2.

4.4 Conclusion

In conclusion, we showed that the transverse confinement of waves in three-dimensional disordered media can be very useful for demonstrating Anderson localization and for measuring the localization length in an experiment. The dependence of the mean-square width σ^2 of a tightly focused beam transmitted through a slab of random medium on the slab thickness L and on time (in a pulsed experiment) is qualitatively different in the diffusive and in the localized regimes of wave propagation. This qualitative difference is due to the position dependence of the diffusion coefficient induced by interferences.

We first considered a continuous monochromatic beam focused to a point at the surface of a disordered slab and showed that the mean-square width σ^2 of the spatially-resolved transmission coefficient $T(\boldsymbol{\rho})$ scales as $L\xi$ in the localized regime, when $\xi \ll L$, in contrast to the relation $\sigma^2 \propto L^2$ in the diffusive regime and at the mobility edge. This result suggests that a measurement of σ^2 gives direct access to the localization length ξ . However, absorption appears to produce the same effect on σ^2 as localization, *i.e.* in the diffusive regime we find $\sigma^2 \propto LL_a$, if the macroscopic absorption length L_a is much smaller than L .

In the second part of the chapter, we replaced the continuous beam by a short pulse. In the localized regime, the mean-square width $\sigma^2(t)$ of the time-dependent, spatially resolved transmission coefficient $T(\boldsymbol{\rho}, t)$ first grows roughly as $t^{1/2}$ and then converges to a constant value $\sigma_\infty^2 \propto L\xi$, in sharp contrast to the relation $\sigma^2(t) \propto Dt$ valid in the diffusive regime. Again, the localization length ξ can be extracted directly from $\sigma^2(t)$, but contrary to the stationary case, $\sigma^2(t)$ does not depend on absorption. This allows one to avoid the risk of confusing localization and absorption. Finally, exactly at the mobility edge, $\sigma^2(t)$ initially grows as $t^{1/2}$ as in the localized regime, until it saturates at $\sigma_\infty^2 \approx L^2$ in the long-time limit.

Self-consistent versus scaling theory

Contents

5.1	The scaling theory of localization	60
5.1.1	Scaling function	60
5.1.2	Regimes of disorder and dimensionality	61
5.1.3	Critical exponent	62
5.2	Stationary transport properties of a slab	63
5.2.1	Total transmission	63
5.2.2	Comparison with the scaling theory	65
5.3	Scaling function and the self-consistent theory	65
5.3.1	Scaling function	65
5.3.2	Critical exponent	66
5.4	Conclusion	68

ONE of the first theories of Anderson localization is the phenomenological scaling theory discussed in Sec. 2.4.1. Its success mainly relies on the fact that it allows deriving many quantitative properties of Anderson localization from very simple arguments. Besides, the scaling theory provides a very elegant description of Anderson transition through a universal scaling function $\beta(g)$ depending only on the dimensionless conductance g and not on the microscopic properties of the disordered system¹.

¹For brevity, in this chapter we call g “conductance” instead of “dimensionless conductance”, thereby assuming $e^2/h = 1$.

In the previous chapters we provided a formulation of the microscopic self-consistent theory of localization adapted to finite open media. This theory features a position-dependent diffusion coefficient. Interestingly, it is possible to derive the results of the scaling theory from the self-consistent theory. This was done in 1982 by D. Vollhardt and P. Wölfle [58]. In this work, however, the size of the system was introduced “by hand” as a lower cutoff $\sim 1/L$ in the integral over momentum in Eq. (2.17b). One can then wonder whether the scaling theory also follows from the generalized form of self-consistent theory with a position dependent diffusion coefficient. Answering this question is the subject of the present chapter. For this purpose, we first remind the main features of the scaling theory as originally introduced by E. Abrahams, P. W. Anderson, D. C. Licciardello and T. V. Ramakrishnan in 1979 [38]. We then apply the generalized microscopic self-consistent theory of localization to characterize stationary transport of waves in a disordered medium with three-dimensional disorder, compare our results to those of the scaling theory, and finally show how the universal scaling function $\beta(g)$ emerges from the microscopic approach.

5.1 The scaling theory of localization

5.1.1 Scaling function

The scaling theory of localization is inspired by the theory of phase transitions and by renormalization group techniques. The idea is to look at a small volume of size L of a larger disordered system. One then makes the assumption that the transport properties of this small volume only depend on its conductance g (Sec. 2.7). Notice that this hypothesis is strong since *a priori* there exist at least two parameters relevant for transport: the energy E and the size L of the medium. From this assumption, the description of the system at larger length scales can be obtained by introducing a dimensionless scaling parameter b and writing:

$$g(L + bL) = f_b[g(L)], \quad (5.1)$$

where f_b is some function depending on b . We then have:

$$\frac{g(L + bL) - g(L)}{bL} = \frac{f_b[g(L)] - g(L)}{bL}. \quad (5.2)$$

We now take the continuous limit $b \rightarrow 0$, which leads to the Gell-Mann and Low equation

$$\frac{d \ln g}{d \ln L} = \beta(g), \quad (5.3)$$

where we have introduced $\beta(g) = \lim_{b \rightarrow 0} [f_b(g) - g]/(bg)$. The scaling theory is a one-parameter theory. The function $\beta(g)$ and the transport properties of the medium only depend on the conductance and not on the microscopic details of disorder.

5.1.2 Regimes of disorder and dimensionality

Far in the extended regime, *i.e.* for $g \gg g_c \sim 1$ according to Thouless criterion (see Sec. 2.7), the conductance is given by Eq. (2.6). On the opposite side of the transition, far in the localized regime, $g \ll g_c$ and the transport is inhibited. The conductance is expected to decrease exponentially with the sample size:

$$g \sim \exp(-L/\xi), \quad (5.4)$$

where ξ is the localization length. From these results and Eq. (5.3) one obtains the limits of the function $\beta(g)$ in any dimension d :

$$\beta(g) = \begin{cases} d - 2, & g \gg g_c \\ \log g + \text{const}, & g \ll g_c. \end{cases} \quad (5.5)$$

Assuming a continuous and monotonic behavior for $\beta(g)$ then allows to sketch it for any g in dimensions $d = 1, 2, 3$ (see Fig. 5.1). The curves of $\beta(g)$ suggest that all

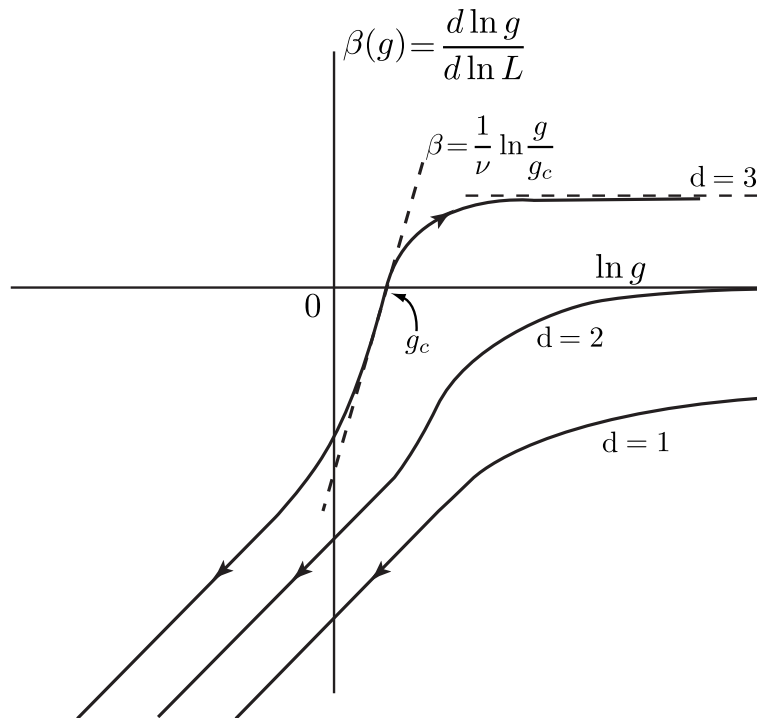


Figure 5.1: Sketch of the scaling function $\beta(g)$ as a function of $\ln g$, where g is the conductance, in dimensions $d = 1, 2$ and 3 . At large values of conductance, the scaling function approaches $\beta(g) = d - 2$, whereas for very small values of conductance, $\beta(g) \rightarrow \ln g + \text{const}$. The arrows denote the direction towards the regime of transport (extended or localized) when the system size increases.

states are localized for $d \leq 2$ (because $\beta(g) < 0$, and thus increasing the system size

always leads to an exponentially small conductance), while a critical point g_c exists for $d = 3$, separating extended ($g > g_c$) from localized ($g < g_c$) states, as already discussed in Sec. 2.1.2.1. g_c is an unstable fixed point since above it the conductance increases with the system size whereas below g decreases with the system size (this is indicated by arrows in Fig. 5.1). This point is also characterized by a scaling invariance due to the fact that g_c is independent of the system size: $\beta(g_c) = 0$.

Note that varying L is not the only way to move along curves $\beta(g)$. One can also change the energy E . For electrons, this energy corresponds to the Fermi energy and for classical waves to the frequency. Whereas the critical point is, in principle, reached by making L tend to the microscopic scale (which is not very interesting since Anderson localization effects do not make sense at the scale of the mean free path), it also corresponds to the critical energy E_c for which the Ioffe-Regel criterion is satisfied.

5.1.3 Critical exponent

In this section, we focus on the case $d = 3$. As we have seen above, in three dimensions there is a phase transition separating the localized regime from the extended one. In the vicinity of this transition, one can use a linear approximation

$$\beta(g) = \frac{1}{\nu} \ln \frac{g}{g_c}. \quad (5.6)$$

This approximation is depicted in Fig. 5.1 by the dotted tangent of slope $1/\nu$ at the point $g = g_c$. Inserting Eq. (5.6) into Eq. (5.3) we obtain a differential equation that can be readily integrated, yielding

$$\ln \frac{g(L)}{g_c(L)} - \ln \frac{g_c(\ell)}{g_c(L)} = \frac{1}{\nu} (\ln L - \ln \ell), \quad (5.7)$$

where we have explicitly indicated the size dependence of the conductance. From Eq. (5.7), the conductance in the vicinity of the critical point reads

$$g(L) = g_c(L) \exp \left(\frac{L}{L_c} \right)^{1/\nu}, \quad (5.8)$$

where $L_c = \ell \delta_g^{-\nu}$ with $\delta_g = \ln[g_c(\ell)/g_c(L)]$. As discussed above, at the critical point there exists a scaling invariance, such that $g_c(L)$ does not depend on L . Therefore, $g_c(L) = g_c(\ell)$ and $g_c(\ell)$ and $g_c(L)$ are both given by the ballistic value of the conductance, at energies E and E_c , respectively: $g_c(\ell) \propto E$ and $g_c(L) \propto E_c$. Since we consider conductance around the critical point, $g_c(\ell) \simeq g_c(L)$ and $\delta_g \simeq [g_c(\ell) - g_c(L)]/g_c(L) \propto (E - E_c)$. We can therefore obtain an expression for the localization length ξ just below the critical point (*i.e.* for $E < E_c$) by identifying Eq. (5.8) in the limit $L_c \gg L$ with the result (5.4) obtained far in the localized regime. This procedure leads to

$$\xi \propto |E - E_c|^{-\nu}. \quad (5.9)$$

The same procedure can be applied just above the critical point (*i.e.* for $E > E_c$) to calculate the diffusion coefficient D . The latter is obtained from the conductance through $D \propto g/L$. By identifying $D \propto g/L$ with the critical value g_c/L_c , we obtain:

$$D \propto (E - E_c)^\nu. \quad (5.10)$$

The divergence of the localization length at the transition allows us to identify ν as the (only) critical exponent of the scaling theory of localization. The role of the critical exponent is illustrated in Fig. 5.2. Calculation of ν has occupied a certain

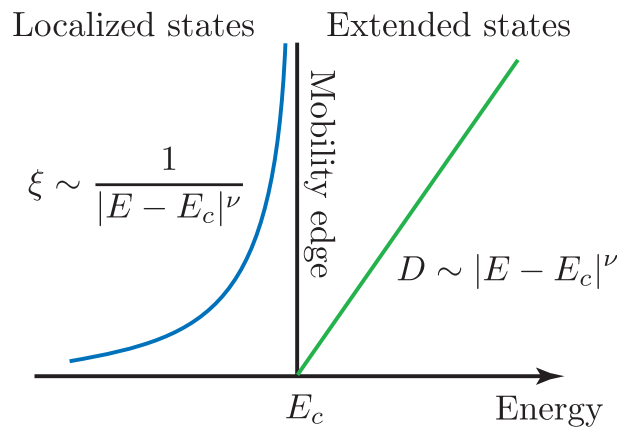


Figure 5.2: Behavior of the localization length ξ and of the diffusion coefficient D , as a function of energy E , around the mobility edge $E = E_c$.

number of theoreticians for the last twenty years. Whereas the ϵ -expansion [59] or the self-consistent theory [39] predict, on their side, $\nu = 1$ (see Sec. 2.4.2.3), the solution of the Anderson tight-binding model leads to $\nu \simeq 1.5$ [60].

5.2 Stationary transport properties of a slab

5.2.1 Total transmission

Let us now confront the main results of the scaling theory to those provided by the self-consistent theory with position-dependent diffusion coefficient developed in Chapter 3. For this purpose, we first consider — as in Sec. 4.2 — the transmission of a continuous plane wave through of a slab confined between the planes $z = 0$ and $z = L$. We wish to calculate the transmission coefficient T of the slab, given by

$$T = -D(z = L, \Omega = 0) \left. \frac{\partial C(\mathbf{q}_\perp = \mathbf{0}, z, z' = \ell, \Omega = 0)}{\partial z} \right|_{z=L}, \quad (5.11)$$

where notations are the same as in Sec. 4.1. From the study carried out in Chapter 4, the transmission coefficient T in the three regimes of propagation (diffusive, localized regimes and mobility edge) can be readily obtained by taking the limit $q_\perp \rightarrow 0$ in

$kl > 1$	$kl = 1$	$kl < 1$
$T \propto \ell/L$	$T \propto (\ell/L)^2$	$T \propto \exp(-L/\xi)$

Table 5.1: Summary of analytical results for the transmission coefficient T of a disordered slab of thickness $L \gg \ell$. We assume $\ell \ll \xi \ll L$ for $kl < 1$.

Eqs. (4.7), (4.9) and (4.11). The results are summarized in Table 5.1. As in Chapter 4, the results we derive for the transmission coefficient rely on the approximate expressions for the position-dependent diffusion coefficient (see Table 4.1). It is therefore important to compare them to those obtained from an exact numerical solution of the self-consistent equations (4.3). This comparison is shown in Fig. 5.3. The agreement between analytical and numerical results is good (at least for

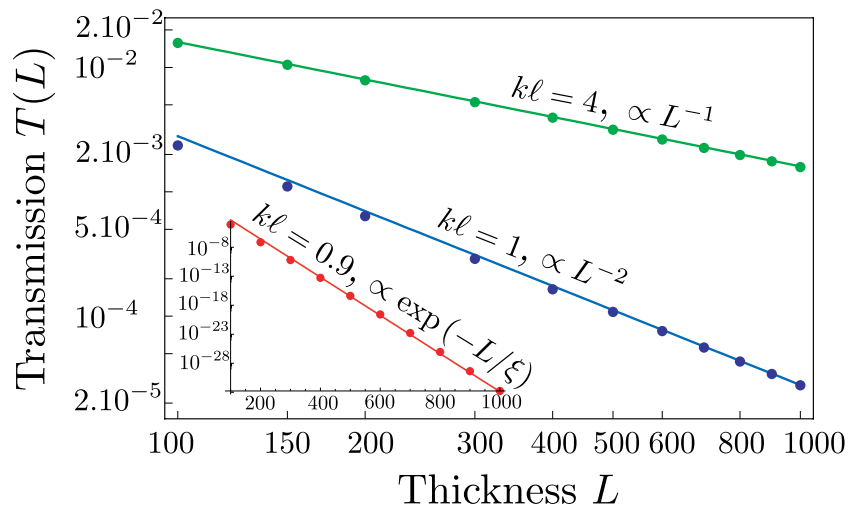


Figure 5.3: Thickness dependence of the transmission coefficient of a disordered slab, in the extended regime ($kl = 4 > 1$), in the localized regime ($kl = 0.9 < 1$) and at the mobility edge ($kl = 1$). In each case the analytical expression of T from Table 5.1 (solid line) is compared to the exact solution of the self-consistent equations (4.3) (symbols).

sufficiently large values of L).

The law $T \propto (\ell/L)^2$ at the mobility edge was recently questioned by S. K. Cheung and Z. Q. Zhang [61], who, instead, put forward a scaling law of the type $T \propto \ln(L)/L^2$, obtained by introducing several assumptions in the self-consistent theory, in order to get rid of the position dependence of the diffusion coefficient. Although Fig. 5.3 does not allow to distinguish between the two laws, we checked, by extending the numerical results presented in this section to values of L up to $\sim 9000\ell$, that the law $T \propto \ln(L)/L^2$ was not compatible with the numerical solution of the self-consistent equations [62].

5.2.2 Comparison with the scaling theory

In order to compare the results shown in Table 5.1 to those of the scaling theory one has to consider conductance. This is a bit problematic in our case because our slab is infinite in the xy plane. As a matter of fact, we are not exactly in the framework of the scaling theory because our slab is not a finite-size sample. However, in the first approximation, a conductance-like quantity can be obtained by simply multiplying the transmission coefficient T by L^2 (this amounts to replace the slab by a cube of side L). With this trick we find that results from Table 5.1 obtained by taking into account the position dependence of the diffusion coefficient are in full agreement with the scaling theory, namely $g \propto L$ in the extended regime, $g \propto \exp(-L/\xi)$ in the localized regime and $g = \text{const}$ at the mobility edge.

5.3 Scaling function and the self-consistent theory

In the previous section, we have calculated the stationary transport properties of a finite disordered medium from the self-consistent theory of localization and have shown the agreement with the predictions of the scaling theory for the conductance. However, the main statement of the scaling theory is the existence of the scaling function $\beta(g)$ depending only on the conductance. In 1982, D. Vollhardt and P. Wölfle [58] showed that this result could be derived from the self-consistent theory with *position independent* diffusion coefficient. In the present section, we extend this proof to the case of the generalized self-consistent theory with *position-dependent* diffusion coefficient.

5.3.1 Scaling function

The position dependence of the diffusion coefficient makes the analytical calculation of the scaling function $\beta(g)$ difficult. We therefore perform a numerical calculation. We make the same assumption $g \sim L^2 T$ as in Sec. 5.2. The prefactor (independent of L) is of no importance here because, if Eq. (5.3) is satisfied, it would simply shift the scaling function along the $\ln g$ axis (see Fig. 5.1).

The scaling theory assumes that all transport properties of the disordered system are governed by a single parameter, the conductance g . This statement is not *a priori* obvious in the framework of the self-consistent theory, since *two* parameters — the thickness L and the disorder strength $k\ell$ — should be specified to calculate g . If the scaling theory is correct however, any changes of L or $k\ell$ should lead to the motion of the point $(\beta(g), g)$ along the same single curve as in Fig. 5.1. The scaling function $\beta(g)$ following from our calculations is shown in Fig. 5.4. It has been obtained by varying L and $k\ell$ independently, thereby confirming the one-parameter hypothesis of the scaling theory. Note, in particular, the agreement with the limit cases given by Eq. (5.5). In calculating $\beta(g)$, we have considered several values of $k\ell$, and for

each of them, varied L in a certain interval, as indicated in Fig. 5.4.

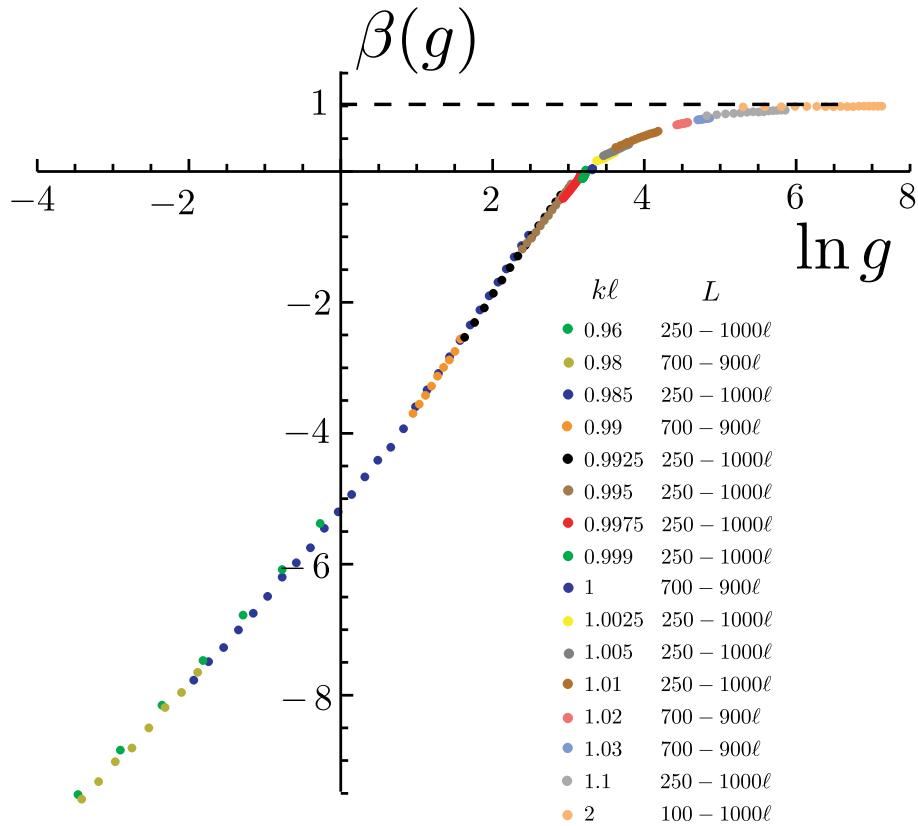


Figure 5.4: Scaling function $\beta(g) = d \ln g / d \ln L$ as a function of the logarithm of conductance g , obtained by solving the self-consistent equations (4.3) numerically. The curve has been obtained by taking different values of $k\ell$ and, for each of them, by varying L in a certain interval, as indicated in the figure.

5.3.2 Critical exponent

It is interesting to calculate of the critical exponent ν in the framework of the self-consistent theory with position-dependent diffusion coefficient. The critical exponent can be obtained in a simple way by evaluating the slope of tangent to the curve $\beta(g)$ around the mobility edge. The main difficulty is that in this region, finite-size effects become important. These effects originate from the fact that the closer one approaches the critical point, the larger the system size has to be to obtain relevant results [63]. Finite-size effects are shown in the left plot of Fig. 5.5, obtained by varying the thickness L for fixed values of $k\ell$, in the same way as in Fig. 5.4. These results are of course not satisfactory when one is interested in fine effects such as the critical exponent of the transition. A way to circumvent this problem consists in fixing $L \gg \ell$ instead of $k\ell$, and varying $k\ell$ in the vicinity of the critical point. This provides much better results, as shown in the right plot of Fig. 5.5, where we have

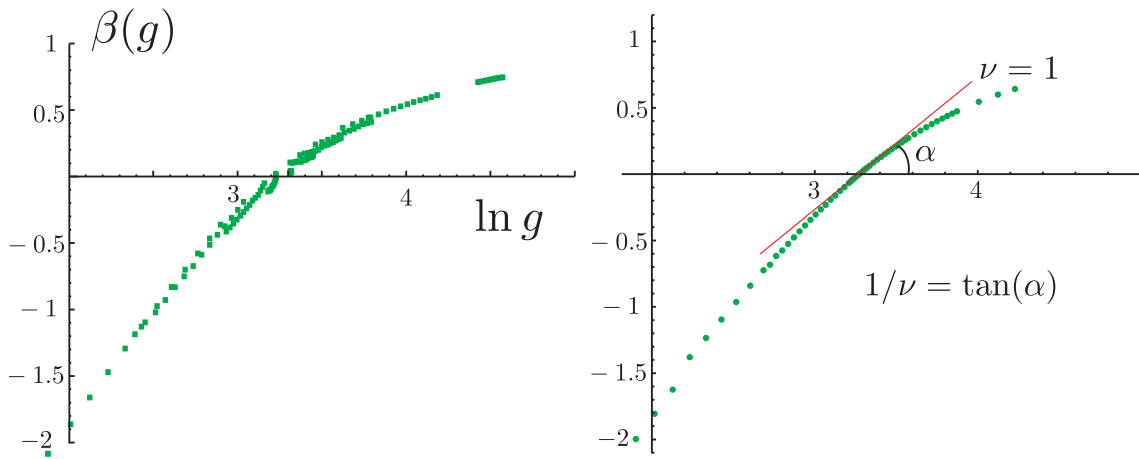


Figure 5.5: Scaling function $\beta(g) = d \ln g / d \ln L$ as a function of $\ln g$ obtained by solving the self-consistent equations of localization numerically in the vicinity of the critical point. Left: $\beta(g)$ obtained by varying L for fixed values of $k\ell$ (these are the same numerical points as in Fig. 5.4). The curve exhibits unwanted finite-size effects (note dispersion of points in the vicinity of $\beta(g) = 0$). Right: $\beta(g)$ obtained by varying $k\ell$ from 0.991 to 1.015 for fixed $L = 700\ell$. The inverse slope of the tangent at the critical point gives the critical exponent $\nu = 1$.

fixed $L = 700\ell$. From this plot, we extract the critical exponent $\nu = 1$. This value is the same as obtained earlier by D. Vollhardt and P. Wölfle from the self-consistent theory with position-independent diffusion coefficient, and it is different from the value $\nu \simeq 1.5$ following from the numerical solution of the Anderson tight-binding model. This discrepancy signals that the self-consistent theory describes only imperfectly the critical point. The reason to this issue may be found in the microscopic description of the transition. As a matter of fact, the diagrammatic series considered in Chapter 3 (sum of interference “loops”) is probably not precise enough to describe some features of the critical point, as the value of the critical exponent. Say differently, the self-consistent theory remains somehow a perturbative approach and is therefore limited when describing the fixed point, which can have properties completely different from the ones observed in the vicinity of $g = g_c$. Today, a part from recent work that put forward a strategy combining the self-consistent theory with a phenomenological momentum dependence of the diffusion coefficient at the critical point [64], a complete analytical description of the Anderson transition in three dimensions is still lacking.

To obtain the function $\beta(g)$ from the microscopic approach, we have used boundary conditions introduced in Sec. 3.4.2 with the extrapolation length $z_0 = 2/3\ell$, corresponding to the absence of internal reflections at boundaries of the disordered slab. In the presence of internal reflections with an intensity reflection coefficient r , the extrapolation length reads [53]

$$z_0 = \frac{2\ell}{3} \frac{1+r}{1-r}. \quad (5.12)$$

An interesting question is to know whether or not the value of the critical exponent depends on r . This can be checked easily by calculating the function $\beta(g)$ for different values of z_0 . We did so for three values of z_0 : $2/3$, 4.67 and 10 , corresponding to $r = 0$, $r = 0.75$ and $r = 0.875$, respectively. The results are shown in Fig. 5.6 and

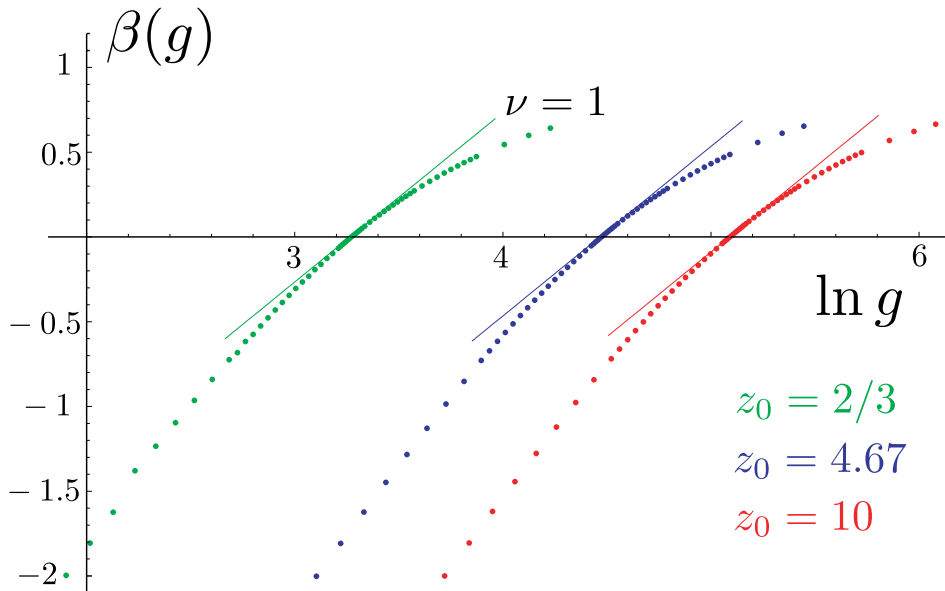


Figure 5.6: Scaling function $\beta(g) = d \ln g / d \ln L$ as a function $\ln g$, obtained by solving the self-consistent equations of localization numerically in the vicinity of the critical point, for three different values of the extrapolation length z_0 , which measures the importance of internal reflections at the boundaries of the disordered medium. These curves have been obtained by fixing $L = 700\ell$, and varying $k\ell$ from 0.991 to 1.015 . The critical exponent remains unchanged when changing z_0 .

prove that internal reflections have no effect on the value of the critical exponent which remains equal to 1 whatever r .

5.4 Conclusion

In this chapter we derived the main results of the scaling theory from the microscopic self-consistent theory of localization with position-dependent diffusion coefficient. In particular, we studied the one-parameter function $\beta(g)$. This allowed us to extract the value $\nu = 1$ for the critical exponent of the Anderson transition. By varying the amount of internal reflections at the boundaries of the disordered sample we demonstrated the independence of the critical exponent of this effect.

Part II

Dynamics of intensity speckle patterns

Intensity correlations in waveguides

Contents

6.1	Intensity correlation function	72
6.1.1	Description of intensity speckle patterns in terms of multiple scattering paths	72
6.1.2	Intensity correlation function	73
6.2	Intensity correlations in waveguides	73
6.2.1	Framework	73
6.2.2	Average intensity	75
6.2.3	Perturbative approach	76
6.2.4	The \mathcal{C}_2 correlation	78
6.2.5	The \mathcal{C}_3 correlation	79
6.2.6	Physical interpretation	79
6.3	Experimental measurement of intensity correlations in waveguides	80
6.3.1	Direct measurements	80
6.3.2	Polarization-resolved measurements	81
6.4	Conclusion	82

THE first part of this thesis concerned average transport properties of disordered media (transmission, conductance, etc). We are now interested in the fluctuations of transport properties. These fluctuations can be seen by eye when a disordered material is irradiated by a continuous beam and a snapshot of the intensity pattern

at some point behind the sample is taken. This pattern exhibits a complicated, highly irregular distribution of dark and bright spots and it is called the speckle pattern [65]. A typical optical speckle pattern is shown in Fig. 6.1.

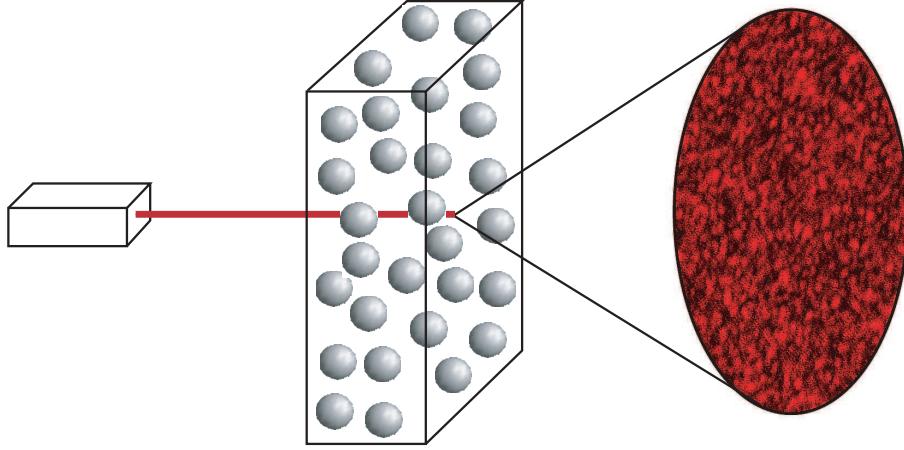


Figure 6.1: An optical speckle pattern (courtesy of W. Bührer).

At first sight, the speckle pattern looks completely random. This is however not true since it can be shown that intensities of even very distant points are weakly correlated. Speckle patterns are characterized by the statistical distribution of intensity fluctuations. Unfortunately, the evaluation of this quantity is often involved. In this chapter, we adopt a simpler approach, which consists in examining intensity correlations between different points. One has to keep in mind that, however, this strategy provides only a partial information about statistics of speckle patterns.

In the present chapter, we remind a few basic facts concerning intensity correlations in disordered media. There exist many reviews on this subject (see for instance those of R. Berkovits and S. Feng [66] and of M. C. W. van Rossum and Th. M. Nieuwenhuizen [17]). In this chapter, we study intensity correlations in a waveguide. Such a geometry has several advantages. First, its physics is simpler than that of three-dimensional samples. Second, from the theoretical point of view the treatment of intensity correlations — generally involved in three-dimensional media — simplifies in waveguides.

6.1 Intensity correlation function

6.1.1 Description of intensity speckle patterns in terms of multiple scattering paths

In order to better understand the origin of speckle patterns, it is instructive to take advantage of the path picture of wave propagation in random media. At time t and at a position \mathbf{r} , the field $\Psi(\mathbf{r}, t)$ is given by a superposition of partial waves $\Psi_i(\mathbf{r}, t)$

all reaching point \mathbf{r} at time t but following different multiple scattering paths i :

$$\Psi(\mathbf{r}, t) = \sum_i \Psi_i(\mathbf{r}, t). \quad (6.1)$$

The intensity at point \mathbf{r} averaged over disorder follows as

$$I(\mathbf{r}, t) = |\Psi(\mathbf{r}, t)|^2 = \sum_i |\Psi_i(\mathbf{r}, t)|^2 + \sum_{i \neq j} \Psi_i(\mathbf{r}, t) \Psi_j^*(\mathbf{r}, t). \quad (6.2)$$

The second sum in Eq. (6.2) contains interference effects between multiply scattered waves. Far in the extended regime, it vanishes when averaged over disorder. These interference effects are at the origin of speckle patterns. Due to them, the intensity is random and can be written as

$$I(\mathbf{r}, t) = \overline{I(\mathbf{r}, t)} + \delta I(\mathbf{r}, t), \quad (6.3)$$

where $\delta I(\mathbf{r}, t)$ is the fluctuating part of intensity. It is the intensity speckle pattern.

6.1.2 Intensity correlation function

In this chapter, we consider only continuous waves, such that the intensity and the speckle pattern do not depend on time (time dependent speckle patterns will be studied in Chapter 7). We thus drop all time dependences from here on. The frequency of all waves is fixed at some value ω_0 . To lighten the notation, we drop this frequency argument from here on.

In general, the statistical properties of the speckle δI can be described by the four-point intensity correlation function between two source points \mathbf{R} and \mathbf{R}' at the input surface of the waveguide and two detector points \mathbf{r} and \mathbf{r}' at the output surface. It is defined as

$$\mathcal{C}(\mathbf{r}, \mathbf{R}; \mathbf{r}', \mathbf{R}') = \frac{\overline{\delta I(\mathbf{r}, \mathbf{R}) \delta I(\mathbf{r}', \mathbf{R}')}}{\overline{I(\mathbf{r}, \mathbf{R})} \times \overline{I(\mathbf{r}', \mathbf{R}')}}, \quad (6.4)$$

where $\delta I(\mathbf{r}, \mathbf{R}) = I(\mathbf{r}, \mathbf{R}) - \overline{I(\mathbf{r}, \mathbf{R})}$. $I(\mathbf{r}, \mathbf{R})$ denotes the intensity measured at the point \mathbf{r} at the output surface of the waveguide and produced by a point-like continuous source located at the point \mathbf{R} at the input surface. Note that in writing the intensity correlation function, we have normalized by the average intensity; other definitions exist in literature.

6.2 Intensity correlations in waveguides

6.2.1 Framework

In the present chapter, we are interested in intensity correlations in a disordered waveguide. In the language of multiple scattering, this terminology refers to a tube-shaped disordered medium of length $L \gg \ell$ along its longitudinal direction z and

narrow along the two other transverse directions (see Fig. 6.2). More specifically, “narrow” here means that the diameter d of the tube obeys

$$\lambda \ll d \lesssim \ell. \quad (6.5)$$

Such a medium is said to be quasi one-dimensional, in the sense that wave propa-

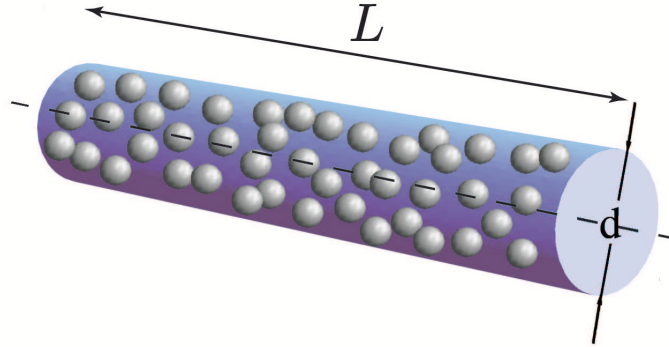


Figure 6.2: Sketch of a disordered waveguide of length $L \gg \ell$ and diameter $d \lesssim \ell$.

gation is three-dimensional since $d \gg \lambda$, but diffusion is one-dimensional along the z direction, since d does not exceed one mean free path. The effective behavior of waves depends on how L compares to the localization length $\xi \sim \ell(kd)^2$ and the mean free path. For short waveguides $L \lesssim \ell$, waves do not see the disorder and propagation is ballistic. For $\ell \ll L \ll \xi$, waves are scattered many times and propagate by diffusion because the localization length is too large for propagation to be affected by the effects of Anderson localization. Finally, for $L > \xi$, Anderson localization must be taken into account. In the following, we only consider the intermediate regime of transport $\ell \ll L \ll \xi$, thereby neglecting the effects of localization on propagation. The different regimes of propagation in a waveguide are summarized in Fig. 6.3.

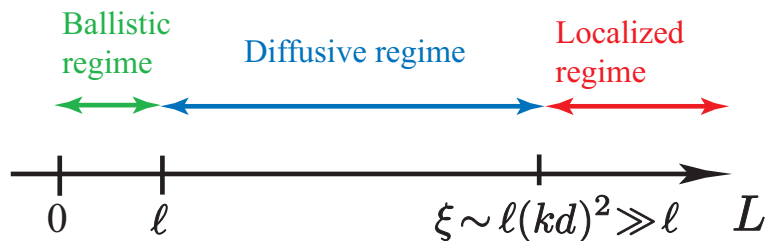


Figure 6.3: Regimes of propagation in a disordered waveguide, depending on the value of L as compared to the mean free path ℓ and the localization length ξ . In this chapter, we only consider the case $\ell \ll L \ll \xi$ where the localization length is large enough, such that waves propagate by diffusion.

At this stage, it is interesting to make the connection with the Thouless criterion discussed in Sec. 2.7. In a waveguide, the electronic dimensionless conductance reads

[16]

$$g = \frac{4N\ell}{3L} \sim \frac{\xi}{L}, \quad (6.6)$$

where $N = k^2 A / (4\pi)$ is the number of transverse modes of the waveguide. One sees that the condition $L \sim \xi$, for which the effects of Anderson localization are expected to take place, coincides with the condition $g \sim 1$, which is nothing but the Thouless criterion! From Eq. (6.6), it follows that the condition $L \ll \xi$ is equivalent to the large conductance limit $g \gg 1$.

6.2.2 Average intensity

We now consider the average intensity $\overline{I(\mathbf{r}, \mathbf{R})}$. Inside the waveguide, a vector \mathbf{r} can be decomposed into a transverse part $\boldsymbol{\rho}$ and a longitudinal part z : $\mathbf{r} = (\boldsymbol{\rho}, z)$. This decomposition is shown in Fig. 6.4. The average intensity is obtained from the

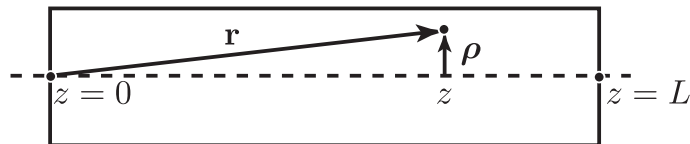


Figure 6.4: In the waveguide, a vector \mathbf{r} is decomposed into a transverse part $\boldsymbol{\rho}$ and a longitudinal part z .

intensity Green's function C_D introduced in Eq. (3.6).

$$\overline{I(\mathbf{r}, \mathbf{R})} = \overline{G(\mathbf{r}, \mathbf{R})G^*(\mathbf{r}, \mathbf{R})} = \frac{c}{4\pi} C_D(\mathbf{r}, \mathbf{R}). \quad (6.7)$$

Since we consider the diffusive propagation of waves ($L \ll \xi$), C_D is obtained by solving the diffusion equation (3.8) for the waveguide geometry. This calculation is straightforward and leads to [16]

$$C_D(\mathbf{r}, \mathbf{R}) = \frac{z_m(L - z_M)}{AD_B L}, \quad (6.8)$$

where A is the cross-section of the waveguide, $z_m = \min(z, z_R)$ and $z_M = \max(z, z_R)$, with z_R the longitudinal part of \mathbf{R} and z that of \mathbf{r} . In deriving Eq. (6.8), we have assumed Dirichlet boundary conditions for simplicity and therefore set the extrapolation length to zero. We can now calculate explicitly the average intensity by inserting Eq. (6.8) into Eq. (6.7). As a first approximation, we set $z_R \simeq \ell$ and $z \simeq L - \ell$, which yields

$$\overline{I(\mathbf{r}, \mathbf{R})} = \frac{3}{4\pi} \frac{\ell}{AL}. \quad (6.9)$$

Note that Eq. (6.9) is approximate because we have used simplified boundary conditions to derive it. From here on, we assume the same simplified boundary conditions for the calculation of the intensity correlation function.

6.2.3 Perturbative approach

In the previous section, we have calculated the average intensity appearing in the denominator of the intensity correlation function (6.4). The calculation of \mathcal{C} is more tricky because it involves an average of a product of two intensities. Each intensity is a sum of products of pairs of multiple scattering paths, starting at points \mathbf{R} and \mathbf{R}' and ending at points \mathbf{r} and \mathbf{r}' (see Fig. 6.5). The usual technique that we adopt

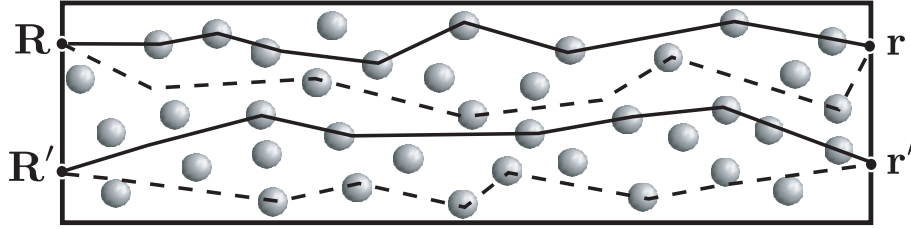


Figure 6.5: The intensity correlation function of a speckle pattern is built from the product of two intensities corresponding to paths starting at points \mathbf{R} and \mathbf{R}' and ending at points \mathbf{r} and \mathbf{r}' .

here consists in expanding \mathcal{C} in powers of $1/g \ll 1$. It was first suggested by S. Feng, C. Kane, P. A. Lee, and A. D. Stone in 1988 [67]. This perturbative approach is only possible in the extended regime where $1/g$ is small, and gives rise to three main contributions \mathcal{C}_1 , \mathcal{C}_2 and \mathcal{C}_3 to \mathcal{C} that we describe below. We detail the calculation of \mathcal{C}_1 and go faster on those of \mathcal{C}_2 and \mathcal{C}_3 which rely on the same mathematical techniques.

6.2.3.1 The \mathcal{C}_1 correlation

The lowest order of perturbation theory in the expansion of the intensity correlation function (6.4) is called \mathcal{C}_1 . This contribution is obtained by pairing the amplitude Green's functions two by two. The diagrammatic representation of \mathcal{C}_1 is depicted in Fig. 6.6a. The two pairs of amplitude Green's function can be factorized to give¹

$$\mathcal{C}_1 = \frac{\left| \overline{G(\mathbf{r}, \mathbf{R}) G^*(\mathbf{r}', \mathbf{R}')} \right|^2}{\overline{I(\mathbf{r}, \mathbf{R})} \times \overline{I(\mathbf{r}', \mathbf{R}')}}. \quad (6.10)$$

Using the diagram of \mathcal{C}_1 , we can rewrite Eq. (6.10) as

$$\mathcal{C}_1 = \frac{\left| \int d^3\mathbf{r}_1 d^3\mathbf{r}_2 \overline{G(\mathbf{r}_1, \mathbf{R}) G^*(\mathbf{r}_1, \mathbf{R}') G(\mathbf{r}, \mathbf{r}_2) G^*(\mathbf{r}', \mathbf{r}_2)} \Gamma_D(\mathbf{r}_2, \mathbf{r}_1) \right|^2}{\overline{I(\mathbf{r}, \mathbf{R})} \times \overline{I(\mathbf{r}', \mathbf{R}')}}, \quad (6.11)$$

where we have made use of the average amplitude Green's functions \overline{G} and $\overline{G^*}$ defined in Eq. (3.5) and of the sum of ladder diagrams Γ_D introduced in Sec. 3.2.2.

¹For the sake of clarity, we drop the spatial arguments of \mathcal{C}_1 .

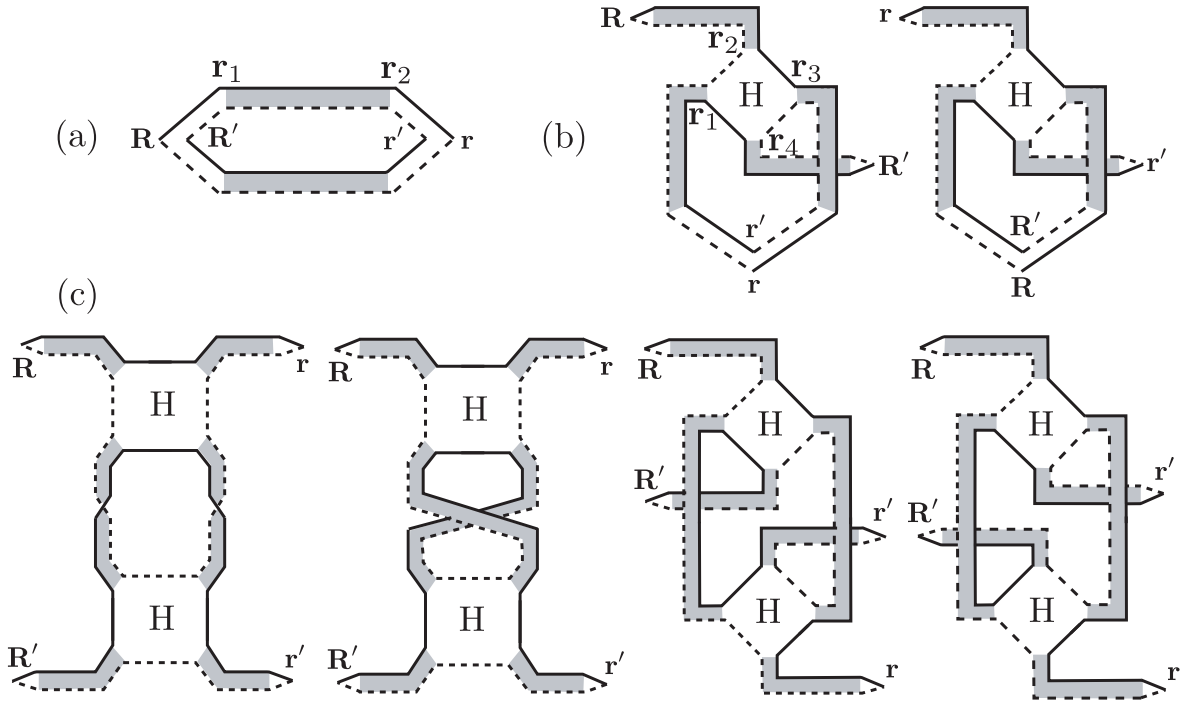


Figure 6.6: Diagrams giving (a) \mathcal{C}_1 , (b) \mathcal{C}_2 and (c) \mathcal{C}_3 contributions to the intensity correlation function. \mathbf{R} and \mathbf{R}' are two source points and \mathbf{r} and \mathbf{r}' are two detector points. Solid and dashed lines denote amplitude Green's functions G and G^* , respectively. Square “ H ” boxes are Hikami boxes (see Appendix A.1). Shaded pairs of Green's functions are sums of ladder diagrams Γ_D , detailed in Fig. 3.2.

Points \mathbf{r}_1 and \mathbf{r}_2 correspond, respectively, to the first and last scattering events of the sequence of ladder diagrams, such that one can set $\mathbf{r}_1 \simeq \mathbf{R}$ and $\mathbf{r}_2 \simeq \mathbf{r}$ as arguments of Γ_D , which varies slowly in space. The latter can then be taken out of the integrals over \mathbf{r}_1 and \mathbf{r}_2 :

$$\mathcal{C}_1 \simeq \frac{\Gamma_D(\mathbf{r}, \mathbf{R})^2 \left| \int d^3\mathbf{r}_1 d^3\mathbf{r}_2 \overline{G}(\mathbf{r}_1, \mathbf{R}) \overline{G}^*(\mathbf{r}_1, \mathbf{R}') \overline{G}(\mathbf{r}, \mathbf{r}_2) \overline{G}^*(\mathbf{r}', \mathbf{r}_2) \right|^2}{\overline{I(\mathbf{r}, \mathbf{R})} \times \overline{I(\mathbf{r}', \mathbf{R}')}}, \quad (6.12)$$

We now make use of Eqs. (3.24) and (6.7), which yield $\Gamma_D(\mathbf{R}, \mathbf{r}) = (4\pi/\ell)^2 \overline{I(\mathbf{r}, \mathbf{R})}$. Intensity terms cancel in the numerator and denominator and we obtain

$$\mathcal{C}_1 \simeq \left(\frac{4\pi}{\ell} \right)^4 \left| \int d^3\mathbf{r}_1 d^3\mathbf{r}_2 \overline{G}(\mathbf{r}_1, \mathbf{R}) \overline{G}^*(\mathbf{r}_1, \mathbf{R}') \overline{G}(\mathbf{r}, \mathbf{r}_2) \overline{G}^*(\mathbf{r}', \mathbf{r}_2) \right|^2. \quad (6.13)$$

Performing the two remaining integrals finally yields

$$\mathcal{C}_1(\Delta r, \Delta R) = F(\Delta r) F(\Delta R), \quad (6.14)$$

where $\Delta R = |\mathbf{R} - \mathbf{R}'|$, $\Delta r = |\mathbf{r} - \mathbf{r}'|$ and $F(x) = \text{sinc}(kx)^2 \exp(-x/\ell)$ with $k = \omega_0/c$ and $\text{sinc}(x) = \sin(x)/x$. For $\Delta R = \Delta r = 0$, \mathcal{C}_1 is equal to unity. This observation

constitutes the well-known Rayleigh law, which expresses the fact that intensity fluctuations are comparable to the average intensity.

6.2.4 The \mathcal{C}_2 correlation

\mathcal{C}_1 gives the main contribution to the intensity correlation function at the zeroth order of perturbation theory. The first order of perturbation theory, called \mathcal{C}_2 , is obtained by introducing an interference effect between the four amplitude Green's functions joining points \mathbf{R} and \mathbf{r} and \mathbf{R}' and \mathbf{r}' in Fig. 6.5. This interference effect is similar to that at the origin of Anderson localization (see Sec. 3.2): it consists of a crossing between four waves that propagate in pairs to some point, where they interchange partners before continuing to the measurement points \mathbf{r} and \mathbf{r}' . This crossing is described by the Hikami box introduced in Chapter 3. The diagram giving \mathcal{C}_2 is the left one of Fig. 6.6b. In real space, the Hikami box reads, for classical waves,

$$H(\mathbf{r}_1, \mathbf{r}_2, \mathbf{r}_3, \mathbf{r}_4) = \delta(\mathbf{r}_1 - \mathbf{r}_2)\delta(\mathbf{r}_1 - \mathbf{r}_3)\delta(\mathbf{r}_1 - \mathbf{r}_4) \frac{\ell^5}{24\pi k^2} \nabla_{\mathbf{r}_1} \cdot \nabla_{\mathbf{r}_3}. \quad (6.15)$$

A detailed derivation of Eq. (6.15) can be found, for instance, in Ref. [16]. Making use of this equation, we can write the left diagram of Fig. 6.6b as

$$\begin{aligned} \mathcal{C}_2 = & \frac{(4\pi/\ell)^4 [\ell^5 / (24\pi k^2)]}{I(\mathbf{r}, \mathbf{R}) \times I(\mathbf{r}', \mathbf{R}')} \int d^3\mathbf{r}_1 \overline{G(\mathbf{r}_1, \mathbf{R})G^*(\mathbf{r}_1, \mathbf{R})} \times \\ & \overline{G(\mathbf{r}_1, \mathbf{R}')G^*(\mathbf{r}_1, \mathbf{R}')} \times \nabla_{\mathbf{r}_1} \overline{G(\mathbf{r}, \mathbf{r}_1)G^*(\mathbf{r}', \mathbf{r}_1)} \cdot \nabla_{\mathbf{r}_1} \overline{G(\mathbf{r}', \mathbf{r}_1)G^*(\mathbf{r}, \mathbf{r}_1)}, \end{aligned} \quad (6.16)$$

where \mathbf{r}_1 denotes the point where the interference effect occurs. Gradients come from the real-space expression of the Hikami box (see Appendix A.1). Decomposing the averages over two amplitude Green's functions in the same spirit as for the calculation of \mathcal{C}_1 we obtain:

$$\begin{aligned} \mathcal{C}_2 = & \frac{\ell c^4}{24\pi k^2} \frac{F(\Delta r)}{I(\mathbf{r}, \mathbf{R}) \times I(\mathbf{r}', \mathbf{R}')} \int d^3\mathbf{r}_1 C_D(\mathbf{r}_1, \mathbf{R})^2 [\nabla_{\mathbf{r}_1} C_D(\mathbf{r}, \mathbf{r}_1)]^2 \\ = & \frac{2}{3g} F(\Delta r). \end{aligned} \quad (6.17)$$

where we have used Eq. (6.8) to perform integrals and introduced the dimensionless conductance g . Eq. (6.17) is, however, not the final result for \mathcal{C}_2 . Indeed, there is another contribution obtained by interchanging the start and end points of the left diagram of Fig. 6.6b. This yields the right diagram. This procedure amounts to substitute $F(\Delta r)$ by $F(\Delta R)$ in Eq. (6.17). The final form of \mathcal{C}_2 is then

$$\mathcal{C}_2(\Delta r, \Delta R) \simeq \frac{2}{3g} [F(\Delta r) + F(\Delta R)]. \quad (6.18)$$

As a result of the first order of perturbation theory, \mathcal{C}_2 is g times smaller than \mathcal{C}_1 for $\Delta r = \Delta R = 0$, but it can dominate for large Δr (when $\Delta R = 0$) or large ΔR (when $\Delta r = 0$).

6.2.5 The \mathcal{C}_3 correlation

The contribution to the intensity correlation function obtained at the second order of perturbation theory is called \mathcal{C}_3 . \mathcal{C}_3 is similar to \mathcal{C}_2 , except that it involves two interference effects in a row. Four diagrams $\mathcal{C}_3^{(1)}$, $\mathcal{C}_3^{(2)}$, $\mathcal{C}_3^{(3)}$ and $\mathcal{C}_3^{(4)}$ describe such a process [68]. They are shown in Fig. 6.6c. As an example, we only outline the calculation of the third one, $\mathcal{C}_3^{(3)}$:

$$\begin{aligned} \mathcal{C}_3^{(3)} = & \frac{(4\pi/\ell)^8 [\ell^5 / (24\pi k^2)]^2}{\overline{I(\mathbf{r}, \mathbf{R})} \times \overline{I(\mathbf{r}', \mathbf{R}')}} \int d^3\mathbf{r}_1 d^3\mathbf{r}_2 \overline{G(\mathbf{r}_2, \mathbf{r}_1) G^*(\mathbf{r}_2, \mathbf{r}_1)}^2 \times \\ & \frac{\overline{\nabla_{\mathbf{r}_1} G(\mathbf{r}_1, \mathbf{R}') G^*(\mathbf{r}_1, \mathbf{R}') \cdot \nabla_{\mathbf{r}_1} G(\mathbf{r}_1, \mathbf{R}) G^*(\mathbf{r}_1, \mathbf{R})}}{\overline{\nabla_{\mathbf{r}_2} G(\mathbf{r}, \mathbf{r}_2) G^*(\mathbf{r}, \mathbf{r}_2) \cdot \nabla_{\mathbf{r}_2} G(\mathbf{r}', \mathbf{r}_2) G^*(\mathbf{r}', \mathbf{r}_2)}}, \end{aligned} \quad (6.19)$$

where \mathbf{r}_1 and \mathbf{r}_2 denote the points where the two interference effects occur. We obtain

$$\begin{aligned} \mathcal{C}_3^{(3)} = & \left(\frac{\ell c^3}{6k^2} \right) \frac{1}{\overline{I(\mathbf{r}, \mathbf{R})} \times \overline{I(\mathbf{r}', \mathbf{R}')}} \int d^3\mathbf{r}_1 \nabla_{\mathbf{r}_1} C_D(\mathbf{r}_1, \mathbf{R}) \cdot \nabla_{\mathbf{r}_1} C_D(\mathbf{r}_1, \mathbf{R}) \times \\ & \frac{\overline{\nabla_{\mathbf{r}_2} C_D(\mathbf{r}_2, \mathbf{r}) \cdot \nabla_{\mathbf{r}_2} C_D(\mathbf{r}_2, \mathbf{r}) \times C_D(\mathbf{r}_2, \mathbf{r}_1)^2}}{2} \\ = & \frac{2}{45g^2}. \end{aligned} \quad (6.20)$$

A similar calculation gives $\mathcal{C}_3^{(1)} = \mathcal{C}_3^{(2)} = 1/(45g^2)$ and $\mathcal{C}_3^{(4)} = \mathcal{C}_3^{(3)} = 2/(45g^2)$, so that $\mathcal{C}_3 = \mathcal{C}_3^{(1)} + \mathcal{C}_3^{(2)} + \mathcal{C}_3^{(3)} + \mathcal{C}_3^{(4)} = 2/(15g^2)$. There are three other contributions to \mathcal{C}_3 , obtained by interchanging source and detector points in the four diagrams of Fig. 6.6c (these diagrams are not shown), in the same way as for \mathcal{C}_2 . The final result is

$$\mathcal{C}_3(\Delta r, \Delta R) \simeq \frac{2}{15g^2} [1 + F(\Delta r) + F(\Delta R) + F(\Delta r)F(\Delta R)]. \quad (6.21)$$

6.2.6 Physical interpretation

Collecting Eqs. (6.14), (6.18) and (6.21), we obtain the complete form of the intensity correlation function at the second order of perturbation theory:

$$\begin{aligned} \mathcal{C}(\Delta r, \Delta R) = & F(\Delta r)F(\Delta R) + \frac{2}{3g} [F(\Delta r) + F(\Delta R)] \\ & + \frac{2}{15g^2} [1 + F(\Delta r) + F(\Delta R) + F(\Delta r)F(\Delta R)]. \end{aligned} \quad (6.22)$$

The physical interpretation of Eq. (6.22) is the following. The \mathcal{C}_1 term gives the main contribution to the fluctuations of intensity transmitted through a disordered waveguide. It is responsible for the grainy aspect of speckle patterns. If we set $\Delta R = 0$ and integrate Eq. (6.22) over detector points \mathbf{r} and \mathbf{r}' , the contributions

of \mathcal{C}_1 and \mathcal{C}_3 become negligible. Therefore, \mathcal{C}_2 gives the main contribution to the correlation function of the fluctuations of the *total transmission*:

$$\frac{1}{A^2} \int_A d^2\mathbf{r} d^2\mathbf{r}' \mathcal{C}(\Delta r, \Delta R = 0) \simeq \frac{1}{A^2} \int_A d^2\mathbf{r} d^2\mathbf{r}' \mathcal{C}_2(\Delta r, \Delta R = 0) = \frac{2}{3g}. \quad (6.23)$$

If now we sum over source points \mathbf{R} and \mathbf{R}' and detector points \mathbf{r} and \mathbf{r}' , the contribution due to \mathcal{C}_3 dominates. Therefore, \mathcal{C}_3 gives the main contribution to the correlation function of the fluctuations of the *transmittance*:

$$\frac{1}{A^4} \int_A d^2\mathbf{r} d^2\mathbf{r}' d^2\mathbf{R} d^2\mathbf{R}' \mathcal{C}(\Delta r, \Delta R) \simeq \frac{1}{A^4} \int_A d^2\mathbf{r} d^2\mathbf{r}' d^2\mathbf{R} d^2\mathbf{R}' \mathcal{C}_3(\Delta r, \Delta R) = \frac{2}{15g^2}. \quad (6.24)$$

There is a remarkable analogy between electronic transport in mesoscopic systems and wave propagation in random media: in a mesoscopic conductor, the transmittance corresponds to the dimensionless conductance g , and Eq. (6.24) is nothing but the (normalized) variance $\overline{\delta G^2}/\overline{G}^2$ of $G = (e^2/h)g$. We therefore obtain

$$\overline{\delta G^2} = \frac{2}{15} \left(\frac{e^2}{h} \right)^2. \quad (6.25)$$

Eq. (6.25) describes one of the most important effects of mesoscopic physics: the variance of conductance fluctuations is a universal constant that depends neither on the sample size, nor on any microscopic parameter of the disordered conductor. These “universal conductance fluctuations” have been extensively studied in mesoscopic systems, both experimentally [69, 70, 71, 72] and theoretically [73, 74, 75] (see Refs. [16] and [17] for reviews).

6.3 Experimental measurement of intensity correlations in waveguides

6.3.1 Direct measurements

Eq. (6.22) was first derived by P. Sebbah *et al.* in 2002 [76]. In their work, these authors also carried out a microwave experiment in order to measure the intensity correlation function. For that purpose, they used miniature source and detector antennas at the input and output surfaces of a disordered sample made of a random mixture of alumina and polystyrene spheres embedded in a long copper tube². By translating the source antenna at the input surface of the tube, they were able to demonstrate the main features of Eq. (6.22). For instance, if we neglect the \mathcal{C}_3 contribution in Eq. (6.22) and set $\Delta R = 0$, we obtain

$$\mathcal{C}(\Delta r, \Delta R = 0) \simeq F(\Delta r) + \frac{2}{3g} [1 + F(\Delta r)]. \quad (6.26)$$

²polystyrene spheres are transparent for microwaves and are just used to randomize the distribution of alumina spheres.

This quantity was measured in the experiment of Ref. [76] as a function of Δr (see the main plot of Fig. 6.7). Similarly, we have

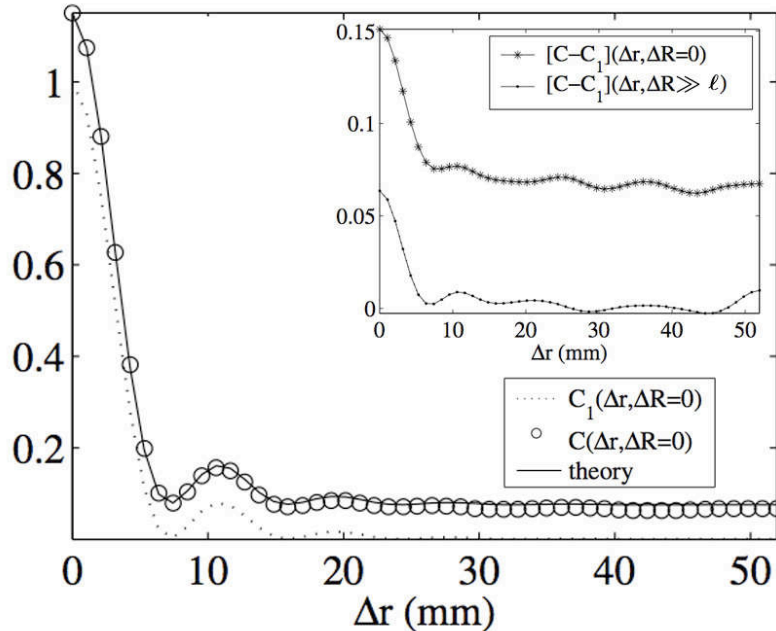


Figure 6.7: Microwave measurement carried out in Ref. [76]. Main plot: measurement of $\mathcal{C}(\Delta r, \Delta R = 0)$ as a function of Δr together with the theoretical $\mathcal{C}_1(\Delta r, \Delta R = 0) = F(\Delta r)$. Inset: measurements of $[\mathcal{C} - \mathcal{C}_1](\Delta r, \Delta R = 0) \simeq [2/(3g)][1 + F(\Delta r)]$ and $[\mathcal{C} - \mathcal{C}_1](\Delta r, \Delta R \gg \ell) \simeq [2/(3g)]F(\Delta r)$.

$$[\mathcal{C} - \mathcal{C}_1](\Delta r, \Delta R = 0) \simeq \frac{2}{3g} [1 + F(\Delta r)], \quad (6.27)$$

and

$$[\mathcal{C} - \mathcal{C}_1](\Delta r, \Delta R \gg \ell) \simeq \frac{2}{3g} F(\Delta r). \quad (6.28)$$

These two quantities were also measured in Ref. [76], as functions of Δr , and are shown in the inset of Fig. 6.7.

6.3.2 Polarization-resolved measurements

The most interesting parts in Eq. (6.22) are the terms proportional to $1/g$ and $1/g^2$, which are manifestations of coherent wave transport in a disordered medium. Unfortunately, these terms are difficult to measure. A solution to this problem was proposed in the Ph.D. thesis of N. Trégourès in 2001 [77] and was realized experimentally by A. A. Chabanov *et al.* in 2004 [78]. It relies on polarization dependence of intensity correlations. Roughly, the idea is the following. Instead of emitting waves from two different source points \mathbf{R} and \mathbf{R}' and measuring them at

two different detector points \mathbf{r} and \mathbf{r}' , the waves are emitted from a single source point \mathbf{R} but with two different polarizations \mathbf{e}_a and $\mathbf{e}_{a'}$, and measured at only one detector point \mathbf{r} , but for two different polarizations \mathbf{e}_b and $\mathbf{e}_{b'}$ ³ (see Fig. 6.8). The

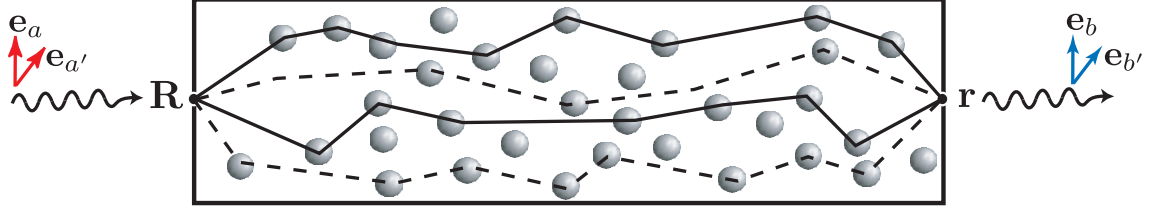


Figure 6.8: Principle of polarization measurements.

calculation of the intensity correlation function taking into account polarization is more difficult because it requires to consider the vector nature of electromagnetic waves. The result is the following [77]:

$$\begin{aligned} \mathcal{C}(\mathbf{e}_b \cdot \mathbf{e}_{b'}, \mathbf{e}_a \cdot \mathbf{e}_{a'}) &= (\mathbf{e}_b \cdot \mathbf{e}_{b'}) \times (\mathbf{e}_a \cdot \mathbf{e}_{a'}) + \frac{2}{3g} (\mathbf{e}_b \cdot \mathbf{e}_{b'} + \mathbf{e}_a \cdot \mathbf{e}_{a'}) \\ &+ \frac{2}{15g^2} [1 + \mathbf{e}_b \cdot \mathbf{e}_{b'} + \mathbf{e}_a \cdot \mathbf{e}_{a'} + (\mathbf{e}_b \cdot \mathbf{e}_{b'}) \times (\mathbf{e}_a \cdot \mathbf{e}_{a'})]. \end{aligned} \quad (6.29)$$

The advantage of polarization measurements is evident from Eq. (6.29): polarization offers a new degree of freedom for measuring independently the \mathcal{C}_1 , \mathcal{C}_2 and \mathcal{C}_3 terms. Setting, for instance, $\mathbf{e}_a \cdot \mathbf{e}_{a'} = \mathbf{e}_b \cdot \mathbf{e}_{b'} = 0$, one obtains $\mathcal{C} = 2/(15g^2) = \mathcal{C}_3$. This technique was successfully used in Ref. [78] to demonstrate universal conductance fluctuations with microwaves.

6.4 Conclusion

In this chapter we laid the basis for the calculation of the intensity correlations in disordered waveguides. We introduced the \mathcal{C}_1 , \mathcal{C}_2 and \mathcal{C}_3 correlations functions and calculated them by means of perturbation theory, where the small parameter is the inverse dimensionless conductance $1/g$. $\mathcal{C}_2 \propto 1/g$ and $\mathcal{C}_3 \propto 1/g^2$ contributions to the total intensity correlation function are manifestations of coherent effects showing up during the propagation of a wave. We showed how these contributions could be resolved by playing, in a clever way, with the polarization of waves.

³ \mathbf{e}_a , $\mathbf{e}_{a'}$, \mathbf{e}_b and $\mathbf{e}_{b'}$ are unit vectors.

Dynamics of intensity speckle patterns

Contents

7.1	Average intensity and intensity correlation function . . .	84
7.1.1	Framework	84
7.1.2	Field correlation function	85
7.1.3	Average intensity	86
7.1.4	Time-dependent intensity correlation function	87
7.2	Dynamic \mathcal{C}_1 and \mathcal{C}_2 correlation functions	87
7.2.1	The \mathcal{C}_1 correlation function	87
7.2.2	The \mathcal{C}_2 correlation function	88
7.3	The \mathcal{C}_3 correlation function	89
7.3.1	Calculation of \mathcal{C}_3	89
7.3.2	Experimental measurement of \mathcal{C}_3	91
7.3.3	Role of absorption	95
7.3.4	Limitation of long times	96
7.4	Conclusion	96

WHEREAS the physics of *stationary* intensity correlations in disordered media is relatively well known, at least in the extended regime, very few results concern the dynamics of speckle patterns. In principle, this dynamics can be caused either by the Brownian motion of scatterers inside the disordered medium, or by the time-dependence of the incoming radiation. The former case was studied by F. Scheffold *et al.* [79] and by G. Maret and F. Scheffold [80] in the late 1990's. In the presence of

mobile scatterers, the \mathcal{C}_1 , \mathcal{C}_2 and \mathcal{C}_3 correlation functions acquire a time-dependent decay reflecting the loss of coherence due to the Brownian motion of scatterers. At long times, $\mathcal{C}_1(\Delta t)$ decreases exponentially, whereas the decay of $\mathcal{C}_2(\Delta t)$ and $\mathcal{C}_3(\Delta t)$ is algebraic¹. The latter was directly observed in Ref. [80], in samples containing a suspension of colloidal particles in water. We show it in Fig. 7.1.

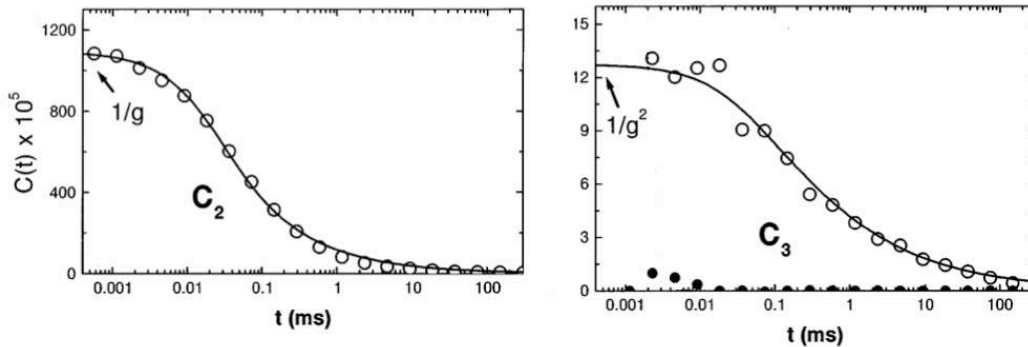


Figure 7.1: Time dependence of $\mathcal{C}_2(\Delta t)$ and $\mathcal{C}_3(\Delta t)$, obtained from the multiple scattering of light in a suspension of colloidal particles in water. The decay of $\mathcal{C}_2(\Delta t)$ and $\mathcal{C}_3(\Delta t)$ at long times is algebraic. The magnitude of \mathcal{C}_3 is less than that of \mathcal{C}_2 by a factor $\sim 1/g$.

The dynamics of intensity correlations and hence of speckle patterns also shows up in samples with static disorder but impinged on by a time-dependent radiation, for instance a short pulse. The experimental study of this problem was initiated by A. A. Chabanov in 2004 [81], and, the same year, S. E. Skipetrov [82] developed a theory for the time dependence of the \mathcal{C}_2 correlation function. In this chapter, we study the time dependence of \mathcal{C}_1 , \mathcal{C}_2 and \mathcal{C}_3 intensity correlation functions in a waveguide irradiated by a short pulse. For the case of \mathcal{C}_3 , we compare our theoretical results to a microwave experiment carried out recently by A. Peña and A. A. Chabanov at the Department of Physics and Astronomy of the University of Texas (San Antonio). The technical calculations of this chapter are reported in Appendix B.

7.1 Average intensity and intensity correlation function

7.1.1 Framework

The situation that we consider in this chapter is shown in Fig. 7.2. A short pulse of duration t_p is sent at time $t = 0$ from a point \mathbf{R} at the input surface of a disordered waveguide of diameter d and length L . The intensity averaged over

¹Here the intensity is measured first at time $t = 0$, and then at time Δt . $\mathcal{C}_i(\Delta t)$ ($i = 1, 2, 3$) corresponds to the intensity correlation between these two measurements.

disorder $\overline{I(\mathbf{r}, \mathbf{R}, t)}$ is measured at time t and at point \mathbf{r} at the output surface. The

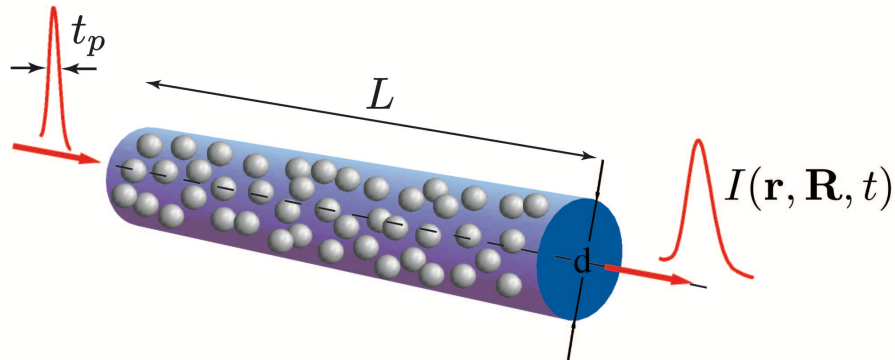


Figure 7.2: Sketch of the physical situation considered in this chapter. A short pulse of duration t_p is sent at time $t = 0$ from a point \mathbf{R} at the input surface of a disordered waveguide of diameter d and length L . The intensity $I(\mathbf{r}, \mathbf{R}, t)$ at point \mathbf{r} at the output surface acquires a time dependence.

theoretical framework is the same as in Sec. 6.2.1, that is we assume that L much exceeds the mean free path, but is much smaller than the localization length. In other words, the dimensionless conductance g is much larger than one. This ensures that waves propagate by diffusion in the waveguide. In the remainder of this chapter, we assume that the incoming pulse is Gaussian:

$$|\Psi_0(\mathbf{R}, t)|^2 = \frac{1}{\sqrt{\pi}t_p} \exp\left(-\frac{t^2}{t_p^2}\right). \quad (7.1)$$

We also restrict ourselves to the limit of long times and short pulses, for which relatively simple results can be derived. If we introduce the Thouless time $t_D = L^2/(\pi^2 D_B)$, these two conditions read

$$t_p \ll t_D \ll t. \quad (7.2)$$

Eq. (7.2) will be assumed in the remainder of the chapter.

7.1.2 Field correlation function

The Fourier component of the field at frequency ω measured at point \mathbf{r} is given by

$$\Psi(\mathbf{r}, \mathbf{R}, \omega) = G(\mathbf{r}, \mathbf{R}, \omega)\Psi_0(\mathbf{R}, \omega), \quad (7.3)$$

where $\Psi_0(\mathbf{R}, \omega)$ is the Fourier transform of $\Psi_0(\mathbf{R}, t)$ with respect to time and G is the amplitude Green's function, obeying the Helmholtz equation (3.2). In real space, Eq. (7.3) can be rewritten as

$$\Psi(\mathbf{r}, \mathbf{R}, t) = \int_{-\infty}^t dt_1 G(\mathbf{r}, \mathbf{R}, t - t_1)\Psi_0(\mathbf{R}, t_1). \quad (7.4)$$

We first calculate the *field correlation function* $\overline{\Psi(\mathbf{r}, \mathbf{R}, t)\Psi(\mathbf{r}', \mathbf{R}', t)}$. The diagrammatic representation of this quantity is shown in Fig. 7.3a. It reads

$$\overline{\Psi(\mathbf{r}, \mathbf{R}, t)\Psi^*(\mathbf{r}', \mathbf{R}', t')} = \int_{-\infty}^t dt_1 \int_{-\infty}^{t'} dt_2 \overline{G(\mathbf{r}, \mathbf{R}, t-t_1)G^*(\mathbf{r}', \mathbf{R}', t'-t_2)} \Psi_0(t_1)\Psi_0^*(t_2) \quad (7.5)$$

We demonstrate in Appendix B the following property

$$\overline{G(\mathbf{r}, \mathbf{R}, t)G^*(\mathbf{r}', \mathbf{R}', t')} = \frac{c}{4\pi} f(\Delta r)f(\Delta R)\delta(t-t')C_D(\mathbf{r}, \mathbf{R}, t), \quad (7.6)$$

where $C_D(\mathbf{r}, \mathbf{R}, t)$ is the Fourier transform of the intensity Green's function introduced in Sec. 3.2.2 and $f(x) = \text{sinc}(kx)\exp[-x/(2\ell)]$. In a waveguide of cross-section A and length L and for Dirichlet boundary conditions, it is given by (see Appendix B for the detailed calculation)

$$C_D(\mathbf{r}, \mathbf{R}, t) = \frac{1}{A} \sum_{n=1}^{\infty} \Phi_n(z)\Phi_n(z_R) \exp\left(-n^2 \frac{t}{t_D}\right), \quad (7.7)$$

where $\Phi_n(z) = \sqrt{2/L}\sin(n\pi z/L)$. As previously, z denotes the longitudinal coordinate of \mathbf{r} and $z_R \simeq \ell$ that of \mathbf{R} . Substituting Eq. (7.6) into Eq. (7.5), we obtain

$$\overline{\Psi(\mathbf{r}, \mathbf{R}, t)\Psi^*(\mathbf{r}', \mathbf{R}', t')} = \frac{c}{4\pi} f(\Delta r)f(\Delta R) \int_{-\infty}^t dt_1 C_D(\mathbf{r}, \mathbf{R}, t-t_1)\Psi_0(t_1)\Psi_0^*(t_1+t'-t). \quad (7.8)$$

Using Eq. (7.7), we obtain

$$\overline{\Psi(\mathbf{r}, \mathbf{R}, t)\Psi^*(\mathbf{r}', \mathbf{R}', t')} = \frac{c}{4\pi A} f(\Delta r)f(\Delta R) \sum_{n=1}^{\infty} \Phi_n(z)\Phi_n(z_R) f^{(n)}(t, t'). \quad (7.9)$$

where

$$\begin{aligned} f^{(n)}(t, t') &= \int_{-\infty}^t \exp\left(-n^2 \frac{t-t_1}{t_D}\right) \Psi_0(t_1)\Psi_0^*(t_1+t'-t) \\ &= \frac{1}{2} \exp\left[\frac{-n^2(t+t')}{2t_D} + \frac{n^4 t_p^2}{4t_D^2} - \frac{(t-t')^2}{4t_p^2}\right] \left[1 + \text{erf}\left(\frac{t+t'}{2t_p} - \frac{n^2 t_p}{2t_D}\right)\right]. \end{aligned} \quad (7.10)$$

The field correlation function (7.9) will be used several times in the following.

7.1.3 Average intensity

The average intensity $\overline{I(\mathbf{r}, \mathbf{R}, t)} = \overline{|\Psi(\mathbf{r}, \mathbf{R}, t)|^2}$ is obtained straightforwardly from the field correlation function (7.9) by setting $\mathbf{r}' = \mathbf{r}$, $\mathbf{R}' = \mathbf{R}$ and $t = t'$:

$$\overline{I(\mathbf{r}, \mathbf{R}, t)} = \frac{c}{4\pi} \frac{1}{2A} \sum_{n=1}^{\infty} \Phi_n(z)\Phi_n(z_R) f^{(n)}(t, t). \quad (7.11)$$

Using Eq. (7.9) and (7.11) we obtain

$$\mathcal{C}_1(\Delta r, \Delta R, t) = F(\Delta r)F(\Delta R), \quad (7.15)$$

where $F(x) = f(x)^2$. Due to the structure of the diagram of Fig. 7.3c, \mathcal{C}_1 does not depend on time. This means that at the lowest order of perturbation theory, the intensity speckle pattern is stationary, despite the time dependence of the incoming excitation.

7.2.2 The \mathcal{C}_2 correlation function

The diagram for time-dependent \mathcal{C}_2 is depicted in Fig. 7.3d. The Hikami box remains unchanged in the dynamic case. From this diagram we obtain

$$\begin{aligned} \mathcal{C}_2 = & \frac{(4\pi/\ell)^4[\ell^5/(24\pi k^2)]}{\overline{I(\mathbf{r}, \mathbf{R}, t)} \times \overline{I(\mathbf{r}', \mathbf{R}', t)}} \int d^3\mathbf{r}_1 \prod_{i=1}^4 \int_{-\infty}^t dt_i \overline{\Psi(\mathbf{r}_1, \mathbf{R}, t_1)\Psi^*(\mathbf{r}_1, \mathbf{R}, t_2)} \times \\ & \overline{\Psi(\mathbf{r}_1, \mathbf{R}', t_3)\Psi^*(\mathbf{r}_1, \mathbf{R}', t_4)} \times \nabla_{\mathbf{r}_1} \overline{G(\mathbf{r}, \mathbf{r}_1, t - t_1)G^*(\mathbf{r}', \mathbf{r}_1, t - t_4)} \cdot \\ & \nabla_{\mathbf{r}_1} \overline{G(\mathbf{r}', \mathbf{r}_1, t - t_3)G^*(\mathbf{r}, \mathbf{r}_1, t - t_2)}, \end{aligned} \quad (7.16)$$

We now make use of Eq. (7.6) to simplify the two pairs of amplitude Green's functions. This yields

$$\begin{aligned} \mathcal{C}_2 = & \frac{2\pi\ell c^2/(3k^2)F(\Delta r)}{\overline{I(\mathbf{r}, \mathbf{R}, t)} \times \overline{I(\mathbf{r}', \mathbf{R}', t)}} \int d^3\mathbf{r}_1 \int_{-\infty}^t dt_1 \int_{-\infty}^t dt_2 \overline{\Psi(\mathbf{r}_1, \mathbf{R}, t_1)\Psi^*(\mathbf{r}_1, \mathbf{R}, t_2)} \times \\ & \overline{\Psi(\mathbf{r}_1, \mathbf{R}', t_2)\Psi^*(\mathbf{r}_1, \mathbf{R}', t_1)} \nabla_{\mathbf{r}_1} C_D(\mathbf{r}, \mathbf{r}_1, t - t_1) \cdot \nabla_{\mathbf{r}_1} C_D(\mathbf{r}', \mathbf{r}_1, t - t_2). \end{aligned} \quad (7.17)$$

Simplifying intensity Green's functions, field correlation functions and intensities with help of Eq. (7.7), (7.9) and (7.12), and performing the integral over \mathbf{r}_1 , we obtain in the limit $t_p \ll t_D \ll t$

$$\mathcal{C}_2 = \frac{2}{3g} \frac{3}{8\pi^2} \frac{\exp(2t/t_D)}{\sin^4(\pi\ell/L)} F(\Delta r) \sum_{m,n,p,q=1}^{\infty} S_{mnpq} T_{mnpq}, \quad (7.18)$$

where

$$S_{mnpq} = mn(-1)^{m+n} \sin\left(\frac{m\pi\ell}{L}\right) \sin\left(\frac{n\pi\ell}{L}\right) \sin\left(\frac{p\pi\ell}{L}\right) \sin\left(\frac{q\pi\ell}{L}\right) f_1(m, n, p, q), \quad (7.19)$$

with

$$\begin{aligned} f_1(m, n, p, q) = & -\delta_{m-n-p-q,0} - \delta_{m+n-p-q,0} + \delta_{m-n+p-q,0} + \delta_{m+n+p-q,0} + \\ & \delta_{m-n-p+q,0} + \delta_{m+n-p+q,0} - \delta_{m-n+p+q,0}, \end{aligned} \quad (7.20)$$

where δ_{ij} is the Kronecker symbol, and

$$T_{mnpq} = \int_{-\infty}^t \frac{dt_1}{t_D} \int_{-\infty}^t \frac{dt_2}{t_D} \exp \left[-m^2 \left(\frac{t-t_1}{t_D} \right) - n^2 \left(\frac{t-t_2}{t_D} \right) \right] f^{(p)}(t_1, t_2) f^{(q)}(t_1, t_2). \quad (7.21)$$

In the limit of short pulses $t_p \ll t_D$, Eq. (7.21) reduces to

$$T_{mnpq} \simeq 4\sqrt{2\pi} \frac{t_p}{t_D} \int_0^t \frac{dt_1}{t_D} \exp \left[-(m^2 + n^2) \frac{t-t_1}{t_D} - (p^2 + q^2) \frac{t_1}{t_D} \right]. \quad (7.22)$$

Further simplifications can be made by noting that Eq. (7.18) consists of a sum of terms that either do not depend on time, or vary linearly with time. At long times the latter becomes the leading term, and it corresponds to $m = n = p = q = 1$. Therefore, we obtain

$$\mathcal{C}_2 = \frac{2}{3g} \frac{6}{(2\pi)^{3/2}} \frac{t_p}{t_D} \frac{t}{t_D} F(\Delta r). \quad (7.23)$$

Finally, as in Sec. 6.2.4, we have to keep in mind that another diagram contributes to \mathcal{C}_2 . It is obtained by interchanging the start and end points \mathbf{r}, \mathbf{r}' and \mathbf{R}, \mathbf{R}' . The final result is

$$\mathcal{C}_2(\Delta r, \Delta R, t) = \frac{2}{3g} \frac{6}{(2\pi)^{3/2}} \frac{t_p}{t_D} \frac{t}{t_D} [F(\Delta r) + F(\Delta R)], \quad t_p \ll t_D \ll t. \quad (7.24)$$

A few comments are in order. First, we notice that \mathcal{C}_2 grows with time. In particular, at long times $t > t_D^2/t_p$, \mathcal{C}_2 exceeds its stationary value $\sim 2/(3g)$. Second, in the regime considered here, the duration of the incident pulse is too short for its shape to be resolved in transmission. Therefore, we expect Eq. (7.24) to be valid for any pulse shape, apart from numerical factors.

Eq. (7.24) was first derived by S. E. Skipetrov in 2004 [82]. Somewhat earlier, the growth of \mathcal{C}_2 with time was observed experimentally by A. A. Chabanov *et al.* [81], even though in the latter work the number of data points were insufficient to confirm the functional dependence of \mathcal{C}_2 on t or t_p .

7.3 The \mathcal{C}_3 correlation function

7.3.1 Calculation of \mathcal{C}_3

Let us now focus on the dynamics of the \mathcal{C}_3 correlation function. As seen in Sec. 6.2.5, three diagrams $\mathcal{C}_3^{(1)}$, $\mathcal{C}_3^{(2)}$, $\mathcal{C}_3^{(3)}$ and $\mathcal{C}_3^{(4)}$ have to be taken into account. For clarity, only $\mathcal{C}_3^{(3)}$ is depicted in Fig. 7.3e. We detail its calculation below. We start

from

$$\begin{aligned}
\mathcal{C}_3^{(3)} &= \frac{(4\pi/\ell)^8 [\ell^5 / (24\pi k^2)]^2}{I(\mathbf{r}, \mathbf{R}, t) \times I(\mathbf{r}', \mathbf{R}', t)} \int d^3\mathbf{r}_1 \int d^3\mathbf{r}_2 \int_{-\infty}^{t_8} dt_1 \int_{-\infty}^{t_7} dt_2 \int_{-\infty}^{t_6} dt_3 \int_{-\infty}^{t_5} dt_4 \\
&\quad \prod_{i=5}^8 \int_{-\infty}^t dt_i \overline{\nabla_{\mathbf{r}_1} \Psi(\mathbf{r}_1, \mathbf{R}, t_1) \Psi^*(\mathbf{r}_1, \mathbf{R}, t_2) \cdot \nabla_{\mathbf{r}_1} \Psi(\mathbf{r}_1, \mathbf{R}', t_3) \Psi^*(\mathbf{r}_1, \mathbf{R}', t_4)} \\
&\quad \times \overline{G(\mathbf{r}_2, \mathbf{r}_1, t_8 - t_1) G^*(\mathbf{r}_2, \mathbf{r}_1, t_5 - t_4)} \times \overline{G(\mathbf{r}_2, \mathbf{r}_1, t_6 - t_3) G^*(\mathbf{r}_2, \mathbf{r}_1, t_7 - t_2)} \\
&\quad \times \overline{\nabla_{\mathbf{r}_2} G(\mathbf{r}', \mathbf{r}_2, t - t_6) G^*(\mathbf{r}', \mathbf{r}_2, t - t_5) \cdot \nabla_{\mathbf{r}_2} G(\mathbf{r}, \mathbf{r}_2, t - t_8) G^*(\mathbf{r}, \mathbf{r}_2, t - t_7)}.
\end{aligned} \tag{7.25}$$

We now follow the same strategy as for \mathcal{C}_2 , and first simplify the pairs of amplitude Green's functions with the help of Eq. (7.6):

$$\begin{aligned}
\mathcal{C}_3^{(3)} &= \frac{(4\pi/\ell)^8 [\ell^5 / (24\pi k^2)]^2}{I(\mathbf{r}, \mathbf{R}, t) \times I(\mathbf{r}', \mathbf{R}', t)} \int d^3\mathbf{r}_1 \int d^3\mathbf{r}_2 \int_{-\infty}^t dt_5 \int_{-\infty}^t dt_7 \int_{-\infty}^{t_7} dt_1 \int_{-\infty}^{t_5} dt_3 \\
&\quad \overline{\nabla_{\mathbf{r}_1} \Psi(\mathbf{r}_1, \mathbf{R}, t_1) \Psi^*(\mathbf{r}_1, \mathbf{R}, t_7 - t_5 + t_3) \cdot \nabla_{\mathbf{r}_1} \Psi(\mathbf{r}_1, \mathbf{R}', t_3) \Psi^*(\mathbf{r}_1, \mathbf{R}', t_5 - t_7 + t_1)} \times \\
&\quad C_D(\mathbf{r}_2, \mathbf{r}_1, t_7 - t_1) C_D(\mathbf{r}_2, \mathbf{r}_1, t_5 - t_3) \times \overline{\nabla_{\mathbf{r}_2} C_D(\mathbf{r}', \mathbf{r}_2, t - t_5) \cdot \nabla_{\mathbf{r}_2} C_D(\mathbf{r}, \mathbf{r}_2, t - t_7)}.
\end{aligned} \tag{7.26}$$

We now simplify intensity Green's functions, field correlation functions and intensities with the help of Eq. (7.7), (7.9) and (7.12), and perform the integral over \mathbf{r}_1 . In the limit $t_p \ll t_D \ll t$ this yields

$$\mathcal{C}_3^{(3)} = \frac{2}{45g^2} \frac{45}{8\pi^4} \frac{\exp(2t/t_D)}{\sin^4(\pi\ell/L)} \sum_{m,n,p,q,r,s=1}^{\infty} U_{mnpqrs} V_{mnpqrs}, \tag{7.27}$$

where

$$\begin{aligned}
U_{mnpqrs} &= mnrs (-1)^{m+n} \sin\left(\frac{m\pi\ell}{L}\right) \sin\left(\frac{n\pi\ell}{L}\right) \sin\left(\frac{r\pi\ell}{L}\right) \sin\left(\frac{s\pi\ell}{L}\right) \\
&\quad \times f_1(m, n, p, q) f_1(r, s, p, q),
\end{aligned} \tag{7.28}$$

and

$$\begin{aligned}
V_{mnpqrs} &= \int_{-\infty}^t \frac{dt_5}{t_D} \int_{-\infty}^t \frac{dt_7}{t_D} \int_{-\infty}^{t_7} \frac{dt_1}{t_D} \int_{-\infty}^{t_5} \frac{dt_3}{t_D} f^{(r)}(t_1, t_7 - t_5 + t_3) f^{(s)}(t_3, t_5 - t_7 + t_1) \\
&\quad \times \exp\left[-m^2 \left(\frac{t - t_5}{t_D}\right) - n^2 \left(\frac{t - t_7}{t_D}\right) - p^2 \left(\frac{t_7 - t_1}{t_D}\right) - q^2 \left(\frac{t_5 - t_3}{t_D}\right)\right].
\end{aligned} \tag{7.29}$$

In the limit of short pulses $t_p \ll t_D$, Eq. (7.29) simplifies to

$$\begin{aligned}
V_{mnpqrs} &\simeq 4\sqrt{2\pi} \frac{t_p}{t_D} \int_0^t \frac{dt_5}{t_D} \int_{t_5 - t_3}^t \frac{dt_7}{t_D} \int_0^{t_5} \frac{dt_3}{t_D} \exp\left[-m^2 \left(\frac{t - t_5}{t_D}\right) - n^2 \left(\frac{t - t_7}{t_D}\right)\right] \\
&\quad \times \exp\left[-(p^2 + q^2 - s^2) \left(\frac{t_5 - t_3}{t_D}\right) - r^2 \frac{t_3}{t_D} - s^2 \frac{t_7}{t_D}\right].
\end{aligned} \tag{7.30}$$

As for \mathcal{C}_2 , a relatively simple result can be obtained in the long time limit $t \gg t_D$. Indeed, when made explicit, the sum in Eq. (7.27) is a polynomial of the third order in time t . It is not possible to calculate exactly all the coefficients of this polynomial. However, when $t \gg t_D$, the term of higher power dominates. It originates from $m = n = p = q = r = s = 1$. From Eqs. (7.27), (7.28) and (7.30) we obtain

$$\mathcal{C}_3^{(3)} = \frac{1}{15g^2} \frac{5\sqrt{2}}{(\pi^3\sqrt{\pi})} \frac{t_p}{t_D} \left(\frac{t}{t_D} \right)^3. \quad (7.31)$$

$\mathcal{C}_3^{(4)}$ (fourth diagram of Fig. 6.6c) is equal to $\mathcal{C}_3^{(3)}$. $\mathcal{C}_3^{(1)}$ and $\mathcal{C}_3^{(2)}$ are equal, but one can show that they do not contain terms proportional to t^3 in the limit $t_p \ll t_D \ll t$, but only terms of powers lower than two. Therefore, their contribution to \mathcal{C}_3 is negligible at long times. Furthermore, as in the stationary case detailed in Sec. 6.2.4, for each of the four diagrams of Fig. 6.6c, there are three other contributions obtained by interchanging start and end points of the diagram. Taking into account all of them finally yields

$$\mathcal{C}_3(\Delta r, \Delta R, t) = \frac{2}{15g^2} \frac{5\sqrt{2}}{(\pi^3\sqrt{\pi})} \frac{t_p}{t_D} \left(\frac{t}{t_D} \right)^3 [1 + F(\Delta r) + F(\Delta R) + F(\Delta r)F(\Delta R)], \quad (7.32)$$

$t_p \ll t_D \ll t.$

Thus, \mathcal{C}_3 increases as the third power of time and becomes larger than its stationary value $2/(15g^2)$ for $t \gg t_D(t_D/t_p)^{1/3}$. As for \mathcal{C}_2 , Eq. (7.32) is expected to hold independent of the shape of the incident pulse, apart from the numerical prefactors.

7.3.2 Experimental measurement of \mathcal{C}_3

In this section, we present the results of an experiment carried out by A. Peña and A. A. Chabanov at the Department of Physics and Astronomy of the University of Texas (San Antonio). The purpose of this work was to provide the experimental support to Eq. (7.32).

The principle of this experiment is the following. In order to measure unambiguously the time dependence of \mathcal{C}_3 , one can take advantage of the vector nature of electromagnetic waves, as described in Sec. 6.3.2. As a matter of fact, similarly to Eq. (6.29), the dynamic intensity correlation function with polarization rotation can be written as

$$\begin{aligned} \mathcal{C}(\mathbf{e}_b \cdot \mathbf{e}_{b'}, \mathbf{e}_a \cdot \mathbf{e}_{a'}, t) &= (\mathbf{e}_b \cdot \mathbf{e}_{b'}) \times (\mathbf{e}_a \cdot \mathbf{e}_{a'}) + \frac{2}{3g} \frac{6}{(2\pi)^{3/2}} \frac{t_p}{t_D} \frac{t}{t_D} (\mathbf{e}_b \cdot \mathbf{e}_{b'} + \mathbf{e}_a \cdot \mathbf{e}_{a'}) \\ &+ \frac{2}{15g^2} \frac{5\sqrt{2}}{(\pi^3\sqrt{\pi})} \frac{t_p}{t_D} \left(\frac{t}{t_D} \right)^3 [1 + \mathbf{e}_b \cdot \mathbf{e}_{b'} + \mathbf{e}_a \cdot \mathbf{e}_{a'} + (\mathbf{e}_b \cdot \mathbf{e}_{b'}) \times (\mathbf{e}_a \cdot \mathbf{e}_{a'})]. \end{aligned} \quad (7.33)$$

When the polarizations of the waves at the source and detector are both rotated by 90° , $\mathbf{e}_b \cdot \mathbf{e}_{b'} = \mathbf{e}_a \cdot \mathbf{e}_{a'} = 0$ and only the time-dependent prefactor of \mathcal{C}_3 remains:

$$\mathcal{C}(0, 0, t) = \frac{2}{15g^2} \frac{5\sqrt{2}}{(\pi^3\sqrt{\pi})} \frac{t_p}{t_D} \left(\frac{t}{t_D} \right)^3. \quad (7.34)$$

For simplicity in the following we denote $\mathcal{C}_3(t) = \mathcal{C}(0, 0, t)$. Measurements of the intensity correlation function are made for microwave radiation transmitted through random mixtures of Al_2O_3 spheres. Alumina spheres with diameter 0.64 cm and index of refraction 3.14 are embedded within Styrofoam shells to produce a sample with alumina volume fraction 0.03. The sample is contained within a copper tube with diameter of 4.4 cm (Fig. 7.4). Linearly polarized microwave radiation



Figure 7.4: Axial view of the sample used in the microwave experiment.

is launched and detected by identical conical horns placed 20 cm in front of and behind the sample, as shown in Fig. 7.5. These horns allow to control the state of linear polarization of the microwave radiation. Microwave field spectra are recorded for cross-polarization orientations of both the source and the detector horns, for 15 000 configurations of disorder, produced by briefly rotating the tube around its axis, in samples of length 61, 76.2, and 91.4 cm. Measurements are made over the frequency range 18.7–19.7 GHz, away from Mie resonances of spheres, and far from the localization threshold. At 19.2 GHz, the number of transverse channels is $N = 54$. The transport mean free path estimated from Mie theory is $\ell = 3.76$ cm, giving the dimensionless conductance $g = 4N\ell/3(L + 2z_0) = 4.10, 3.33, \text{ and } 2.81$ for $L = 61, 76.2, \text{ and } 91.4$ cm, respectively².

In the experiment, no “real” pulse is sent through the disordered medium. Rather, the temporal response to a Gaussian pulse of width t_p peaked at $t = 0$ is reconstructed by taking the Fourier transform of the measured field spectrum multiplied by a Gaussian envelope of width $(2\pi t_p)^{-1}$, and centered at the frequency 19.2 GHz. The field of the time response is squared to obtain the transmitted intensity. Ensemble-averaged intensity $\overline{I}(t)$ is shown in Fig. 7.6 for the three sample lengths and for a pulse duration $t_p = 1.8$ ns. At short times ($t < 100$ ns), the average intensity decays exponentially, in agreement with diffusion theory (Eq. (7.12)). The deviations from this exponential decay observed at long times are due to weak localization effects in the disordered sample. They were studied in Refs. [57, 47, 83].

²Note that here we have accounted for the finite value of the extrapolation length $z_0 = 2\ell/3$ to obtain a precise value of the dimensionless conductance.

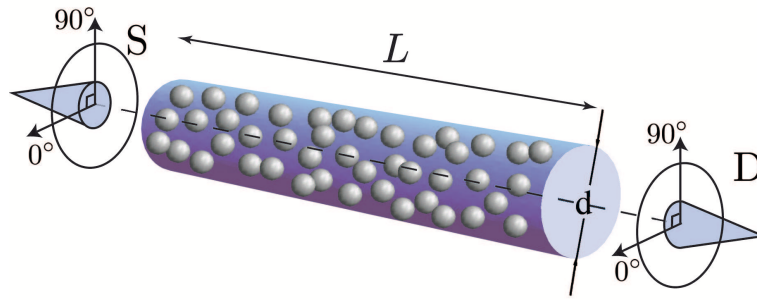


Figure 7.5: Drawing of the experimental setup. Source (S) and detector (D) horns are positioned in front of and behind the disordered sample of length L and diameter d . These horns allow to control the state of linear polarization of emitted and detected waves. Experimental measurements are made for two polarizations 0 and 90° of both emitted and detected waves, obtained by rotating the horns about their axis (z axis).

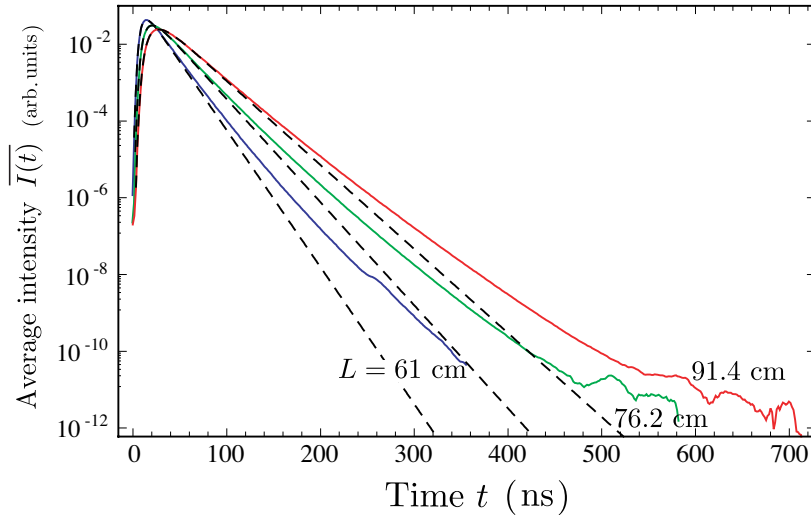


Figure 7.6: Average transmitted intensity as a function of time, for the three sample lengths $L = 61$ (blue), 76.2 (green), and 91.4 cm (red), for a pulse duration $t_p = 1.8$ ns. Dashed lines are theoretical fits to the data by diffusion theory at short times (up to ~ 100 ns). Diffusion times t_D extracted from the fits are $t_D = 17.5$, 27.3 and 39.6 ns, respectively.

These deviations are of order $1/g$ for $g \gg 1$ and, therefore, taking them into account would yield negligible corrections of order $1/g^3$ or higher in Eq. (7.34). Fits of the average intensity by diffusion theory at short times $t < 100$ ns (dashed lines of Fig. 7.6) give the Thouless times $t_D = 17.5$, 27.3 , and 39.6 ns for samples of lengths 61 , 76.2 , and 91.4 cm, respectively.

Experimental curves of $\mathcal{C}_3(t)$ for pulse durations $t_p = 0.9$, 1.2 , and 1.8 ns are shown in Fig. 7.7, for the three sample lengths. The experimental data are fitted

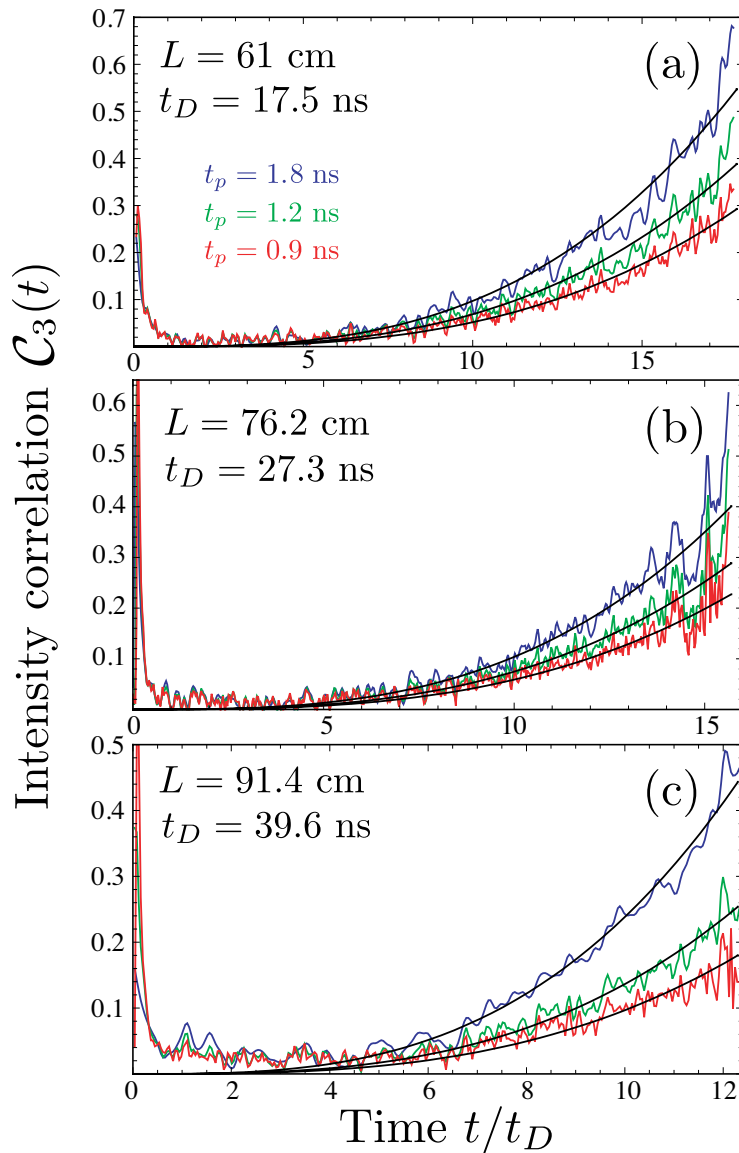


Figure 7.7: $\mathcal{C}_3(t)$ measured in samples of three different lengths L , for three different pulse durations t_p . The diffusion time t_D , extracted from the fit to average intensity $\overline{I(t)}$, is given for each sample. Black smooth lines are theoretical fits using Eq. (7.34) with $g = 4.17$ (a), 3.21 (b) and 1.85 (c) as the only fit parameter for each sample. Only the data corresponding to $t > 3t_D$ were used for fitting.

by Eq. (7.34), using g as the only fit parameter and imposing that g is the same for the three pulse durations for a given L . The values of g found from the fits are 4.17, 3.21 and 1.85 for samples of lengths 61, 76.2, and 91.4 cm, respectively. These values differ only slightly from the estimates, except for the longest sample. It is necessary to go beyond the two H -box diagrams of Fig. 7.3e for a better quantitative agreement with the data for samples with small values of g .

To demonstrate that Eq. (7.34) correctly captures the key scaling properties of

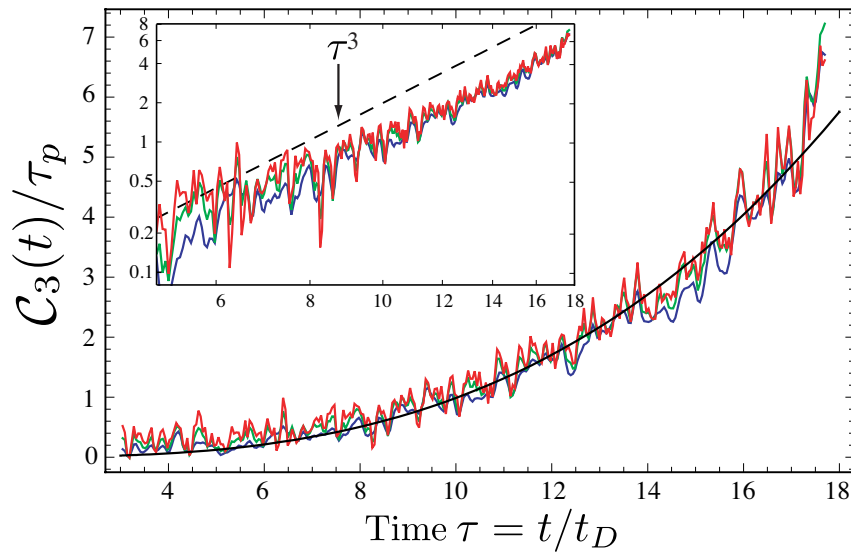


Figure 7.8: Intensity correlation $\mathcal{C}_3(t)$ divided by the dimensionless pulse duration $\tau_p = t_p/t_D$, as a function of dimensionless time $\tau = t/t_D$ for $L = 61$ cm and the same three different t_p 's as in Fig. 7.7. Only long times $t \gg t_D$ are shown. The solid smooth curve is a fit to the data with $g = 4.17$ as the only fit parameter. The inset shows the same plot in the log-log scale.

$\mathcal{C}_3(t)$ for $t \gg t_D$, we introduce the dimensionless time $\tau = t/t_D$ and the normalized pulse duration $\tau_p = t_p/t_D$, and plot $\mathcal{C}_3(t)/\tau_p$ versus τ for $L = 61$ cm in Fig. 7.8. The three curves corresponding to the three different pulse durations fall on a single curve, thereby demonstrating $\mathcal{C}_3(t) \propto \tau_p$. The same data plotted on a log-log scale (inset of Fig. 7.8) show that $\mathcal{C}_3(t) \propto \tau^3$. Thus, $\mathcal{C}_3(t) \propto \tau_p \tau^3$, as predicted by Eq. (7.34).

7.3.3 Role of absorption

Absorption can be readily included into the calculation of $\mathcal{C}_3(t)$ by introducing an additional exponential decay into the intensity Green's function:

$$C_D(\mathbf{r}, \mathbf{R}, t) = \frac{1}{A} \sum_{n=1}^{\infty} \Phi_n(z) \Phi_n(z_R) \exp\left(-n^2 \frac{t}{t_D} - \frac{t}{t_a}\right), \quad (7.35)$$

where t_a is the absorption time. The calculation of \mathcal{C}_3 then follows exactly the same lines as above. We find that provided that $t_a \gg t_p$, the result (7.32) remains unchanged, which is not surprising because for very short pulses scattering paths are all of almost the same length, and therefore suffer from absorption to the same extent. Absorption then cancels when normalizing \overline{II} by $\overline{I} \times \overline{I}$. Note that the condition $t_a \gg t_p$ can be readily met in practice, opening interesting perspectives for probing scattering parameters of random media without necessarily knowing absorption inside the medium.

In the experiment described above, the absorption time $t_a = 39.7$ ns is large as compared to the three values of $t_p = 0.9, 1.2,$ and 1.8 ns. The criterion $t_a \gg t_p$ for negligible absorption is therefore fulfilled.

7.3.4 Limitation of long times

The dynamic study presented above might not be valid for times exceeding the Heisenberg time $t_H = gt_D$. The Heisenberg time is the typical time needed for a wave (or quantum particle) to visit the whole system (the whole waveguide, in our case). After the Heisenberg time, the wave has to pass by those parts of the sample that it has already visited before. The probability for several paths to cross then becomes of the order of one. For this situation, the approach adopted in this chapter and treating such crossings as a perturbative effect, might not be valid any longer. Therefore, our results (7.24) and (7.32) might break down for $t > t_H$.

Another characteristic length scale can be pointed out by comparing the orders of magnitude of $\mathcal{C}_2(t)$ and $\mathcal{C}_3(t)$. Such a comparison suggests an important time scale, $t_q = \sqrt{g}t_D$, intermediate between the Thouless time t_D and the Heisenberg time t_H . This time scale appeared previously in the context of weak localization in classically chaotic [84, 85] and disordered [45] systems, but its role in the analysis of fluctuations of transport properties has never been identified. Because for short pulses in the long-time limit we can write $\mathcal{C}_2(t) \sim (t_p/t_q)(t/t_q)$ and $\mathcal{C}_3(t) \sim (t_p/t_q)(t/t_q)^3$, the formally next-order contribution (in $1/g$ expansion) to the intensity correlation function, $\mathcal{C}_3(t)$ becomes larger than $\mathcal{C}_2(t)$ when $t > t_q$. Even though this might indicate that some new physics comes into play at such long times, $\mathcal{C}_3(t)$ of Eq. (7.34) agrees well with the experimental data for $t > t_q$, and as a matter of fact, even for $t > t_H$.

7.4 Conclusion

In this chapter, we derived the time dependences of the \mathcal{C}_1 , \mathcal{C}_2 and \mathcal{C}_3 correlation functions, describing the response of a disordered waveguide with static disorder to a short pulsed excitation. We first recovered the results of Ref. [82], where the author found a linear growth of \mathcal{C}_2 with the delay time from the exciting pulse (Eq. (7.24)). This growth can be qualitatively understood from the following reasoning. In a semi-classical path picture, a pair of two fields propagating along a common multiple scattering path during a time interval t can be seen as a curvilinear tube of diameter λ^{d-1} and of length $s = ct$. The analogy between such a tube and a sum of ladder diagrams is illustrated in Fig. 7.9. Roughly, from the diagram of Fig. 7.3d, $\mathcal{C}_2(t)$ is given by the probability $p(t)$ for two of such tubes to cross somewhere inside the medium, during the time interval t . This probability is given by the ratio of the volume $\lambda^2 ct$ of the tube to the total volume $V = AL$ of the waveguide. Then we find

$$\mathcal{C}_2(t) \sim p(t) = \frac{sct}{AL} \sim \frac{1}{g} \frac{t}{t_D}, \quad (7.36)$$

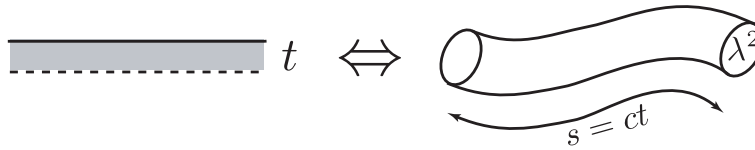


Figure 7.9: Semi-classical picture of wave propagation. A sum of ladder diagrams can be seen as a tube of diameter λ^{d-1} and of length $s = ct$.

in agreement with the more rigorous Eq. (7.24).

In a second time, we derived the time dependence of the \mathcal{C}_3 correlation function, and found a t^3 enhancement of the latter at long times, allowing $\mathcal{C}_3(t)$ to reach values well in excess of the stationary result $2/(15g^2)$. Remarkably, it turns out that this behavior can be explained by a semi-classical picture as well! \mathcal{C}_3 involves two crossings in a row between two pairs of multiple scattering paths. The probability that these paths cross first during the time interval $(0, t')$ and then a second time during the time interval (t', t) is $p(t')p(t - t')$. \mathcal{C}_3 is obtained by integrating over t' from 0 to t :

$$\mathcal{C}_3(t) \sim \int_0^t p(t')p(t - t') = \int_0^t \frac{sc t'}{AL} \frac{sc(t - t')}{AL} \sim \frac{1}{g^2} \left(\frac{t}{t_D} \right)^3. \quad (7.37)$$

The growth of \mathcal{C}_3 with time, as well as its proportionality to the pulse duration³, was confirmed experimentally by a microwave experiment carried out in the group of A. A. Chabanov.

Note that the study of \mathcal{C}_3 presented in this chapter is valid for both electronic transport in mesoscopic systems and wave propagation in random media. In particular, Eq. (7.34) is the dynamic counterpart of stationary conductance fluctuations (6.24). Incidentally, one sees that dynamic conductance fluctuations are not universal, *i.e.*, depend on sample parameters, unlike in the stationary case.

Finally, a comparative analysis of $\mathcal{C}_3(t)$ and $\mathcal{C}_2(t)$ allowed us to identify a new characteristic time scale t_q , being intermediate between the Thouless and Heisenberg times, and to explain its role in statistics of dynamic transport.

³not explained by the above semi-classical picture.

Part III

Bose-Einstein condensates expanding in random potentials

Bose-Einstein condensates and disorder

Contents

8.1	Bose-Einstein condensates	103
8.1.1	Quantum gases: elementary considerations	103
8.1.2	Nonuniform and weakly interacting Bose-Einstein condensates	103
8.2	Bose-Einstein condensate expanding in a random potential: a toy model	105
8.3	Release of the condensate from the trap	106
8.3.1	Thomas-Fermi regime	107
8.3.2	Opening of the trap. Scaling	108
8.3.3	Momentum distribution at long times	109
8.4	Conclusion	109

THE last years have seen the encounter of two communities: the community of cold atoms and the one of disorder in mesoscopic physics. From this encounter is notably born the full-fledged field of research of Bose-Einstein condensates (BECs) in random potentials. This problem is the “matter-wave counterpart” of that of a classical wave propagating in a random medium. The large number of high-quality publications of the last few years testify of the great interest of physicists for BECs in random potentials. Research in this field largely benefits from the advances of new experimental techniques, among which the now common possibility to cool

and trap atoms, and to produce optical random potentials. The main interest of experiments with Bose-Einstein condensates is their great versatility. For instance, the strength of atomic interactions can be tuned almost at will by taking advantage of Feshbach resonances, thus exploiting the dependence of the range of the interaction potential on an external magnetic field. In the same way, optical potentials used to produce disorder or confine condensates in particular directions of space offer an unprecedented experimental control. Bose-Einstein condensates thus appear to be ideal systems to study the interplay between disorder and interactions. This is the main reason why they are currently extensively used to revisit many problems of condensed-matter physics. In this context, the number of problems that can be studied is very large and it would be futile to list them all here. The interested reader is invited to consult the recent review of L. Fallani *et al.* [86].

Among popular subjects of mesoscopic physics, one which plays a primordial role in the study of BECs in the presence of disorder is certainly Anderson localization. In 2005, several attempts were made to observe this phenomenon for BECs expanding in one-dimensional random potentials [87, 88, 89]. In 2007, L. Sanchez-Palencia *et al.* proposed the first theoretical study of localization of condensates in one dimension [96]. The experimental observation of this phenomenon was finally achieved in 2008, and was reported in two Nature papers from the groups of A. Aspect in Orsay [35] and M. Inguscio in Florence [90].

Upcoming experiments will undoubtedly focus on the three-dimensional expansion of BECs in random potentials. Indeed, this situation is very rich because, as discussed in the first part of this thesis, in three dimensions a critical energy separates localized from extended states, unlike in one dimension where all states are localized. Recently, B. Shapiro studied theoretically the *diffusive* expansion of a BEC in a three-dimensional random potential, which takes place when disorder is sufficiently weak [91]. Later, S. E. Skipetrov *et al.* addressed the same problem but in the opposite situation where the disorder is strong and leads to Anderson localization of the condensate [92].

Another interesting subject concerns the extent of mesoscopic correlations discussed in the second part of this thesis to the case of BECs expanding in random potentials. As we saw in Chapter 6, a monochromatic wave propagating in a disordered medium generates a speckle pattern. From the fundamental point of view, the case of a condensate expanding in a random potential is very similar. One can therefore wonder if an equivalent of intensity speckle patterns exists for BECs, and if yes, what are its properties? These questions are the central issue of Chapter 9.

Finally, in the study of BECs expanding in random potentials, interactions between atoms are often ignored in the theoretical treatment because they strongly complicate the analysis. However, although in principle these interactions can be made very small experimentally, they always exist and their precise role in the presence of disorder, particularly when strong, is still an open question. In Chapter 10, we investigate the role of weak interactions on the expansion of a condensate.

Before considering BECs expanding in random potentials, it is useful to remind a few basic facts concerning matter waves. The physics of the latter is a bit different

from that of other waves that have been considered until now in this thesis. This is the subject of the present chapter.

8.1 Bose-Einstein condensates

The purpose of this section is to remind some basic physics of Bose gases and to introduce the main hypotheses and standard theoretical tools necessary for the proper description of Bose-Einstein condensates in the presence of disorder. The concepts developed in this section are very general and should be seen as a basis for the understanding of the next chapters.

8.1.1 Quantum gases: elementary considerations

Quantum gases are systems of particles that cannot be described by classical Maxwell-Boltzmann statistics but require a quantum mechanical treatment. For these systems, the thermal de Broglie wavelength $\lambda_T = \sqrt{2\pi\hbar^2/mk_B T}$ is much larger than the interparticle distance $n^{-1/3}$, where $n = N/V$ is the atomic density of the gas of N atoms in the volume V . Experimentally, quantum gases are obtained from alkali atoms maintained in the state of vapor at very low temperatures.

The case of gases composed of bosons (particles with integer spin) is very peculiar. In 1925, A. Einstein, on the basis of an article by S. N. Bose, published one year earlier and dealing with photon gases, predicted the occurrence of a phase transition in a gas of massive bosons. This phase transition corresponds to the macroscopic occupation of a single quantum state at low temperatures $T < T_c$. Today, this phenomenon is known as the “Bose-Einstein condensation”. A simple estimate of the condensation temperature T_c can be obtained by requiring that λ_T is equal to $n^{-1/3}$:

$$T_c \sim \frac{\hbar^2 n^{2/3}}{mk_B}. \quad (8.1)$$

In the case of alkali atoms, condensation temperatures usually range from 100 nK to a few μ K. The first Bose-Einstein condensate of alkali atoms was experimentally realized in 1995 by the teams of W. Ketterle at MIT [93] and E. Cornell and C. Wiemann at Boulder [94] in vapors of Rubidium and Sodium (see Fig. 8.1). In 2001, they were awarded the Nobel prize for this achievement. Since then, many other atomic species have been condensed and Bose-Einstein condensation has become the know-how of numerous laboratories.

8.1.2 Nonuniform and weakly interacting Bose-Einstein condensates

The phenomenon of Bose-Einstein condensation makes part of the natural behavior of Bose gases at low temperatures. It is quite well understood in the ideal case of a uniform gas (*i.e.*, with constant density in space) of noninteracting atoms. More

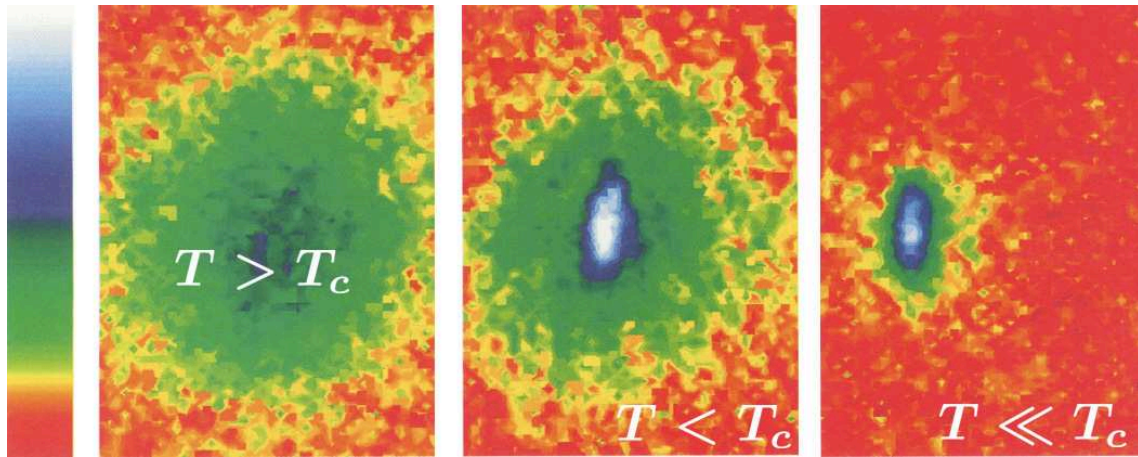


Figure 8.1: Velocity distribution (in false colors) of a cloud of ^{87}Rb atoms above and below the condensation temperature T_c , from [94]. For $T > T_c$, the distribution is Maxwell-Boltzmann. Below T_c , atoms start condensing in the same quantum state (blue-white ellipse) whose wave function has an anisotropy reflecting that of the confining potential.

details on this subject can be found, for instance, in the book of L. Pitaevskii and S. Stringari [95]. However, in practice, condensates are often produced in confining optical potentials (called “traps”), where gases are naturally nonuniform. Besides, atomic interactions are always present and may affect the properties of the gas. It is therefore important to develop a theoretical playground for the description of these more general situations. For the sake of simplicity, from here on we assume zero temperature.

8.1.2.1 Hartree ansatz

In this thesis, we always assume that interactions between atoms are “not too strong”. This situation is frequently encountered in practice, and allows for a mean-field theoretical description of Bose-Einstein condensation. More quantitatively, the condition of weak interactions can be written as

$$n^{-1/3} \gg a_s, \quad (8.2)$$

where a_s is the scattering length of the interaction potential. Condition (8.2) amounts to say that the Bose gas is sufficiently dilute. Keeping this condition in mind, the mean-field description of a Bose-Einstein condensate of $N \gg 1$ atoms consists in assuming that all atoms are described by the same wave function ϕ . In other words, atoms are considered to be independent. This is the “Hartree ansatz” which leads to the following expression for the N-particle wave function $\Theta(\mathbf{r}_1, \dots, \mathbf{r}_N)$ of the gas:

$$\Theta(\mathbf{r}_1, \dots, \mathbf{r}_N) = \prod_{i=1}^N \phi(\mathbf{r}_i). \quad (8.3)$$

From this ansatz, one defines the “wave function of the condensate” as $\psi = \sqrt{N}\phi$. In the following, we shall always refer to this quantity when speaking of the condensate. ψ is normalized to the total number N of particles of the condensate:

$$\int d^3\mathbf{r}|\psi(\mathbf{r})|^2 = N. \quad (8.4)$$

8.1.2.2 Gross-Pitaevskii equation

We have now all tools to introduce the stationary Gross-Pitaevskii equation which governs the equilibrium behavior of a Bose-Einstein condensate in an external potential V_{ext} :

$$\mu\psi(\mathbf{r}) = \left[\frac{-\hbar^2}{2m}\nabla_{\mathbf{r}}^2 + V_{\text{ext}}(\mathbf{r}) + g_0|\psi(\mathbf{r})|^2 \right] \psi(\mathbf{r}). \quad (8.5)$$

Here g_0 is the strength of interactions; in three dimensions, $g_0 = 4\pi\hbar^2 a_s/m$. The chemical potential μ is the energy needed to remove an atom from the condensate. Notice that Eq. (8.5) is nothing but a stationary Schrödinger equation at energy μ and with an additional nonlinear term. Its derivation from the Hartree ansatz (8.3) is given in Appendix C. As an example of application of the stationary Gross-Pitaevskii equation, we mention the — frequently encountered — case of a condensate maintained in its equilibrium state by an external confining potential. This problem is treated in Sec. 8.2.

Eq. (8.5) is a stationary equation. In some situations, however, one can be interested in the dynamic behavior of a BEC. This happens, for instance, when a condensate expands freely in an external random potential (this situation is also considered in Sec. 8.2). In this case, the wave function of the condensate $\psi(\mathbf{r}, t)$ depends on time and Eq. (8.5) must be replaced by the dynamic Gross-Pitaevskii equation

$$i\hbar\partial\psi(\mathbf{r}, t) = \left[\frac{-\hbar^2}{2m}\nabla_{\mathbf{r}}^2 + V_{\text{ext}}(\mathbf{r}, t) + g_0|\psi(\mathbf{r}, t)|^2 \right] \psi(\mathbf{r}, t). \quad (8.6)$$

A derivation of this equation is given in Appendix C. Obviously, the total number of atoms is conserved during the time evolution of the condensate:

$$\int d^3\mathbf{r}|\psi(\mathbf{r}, t)|^2 = N. \quad (8.7)$$

8.2 Bose-Einstein condensate expanding in a random potential: a toy model

Experimentally, BECs are usually produced inside traps generated by means of optical or magneto-optical techniques. In the experiments on BEC expansion in random potentials, the trap is turned off and the condensate starts to expand in an external optical random potential. Theoretical treatment of this problem requires to solve the Gross-Pitaevskii equation (8.6) with $V_{\text{ext}}(\mathbf{r}, t) = V_{\omega}(\mathbf{r}, t) + V(\mathbf{r})$, where

V_ω is a harmonic potential of frequency ω describing the trap and V is the random potential. The process of turning off of the trap is described by the time dependence of V_ω .

Unfortunately, solving Eq. (8.6) for this particular scenario is a formidable task that is doomed to fail. To simplify the problem, it is convenient to make use of a toy model which consists in separating the initial process of release from later stages of expansion. This model was initially proposed in [96] in the context of Anderson localization of BECs. We shall make use of it in the next two chapters. In this model, the expansion scenario is divided in three distinct stages that describe, respectively, the trapping of the BEC, the release process and finally the expansion in the random potential. At the first stage, the condensate is in its equilibrium state inside the trap V_ω . No random potential is initially present, and atomic interactions are typically strong. We assume this stage to take place at times $t < 0$. At time $t = 0$, the trap is turned off and the second stage starts. For times $t \ll 1/\omega$, interactions mainly drive the expansion of the condensate and the random potential can be neglected (this stage is described in detail in Sec. 8.3). Finally, for times $t \gg 1/\omega$, the local density of the condensate becomes low and the role of interactions is expected to be negligible. Hence, interactions can be excluded from consideration. The three stages are summarized in Fig. 8.2.

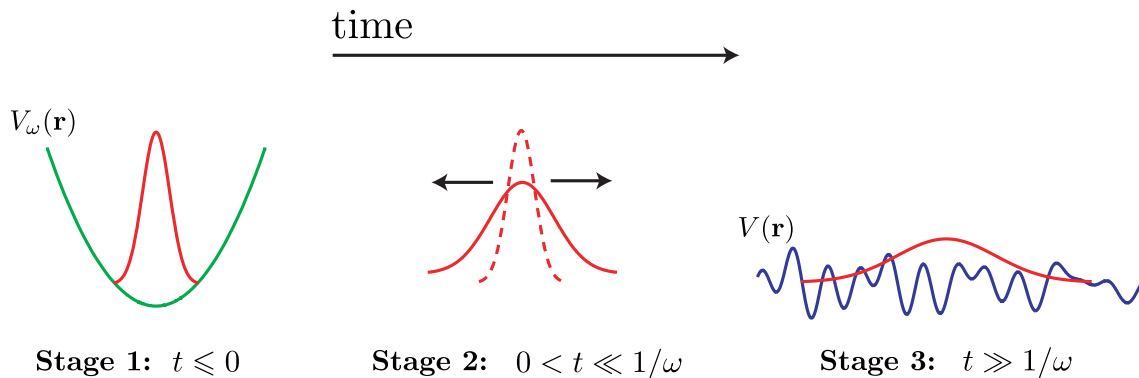


Figure 8.2: Toy model describing the expansion of a BEC produced in a trap of potential V_ω . At the stage 1, the BEC is in its equilibrium state inside the trap. At $t = 0$ the trap is turned off and the BEC starts expanding. At this stage, the expansion is driven by interactions and the random potential $V(\mathbf{r})$ can be neglected (stage 2). Finally, for times $t \gg 1/\omega$, interactions become negligible and the expansion is driven exclusively by the random potential (stage 3).

8.3 Release of the condensate from the trap

Although the initial release process of the condensate from the trap (stages 1 and 2 of our previous discussion) is not the central issue in our study of Bose-Einstein condensates, we detail it in this section because the knowledge of the state of the

condensate in the beginning of stage 3 will be needed in the next chapters. More precisely, in this section we evaluate the momentum distribution of a freely expanding BEC at $t \gg 1/\omega$. This amounts to study the expansion of an interacting condensate in a time dependent harmonic trap. This problem was investigated theoretically by Y. Kagan *et al.* [97] and Y. Castin and R. Dum [98]. As discussed in Sec. 8.2, due to the strong atomic interactions, the random potential can be neglected during this stage.

8.3.1 Thomas-Fermi regime

Consider a BEC in its equilibrium state, trapped in a three-dimensional, symmetric harmonic potential $V_\omega(\mathbf{r}) = m\omega^2 r^2/2$. The wave function $\psi_0(\mathbf{r})$ ¹ of the condensate then obeys the stationary Gross-Pitaevskii equation

$$\mu\psi_0(\mathbf{r}) = \left[\frac{-\hbar^2}{2m} \nabla_{\mathbf{r}}^2 + V_\omega(\mathbf{r}) + g_0 |\psi_0(\mathbf{r})|^2 \right] \psi_0(\mathbf{r}). \quad (8.8)$$

We assume repulsive interactions inside the trap: $g_0 > 0$. The interaction energy is large as compared to the kinetic energy. Neglecting the kinetic term $-\hbar^2 \nabla_{\mathbf{r}}^2 / (2m)$ in Eq. (8.8), we obtain

$$\psi_0(\mathbf{r}) = \sqrt{\frac{\mu - V_\omega(\mathbf{r})}{g_0}}, \quad (8.9)$$

when $\mu > V_\omega(\mathbf{r})$ and 0 otherwise. For a harmonic $V_\omega(\mathbf{r})$, the density profile $|\psi_0(\mathbf{r})|^2$ has therefore the shape of an inverted parabola. Eq. (8.9) characterizes the local equilibrium between the interaction energy, on the one hand, and the trap potential, on the other hand, according to the relation

$$g_0 |\psi_0(\mathbf{r})|^2 + V_\omega(\mathbf{r}) = \mu. \quad (8.10)$$

This Thomas-Fermi equilibrium is depicted in Fig. 8.3.

Let us now characterize the Thomas-Fermi regime a bit more precisely. In the absence of interactions, the typical extent a_0 of the condensate can be obtained by applying the virial theorem to a condensate without interactions in its equilibrium state in a harmonic trap. Requiring that the kinetic energy of an atom $\sim \hbar^2 / (2ma_0^2)$ equals its potential energy $\sim m\omega^2 a_0^2 / 2$ we obtain $a_0 \sim \sqrt{\hbar / m\omega}$. In the Thomas-Fermi regime, however, repulsive interactions are strong and one expects the typical extent R_0 of the condensate to be much larger than a_0 . R_0 follows from Eq. (8.9):

$$R_0 = \sqrt{\frac{2\mu}{m\omega^2}}. \quad (8.11)$$

Applying the condition $R_0 \gg a_0$, we finally obtain

$$\mu \gg \hbar\omega, \quad (8.12)$$

which is the fundamental inequality of the Thomas-Fermi regime.

¹In this section, we add the subscript “0” to the wave function to indicate that we deal with the initial process of the expansion scenario.

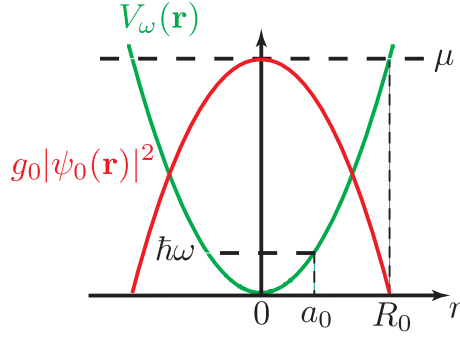


Figure 8.3: Drawing of a Bose-Einstein condensate of chemical potential μ trapped in a harmonic potential $V_\omega(\mathbf{r})$, in the Thomas-Fermi regime characterized by the local equilibrium between the interaction energy $g_0|\psi_0(\mathbf{r})|^2$ and the harmonic potential. In this regime, the typical extent of the condensate is R_0 , which is much larger than its extent a_0 in the absence of interactions.

8.3.2 Opening of the trap. Scaling

The process of opening of the trap is modeled by a time-dependent trap potential. The Gross-Pitaevskii equation then reads

$$i\hbar\partial_t\psi(\mathbf{r},t) = \left[\frac{-\hbar^2}{2m}\nabla_{\mathbf{r}}^2 + V_\omega(\mathbf{r},t) + g_0|\psi(\mathbf{r},t)|^2 \right] \psi(\mathbf{r},t). \quad (8.13)$$

A brutal turning off of V_ω at $t = 0$ is described by

$$V_\omega(\mathbf{r},t) = \frac{1}{2}m\omega(t)^2r^2, \quad (8.14)$$

with $\omega(t) = \omega = \text{const}$ for $t < 0$ and $\omega(t) = 0$ for $t > 0$. Although immediately after the release from the trap, interactions are still strong, we cannot directly neglect the kinetic term in Eq. (8.13) as in Sec. 8.3.1, because the interaction energy $g_0|\psi(\mathbf{r},t)|^2$ is progressively converted into the kinetic energy during expansion. The idea of [97, 98] is to make use of a unitary transformation of the wave function including, notably, a scaling in \mathbf{r} , in order to get rid of the kinetic term in Eq. (8.13). By making such a transformation one obtains the following solution of Eq. (8.13) (see Refs. [97, 98] for details):

$$\psi(\mathbf{r},t) = \exp \left[-i\beta(t) + imr^2 \frac{\dot{\lambda}(t)}{2\hbar\lambda(t)} \right] \frac{\psi_0(\mathbf{r}/\lambda(t))}{\lambda(t)^{3/2}}, \quad (8.15)$$

where λ and β are two scaling functions that obey

$$\dot{\beta}(t) = \frac{\mu}{\hbar\lambda(t)^3} \text{ and } \ddot{\lambda}(t) = \frac{\omega^2}{\lambda(t)^4}, \quad (8.16)$$

and ψ_0 is the wave function at $t = 0$ given by Eq. (8.9). Eq. (8.15) shows that the inverted parabola shape of the density profile is preserved during the expansion. More important, solution (8.15) also preserves the normalization of the wave function $\int d^3\mathbf{r}|\psi(\mathbf{r},t)|^2 = N$.

8.3.3 Momentum distribution at long times

We are interested in the momentum distribution of the condensate at long times. Its calculation requires the knowledge of the functions λ and β . Although Eqs. (8.16) do not admit any analytical solutions, a numerical study indicates that at long times $t \gg 1/\omega$, $\lambda(t) \simeq \sqrt{2/3}\omega t$. Substituting this solution into Eq. (8.15), we obtain

$$\psi(\mathbf{k}, t) = \exp[-i\beta(t)] \left(\frac{3}{2\omega t}\right)^{3/2} \int d^3\mathbf{r} \psi_0\left(\sqrt{\frac{3}{2}}\frac{r}{\omega t}\right) \exp\left(\frac{imr^2}{2t} - i\mathbf{k} \cdot \mathbf{r}\right). \quad (8.17)$$

The integral over \mathbf{r} can be evaluated by means of the stationary phase approximation. At long times $t \gg 1/\omega$, this gives the momentum distribution of the condensate that we denote $|\phi_0(\mathbf{k})|^2$:

$$|\psi(\mathbf{k}, t \gg 1/\omega)|^2 = |\phi_0(\mathbf{k})|^2 = |\phi_0(\mathbf{0})|^2 \left(1 - \frac{k^2}{2k_\mu^2}\right) \mathcal{H}\left(1 - \frac{k}{\sqrt{2}k_\mu}\right), \quad (8.18)$$

where we have introduced the wave number $k_\mu = \sqrt{2m\mu/\hbar^2}$ at energy μ and the Heaviside step function \mathcal{H} .

Although we have considered a three-dimensional initial trap, Eq. (8.18) turns out to be valid in any dimension. That is the reason why we have not detailed the exact prefactor $|\phi_0(\mathbf{0})|^2$ in front of the momentum distribution. This prefactor can be readily obtained by making use of conservation of the total number of atoms and depends on the dimensionality. In the following two chapters, we consider both expansion in a waveguide of cross-section A (quasi one-dimensional geometry) and expansion in an unbounded three-dimensional space. We have, respectively,

$$|\phi_0^{\text{quasi-1D}}(\mathbf{0})|^2 = \frac{6\pi N A}{4\sqrt{2}k_\mu} \quad \text{and} \quad |\phi_0^{\text{3D}}(\mathbf{0})|^2 = \frac{15\pi^2 N}{2\sqrt{2}k_\mu^3}. \quad (8.19)$$

8.4 Conclusion

In this introductory chapter we laid foundations of the theory of weakly interacting Bose-Einstein condensates in the presence of an external potential, by introducing the dynamic Gross-Pitaevskii equation. We also presented a theoretical toy model allowing for a coherent description of experiments with BECs expanding in random potentials: the condensate is produced in a trap (initial stage), from where it is released. The expansion of the condensate can then be divided in two stages. At the first stage the expansion is mainly driven by atomic interactions, whereas at the second stage interactions become weak. The next two chapters will describe the expansion of the condensate in the random potential starting from the moment in time when interactions become negligible (Chapter 9) or weak (Chapter 10).

We end up this section with a few quantitative estimates. We introduced several length scales throughout this chapter: the scattering length a_s of the interaction potential, the extent a_0 of a non-interacting trapped condensate, the extent R_0 of a

strongly interacting trapped condensate and the wave number k_μ at energy μ ($1/k_\mu$ is sometimes called the healing length). Anticipating the next chapter, we can also introduce the mean free path ℓ , the average distance between two scattering events for an atom in the random potential. All these length scales typically order in the following way:

$$\underbrace{a_s}_{1 \text{ nm}} \ll \underbrace{1/k_\mu}_{0.1 \text{ } \mu\text{m}} \ll \underbrace{a_0}_{1 \text{ } \mu\text{m}} \ll \underbrace{R_0 \sim \ell}_{10 \text{ } \mu\text{m}}. \quad (8.20)$$

Note in particular that, for a usual atomic density of 10^{15} cm^{-3} , we have $n^{-1/3} \sim 100 \text{ nm}$ which is much larger than the scattering length. Condition (8.2) is thus typically fulfilled in experiments with BECs². Finally, in typical experiments the expansion of the condensate lasts for a few seconds, and the time $1/\omega$ after which Eq. (8.18) applies is typically $\sim 30 \text{ ms}$.

²Except, of course, in those dealing with particularly strong interactions, like in [99], where the authors observed the first hints suggesting a Bose-glass phase for a strongly interacting BEC in a random potential.

CHAPTER 9

Matter-wave speckle patterns

Contents

9.1 Preliminaries	112
9.1.1 Gross-Pitaevskii equation	112
9.1.2 Random potential	113
9.1.3 Quasi one-dimensional geometry	114
9.2 Density speckle and average density profile	115
9.2.1 Density speckle pattern	115
9.2.2 Average density profile of a BEC expanding in a quasi one-dimensional waveguide	116
9.2.3 Validity of the analysis	118
9.3 \mathcal{C}_1 and \mathcal{C}_2 correlation functions	119
9.3.1 Diagrammatic approach	119
9.3.2 Short-range \mathcal{C}_1 correlation	119
9.3.3 Long-range \mathcal{C}_2 correlation	120
9.4 Conclusion	125

ARMED with the considerations of Chapter 8 we can now get to the heart of the matter and study the expansion of a Bose-Einstein condensate in a random potential. In the present chapter we are interested in the statistical fluctuations of the atomic density $n(\mathbf{r}, t)$ due to the randomness of the potential. Recently, P. Henseler and

B. Shapiro [100] showed that a BEC in a random potential is characterized by a complicated, highly irregular density pattern reminiscent of what we know as speckle in optics (see Chapter 6). According to Ref. [100], multiple scattering from the potential completely randomizes $n(\mathbf{r}, t)$ and reduces the correlation length of atomic speckle pattern to a value of the order of the healing length $1/k_\mu$ of the initial trapped condensate, which is the minimal possible correlation length for a coherent matter wave. The “matter-wave speckle pattern” is therefore a random arrangement of small regions of high and low density. The short-range correlation associated with this structure is called \mathcal{C}_1 by analogy with the case of classical waves studied in Chapter 6. Physically, this correlation results from the scattering of the condensate immediately preceding the observation and can thus be seen as a diffraction-like effect. The key point is that, in principle, the macroscopic coherence of the condensate should give rise to genuine interference effects that were ignored in Ref. [100]. For classical waves, these correlations are long-range and are called \mathcal{C}_2 . The purpose of this chapter is to investigate these correlations in an expanding BEC and to answer the following two questions: are these correlations still long-range for BECs? Do they vary with time and how do they compare to the short-range correlations introduced in Ref. [100]?

This chapter is divided in three parts. First, we introduce the model of random potential and the quasi one-dimensional geometry. We then study the density profile of a BEC during expansion in the random potential and discuss the notion of “matter-wave speckle pattern” by calculating the short-range \mathcal{C}_1 density correlations introduced in Ref. [100]. Finally, in the third part we develop the formalism which allows us to analyze to the long-range \mathcal{C}_2 density correlations.

9.1 Preliminaries

9.1.1 Gross-Pitaevskii equation

From here on, the origin of time is chosen at a time $\gg 1/\omega$ after the release of the condensate from the trap (see the toy model of Sec. 8.2), *i.e.* when the condensate is sufficiently dilute and atomic interactions weak. As a consequence, in this chapter we neglect atomic interactions. We shall come back to this assumption in Chapter 10.

For $t > 0$, the wave function of the condensate $\psi(\mathbf{r}, t)$ obeys the Gross-Pitaevskii equation (8.6) which, in the absence of interactions, reduces to a linear Schrödinger equation:

$$i\hbar \frac{\partial \psi(\mathbf{r}, t)}{\partial t} = \left[-\frac{\hbar^2}{2m} \nabla_{\mathbf{r}}^2 + V_{\text{ext}}(\mathbf{r}) \right] \psi(\mathbf{r}, t), \quad (9.1)$$

with the initial condition $\psi(\mathbf{r}, t = 0) = \phi_0(\mathbf{r})$, where ϕ_0 has been introduced in Sec. 8.3.3. The potential $V_{\text{ext}}(\mathbf{r}) = V_{\perp}(r) + V(\mathbf{r})$, where $V(\mathbf{r})$ is the random potential and $V_{\perp}(r)$ is a confining potential. Both are described in details in Secs. 9.1.2 and 9.1.3.

It is important to understand the physical meaning of the chemical potential μ . We saw in Chapter 8 that immediately after the release of the condensate from its trap, μ is the typical energy of atomic interactions (Eq. (8.10)). When the trap is turned off, this energy is converted into kinetic energy, until interactions become negligible. Therefore, in this chapter, μ gives the typical kinetic energy of atoms.

9.1.2 Random potential

As in the first two parts of this thesis, we assume a white-noise Gaussian statistics for the random potential (disorder) $V(\mathbf{r})$. The correlation function of the random potential reads [16]

$$\overline{V(\mathbf{r})V(\mathbf{r}')} = \frac{\hbar^4\pi}{m^2\ell}\delta(\mathbf{r} - \mathbf{r}'). \quad (9.2)$$

If this model has the merit of being simple from the theoretical point of view, it is not well adapted to the direct description of experiments. That is the reason why at the end of the chapter we shall also discuss the more physical case of the correlated “speckle potential”. Note that the term “speckle” here comes from the fact that the light beam used to produce the random potential is transmitted through a diffusive plate and thus generates an optical speckle. It should not be confused with the term “speckle” used throughout this chapter and referring to the random density pattern generated by the expanding condensate itself. The correlation function of the correlated speckle potential is given by [101]

$$\overline{V(\mathbf{r})V(\mathbf{r}')} = v_R^2 \left[\frac{\sin(|\mathbf{r} - \mathbf{r}'|/\sigma_R)}{|\mathbf{r} - \mathbf{r}'|/\sigma_R} \right]^2, \quad (9.3)$$

where v_R and σ_R are the amplitude and the correlation length of the random potential, respectively. The limit $v_R \rightarrow \infty$ and $\sigma_R \rightarrow 0$ with $v_R^2\sigma_R^3 = \text{const} = \hbar^4/(m^2\ell\sqrt{\pi})$ corresponds to the uncorrelated white-noise random potential (9.2). A typical realization of the speckle potential is drawn in Fig. 9.1.

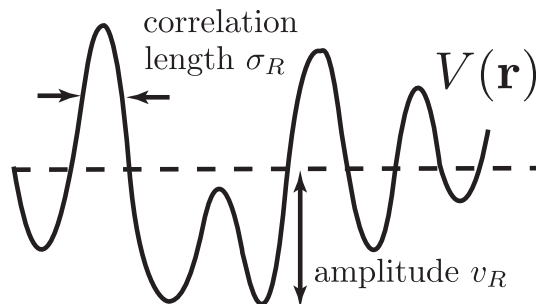


Figure 9.1: Drawing of a typical realization of the speckle potential as a function of position (in one dimension for clarity). The amplitude v_R and the correlation length σ_R are indicated.

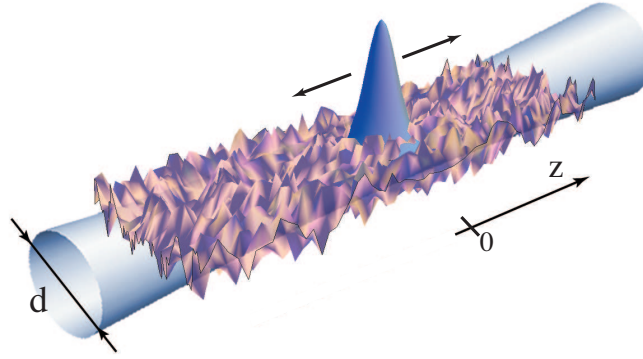


Figure 9.2: Drawing of a BEC expanding in a three-dimensional random potential and confined transversally to a waveguide of typical diameter d . We assume $2\pi/k_\mu \ll d \lesssim \ell$.

9.1.3 Quasi one-dimensional geometry

The potential $V_\perp(r)$ that appears in Eq. (9.1) is used to confine the BEC in particular directions of space. In this chapter, we assume that when expanding in the random potential, the condensate is constrained in a “tube” of diameter d and transverse cross-section $A = \pi d^2/4$. In experiments, this “tube” can be realized by means of a confining optical or magneto-optical potential in the transverse direction. For the sake of simplicity, $V_\perp(r)$ is chosen to be zero for $r < d/2$ and infinite for $r > d/2$ ¹. This geometry is depicted in Fig. 9.2. The confining potential $V_\perp(r)$ restricts the expansion of the BEC to a quasi one-dimensional waveguide:

$$2\pi/k_\mu \ll d \lesssim \ell. \quad (9.4)$$

Eq. (9.4) is the matter-wave counterpart of Eq. (6.5) and carries the same physical meaning: the first inequality indicates that the condensate expands in a *three-dimensional* space, whereas the second inequality imposes a *one-dimensional* diffusion process along the longitudinal direction. In quasi one-dimensional geometry, the localization length at energy μ is typically $\xi_\mu \sim \ell(k_\mu d)^2$. From this expression, we immediately deduce that when $k_\mu d \gg 1$ (first inequality (9.4)), the localization length much exceeds the mean free path. Therefore, the condensate starts to “feel” the effects of Anderson localization only after an initial stage of diffusive expansion. This is the main difference with recent experiments [87, 88, 89, 35, 90] which focused on the purely one-dimensional case $k_\mu d \sim 1$ and $\xi_\mu \sim \ell$.

To sum up, the condition (9.4) implies the following scenario: the condensate expands by diffusion along the longitudinal direction until $|z| \sim \xi_\mu \gg \ell$ before it starts to be affected by the effects of Anderson localization. The macroscopic expansion is one-dimensional along the z -direction, but at the microscopic scales the atoms of the condensate see a fully three-dimensional random potential.

¹In experiments [87, 88, 89, 35, 90], V_\perp is roughly harmonic, such that the transverse confining tube resembles more a hyperboloid of weak curvature.

9.2 Density speckle and average density profile

9.2.1 Density speckle pattern

When dealing with a Bose-Einstein condensate expanding in a random potential, a natural quantity of interest is the atomic density $n(\mathbf{r}, t) = |\psi(\mathbf{r}, t)|^2$. Due to the random potential, this quantity is random, namely it rapidly fluctuates as a function of position. It is convenient to decompose n in a sum of its statistical mean (over many realizations of the random potential) \bar{n} and its fluctuating part δn which is a random function. For a given realization of random potential, the density profile n typically looks like the blue curve depicted in Fig. 9.3. It fluctuates due to δn : this profile is the “density speckle pattern”. On the contrary, the *average* density profile \bar{n} does not fluctuate. It is depicted by the smooth red curve in Fig. 9.3.

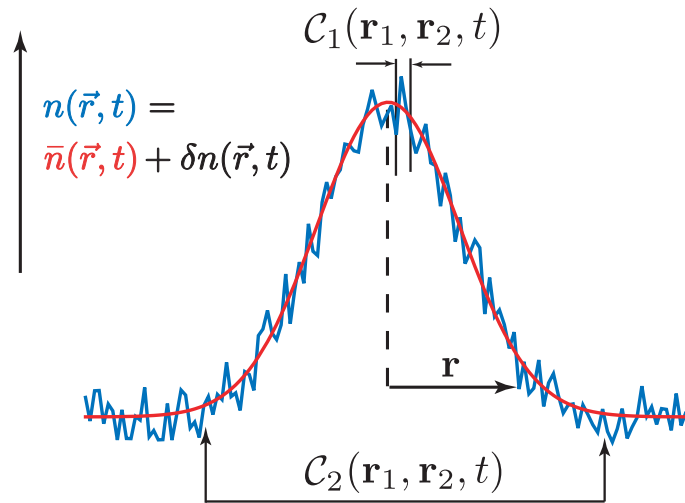


Figure 9.3: Typical density profile $n(\mathbf{r}, t)$ of the condensate (blue curve). The speckle disappears when the average over realizations of disorder is taken (red curve). The \mathcal{C}_1 part of the correlation function of density fluctuations is short-range and the \mathcal{C}_2 part is long-range.

Generally speaking, the statistics of the random function δn can be characterized by the two-point correlation function

$$\frac{\overline{\delta n(\mathbf{r}_1, t_1) \delta n(\mathbf{r}_2, t_2)}}{\overline{n(\mathbf{r}_1, t_1)} \times \overline{n(\mathbf{r}_2, t_2)}}. \quad (9.5)$$

Eq. (9.5) is the matter-wave counterpart of the intensity correlation function (6.4) that we defined for classical waves. For the sake of simplicity, in the following we restrict our consideration to the case $t_1 = t_2 = t$. Although the exact calculation of this correlation function is hopeless, by analogy with Eq. (6.2.3), we can formally decompose it in two parts \mathcal{C}_1 and \mathcal{C}_2 that are the zeroth and first order of perturbation

theory in the strength of the random potential, respectively:².

$$\frac{\overline{\delta n(\mathbf{r}_1, t)\delta n(\mathbf{r}_2, t)}}{n(\mathbf{r}_1, t) \times n(\mathbf{r}_2, t)} = \mathcal{C}_1(\mathbf{r}_1, \mathbf{r}_2, t) + \mathcal{C}_2(\mathbf{r}_1, \mathbf{r}_2, t). \quad (9.6)$$

Here we consider a slightly different situation than that studied in Chapter 6 for classical waves. Indeed, now we are not interested in the speckle pattern observed in transmission through the waveguide, but in the speckle pattern inside the waveguide. In other words, we study correlations between points \mathbf{r}_1 and \mathbf{r}_2 inside the waveguide. By analogy with previous works on optical speckle patterns [67, 102, 103, 104], \mathcal{C}_1 and \mathcal{C}_2 are expected to be short- and long-range, respectively. Here “short-” or “long-range” refers to the range of the corresponding correlation function in space: \mathcal{C}_1 is expected to be non-zero only for points \mathbf{r}_1 and \mathbf{r}_2 that are close to each other, whereas \mathcal{C}_2 is expected to decay slowly with $|\mathbf{r}_1 - \mathbf{r}_2|$. The role of \mathcal{C}_1 and \mathcal{C}_2 correlation functions is illustrated in Fig. 9.3.

9.2.2 Average density profile of a BEC expanding in a quasi one-dimensional waveguide

Let us first look at the average density profile $\bar{n}(\mathbf{r}, t) = \overline{|\psi(\mathbf{r}, t)|^2}$ of an expanding BEC in a waveguide. We start from the Gross-Pitaevskii equation (9.1). The wave function of the condensate at time t and position \mathbf{r} is given by

$$\psi(\mathbf{r}, t) = \int \frac{d\epsilon}{2\pi} \int d^3\mathbf{r}' G_\epsilon(\mathbf{r}, \mathbf{r}') \phi_0(\mathbf{r}') e^{-i\epsilon t/\hbar}, \quad (9.7)$$

where G_ϵ is the Green’s function of Eq. (9.1). $\phi_0(\mathbf{r})$ is the initial wave function of the condensate (Sec. 8.18). The atomic density averaged over realizations of the random potential then reads

$$\begin{aligned} \bar{n}(\mathbf{r}, t) = \overline{|\psi(\mathbf{r}, t)|^2} &= \int \frac{d\epsilon_1}{2\pi} \frac{d\epsilon_2}{2\pi} \int d^3\mathbf{r}_1 d^3\mathbf{r}_2 \overline{G_{\epsilon_1}(\mathbf{r}, \mathbf{r}_1) G_{\epsilon_2}^*(\mathbf{r}, \mathbf{r}_2)} \times \\ &\times \phi_0(\mathbf{r}_1) \phi_0^*(\mathbf{r}_2) e^{-i(\epsilon_1 - \epsilon_2)t/\hbar}. \end{aligned} \quad (9.8)$$

The calculation of the four integrals in Eq. (9.8) requires the knowledge of the product $\overline{GG^*}$. In the weak disorder limit $k_\mu \ell \gg 1$ it is given by the diagram depicted in Fig. 9.4. The gray part of this diagram represents, as usual, a sum of ladder diagrams detailed in Fig. 3.2.

At large distances $z \gg \ell$ and long times $t \gg \ell/v_\mu$, where $v_\mu = \hbar k_\mu/m$ is the velocity of an atom with kinetic energy μ , \bar{n} is independent of the transverse directions x, y and Eq. (9.8) leads to [91, 100]

$$\bar{n}(z, t) = \int_{-\infty}^{\infty} \frac{dk}{2\pi} |\phi_0(k)|^2 C_{\epsilon_k}(z, t), \quad (9.9)$$

²Note that this decomposition is not the end of the story since we saw in Chapter 6 that a classical wave propagating in a disordered medium generates second-order \mathcal{C}_3 correlations as well. These correlations should also exist for condensates. However, their role is still an open question. They will not be considered in this chapter.

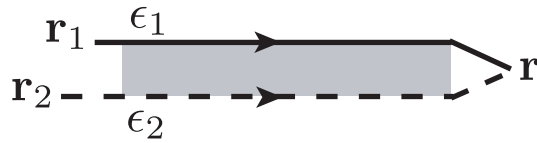


Figure 9.4: Main diagram contributing to $\overline{G_{\epsilon_1}(\mathbf{r}, \mathbf{r}_1)G_{\epsilon_2}^*(\mathbf{r}, \mathbf{r}_2)}$ in the weak disorder limit. The solid and dashed lines represent Green's functions G_{ϵ_1} and $G_{\epsilon_2}^*$, respectively. The gray part connecting G and G^* symbolizes a sum of ladder diagrams. This sum is detailed in Fig. 3.2.

where $\epsilon_k = \hbar^2 k^2 / (2m)$ and $C_\epsilon(z, t)$ is the probability to find an atom of energy ϵ , initially located at the origin, in the vicinity of $\mathbf{r} = (x, y, z)$ after a time t . The physical interpretation of Eq. (9.9) is transparent. However, its complete derivation from Eq. (9.8) is quite involved, and has been reported in Appendix D. The ‘‘diffusion propagator’’ C_ϵ has already been introduced in the first part of this thesis for classical waves, as a solution of the diffusion equation (3.8). There is no difference in the case of matter waves, and in the quasi one-dimensional geometry it is given by

$$C_\epsilon(z, t) = \frac{1}{A\sqrt{4\pi D_\epsilon t}} \exp\left(\frac{-z^2}{4D_\epsilon t}\right). \quad (9.10)$$

As compared to Eq. (3.8) for the diffusion propagator C_D , here we have dropped the subscript ‘‘ D ’’ for clarity and introduced the energy argument ϵ to indicate that C_ϵ describes propagation of an atom of energy ϵ . In the same spirit, we have replaced the subscript B in the Boltzmann diffusion coefficient D_B by ϵ . For matter-waves, this diffusion coefficient reads $D_\epsilon = v_\epsilon \ell / 3$, where $v_\epsilon = \sqrt{2\epsilon/m}$ is the velocity of an atom of energy ϵ . We remind that the constant A in Eq. (9.10) refers to the cross-section of the waveguide. Note that the fact that the average density profile only depends on the longitudinal position z is inherent of the quasi one-dimensional geometry: along the transverse directions x and y , n does fluctuate but \bar{n} is uniform.

The explicit calculation of $\bar{n}(\mathbf{r}, t)$ from Eqs. (9.9), (9.10) and (8.18) is straightforward and leads to:

$$\bar{n}(z, t) = \frac{N}{A\sqrt{D_\mu t}} h_1\left(\frac{z}{D_\mu t}\right), \quad (9.11)$$

where

$$h_1(x) = \frac{1}{160\sqrt{2}} \left\{ \sqrt{\frac{4\sqrt{2}}{\pi}} (96 + 2\sqrt{2}x - x^2) \exp\left(\frac{-x}{4\sqrt{2}}\right) + \sqrt{x}(-120 + x^2) \left[1 - \operatorname{erf}\left(\sqrt{\frac{x}{4\sqrt{2}}}\right) \right] \right\}, \quad (9.12)$$

with $\operatorname{erf}(x) = \int_0^x \exp(-u^2) du$. As the condensate expands, its typical size grows with time according to $\langle z^2 \rangle = \int z^2 \bar{n}(z, t) dz \simeq D_\mu t$. The linear growth of $\langle z^2 \rangle$ with time is typical for the diffusion process (this is a direct consequence of Eq. (2.1)).

It is interesting to note that the expansion of the condensate is characterized by a single parameter $D_\mu = v_\mu \ell / 3$: all goes as if the condensate behaved like a single atom of energy μ . D_μ can thus be regarded as the typical diffusion coefficient of the condensate.

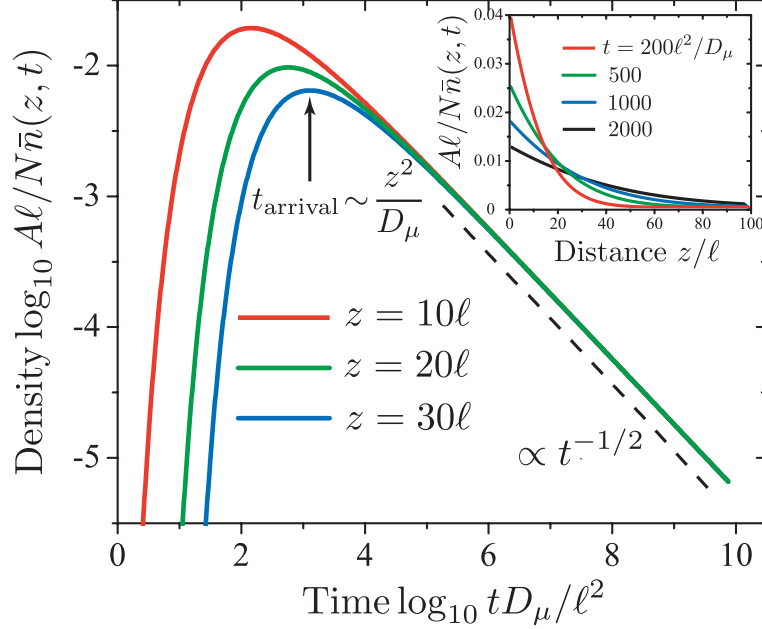


Figure 9.5: Ensemble-averaged atomic density \bar{n} of a BEC expanding in a three-dimensional random potential inside a quasi one-dimensional optical waveguide. The main plot shows \bar{n} as a function of time for three different distances z . The dashed line is a $1/\sqrt{t}$ asymptote. The inset shows \bar{n} as a function of z .

Profiles of atomic density are plotted as functions of z in the inset of Fig. 9.5. In the main plot of Fig. 9.5 we show \bar{n} as a function of time. The density reaches a maximum at the “arrival time” $t_{\text{arrival}} \sim z^2/D_\mu \sim (\ell/v_\mu)(z/\ell)^2$ and decays as $1/\sqrt{t}$ at long times $t > t_{\text{arrival}}$. This long-time limit is the most interesting regime to which we restrict our analysis from here on.

9.2.3 Validity of the analysis

As discussed in Sec. 9.1.3, in the waveguide geometry the localization length is given by $\xi_\mu \sim \ell(k_\mu d)^2$, and it is much larger than the mean free path, if $k_\mu d \gg 1$. For relatively short times, the typical extent of the condensate is much smaller than ξ_μ , such that the diffusive approach developed in this chapter is valid. However, the condensate expands along the z axis, and there exists some (long) time after which it starts feeling the effects of Anderson localization. This happens when the typical size of the condensate becomes of the order of the localization length ξ_μ . We have seen in the previous section that the typical size of the condensate at time t is given

by

$$\sqrt{\langle z^2 \rangle} \simeq \sqrt{D_\mu t}. \quad (9.13)$$

The condition $\sqrt{\langle z^2 \rangle} \simeq \xi_\mu$ leads to the following characteristic time after which the diffusion approach breaks down and Anderson localization sets in:

$$t_{\text{loc}} \sim \left(\frac{\ell}{v_\mu} \right) (k_\mu d)^4. \quad (9.14)$$

In all the following reasonings, we shall assume that $t < t_{\text{loc}}$. Interestingly, Eq. (9.14) could have been obtained in yet another way, by noticing that the prediction $\bar{n} \rightarrow 0$ for $t \rightarrow \infty$ of Eq. (9.11) is wrong because at very long times, localization “freezes” \bar{n} at values of the order of $N/(A\xi_\mu)$. By comparing $N/(A\xi_\mu)$ with the long-time limit of Eq. (9.11), one recovers the characteristic time t_{loc} of Eq. (9.14).

9.3 \mathcal{C}_1 and \mathcal{C}_2 correlation functions

9.3.1 Diagrammatic approach

In general, the calculation of density correlation functions is a difficult problem because it implies averaging a product of four wave functions over disorder. For matter waves, the problem is even more complicated because it implies a summation over energies of all atoms composing the condensate. From Eq. (9.7), the density correlation function (9.6) writes in a very general form:

$$\overline{\delta n(\mathbf{r}, t) \delta n(\mathbf{r}', t)} = \frac{1}{(2\pi)^4} \int \prod_{j=1}^4 d^3 \mathbf{r}_j d\epsilon_j e^{-\frac{i}{\hbar}(\epsilon_1 - \epsilon_2)t - \frac{i}{\hbar}(\epsilon_3 - \epsilon_4)t} K(\mathbf{r}, t; \mathbf{r}', t'; \{\mathbf{r}_j\}, \{\epsilon_j\}) \phi_0(\mathbf{r}_1) \phi_0^*(\mathbf{r}_2) \phi_0(\mathbf{r}_3) \phi_0^*(\mathbf{r}_4), \quad (9.15)$$

where the six-point kernel K is given by the connected part of a product of four Green’s functions, averaged over disorder:

$$K = \frac{G_{\epsilon_1}(\mathbf{r}, \mathbf{r}_1) G_{\epsilon_2}^*(\mathbf{r}, \mathbf{r}_2) G_{\epsilon_3}(\mathbf{r}', \mathbf{r}_3) G_{\epsilon_4}^*(\mathbf{r}', \mathbf{r}_4)}{G_{\epsilon_1}(\mathbf{r}, \mathbf{r}_1) G_{\epsilon_2}^*(\mathbf{r}, \mathbf{r}_2) \times G_{\epsilon_3}(\mathbf{r}', \mathbf{r}_3) G_{\epsilon_4}^*(\mathbf{r}', \mathbf{r}_4)}. \quad (9.16)$$

We stress that by writing Eqs. (9.15) and (9.16) we do nothing else than multiplying four wave functions (9.7). These equations are therefore still very general. Physically, density correlations result from interference processes between four scattering paths. These processes are encoded in the kernel K . In the next two sections, we consider \mathcal{C}_1 and \mathcal{C}_2 parts of the correlation function.

9.3.2 Short-range \mathcal{C}_1 correlation

We now consider the short-range part \mathcal{C}_1 of the density correlation function (9.6). The physical process leading to \mathcal{C}_1 involves four scattering paths that propagate in

independent pairs. Therefore, in some sense \mathcal{C}_1 does not really describe a genuine interference effect. The diagram of Fig. 9.6 gives the main contribution K_1 to the kernel K . By substituting the diagram K_1 into Eq. (9.15) we obtain:

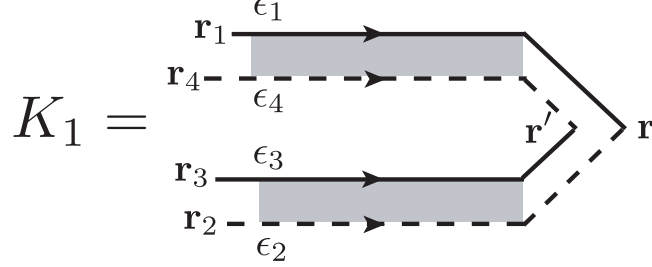


Figure 9.6: Diagram contributing to \mathcal{C}_1 . The meaning of lines and symbols is the same as in Fig. 9.4.

$$\mathcal{C}_1(\mathbf{r}, \mathbf{r}', t) = \frac{\left| \int \frac{d\epsilon_1}{2\pi} \frac{d\epsilon_4}{2\pi} \int d^3\mathbf{r}_1 d^3\mathbf{r}_4 e^{-\frac{i}{\hbar}(\epsilon_1 - \epsilon_4)t} \overline{G_{\epsilon_1}(\mathbf{r}, \mathbf{r}_1)} G_{\epsilon_4}^*(\mathbf{r}', \mathbf{r}_4) \phi_0(\mathbf{r}_1) \phi_0^*(\mathbf{r}_4) \right|^2}{\overline{n}(\mathbf{r}, t) \overline{n}(\mathbf{r}', t)}. \quad (9.17)$$

The calculation of the numerator of Eq. (9.18) is very similar to the calculation of \overline{n} . The result is

$$\mathcal{C}_1(\mathbf{r}, \mathbf{r}', t) = \frac{\left| \int_{-\infty}^{\infty} \frac{dk}{2\pi} C_{\epsilon_k}(z, t) \frac{\sin(k\Delta r)}{k\Delta r} \exp\left(\frac{-\Delta r}{2\ell}\right) |\phi_0(k)|^2 \right|^2}{\overline{n}(z, t) \overline{n}(z', t)}, \quad (9.18)$$

where $\Delta r = |\mathbf{r} - \mathbf{r}'|$. Densities at points \mathbf{r} and \mathbf{r}' appearing in the denominator of Eq. (9.18) are given by Eq. (9.11). The integral of the numerator has no analytical expression. It has to be evaluated numerically. \mathcal{C}_1 is plotted in Fig. 9.7 as a function of Δr . The correlation falls to zero for very short distances $\Delta r \sim 1/k_\mu$. Physically, this proves the very existence of the density speckle, consisting of an irregular pattern made of small regions of high and low density. The typical speckle size is $1/k_\mu$, the decay length of the correlation function. Surprisingly, \mathcal{C}_1 does practically not vary with time. This means that the typical speckle size remains unchanged as the condensate expands!

9.3.3 Long-range \mathcal{C}_2 correlation

The long-range part of the correlation function — \mathcal{C}_2 — can be obtained by using a next-order contribution to K : K_2 given by the diagram depicted in Fig. 9.8. This diagram represents an interference process between four matter waves that propagate in pairs to some point, where they interchange partners before continuing to the measurement points \mathbf{r} and \mathbf{r}' . A proper treatment of such a crossing of wave paths is guaranteed by the use of the Hikami box diagram — the H box in Fig. 9.8 — that has been introduced in Chapter 3. From Fig. 9.8, we find

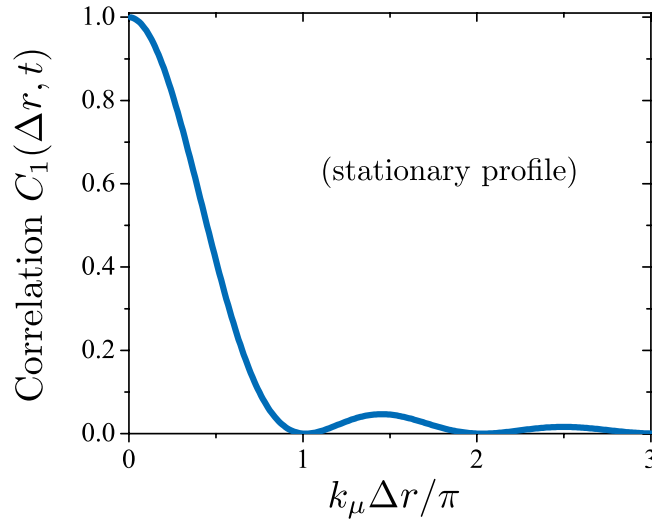


Figure 9.7: \mathcal{C}_1 correlation function as a function of the distance $\Delta r = |\mathbf{r} - \mathbf{r}'|$ between two points \mathbf{r} and \mathbf{r}' . The typical decay length is $1/k_\mu$. This profile is independent of time.

$$K_2 = \frac{H(\mathbf{r}_5, \mathbf{r}_6, \mathbf{r}_7, \mathbf{r}_8) \times \overline{G_{\epsilon_1}(\mathbf{r}_1, \mathbf{r}_8) G_{\epsilon_4}^*(\mathbf{r}_4, \mathbf{r}_8)} \times \overline{G_{\epsilon_3}(\mathbf{r}_3, \mathbf{r}_6) G_{\epsilon_2}^*(\mathbf{r}_2, \mathbf{r}_6)} \times \overline{G_{\epsilon_1}(\mathbf{r}, \mathbf{r}_5) G_{\epsilon_2}^*(\mathbf{r}, \mathbf{r}_5)} \times \overline{G_{\epsilon_3}(\mathbf{r}', \mathbf{r}_7) G_{\epsilon_4}^*(\mathbf{r}', \mathbf{r}_7)}}{(9.19)}$$

For matter waves, the Hikami box reads [16]

$$H(\mathbf{r}_5, \mathbf{r}_6, \mathbf{r}_7, \mathbf{r}_8) = \delta(\mathbf{r}_5 - \mathbf{r}_6) \delta(\mathbf{r}_6 - \mathbf{r}_7) \delta(\mathbf{r}_5 - \mathbf{r}_7) \frac{\ell^5 m^3}{3\pi \hbar^3 \epsilon_1} \nabla_{\mathbf{r}_5} \cdot \nabla_{\mathbf{r}_7}. \quad (9.20)$$

Substituting Eq. (9.19) into Eq. (9.15) and making use of Eq. (9.20), we obtain

$$\begin{aligned} \overline{\delta n(\mathbf{r}, t) \delta n(\mathbf{r}', t)} &= \frac{1}{(2\pi)^4} \int d^3 \mathbf{r}'' \prod_{j=1}^4 d\epsilon_j d^3 \mathbf{r}_j e^{-\frac{i}{\hbar}(\epsilon_1 - \epsilon_2)t - \frac{i}{\hbar}(\epsilon_3 - \epsilon_4)t} \times \\ &\nabla_{\mathbf{r}''} \left[\overline{G_{\epsilon_1}(\mathbf{r}_1, \mathbf{r}'') G_{\epsilon_4}^*(\mathbf{r}_4, \mathbf{r}'')} \right] \cdot \nabla_{\mathbf{r}''} \left[\overline{G_{\epsilon_3}(\mathbf{r}_3, \mathbf{r}'') G_{\epsilon_2}^*(\mathbf{r}_2, \mathbf{r}'')} \right] \times \\ &\overline{G_{\epsilon_1}(\mathbf{r}, \mathbf{r}'') G_{\epsilon_2}^*(\mathbf{r}, \mathbf{r}'')} \times \overline{G_{\epsilon_3}(\mathbf{r}', \mathbf{r}'') G_{\epsilon_4}^*(\mathbf{r}', \mathbf{r}'')} \phi(\mathbf{r}_1) \phi^*(\mathbf{r}_2) \phi(\mathbf{r}_3) \phi^*(\mathbf{r}_4). \end{aligned} \quad (9.21)$$

After some algebra, Eq. (9.21) becomes

$$\begin{aligned} \overline{\delta n(\mathbf{r}, t) \delta n(\mathbf{r}', t)} &= \frac{2\pi \ell \hbar^2 A}{3m^2 (2\pi)^4} \int_{-\infty}^{\infty} dz_1 \left[\prod_{j=1}^2 dk_j d\Omega_j |\phi(k_j)|^2 P_{\epsilon_{k_j}}(z_1, \Omega_j) \right] \\ &\times \partial_{z_1} C_{\epsilon_-}(z - z_1, \Omega_-) \partial_{z_1} C_{\epsilon_+}(z' - z_1, \Omega_+) e^{-i(\Omega_+ + \Omega_-)t}, \end{aligned} \quad (9.22)$$

where $\epsilon_{\pm} = [\epsilon_{k_1} + \epsilon_{k_2} \pm \hbar(\Omega_1 - \Omega_2)/2]/2$ and $\Omega_{\pm} = \pm(\epsilon_{k_1} - \epsilon_{k_2}) + (\Omega_1 + \Omega_2)/2$. Here we have introduced the three-dimensional diffusion propagator

$$C_{\epsilon}(z, \Omega) = \exp(-|z| \sqrt{-i\Omega/D_{\epsilon}}) / 2A \sqrt{-i\Omega D_{\epsilon}}, \quad (9.23)$$

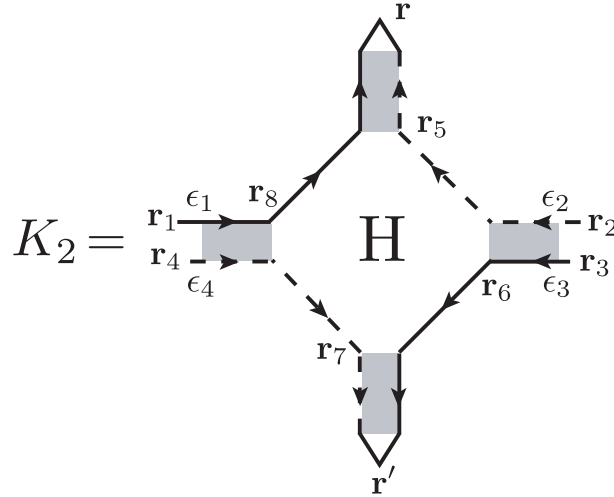


Figure 9.8: Diagram for the kernel K_2 generating the long-range correlation function of density fluctuations \mathcal{C}_2 . Lines and symbols have the same meaning as in the diagrams of Fig. 9.4. H is the Hikami box whose expression is given in the main text.

which is nothing but the Fourier transform of Eq. (9.10) with respect to time.

At first sight, the physical meaning of Eq. (9.22) is not at all obvious. The multiple integral is difficult to perform due to the complicated coupling between energies and momenta. However it can be evaluated numerically by means of the Monte-Carlo integration technique, and allows for partial analytical analysis in some special cases, as we now show.

9.3.3.1 Variance of the atomic density

The simplest quantity that Eq. (9.22) allows us to study is the correction to the (normalized) variance of the atomic density fluctuations:

$$\frac{\overline{\delta n^2(\mathbf{r}, t)}}{\overline{n^2(\mathbf{r}, t)}} = \underbrace{\mathcal{C}_1(\mathbf{r}, \mathbf{r}, t)}_{=1} + \mathcal{C}_2(\mathbf{r}, \mathbf{r}, t). \quad (9.24)$$

The \mathcal{C}_2 term in Eq. (9.24) follows from Eq. (9.22) and can be conveniently written as

$$\mathcal{C}_2(\mathbf{r}, \mathbf{r}, t) = \frac{2}{k_\mu^2 A \sqrt{k_\mu \ell}} c(\zeta, \tau), \quad (9.25)$$

Here we have introduced dimensionless variables $\zeta = z\sqrt{k_\mu \ell}/\ell$ and $\tau = t\mu/\hbar$ that feature natural spatial and temporal scales of the problem. A combinatorial factor 2 has been added. The dependence of \mathcal{C}_2 on position ζ and time τ appears to be given by a universal function $c(\zeta, \tau)$ that does not depend on any parameters of the problem. We plot this function in Fig. 9.9 for three fixed values of τ . It is quadratic in ζ for small $\zeta \ll \tau^{1/4}$: $c(\zeta, \tau) \simeq A_1 \tau^{3/4} [1 - A_2 (\zeta/\tau^{1/4})^2]$ and decays as $A_3 \tau/\zeta$ for

$\zeta \gg \tau^{1/4}$. Here $A_1 \simeq 6.3$, $A_2 \simeq 0.3$ and $A_3 \simeq 1.9$ are constants that have to be calculated numerically.

$c(\zeta, \tau)$ grows with time as $\tau^{3/4}$ for $\zeta \ll \tau^{1/4}$ as we also show in the inset of Fig. 9.9. This amplification of $c(\zeta, \tau)$ with time can make \mathcal{C}_2 significant for large τ , despite the small prefactor in front of c in Eq. (9.25). In particular, $\mathcal{C}_2(\mathbf{r}, \mathbf{r}, t)$ becomes of order 1 (*i.e.*, of the same order as \mathcal{C}_1) for

$$t \sim (\ell/v_\mu)(k_\mu d)^{8/3}(k_\mu \ell)^{-1/3}, \quad (9.26)$$

which is still smaller than the localization time t_{loc} that limits the validity of our analysis (see Sec. 9.2.3).

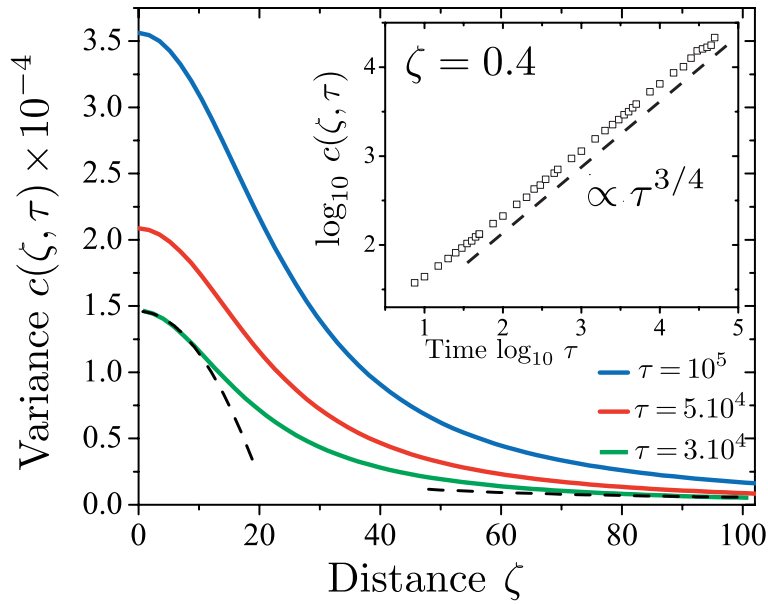


Figure 9.9: Position dependence of the correction c to the variance of atomic density in an expanding BEC for three different times $\tau = t\mu/\hbar$. The dimensionless distance is $\zeta = z\sqrt{k_\mu\ell}/\ell$. The dashed lines show analytic results $A_1\tau^{3/4}[1 - A_2(\zeta/\tau^{1/4})^2]$ (small ζ) and $A_3\tau/\zeta$ (large ζ) for $\tau = 3 \times 10^4$. The numerical constants A_1 , A_2 and A_3 are given in the text. The inset shows the time dependence of c for a given (small) $\zeta = 0.4$.

9.3.3.2 Correlation between distant points

We now treat the particular case of correlations of density at two points symmetric with respect to the origin: $z = -z' = \Delta z/2 \gg \ell$. The result is expected to be qualitatively similar for any sufficiently distant z and z' of opposite sign. Eq. (9.22) yields

$$\mathcal{C}_2(\mathbf{r}, \mathbf{r}', t) = \frac{1}{k_\mu^2 A \sqrt{k_\mu \ell}} c_2(\Delta\zeta, \tau). \quad (9.27)$$

We show c_2 in Fig. 9.10 as a function of $\Delta\zeta$ for three different times. For small distances $\Delta\zeta \ll \tau^{1/4}$, the correlation decays linearly with $\Delta\zeta$: $c_2(\Delta\zeta, \tau) \simeq A_1\tau^{3/4}(1 - A_4\Delta\zeta/\tau^{1/4})$, where $A_4 \simeq 2$. At $\Delta\zeta \sim \tau^{1/4}$, it becomes *negative* and reaches a minimum. For longer distances $\Delta\zeta \gg \tau^{1/4}$, c_2 remains negative whereas its magnitude decays only algebraically: $c_2 \simeq -A_5\tau/\Delta\zeta$ with $A_5 \simeq 1.2$. In addition to having long range is space, C_2 correlation grows in magnitude with time (see the inset of Fig. 9.10), similarly to the variance of δn . This property should facilitate its experimental observation.

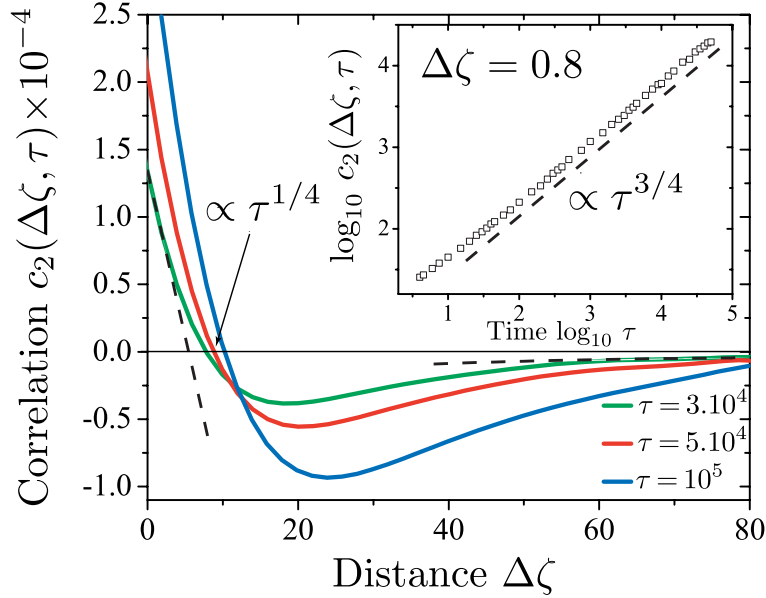


Figure 9.10: Long-range correlation function c_2 versus dimensionless distance $\Delta\zeta = 2\zeta$ (solid lines) for three different times $\tau = t\mu/\hbar$. The dashed lines show asymptotes $A_1\tau^{3/4}(1 - A_4\Delta\zeta/\tau^{1/4})$ and $-A_5\tau/\Delta\zeta$ for $\tau = 3 \times 10^4$. The numerical constants A_1 , A_4 and A_5 are given in the text. The inset shows the time dependence of the correlation for $\Delta\zeta = 0.8$.

Negative correlations of atomic density in an expanding BEC could be anticipated from the conservation of atom number N which implies $\int d^3\mathbf{r} \delta n(\mathbf{r}, t) \delta n(\mathbf{r}', t) = 0$ and thus requires that the integrand must change sign. (Note that Eq. (9.22) obeys this condition *exactly*.) The important result of our work is to show that negative correlations occur at large distances between points \mathbf{r} and \mathbf{r}' and that they become increasingly important as the condensate expands. Negative correlations of similar origin were predicted to exist in reflection of waves from a thick disordered slab [105]. The analysis of long-range correlations introduces a new characteristic length scale $\zeta^* \sim \tau^{1/4}$ or $z^* \sim (D_\mu t \cdot \ell/k_\mu)^{1/4}$ which is much smaller than the root mean square size of the condensate $\langle z^2 \rangle^{1/2}$. It determines the typical separation between two points, situated symmetrically with respect to the initial location of the condensate, at which density correlations change sign.

9.3.3.3 Physical interpretation of \mathcal{C}_1 and \mathcal{C}_2

From the calculation of \mathcal{C}_1 and \mathcal{C}_2 , we can refine the qualitative scenario of condensate expansion given in the beginning of the chapter (Fig. 9.3). During the expansion, the randomness of the potential makes the density of the condensate fluctuate at short length scales, and these fluctuations do not vary in time. At short times after the beginning of the expansion, the effect of \mathcal{C}_2 is weak and correlations between different points of the condensate are mainly given by \mathcal{C}_1 . After a certain time, however, distant points start to be anti-correlated (\mathcal{C}_2 becomes negative). This anti-correlation may show up through a random displacement of the center of mass M of the condensate. Since the magnitude of \mathcal{C}_2 increases with time, we expect this displacement to increase as well. We can estimate the mean-square amplitude $\langle z_{\text{CM}}^2 \rangle = \int d^3\mathbf{r} \int d^3\mathbf{r}' z z' \overline{\delta n(\mathbf{r}, t) \delta n(\mathbf{r}', t)}$ of this random displacement by identifying it with the distance Δz at which \mathcal{C}_2 become negative. We thus deduce $\sqrt{\langle z_{\text{CM}}^2 \rangle} \propto t^{1/4}$. This scenario is illustrated in Fig. 9.11.

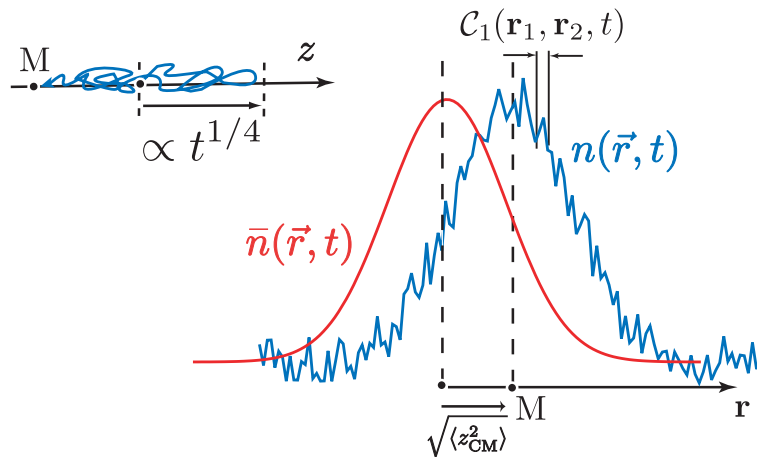


Figure 9.11: Drawing of the density speckle pattern (blue curve) at a given time. The average density profile of the condensate is indicated in red. \mathcal{C}_1 describes the short-range density fluctuations that do not vary with time. \mathcal{C}_2 describes the random displacement of the center of mass M of the condensate. The root mean-square amplitude $\sqrt{\langle z_{\text{CM}}^2 \rangle}$ of this random displacement (inset) grows with time as $t^{1/4}$.

9.4 Conclusion

We investigated the structure of the density speckle pattern generated by a Bose-Einstein condensate expanding in a disordered waveguide. Our study showed that this structure is very different from that of a typical intensity speckle pattern produced, for instance, by a monochromatic light propagating in a disordered medium. Even though at short length scales the density speckle pattern $n(\mathbf{r}, t)$ is made of small independent spots, the macroscopic coherence of the condensate imposes correlations between distant points, enhanced at long times. As a consequence, the

density speckle pattern appears to have a much more complex and nontrivial spatial structure than just a random arrangement of small regions of high and low density. One may interpret the long-range correlations as a sign of random displacement of the center of mass of the condensate, growing with time.

Although in the present chapter we considered the uncorrelated, white-noise random potential, our results can be generalized to correlated potentials in a standard way [101]. In the first approximation, it is sufficient to replace the scattering mean free path by the transport mean free path ℓ_B at energy μ . For the speckle potential (Eq. (9.3)), the latter is given by

$$\ell_B = \frac{3k_\mu \hbar^4}{2\pi m^2 v_R^2 \sigma_R^2}. \quad (9.28)$$

We estimate that the long-range correlations should be directly observable under conditions of the experiment of Ref. [35] with a three-dimensional random potential and a slightly weaker transverse confinement of the condensate.

CHAPTER 10

Study of interactions

Contents

10.1 Perturbative treatment	128
10.2 Expansion in the absence of interactions	129
10.2.1 Diffusive expansion	130
10.2.2 Anderson localization	131
10.3 Nonlinear correction to the atomic density	133
10.3.1 Mean free path	133
10.3.2 Diffusion coefficient	134
10.4 Conclusion	137

IN the previous chapter we studied the diffusive expansion of a Bose-Einstein condensate in a quasi one-dimensional waveguide and discussed the structure of the density speckle pattern. Atomic interactions were neglected during expansion. At long times, the assumption of negligible interactions is known to be true in the absence of disorder [95]. At first sight, the same assumption seems also legitimate in the presence of a random potential because the condensate gets increasingly dilute during the expansion process. Therefore, provided that the disorder is weak enough, the neglect of interactions seems to be a good approximation.

In the presence of a random potential, the assumption of negligible role of interactions was validated by numerical simulations in one dimension [96]. However, even in one dimension, no consensus on the effect of interactions on the expansion of BECs exists. Indeed, recent works suggest that even weak interactions may significantly affect the expansion of a condensate for a sufficiently strong disorder

[106, 107]. In higher dimensions and, especially, in three dimensions, there is neither analytical nor numerical work about this issue.

In this last chapter on Bose-Einstein condensates, we consider the expansion of a BEC in a three-dimensional random potential, in the absence of any confinement. Note that, in contrast to the case of the waveguide studied in Chapter 9, in three dimensions a critical energy separates localized from extended states (see the first part of the thesis). This leads to Anderson localization of the condensate under certain conditions. A systematic study of this issue was proposed recently by S. E. Skipetrov *et al.* [92]. Somewhat earlier, diffusive expansion of a BEC in a three-dimensional random potential was studied by B. Shapiro [91], neglecting effects of Anderson localization. In these works, however, atomic interactions were ignored during the expansion of BEC.

In this chapter, we put forward the first analytical study of nonlinear corrections due to atomic interactions to the density of a BEC expanding in a three-dimensional random potential. We make use of a perturbative approach in the interaction parameter g_0 of the dynamic Gross-Pitaevskii equation (8.6), and neglect Anderson localization. Therefore, we are interested in the effect of interactions on the *diffusive* expansion of the condensate.

The chapter is organized as follows. First, we introduce the main lines of our perturbative approach starting from the Gross-Pitaevskii equation. Second we detail the behavior of the average atomic density as a function of the amount of disorder, which allows us to define the limits of validity of the diffusion theory. Third, we calculate explicitly the first-order nonlinear correction to the average atomic density at long times. The effect of interactions on expansion, as well as the range of validity of our approach, are discussed in detail.

10.1 Perturbative treatment

Consider a weakly interacting Bose-Einstein condensate of $N \gg 1$ atoms of mass m expanding in a three-dimensional random potential $V(\mathbf{r})$. Again, the origin of time is chosen within the third stage of the toy model described in Chapter 8, which ensures that interactions are not too strong. As in Chapter 9, we calculate the density profile of the condensate, but this time without neglecting interactions. We still assume that the random potential follows a white-noise Gaussian statistics: $\overline{V(\mathbf{r})V(\mathbf{r}')} = (\hbar^4\pi/m^2\ell)\delta(\mathbf{r} - \mathbf{r}')$, where ℓ is the mean free path and the overline denotes averaging over realizations of the random potential. We treat the condensate in the framework of the dynamic Gross-Pitaevskii equation that we recall below:

$$i\hbar\frac{\partial\psi}{\partial t} = \left[-\frac{\hbar^2}{2m}\nabla_{\mathbf{r}}^2 + V(\mathbf{r}) + g_0|\psi|^2 \right] \psi. \quad (10.1)$$

Here $\psi(\mathbf{r}, t)$ is the wave function of the condensate and $g_0 = 4\pi\hbar^2 a_s/m$ is the strength of interactions, with a_s the scattering length. Note that the following reasoning is valid for both repulsive ($a_s > 0$) and attractive ($a_s < 0$) interactions. By Fourier

transforming Eq. (10.1) with respect to time, we obtain

$$\left[-\epsilon - \frac{\hbar^2}{2m} \nabla_{\mathbf{r}}^2 + V(\mathbf{r}) \right] \psi_{\epsilon}(\mathbf{r}) + g_0 \int_{-\infty}^{\infty} \frac{d\epsilon_1}{2\pi} \int_{-\infty}^{\infty} \frac{d\epsilon_2}{2\pi} \psi_{\epsilon_1}(\mathbf{r}) \psi_{\epsilon_2}^*(\mathbf{r}) \psi_{\epsilon-\epsilon_1+\epsilon_2}(\mathbf{r}) = 0. \quad (10.2)$$

Here $\psi_{\epsilon}(\mathbf{r}) = \int dt \psi(\mathbf{r}, t) \exp(i\epsilon t/\hbar)$. To describe the effect of weak interactions ($|g_0| \ll 1$) on the expansion of the condensate, we make use of perturbation theory and write $\psi_{\epsilon}(\mathbf{r}) = \psi_{\epsilon}^{(0)}(\mathbf{r}) + \delta\psi_{\epsilon}(\mathbf{r})$, where $|\delta\psi_{\epsilon}| \ll |\psi_{\epsilon}^{(0)}|$. A precise condition of validity of this approach will be given later on (see Sec. 10.3.2). In the following, the superscript (0) will refer to quantities free of interactions. Inserting this expression into Eq. (10.2) and keeping only the lowest-order terms in $\delta\psi_{\epsilon}$ and g_0 , we find that $\psi_{\epsilon}^{(0)}$ obeys the linear Schrödinger equation

$$\left[-\epsilon - \frac{\hbar^2}{2m} \nabla_{\mathbf{r}}^2 + V(\mathbf{r}) \right] \psi_{\epsilon}^{(0)}(\mathbf{r}) = 0, \quad (10.3)$$

whereas the first-order term $\delta\psi_{\epsilon}$ satisfies

$$\left[-\epsilon - \frac{\hbar^2}{2m} \nabla_{\mathbf{r}}^2 + V(\mathbf{r}) \right] \delta\psi_{\epsilon}(\mathbf{r}) = g_0 \int_{-\infty}^{\infty} \frac{d\epsilon_1}{2\pi} \int_{-\infty}^{\infty} \frac{d\epsilon_2}{2\pi} \psi_{\epsilon_1}^{(0)}(\mathbf{r}) \psi_{\epsilon_2}^{(0)*}(\mathbf{r}) \psi_{\epsilon-\epsilon_1+\epsilon_2}^{(0)}(\mathbf{r}). \quad (10.4)$$

Eqs. (10.3) and (10.4) form the basis for studying the behavior of the time-dependent ensemble-averaged atomic density $\bar{n}(\mathbf{r}, t) = \overline{|\psi(\mathbf{r}, t)|^2}$. By expanding \bar{n} and keeping only the lowest-order terms in $\delta\psi$, we readily obtain

$$\bar{n}(\mathbf{r}, t) \simeq \bar{n}^{(0)}(\mathbf{r}, t) + \overline{\Delta n}(\mathbf{r}, t), \quad (10.5)$$

where $\bar{n}^{(0)}(\mathbf{r}, t) = \overline{|\psi^{(0)}(\mathbf{r}, t)|^2}$ is the atomic density in the absence of interactions and $\overline{\Delta n}(\mathbf{r}, t) = 2\text{Re}[\overline{\psi^{(0)*}(\mathbf{r}, t) \delta\psi(\mathbf{r}, t)}]$ is the first-order correction to \bar{n} , with $\psi^{(0)}(\mathbf{r}, t)$ and $\delta\psi(\mathbf{r}, t)$ the Fourier transforms of $\psi_{\epsilon}^{(0)}(\mathbf{r})$ and $\delta\psi_{\epsilon}(\mathbf{r})$, respectively. The next two sections are devoted to the separate study of $\bar{n}^{(0)}$ and $\overline{\Delta n}$.

10.2 Expansion in the absence of interactions

In this section we derive the average density profile $\bar{n}^{(0)}(\mathbf{r}, t)$ free of interactions, in three dimensions. Here the situation is a bit more complicated than in the quasi one-dimensional waveguide of Chapter 9 because we know that in three dimensions, a critical energy ϵ_c separates localized states from extended ones. A part of atoms may propagate by diffusion in the random potential, whereas another part may remain localized in a small region of space. S. E. Skipetrov *et al.* [92] showed that in three dimensions, the behavior of the atomic density is controlled by a single parameter, equal to the ratio of the chemical potential μ to the critical energy $\epsilon_c = \hbar^2/(2m\ell^2)$:

$$\frac{\mu}{\epsilon_c} = (k_{\mu}\ell)^2. \quad (10.6)$$

When $k_\mu \ell \gg 1$, one expects that the condensate expands mostly by diffusion, whereas when $k_\mu \ell$ is of the order of one, localization effects become important. The case of $k_\mu \ell \gg 1$ was studied by B. Shapiro in 2007 [91] whereas the opposite situation $k_\mu \ell \sim 1$ was studied by S. E. Skipetrov *et al.* in 2008 [92]. In this section, we give a detailed study of the cross-over between the regimes of weak disorder $k_\mu \ell \gg 1$ and Anderson localization $k_\mu \ell \sim 1$, which was not clearly identified in Refs. [91] and [92].

10.2.1 Diffusive expansion

Let us first assume that $k_\mu \ell \rightarrow \infty$, which amounts to say that the condensate expands purely by diffusion, since the critical energy is zero according to Eq. (10.6). In the absence of interactions, the reasoning is exactly the same as in Sec. 9.2.2 of Chapter 9. The wave function of the condensate at time t and position \mathbf{r} is given by

$$\psi^{(0)}(\mathbf{r}, t) = \int \frac{d\epsilon}{2\pi} \int d^3\mathbf{r}' G_\epsilon(\mathbf{r}, \mathbf{r}') \phi_0(\mathbf{r}') e^{-i\epsilon t/\hbar}, \quad (10.7)$$

where G_ϵ is the Green's function of Eq. (10.3). As in Chapter 9, we consider large distances $r \gg \ell$ and long times $t \gg (\ell/v_\mu)$, where $v_\mu = \hbar k_\mu/m$ is the velocity of an atom with kinetic energy μ . The mean free time ℓ/v_μ separates the ballistic regime $t \lesssim \ell/v_\mu$ from the multiple scattering one $t \gg \ell/v_\mu$. In the latter case, the atoms are scattered many times on the random potential. Under these assumptions, we derive (see Appendix D for the detailed calculation):

$$\bar{n}^{(0)}(\mathbf{r}, t) = \overline{|\psi^{(0)}(\mathbf{r}, t)|^2} = \int \frac{d^3\mathbf{k}}{(2\pi)^3} |\phi_0(\mathbf{k})|^2 C_{\epsilon_k}(\mathbf{r}, t). \quad (10.8)$$

Eq. (10.8) is the counterpart of Eq. (9.9) in three dimensions. Here $C_\epsilon(\mathbf{r}, t) = \exp(-|\mathbf{r} - \mathbf{r}'|^2/4D_\epsilon t)/(4\pi D_\epsilon t)^{3/2}$ is the diffusion propagator in three dimensions for a particle with energy ϵ . The initial momentum distribution of the condensate $|\phi_0(\mathbf{k})|^2$ is given by Eq. (8.18). The calculation of the integral in Eq. (10.8) is straightforward and leads to:

$$\bar{n}^{(0)}(\mathbf{r}, t) = \frac{N}{(D_\mu t)^{3/2}} h_2 \left(\frac{r^2}{\sqrt{D_\mu t}} \right), \quad (10.9)$$

where

$$h_2(x) = \frac{1}{35842^{3/4} \pi^{3/2}} \left\{ (640 - 256\sqrt{2}x - 4x^2 + \sqrt{2}x^3) \exp\left(\frac{-x}{4\sqrt{2}}\right) - 2^{1/4} \sqrt{\pi} x^{3/2} (-280 + x^2) \left[1 - \operatorname{erf}\left(\frac{\sqrt{x}}{\sqrt{4\sqrt{2}}}\right) \right] \right\}. \quad (10.10)$$

As for the quasi one-dimensional case, in three dimensions the density profile is controlled by a single parameter $D_\mu = v_\mu \ell/3$, which can be regarded as the typical

diffusion coefficient of the condensate. We plot the density profile in Fig. 10.1 as a function of time for three different distances r . In three dimensions, $\bar{n}^{(0)}(\mathbf{r}, t)$ decays as $t^{-3/2}$ in the long time limit $t \gg t_{\text{arrival}}$, where $t_{\text{arrival}} \sim r^2/D_\mu \sim (\ell/v_\mu)(r/\ell)^2$ is the ‘‘arrival’’ time at which the density reaches the maximum.

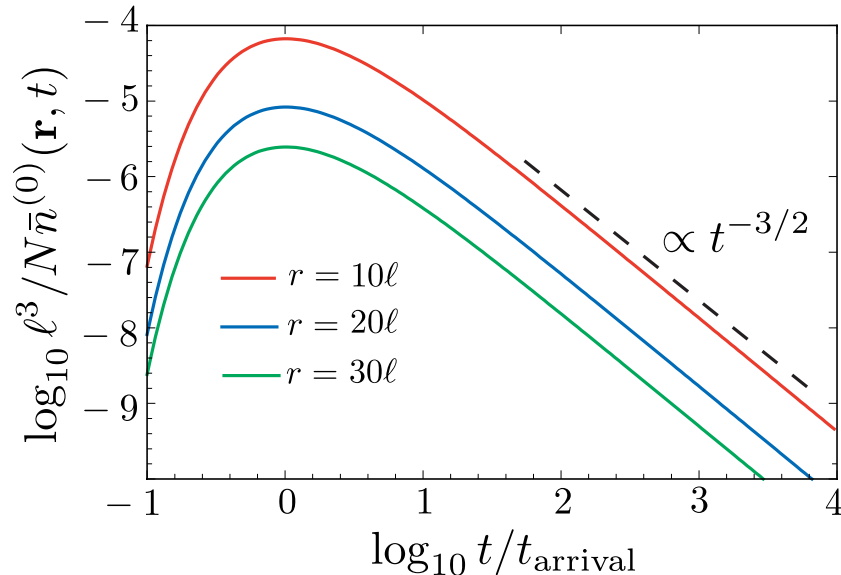


Figure 10.1: Ensemble-averaged atomic density $\bar{n}^{(0)}(\mathbf{r}, t)$ of a BEC expanding without interactions in a three-dimensional random potential, in the regime of weak disorder $k_\mu \ell \gg 1$, as a function of time and for three different distances $r = |\mathbf{r}|$ from the initial location of the condensate. The dashed line is a $1/t^{3/2}$ asymptote. The time is in units of t_{arrival} , such that all maxima fall in the same abscissa.

10.2.2 Anderson localization

Eq. (10.9) describes a purely diffusive expansion and does not include the effects of Anderson localization. When $k_\mu \ell$ is finite, a part of atoms inside the condensate start to ‘‘localize’’. For them, diffusion theory is not valid anymore. What happens then with the atomic density? This question was raised in Ref. [92], where the authors studied the atomic density for values of $k_\mu \ell$ of the order of one. Here we summarize their result and make a link with the diffusive calculation of Sec. 10.2.1.

For $t > t_{\text{arrival}}$ and moderate values of $k_\mu \ell$, the authors of Ref. [92] found that $\bar{n}^{(0)} \propto 1/t$ for $t > t_{\text{arrival}}$, in contrast to the $t^{-3/2}$ behavior discussed above. When $k_\mu \ell$ is increased, the $1/t$ decay is expected to cross over to the $1/t^{3/2}$ decay typical for diffusion. To illustrate this cross-over, we plot $\bar{n}^{(0)}(\mathbf{r}, t)$ including localization effects in Fig. 10.2 for three values of $k_\mu \ell$ and for $r = 10\ell$ (three upper curves, orange, green and blue). These curves are obtained from the self-consistent theory of Anderson localization discussed in the first part of the manuscript. We do not give here the details of this calculation, which is not the central issue of this chapter. They can be found in Ref. [92]. The lower red curve in Fig. 10.2 is obtained from Eq. (10.9),

i.e. by neglecting Anderson localization effects. For $k_\mu \ell = 3$, a significant fraction of

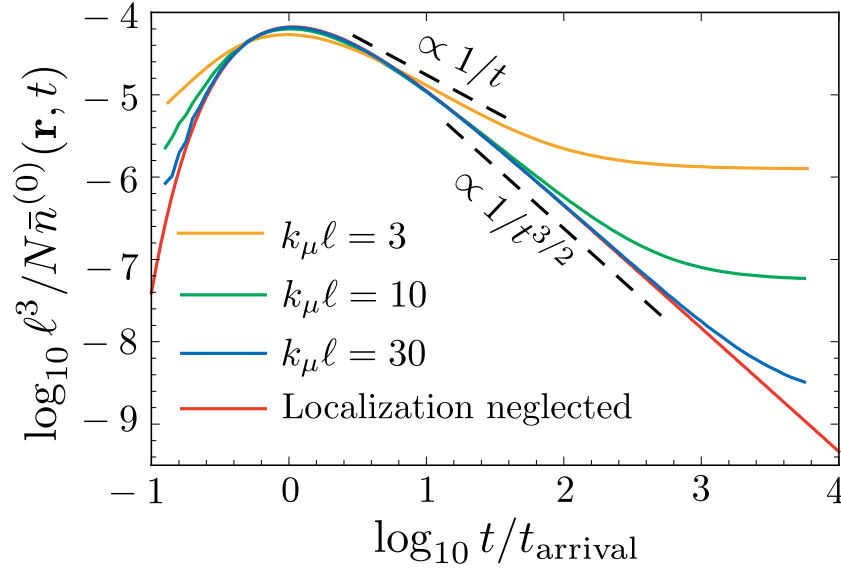


Figure 10.2: Ensemble-averaged atomic density $\bar{n}^{(0)}(\mathbf{r}, t)$ of a BEC expanding without interactions in a three-dimensional random potential, for three different values of the disorder parameter $k_\mu \ell$ and for $r = 10\ell$ (orange, green and blue upper curves). Here, unlike Fig. 10.1, the effects of Anderson localization are fully taken into account. For moderate values of $k_\mu \ell$, the curves exhibit first a $1/t$ decay and then saturation at some constant value. When $k_\mu \ell \gg 1$, the atomic density exhibits a $1/t^{3/2}$ decay, before saturating at very long times as well. The red lower curve is obtained from Eq. (10.9), *i.e.* by neglecting Anderson localization effects.

atoms is localized. Right after the maximum of $\bar{n}^{(0)}$, all diffusive atoms have already flown away and $\bar{n}^{(0)} \propto 1/t$. For weak disorder ($k_\mu \ell = 30$ in Fig. 10.2), the situation is very different: most atoms of the condensate propagate diffusively. Therefore, the atomic density exhibits a $1/t^{3/2}$ decay characteristic for diffusion. Whatever $k_\mu \ell$ however, at very long times the atomic density saturates at a constant value $\bar{n}_{\text{loc}}^{(0)} \sim u(k_\mu \ell)(N/r^3)(\ell/r)^{1/\nu}$, where ν is the critical exponent of the localization transition, and $u(k_\mu \ell) \propto 1/(k_\mu \ell)^3$ for $k_\mu \ell \gg 1$ and $u(k_\mu \ell) \propto \text{const}$ for $k_\mu \ell \ll 1$. This saturation has been also pointed out in Ref. [92]. Roughly, the $1/t$ behavior is due to anomalously diffusing atoms, that is atoms of energy $\epsilon \sim \epsilon_c$, whereas the saturation at long times is due to strongly localized atoms of energy $\epsilon < \epsilon_c$.

We can estimate the time after which the diffusive approach of Sec. 10.2 breaks down by requiring that the saturation value $\bar{n}_{\text{loc}}^{(0)}$ is smaller than the limit $\bar{n}_{\text{dif}}^{(0)} \sim N/(D_\mu t)^{3/2}$ of Eq. (10.9) at long times $t \gg t_{\text{arrival}}$. This yields

$$t_{\text{loc}} \sim (\ell/v_\mu)(r/\ell)^{2(1+1/3\nu)}(k_\mu \ell)^2 \quad (10.11)$$

as the maximum time at which diffusion model can be applied. When $k_\mu \ell \gg 1$ and $r \gg \ell$, t_{loc} is always much larger than t_{arrival} and the diffusion model is hence valid in a broad time interval.

To sum up, for $k_\mu \ell \gg 1$, the condensate behaves diffusively ($\bar{n}^{(0)} \propto t^{-3/2}$) until $t = t_{\text{loc}}$, and beyond localization effects start to “freeze” the density profile at $n^{(0)} = \bar{n}_{\text{loc}}^{(0)}$. The conditions $k_\mu \ell \gg 1$ and $t \ll t_{\text{loc}}$ will be assumed throughout the remainder of the chapter, *i.e.* we shall neglect Anderson localization effects.

10.3 Nonlinear correction to the atomic density

We are now interested in the first-order nonlinear correction $\overline{\Delta n}$ to the density profile (Eq. (10.5)). We first discuss the effect of interactions on the mean free path, and then develop a diagrammatic approach for calculating $\overline{\Delta n}$.

10.3.1 Mean free path

It should be noted that the mean free path ℓ is, in principle, modified in the presence of interactions. However, in the following we shall neglect the nonlinear corrections to ℓ . This approximation is legitimate in the limit of long times, as we now show by making use of a criterion initially developed in [108] for classical waves.

The mean free path is weakly affected by interactions provided that the scattering on the effective potential $g_0|\psi(\mathbf{r}, t)|^2 = g_0n(\mathbf{r}, t)$ is weak as compared to the scattering on the random potential. In other words, the mean free path $\ell^{(1)}$ associated with the effective potential $g_0n(\mathbf{r}, t)$ should be much larger than the mean free path ℓ associated with the random potential. In Born approximation, the mean free path is obtained from the Fourier transform $B(\mathbf{k})$ of the correlation function of the random potential [16]. For a random potential $V(\mathbf{r})$ with $\overline{V(\mathbf{r})V(\mathbf{r}')}$ depending only on $\mathbf{r} - \mathbf{r}'$, the mean free path ℓ is given by

$$\frac{1}{\ell} = \frac{2\pi\nu_0}{\hbar v_\mu} \langle B(\mathbf{k} - \mathbf{k}') \rangle_\theta, \quad (10.12)$$

where $\nu_0 = mk_\mu/2\pi^2\hbar^2$ is the density of states at energy μ . $\langle \dots \rangle_\theta = 1/(4\pi) \times \int_0^\pi (\dots) 2\pi \sin\theta d\theta$ denotes averaging over directions of \mathbf{k}' (see Fig. 10.3).

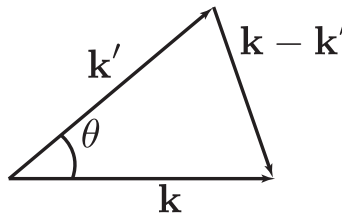


Figure 10.3: Wavevectors \mathbf{k} and \mathbf{k}' .

In order to make use of Eq. (10.12) for calculating $\ell^{(1)}$, we need to know the correlation function $g_0^2 \overline{\delta n(\mathbf{r}, t) \delta n(\mathbf{r}', t)}$. This correlation function can be approximated by the short-range “ \mathcal{C}_1 ” correlation function of density, which was discussed in Chapter 9. We neglect here the contribution due to the long-range “ \mathcal{C}_2 ” part

of the density correlation function. This would be questionable for a condensate expanding in a quasi one-dimensional waveguide where, as we saw in Chapter 9, \mathcal{C}_2 dominates at long times. However, the situation is different in three dimensions in the absence of any confinement, where we expect \mathcal{C}_2 to decay with time. Indeed, let us consider a quasi-monochromatic wave pulse emitted from some point in an unbounded three-dimensional disordered medium. A straightforward calculation similar to that of Chapter 9 yields $\mathcal{C}_2 \propto (1/t^2)/(k\ell)^2$ in the limit of long times. \mathcal{C}_2 is therefore negligible with respect to \mathcal{C}_1 .

From Ref. [100] and Chapter 9, we have the following approximate result for \mathcal{C}_1 :

$$\overline{\delta n(\mathbf{r}, t)\delta n(\mathbf{r}', t)} \simeq \frac{2\pi\ell}{k_\mu^2} \bar{n}^{(0)}(\mathbf{r}, t)^2 \delta(\mathbf{r} - \mathbf{r}'), \quad (10.13)$$

where $\bar{n}^{(0)}(\mathbf{r}, t) \simeq N/(D_\mu t)^{3/2}$ for $t \gg t_{\text{arrival}}$. We therefore obtain from Eq. (10.12)

$$\ell^{(1)} \simeq (\hbar^4 \pi / m^2) (k_\mu^2 / 2\pi\ell) (D_\mu t)^3 / (g_0^2 N^2). \quad (10.14)$$

The condition $\ell^{(1)} \gg \ell$ then gives

$$t \gg t_1 = p_0^{2/3} \left(\frac{\ell}{v_\mu} \right) \frac{1}{(k_\mu \ell)^{1/3}}, \quad (10.15)$$

where we have introduced a dimensionless parameter $p_0 = a_s N / \ell \sqrt{k_\mu \ell}$ that includes both interaction and disorder strengths. At this point, it is sufficient to keep in mind that in the weak disorder limit and under conditions of typical experiments, $p_0 \ll 1$. For instance, with the data from Refs. [35] and [88], we estimate $p_0 \sim 10^{-2}$. Therefore, the characteristic time t_1 is much smaller than ℓ/v_μ , such that the criterion (10.15) is automatically satisfied for long times $t \gg \ell/v_\mu$.

10.3.2 Diffusion coefficient

We now consider $\overline{\Delta n}(\mathbf{r}, t)$. From Eq. (10.4) we obtain

$$\delta\psi(\mathbf{r}, t) = \int \frac{d\epsilon}{2\pi} \int d^3\mathbf{r}' G_\epsilon(\mathbf{r}, \mathbf{r}') S(\mathbf{r}') e^{-i\epsilon t/\hbar}, \quad (10.16)$$

where $S(\mathbf{r}')$ is the right-hand side of Eq. (10.4) evaluated at \mathbf{r}' . Combining Eqs. (10.7) and (10.16) we obtain

$$\begin{aligned} \overline{\Delta n}(\mathbf{r}, t) &= 2\text{Re} \left[\overline{\psi^{(0)*}(\mathbf{r}, t)\delta\psi(\mathbf{r}, t)} \right] \\ &= 2\text{Re} \left[\frac{g_0}{(2\pi)^4} \int \prod_{j=1}^4 d\epsilon_j d^3\mathbf{r}_j d^3\mathbf{r}' e^{(-i/\hbar)(\epsilon_1 - \epsilon_2)t} K(\mathbf{r}, t; \mathbf{r}', \{\mathbf{r}_j\}, \{\epsilon_j\}) \right. \\ &\quad \left. \times \phi_0(\mathbf{r}_1)\phi_0^*(\mathbf{r}_2)\phi_0(\mathbf{r}_3)\phi_0^*(\mathbf{r}_4) \right], \end{aligned} \quad (10.17)$$

where the six-point kernel K is given by the connected part of a product of five Green's functions, averaged over disorder:

$$K = \overline{G_{\epsilon_1}(\mathbf{r}, \mathbf{r}')G_{\epsilon_2}^*(\mathbf{r}, \mathbf{r}_2)G_{\epsilon_3}(\mathbf{r}', \mathbf{r}_3)G_{\epsilon_4}^*(\mathbf{r}', \mathbf{r}_4)G_{\epsilon_1-\epsilon_3+\epsilon_4}(\mathbf{r}', \mathbf{r}_1)}. \quad (10.18)$$

The problem therefore reduces to finding the largest contribution to the kernel K in the weak disorder limit $k_\mu \ell \gg 1$. This contribution is given by the diagram depicted in Fig. 10.4a. The diagram describes interaction of four matter waves at a point \mathbf{r}' . Diagrams of this type were introduced some time ago by V. M. Agranovich and V. E. Kravtsov for classical waves in the context of nonlinear optics of disordered media [109, 110, 111]. The situation is more general here since K contains a product of Green's functions at five different energies. Writing down explicitly the diagram

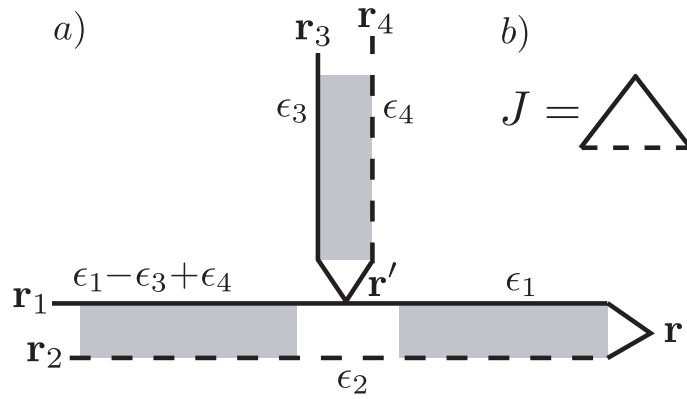


Figure 10.4: a) Diagram for the kernel K giving the first nonlinear correction to the atomic density. The solid and dashed lines represent Green's functions G_{ϵ_i} and $G_{\epsilon_j}^*$, respectively, where $\epsilon_i = \epsilon_1, \epsilon_3$ or $\epsilon_1 - \epsilon_3 + \epsilon_4$ and $\epsilon_j = \epsilon_2$ or ϵ_4 . Shaded rectangles symbolize averages of products of two Green's functions, $\overline{G_{\epsilon_i}G_{\epsilon_j}^*}$. b) Diagram J of Eq. (10.19).

of Fig. 10.4a, we obtain

$$\begin{aligned} \overline{\Delta n}(\mathbf{r}, t) = & 2\text{Re} \left[\frac{g_0 J}{(2\pi)^4} \left(\frac{\hbar v_\mu}{2\pi \nu_0 \ell} \right)^2 \int \prod_{j=1}^4 d\epsilon_j d^3 \mathbf{r}_j d^3 \mathbf{r}' e^{(-i/\hbar)(\epsilon_1 - \epsilon_2)t} \right. \\ & \times \phi(\mathbf{r}_1) \phi^*(\mathbf{r}_2) \phi(\mathbf{r}_3) \phi^*(\mathbf{r}_4) \overline{G_{\epsilon_1}(\mathbf{r}, \mathbf{r}')G_{\epsilon_2}^*(\mathbf{r}, \mathbf{r}')} \\ & \left. \times \overline{G_{\epsilon_3}(\mathbf{r}', \mathbf{r}_3)G_{\epsilon_4}^*(\mathbf{r}', \mathbf{r}_4)} \times \overline{G_{\epsilon_1-\epsilon_3+\epsilon_4}(\mathbf{r}', \mathbf{r}_1)G_{\epsilon_2}^*(\mathbf{r}', \mathbf{r}_2)} \right], \quad (10.19) \end{aligned}$$

where, we remind, $\nu_0 = mk_\mu/(2\pi^2 \hbar^2)$ is the density of states at energy μ and

$$J = \int d^3 \mathbf{k} / (2\pi)^3 \overline{G^2}(\mathbf{k}) \overline{G^*}(\mathbf{k}) = -i(\ell/v_\mu) [4\pi^3 \nu_0^2 \ell / (\hbar k_\mu^2)] \quad (10.20)$$

is the diagram depicted in Fig. 10.4b. Now we introduce new variables $\Omega = \epsilon_1 - \epsilon_2$, $\Omega' = \epsilon_3 - \epsilon_4$, $\epsilon = (\epsilon_1 + \epsilon_2)/2$, $\epsilon' = (\epsilon_3 + \epsilon_4)/2$, and make use of the following formula

that follows straightforwardly from Appendix D:

$$\int d^3\mathbf{r}_3 d^3\mathbf{r}_4 \overline{G_{\epsilon_3}^*(\mathbf{r}_3, \mathbf{r}') G_{\epsilon_4}^*(\mathbf{r}_4, \mathbf{r}') \phi(\mathbf{r}_3) \phi^*(\mathbf{r}_4)} = -\frac{2}{\hbar} \int \frac{d^3\mathbf{k}'}{(2\pi)^3} C_{\epsilon'}(\mathbf{r}', \Omega') \text{Im} \overline{G_{\epsilon'}(\mathbf{k}')} |\phi(\mathbf{k}')|^2. \quad (10.21)$$

Here $C_\epsilon(\mathbf{r}, \Omega) = \exp(-|\mathbf{r}| \sqrt{-i\Omega/\hbar D_\epsilon}) / (4\pi D_\epsilon |\mathbf{r}|)$ is the Fourier transform of the diffusion propagator at energy ϵ . Similar relations hold for the integrals over \mathbf{r}_1 and \mathbf{r}_2 . In the weak disorder limit $k_\mu \ell \gg 1$, $\text{Im} \overline{G_{\epsilon'}(\mathbf{k}')}$ can be approximated by the free-space expression $-\pi \delta(\epsilon' - \epsilon_{k'})$ (see Appendix D). This finally leads to

$$\begin{aligned} \overline{\Delta n}(\mathbf{r}, t) = & 2\text{Re} \left[\frac{g_0 J}{(2\pi)^3} \frac{v_\mu^2}{\nu_0 \hbar \ell^2} \int d^3\mathbf{r}' \int \frac{d^3\mathbf{k}}{(2\pi)^3} \int \frac{d^3\mathbf{k}'}{(2\pi)^3} \int d\Omega \int d\Omega' e^{-i\Omega t/\hbar} \right. \\ & \left. \times |\phi(\mathbf{k})|^2 |\phi(\mathbf{k}')|^2 C_{\epsilon_k}(\mathbf{r}', \Omega - \Omega') C_{\epsilon_{k'}}(\mathbf{r}', \Omega') C_{\epsilon_k + \Omega'/2}(\mathbf{r} - \mathbf{r}', \Omega) \right]. \end{aligned} \quad (10.22)$$

The main difficulty of Eq. (10.22) lies in the four coupled integrals over energies and momenta, which make the exact calculation of $\overline{\Delta n}$ complicated. However, after some algebra and in the limit of long times, all integrals can be performed. The main lines of this calculation are reported in Appendix E. We find that for $t \gg t_2 = (\ell/v_\mu)(r/\ell)^4(k_\mu \ell)$, $\overline{\Delta n}$ becomes position independent, and

$$\overline{\Delta n}(\mathbf{r}, t) \simeq -p_0 \frac{N}{(D_\mu t)^{3/2}}. \quad (10.23)$$

It is quite remarkable that the first-order correction $\overline{\Delta n}$ has exactly the same time dependence as $\bar{n}^{(0)}$ at long times. Comparison of Eq. (10.23) to $\bar{n}_{\text{diff}}^{(0)} \simeq N/(D_\mu t)^{3/2}$ provides the criterion $p_0 \ll 1$ as a condition of validity of our perturbative approach. As discussed in Sec. 10.3.1, this criterion is usually satisfied in typical experiments, which validates the assumption of negligible interactions during expansion made in previous works [91, 100].

A few comments are in order. First, the negative sign in Eq. (10.23) indicates that repulsive interactions ($p_0 > 0$) tend to reinforce the diffusion process, whereas attractive interactions slow it down, which might have been expected. This appears more clearly if one writes the total density profile as

$$\bar{n}(\mathbf{r}, t) \simeq \frac{N}{(D_{\text{eff}} t)^{3/2}}, \quad t_2 \ll t \ll t_{\text{loc}}, \quad (10.24)$$

where we have defined an effective diffusion coefficient $D_{\text{eff}} = D_\mu / (1 - p_0)^{2/3}$ taking interactions into account. For repulsive interactions, for example, $p_0 > 0$ and therefore $D_{\text{eff}} > D_\mu$. Thus repulsive interactions seem to compete with localization, even though calculations of higher-order diagrams or a complete study of interactions within the localized regime would be necessary to confirm this effect.

Another important remark is that the magnitude of the correction term (10.23) can be modified by increasing the strength of disorder at a constant strength of

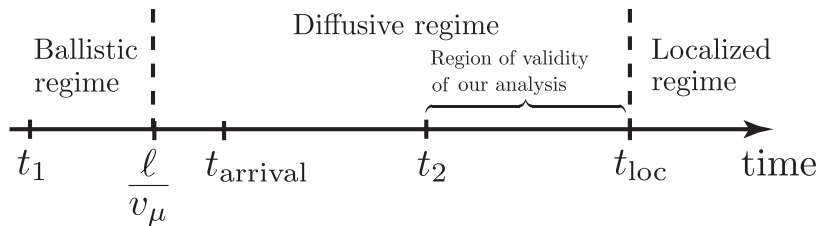


Figure 10.5: Ordering of time scales that we use throughout the chapter. ℓ/v_μ is the mean free time, t_1 is the time after which the mean free path is not affected by interactions, t_{arrival} is the time at which the atomic density free of interactions is maximum, t_2 is the limit of long times for nonlinear corrections to the atomic density, and t_{loc} is the time after which Anderson localization cannot be neglected anymore. In this sketch, the limits of weak disorder $k_\mu\ell \gg 1$ and large distances $r \gg \ell$ are assumed.

interactions, or vice versa. For extremely weak disorder ($k_\mu\ell \rightarrow \infty$), p_0 vanishes and $D_{\text{eff}} \simeq D_\mu$ whatever the interaction strength. In particular, if we extrapolate our calculation to $k_\mu\ell \sim 1$, we find that even weak interactions may significantly affect the expansion of the condensate. In this case, the scattering length a_s must be much less than ℓ/N to justify the neglect of interactions. This refines the condition of validity for the results of Ref. [92], where interactions were assumed weak, but no precise condition of weakness was given.

Our result (10.23) is only valid in the time interval $[t_2, t_{\text{loc}}]$. For weak disorder, $t_2 \ll t_{\text{loc}}$, which guarantees to Eq. (10.23) a broad range of validity. For the sake of clarity we summarize all the time scales that we introduced above in Fig. 10.5.

10.4 Conclusion

We developed a perturbative technique to study interaction corrections to the density of a Bose-Einstein condensate expanding in a three-dimensional random potential. Our results apply to the case of weak disorder. We showed that at the first-order of perturbation theory and at long times, interactions simply renormalize the effective diffusion coefficient of the condensate. Repulsive interactions between atoms accelerate the diffusion process whereas attractive interactions slow it down. In addition, we found that the effect of interactions on the average density is controlled by a single parameter p_0 , depending on both disorder and interaction strengths. Remarkably, the corrections to the density profile tend to increase when disorder becomes stronger, at a fixed strength of interactions. Our main result (10.23) was derived under the assumption of a white-noise, uncorrelated random potential. We expect it to remain qualitatively valid for correlated (speckle) potentials used in experiments too, provided that the mean free path ℓ is replaced by the transport mean free path ℓ_B given by Eq. (9.28). The calculation of higher-order interaction corrections would be of considerable interest in order to validate our main conclusions,

even if this rises important yet purely technical difficulties.

Conclusion

This thesis was an opportunity to study a number of new topics related to wave propagation in the presence of disorder. Most of the theoretical problems presented here were developed in parallel with a rich experimental research. We explored time-dependent aspects of wave propagation in random media, focusing especially on electromagnetic and matter waves. Dynamics of electromagnetic waves provides new signatures of coherent effects in transport, notably Anderson localization, and is often unaffected by absorption. This offers an ideal playground for experimental investigations. As far as matter waves are concerned, the dynamics of Bose-Einstein condensates expanding in random potentials offers a unique opportunity to study both Anderson localization and effects of atomic interactions.

First, we demonstrated a generalized version of the self-consistent theory of Anderson localization, based on the position dependence of the diffusion coefficient. Under this form, the self-consistent theory is suitable for description of random media of finite size. It is able to describe effects that cannot be accounted for by the self-consistent theory with position independent diffusion coefficient. An example of such an effect is the confinement of waves in the plane perpendicular to the direction of observation in three-dimensional random media. We showed that the self-consistent theory with position-dependent diffusion coefficient was fully compatible with the predictions of the one-parameter scaling theory of Anderson localization. The value of the critical exponent of the Anderson transition was found to be one.

Second, we investigated the dynamics of intensity speckle patterns in random media irradiated by short pulses. We showed that the \mathcal{C}_3 correlation function was strongly enhanced at long times. In the steady-state case, this correlation function is responsible for the universal conductance fluctuations, well known in mesoscopic physics. We showed that the dynamics of conductance fluctuations was not universal, since \mathcal{C}_3 then depends on the mean free path, the sample size and the pulse duration. Our theoretical study was carried out in collaboration with the experimental team of A. A. Chabanov (San Antonio). The growth of \mathcal{C}_3 with time as well

as its nonuniversal character were confirmed in a microwave experiment.

The last part of this thesis was devoted to the study of Bose-Einstein condensates expanding in random potentials. We analyzed matter-wave speckle patterns, reminiscent to intensity speckle patterns known for electromagnetic waves. For this purpose, we calculated the \mathcal{C}_1 and \mathcal{C}_2 correlation functions of the atomic density in a waveguide where the condensate expands. Whereas the \mathcal{C}_1 correlation function is short-range and remains constant in time during expansion, \mathcal{C}_2 is long-range and time-dependent. Furthermore, the latter grows with time and can take negative values. We interpreted these properties by suggesting a random displacement of the center of mass of the condensate. This displacement is expected to increase with time.

Our study of matter-wave speckle patterns was carried out by neglecting atomic interactions. The precise role of the latter is still a subject of debate. As a step towards a better understanding of their interplay with disorder, we studied the expansion of a Bose-Einstein condensate in a three-dimensional random potential, in the presence of weak interactions. We found that for weak disorder, interactions only renormalize the effective diffusion coefficient of the condensate but do not change the global behavior of the atomic density.

A number of subjects treated in this thesis still raise many questions. As far as the self-consistent theory is concerned, the value of the critical exponent of the Anderson transition is still an open problem. Indeed, despite the fact that we properly took into account finite-size effects, the value of this exponent is still in disagreement with the predictions of the Anderson tight-binding model.

The behavior of dynamic intensity correlations remains unknown in the localized regime. Indeed, at the onset of Anderson localization, the perturbative approach becomes insufficient to describe speckle patterns.

Finally, the field of Bose-Einstein condensates in random potentials is constantly evolving. Our study of interactions was carried out at the first order of perturbation theory. It is likely that the expansion of the condensate is drastically modified in the presence of stronger interactions or stronger disorder. Exploring the interplay between Anderson localization and interactions in three-dimensions would be extremely interesting, although it is a difficult task. Diagrammatic theories remain, however, a valuable tool for this investigation.

APPENDIX A

Derivation of self-consistent equations

This appendix contains a collection of mathematical results used at different steps of the derivation in Chapter 3. Here we neglect the difference in frequencies ω_1 and ω_2 in the arguments of \overline{G} and \overline{G}^* , respectively, and set $\omega_1 = \omega_2 = \omega_0$ for all amplitude Green's functions. This is justified under the assumption of slow dynamics ($\Omega = \omega_1 - \omega_2 \ll \omega_0, c/\ell$). To lighten the notation, we omit the frequency argument of \overline{G} and \overline{G}^* . We also use $d\mathbf{x}$ instead of $d^3\mathbf{x}$ to denote three-dimensional integration over a vector \mathbf{x} .

A.1 Hikami box

In this first section, we calculate the Fourier transform $\tilde{H}(\mathbf{q})$ of the function $H(\mathbf{r}, \mathbf{r}')$ introduced in Sec. 3.2.3 with respect to $\mathbf{r} - \mathbf{r}'$. In all generality one can write

$$H(\mathbf{r}, \mathbf{r}') = \int d\mathbf{r}_1 d\mathbf{r}_2 H(\mathbf{r}, \mathbf{r}_1, \mathbf{r}', \mathbf{r}_2), \quad (\text{A.1})$$

where $H(\mathbf{r}, \mathbf{r}_1, \mathbf{r}', \mathbf{r}_2)$ is the Hikami box shown Fig. A.1. This diagram is a sum of three contributions: $H^{(A)}(\mathbf{r}, \mathbf{r}_1, \mathbf{r}', \mathbf{r}_2)$, $H^{(B)}(\mathbf{r}, \mathbf{r}_1, \mathbf{r}', \mathbf{r}_2)$ and $H^{(C)}(\mathbf{r}, \mathbf{r}_1, \mathbf{r}', \mathbf{r}_2)$. As an example, we calculate $H^{(B)}$:

$$H^{(B)}(\mathbf{r}, \mathbf{r}') = \int d\mathbf{r}_1 d\mathbf{r}_2 H^{(B)}(\mathbf{r}, \mathbf{r}_1, \mathbf{r}', \mathbf{r}_2). \quad (\text{A.2})$$

From Fig. A.1 we obtain

$$\begin{aligned} H^{(B)}(\mathbf{r}, \mathbf{r}') &= \frac{4\pi}{\ell} \int d\mathbf{r}_1 d\mathbf{r}_2 d\mathbf{r}_3 \overline{G}(\mathbf{r}, \mathbf{r}_3) \overline{G}(\mathbf{r}_3, \mathbf{r}_1) \overline{G}^*(\mathbf{r}_1, \mathbf{r}') \\ &\times \overline{G}^*(\mathbf{r}, \mathbf{r}_2) \overline{G}(\mathbf{r}_2, \mathbf{r}_3) \overline{G}(\mathbf{r}_3, \mathbf{r}'). \end{aligned} \quad (\text{A.3})$$

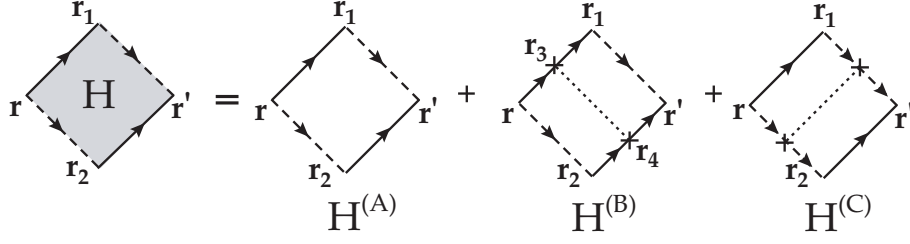


Figure A.1: Hikami box $H(\mathbf{r}, \mathbf{r}_1, \mathbf{r}', \mathbf{r}_2)$. Diagrammatic notation is the same as in Fig. 3.2.

By replacing the Green's functions in Eq. (A.3) by their Fourier transforms, we obtain

$$\begin{aligned}
H^{(B)}(\mathbf{r}, \mathbf{r}') &= \frac{4\pi}{\ell(2\pi)^{18}} \int d\mathbf{r}_1 d\mathbf{r}_2 d\mathbf{r}_3 d\mathbf{k}_1 \dots d\mathbf{k}_6 \overline{G}(\mathbf{k}_1) \overline{G}(\mathbf{k}_2) \overline{G}^*(\mathbf{k}_3) \\
&\times \overline{G}^*(\mathbf{k}_4) \overline{G}(\mathbf{k}_5) \overline{G}(\mathbf{k}_6) e^{-i\mathbf{r}_3(\mathbf{k}_1 - \mathbf{k}_2 + \mathbf{k}_5 - \mathbf{k}_6)} e^{-i\mathbf{r}_1(\mathbf{k}_2 - \mathbf{k}_3)} \\
&\times e^{-i\mathbf{r}_2(\mathbf{k}_4 - \mathbf{k}_5)} e^{-i\mathbf{r}'(-\mathbf{k}_1 - \mathbf{k}_4)} e^{-i\mathbf{r}'(\mathbf{k}_3 + \mathbf{k}_6)}. \tag{A.4}
\end{aligned}$$

Performing the integrals over \mathbf{r}_1 , \mathbf{r}_2 and \mathbf{r}_3 leads to

$$\begin{aligned}
H^{(B)}(\mathbf{r}, \mathbf{r}') &= \frac{4\pi}{\ell(2\pi)^9} \int d\mathbf{k}_1 d\mathbf{k}_2 d\mathbf{k}_4 \overline{G}(\mathbf{k}_1) |\overline{G}(\mathbf{k}_2)|^2 |\overline{G}(\mathbf{k}_4)|^2 \overline{G}(\mathbf{k}_1 - \mathbf{k}_2 + \mathbf{k}_4) \\
&\times e^{-i(\mathbf{r} - \mathbf{r}')(\mathbf{k}_1 + \mathbf{k}_4)}. \tag{A.5}
\end{aligned}$$

From Eq. (A.5) one sees that $H^{(B)}(\mathbf{r}, \mathbf{r}')$ depends only on the difference $\mathbf{r} - \mathbf{r}'$. Its Fourier transform with respect to this variable is, in the limit of small $q = |\mathbf{q}|$,

$$\tilde{H}^{(B)}(\mathbf{q}) = \frac{4\pi}{\ell(2\pi)^6} \left[\int d\mathbf{k} \overline{G}(\mathbf{q} - \mathbf{k}) |\overline{G}(\mathbf{k})|^2 \right]^2 = -\frac{\ell^3}{16\pi k^2} (1 - q^2 \ell^2 / 3)^2. \tag{A.6}$$

The calculation of diagrams $\tilde{H}^{(A)}(\mathbf{q})$ and $\tilde{H}^{(C)}(\mathbf{q})$ follows the same lines. We finally obtain

$$\tilde{H}^{(A)}(\mathbf{q}) = \frac{\ell^3}{8\pi k^2} (1 - q^2 \ell^2 / 3) \tag{A.7}$$

and $\tilde{H}^{(C)}(\mathbf{q}) = \tilde{H}^{(B)}(\mathbf{q})$. Hence

$$\tilde{H}(\mathbf{q}) = \tilde{H}^{(A)}(\mathbf{q}) + \tilde{H}^{(B)}(\mathbf{q}) + \tilde{H}^{(C)}(\mathbf{q}) \simeq \frac{\ell^5 q^2}{24\pi k^2} = \frac{D_B \ell^4 q^2}{8\pi c k^2}, \tag{A.8}$$

where $D_B = c\ell/3$.

A.2 Function $\mathbf{H}_f(\mathbf{r}, \mathbf{r}')$

We now present a demonstration of Eq. (3.15). Consider Eq. (3.14), where $H(\mathbf{r}, \mathbf{r}_1, \mathbf{r}', \mathbf{r}_2)$ is the Hikami box. As the latter is a sum of three contributions

$H^{(A)}(\mathbf{r}, \mathbf{r}_1, \mathbf{r}', \mathbf{r}_2)$, $H^{(B)}(\mathbf{r}, \mathbf{r}_1, \mathbf{r}', \mathbf{r}_2)$ and $H^{(C)}(\mathbf{r}, \mathbf{r}_1, \mathbf{r}', \mathbf{r}_2)$ (see Fig. A.1), we have to perform three integrals. The second one, for example, is

$$\mathbf{H}_f^{(B)}(\mathbf{r}, \mathbf{r}') = \int d\mathbf{r}_1 d\mathbf{r}_2 (\mathbf{r}_1 + \mathbf{r}_2 - 2\mathbf{r}) H^{(B)}(\mathbf{r}, \mathbf{r}_1, \mathbf{r}', \mathbf{r}_2). \quad (\text{A.9})$$

The two other integrals $\mathbf{H}_f^{(A)}$ and $\mathbf{H}_f^{(C)}$ are defined similarly. In the following, we focus on the calculation of $\mathbf{H}_f^{(B)}$, the calculation being similar for $\mathbf{H}_f^{(A)}$ and $\mathbf{H}_f^{(C)}$. Eq. (A.9) can be rewritten as

$$\begin{aligned} \mathbf{H}_f^{(B)}(\mathbf{r}, \mathbf{r}') &= \frac{4\pi}{\ell} \int d\mathbf{r}_1 d\mathbf{r}_2 d\mathbf{r}_3 (\mathbf{r}_1 + \mathbf{r}_2 - 2\mathbf{r}) \overline{G}(\mathbf{r}, \mathbf{r}_3) \overline{G}(\mathbf{r}_3, \mathbf{r}_1) \overline{G}^*(\mathbf{r}_1, \mathbf{r}') \\ &\times \overline{G}^*(\mathbf{r}, \mathbf{r}_2) \overline{G}(\mathbf{r}_2, \mathbf{r}_3) \overline{G}(\mathbf{r}_3, \mathbf{r}'). \end{aligned} \quad (\text{A.10})$$

By replacing the Green's functions in Eq. (A.10) by their Fourier transforms, we obtain

$$\begin{aligned} \mathbf{H}_f^{(B)}(\mathbf{r}, \mathbf{r}') &= \frac{4\pi}{\ell(2\pi)^{18}} \int d\mathbf{r}_1 d\mathbf{r}_2 d\mathbf{r}_3 d\mathbf{k}_1 \dots d\mathbf{k}_6 \overline{G}(\mathbf{k}_1) \overline{G}(\mathbf{k}_2) \overline{G}^*(\mathbf{k}_3) \\ &\times \overline{G}^*(\mathbf{k}_4) \overline{G}(\mathbf{k}_5) \overline{G}(\mathbf{k}_6) (\mathbf{r}_1 + \mathbf{r}_2 - 2\mathbf{r}) \\ &\times e^{-i\mathbf{r}_3(\mathbf{k}_1 - \mathbf{k}_2 + \mathbf{k}_5 - \mathbf{k}_6)} e^{-i\mathbf{r}_1(\mathbf{k}_2 - \mathbf{k}_3)} e^{-i\mathbf{r}_2(\mathbf{k}_4 - \mathbf{k}_5)} e^{-i\mathbf{r}(-\mathbf{k}_1 - \mathbf{k}_4)} e^{-i\mathbf{r}'(\mathbf{k}_3 + \mathbf{k}_6)} \\ &= \mathbf{K}_1(\mathbf{r}, \mathbf{r}') + \mathbf{K}_2(\mathbf{r}, \mathbf{r}') + \mathbf{K}(\mathbf{r}, \mathbf{r}'), \end{aligned} \quad (\text{A.11})$$

where $\mathbf{K}_1(\mathbf{r}, \mathbf{r}')$ is the part of Eq. (A.11) with the integrand proportional to \mathbf{r}_1 , $\mathbf{K}_2(\mathbf{r}, \mathbf{r}')$ is the part with the integrand proportional to \mathbf{r}_2 , and $\mathbf{K}(\mathbf{r}, \mathbf{r}')$ is the one with the integrand proportional to $-2\mathbf{r}$. Let us first consider $\mathbf{K}_1(\mathbf{r}, \mathbf{r}')$. In this term, the integrals over \mathbf{r}_2 and \mathbf{r}_3 give respectively $(2\pi)^3 \delta(\mathbf{k}_4 - \mathbf{k}_5)$ and $(2\pi)^3 \delta(\mathbf{k}_1 - \mathbf{k}_2 + \mathbf{k}_5 - \mathbf{k}_6)$, and the integral over \mathbf{r}_1 gives $-i(2\pi)^3 \nabla_{\mathbf{k}_3} \delta(\mathbf{k}_3 - \mathbf{k}_2)$. We have then

$$\begin{aligned} \mathbf{K}_1(\mathbf{r}, \mathbf{r}') &= \frac{-4\pi i}{\ell(2\pi)^9} \int d\mathbf{k}_1 d\mathbf{k}_2 d\mathbf{k}_4 \overline{G}(\mathbf{k}_1) \overline{G}(\mathbf{k}_2) \overline{G}^*(\mathbf{k}_4) \overline{G}(\mathbf{k}_4) \overline{G}(\mathbf{k}_1 - \mathbf{k}_2 + \mathbf{k}_4) \\ &\times e^{-i\mathbf{r}(-\mathbf{k}_1 - \mathbf{k}_4)} \int d\mathbf{k}_3 [\nabla_{\mathbf{k}_3} \delta(\mathbf{k}_3 - \mathbf{k}_2)] \overline{G}^*(\mathbf{k}_3) e^{-i\mathbf{r}'(\mathbf{k}_3 + \mathbf{k}_1 - \mathbf{k}_2 + \mathbf{k}_4)}. \end{aligned} \quad (\text{A.12})$$

The integral over \mathbf{k}_3 is equal to $-\left[\nabla_{\mathbf{k}_2} \overline{G}^*(\mathbf{k}_2) - i\mathbf{r}' \overline{G}^*(\mathbf{k}_2)\right] e^{-i\mathbf{r}'(\mathbf{k}_1 + \mathbf{k}_4)}$ and hence

$$\begin{aligned} \mathbf{K}_1(\mathbf{r}, \mathbf{r}') &= \frac{4\pi i}{\ell(2\pi)^9} \int d\mathbf{k}_1 d\mathbf{k}_2 d\mathbf{k}_4 \overline{G}(\mathbf{k}_1) \overline{G}(\mathbf{k}_2) \overline{G}^*(\mathbf{k}_4) \\ &\times \overline{G}(\mathbf{k}_4) \left[\nabla_{\mathbf{k}_2} \overline{G}^*(\mathbf{k}_2)\right] \overline{G}(\mathbf{k}_1 - \mathbf{k}_2 + \mathbf{k}_4) e^{i(\mathbf{r} - \mathbf{r}')(\mathbf{k}_1 + \mathbf{k}_4)} \\ &+ \frac{4\pi \mathbf{r}'}{\ell(2\pi)^9} \int d\mathbf{k}_1 d\mathbf{k}_2 d\mathbf{k}_4 \overline{G}(\mathbf{k}_1) \overline{G}(\mathbf{k}_2) \overline{G}^*(\mathbf{k}_4) \\ &\times \overline{G}(\mathbf{k}_4) \overline{G}^*(\mathbf{k}_2) \overline{G}(\mathbf{k}_1 - \mathbf{k}_2 + \mathbf{k}_4) e^{i(\mathbf{r} - \mathbf{r}')(\mathbf{k}_1 + \mathbf{k}_4)}. \end{aligned} \quad (\text{A.13})$$

The second term on the right-hand side is nothing but $\mathbf{r}' H^{(B)}(\mathbf{r}, \mathbf{r}')$, where

$$H^{(B)}(\mathbf{r}, \mathbf{r}') = \int d\mathbf{r}_1 d\mathbf{r}_2 H^{(B)}(\mathbf{r}, \mathbf{r}_1, \mathbf{r}', \mathbf{r}_2). \quad (\text{A.14})$$

In the first term on the right-hand side of Eq. (A.13) we change the variables $\mathbf{k}_1 \rightarrow \mathbf{k}$, $\mathbf{k}_2 \rightarrow \mathbf{k}'$, and $\mathbf{k}_1 + \mathbf{k}_4 \rightarrow \mathbf{q}$. Eq. (A.13) becomes

$$\begin{aligned} \mathbf{K}_1(\mathbf{r}, \mathbf{r}') &= \frac{4\pi i}{\ell(2\pi)^9} \int d\mathbf{k} d\mathbf{k}' d\mathbf{q} \overline{G}(\mathbf{k}) \overline{G}(\mathbf{k}') \overline{G}^*(\mathbf{q} - \mathbf{k}) \\ &\times \overline{G}(\mathbf{q} - \mathbf{k}) \left[\nabla_{\mathbf{k}'} \overline{G}^*(\mathbf{k}') \right] \overline{G}(\mathbf{q} - \mathbf{k}') e^{i\mathbf{q}(\mathbf{r} - \mathbf{r}')} \\ &+ \mathbf{r}' H^{(B)}(\mathbf{r}, \mathbf{r}'). \end{aligned} \quad (\text{A.15})$$

In the limit of small \mathbf{q} , we have $1/(2\pi)^3 \int d\mathbf{k} \overline{G}(\mathbf{k}) \overline{G}^*(\mathbf{q} - \mathbf{k}) \overline{G}(\mathbf{q} - \mathbf{k}) = -i\ell^2(1 - q^2\ell^2/3)/(8\pi k)$ and

$$\begin{aligned} \mathbf{K}_1(\mathbf{r}, \mathbf{r}') &= \frac{1}{(2\pi)^3} \int d\mathbf{q} e^{i\mathbf{q}(\mathbf{r} - \mathbf{r}')} \frac{\ell}{2k} \left(1 - \frac{q^2\ell^2}{3} \right) \\ &\times \frac{1}{(2\pi)^3} \int d\mathbf{k}' \overline{G}(\mathbf{k}') \overline{G}(\mathbf{q} - \mathbf{k}') \nabla_{\mathbf{k}'} \overline{G}^*(\mathbf{k}') \\ &+ \mathbf{r}' H^{(B)}(\mathbf{r}, \mathbf{r}'). \end{aligned} \quad (\text{A.16})$$

A similar calculation gives

$$\begin{aligned} \mathbf{K}_2(\mathbf{r}, \mathbf{r}') &= -\frac{1}{(2\pi)^3} \int d\mathbf{q} e^{i\mathbf{q}(\mathbf{r} - \mathbf{r}')} \frac{\ell}{2k} \left(1 - \frac{q^2\ell^2}{3} \right) \\ &\times \frac{1}{(2\pi)^3} \int d\mathbf{k}' \overline{G}(\mathbf{k}') \overline{G}(\mathbf{q} - \mathbf{k}') \nabla_{\mathbf{k}'} \overline{G}^*(\mathbf{k}') \\ &+ \mathbf{r} H^{(B)}(\mathbf{r}, \mathbf{r}'). \end{aligned} \quad (\text{A.17})$$

Besides, it follows straightforwardly from Eq. (A.10) that $\mathbf{K}(\mathbf{r}, \mathbf{r}') = -2\mathbf{r} H^{(B)}(\mathbf{r}, \mathbf{r}')$. Combined with Eqs. (A.16) and (A.17), this yields

$$\begin{aligned} \mathbf{H}_f^{(B)}(\mathbf{r}, \mathbf{r}') &= \mathbf{K}_1(\mathbf{r}, \mathbf{r}') + \mathbf{K}_2(\mathbf{r}, \mathbf{r}') + \mathbf{K}(\mathbf{r}, \mathbf{r}') \\ &= -(\mathbf{r} - \mathbf{r}') H^{(B)}(\mathbf{r}, \mathbf{r}'). \end{aligned} \quad (\text{A.18})$$

The calculation of $\mathbf{H}^{(A)}$ and $\mathbf{H}^{(C)}$ follows the same lines. We obtain

$$\begin{aligned} \mathbf{H}_f^{(A)}(\mathbf{r}, \mathbf{r}') &= \int d\mathbf{r}_1 d\mathbf{r}_2 (\mathbf{r}_1 + \mathbf{r}_2 - 2\mathbf{r}) H^{(A)}(\mathbf{r}, \mathbf{r}_1, \mathbf{r}', \mathbf{r}_2) \\ &= -(\mathbf{r} - \mathbf{r}') H^{(A)}(\mathbf{r}, \mathbf{r}') \end{aligned} \quad (\text{A.19})$$

and

$$\begin{aligned} \mathbf{H}_f^{(C)}(\mathbf{r}, \mathbf{r}') &= \int d\mathbf{r}_1 d\mathbf{r}_2 (\mathbf{r}_1 + \mathbf{r}_2 - 2\mathbf{r}) H^{(C)}(\mathbf{r}, \mathbf{r}_1, \mathbf{r}', \mathbf{r}_2) \\ &= -(\mathbf{r} - \mathbf{r}') H^{(C)}(\mathbf{r}, \mathbf{r}'). \end{aligned} \quad (\text{A.20})$$

Combining Eqs. (A.18), (A.19), and (A.20) we find

$$\begin{aligned} \mathbf{H}_f(\mathbf{r}, \mathbf{r}') &= \mathbf{H}_f^{(A)}(\mathbf{r}, \mathbf{r}') + \mathbf{H}_f^{(B)}(\mathbf{r}, \mathbf{r}') + \mathbf{H}_f^{(C)}(\mathbf{r}, \mathbf{r}') \\ &= -(\mathbf{r} - \mathbf{r}') H(\mathbf{r}, \mathbf{r}'), \end{aligned} \quad (\text{A.21})$$

which is Eq. (3.15) of the main text.

A.2 Fourier transform

We show here that the inverse Fourier transform of Eq. (3.18) with respect to \mathbf{q} is given by Eq. (3.19). As a function of \mathbf{q} , Eq. (3.18) is a sum of two terms proportional to $(i\mathbf{q})^2$ and $i\mathbf{q}$, respectively. The inverse Fourier transform of $i\mathbf{q}$ is

$$\int \frac{d\mathbf{q}}{(2\pi)^3} i\mathbf{q} e^{i\mathbf{q}\cdot\Delta\mathbf{r}} = \nabla_{\Delta\mathbf{r}} \left[\int \frac{d\mathbf{q}}{(2\pi)^3} e^{i\mathbf{q}\cdot\Delta\mathbf{r}} \right] = \nabla_{\Delta\mathbf{r}} \delta(\Delta\mathbf{r}). \quad (\text{A.22})$$

Similarly, the inverse Fourier transform of $(i\mathbf{q})^2$ is $\Delta_{\Delta\mathbf{r}} \delta(\Delta\mathbf{r})$. This leads directly to Eq. (3.19).

A.3 Series of interference loops

Here we obtain Eq. (3.22) from the series of Eq. (3.21). The idea is to apply the operator $-i\Omega - D_B \Delta_{\mathbf{r}}$ to both sides of Eq. (3.21). The first term on the right-hand side is transformed into $\delta(\mathbf{r} - \mathbf{r}')$ since $C_D(\mathbf{r}, \mathbf{r}_1, \Omega)$ obeys Eq. (3.8), and for each of the next terms the first multiplier $C_D(\mathbf{r}, \mathbf{r}_1, \Omega)$ in the integrands is transformed into $\delta(\mathbf{r} - \mathbf{r}_1)$ for the same reason. Eq. (3.21) becomes

$$\begin{aligned} [-i\Omega - D_B \Delta_{\mathbf{r}}] C(\mathbf{r}, \mathbf{r}', \Omega) &= \delta(\mathbf{r} - \mathbf{r}') \\ &+ \frac{4\pi c}{\ell^2} \int \delta(\mathbf{r} - \mathbf{r}_1) X(\mathbf{r}_1, \mathbf{r}_2, \Omega) C_D(\mathbf{r}_2, \mathbf{r}', \Omega) d\mathbf{r}_1 d\mathbf{r}_2 \\ &+ \left(\frac{4\pi c}{\ell^2} \right)^2 \int \delta(\mathbf{r} - \mathbf{r}_1) X(\mathbf{r}_1, \mathbf{r}_2, \Omega) C_D(\mathbf{r}_2, \mathbf{r}_3, \Omega) \\ &\times X(\mathbf{r}_3, \mathbf{r}_4, \Omega) C_D(\mathbf{r}_4, \mathbf{r}', \Omega) d\mathbf{r}_1 d\mathbf{r}_2 d\mathbf{r}_3 d\mathbf{r}_4 + \dots \end{aligned} \quad (\text{A.23})$$

Performing integrations over \mathbf{r}_1 we obtain

$$\begin{aligned} [-i\Omega - D_B \Delta_{\mathbf{r}}] C(\mathbf{r}, \mathbf{r}', \Omega) &= \delta(\mathbf{r} - \mathbf{r}') + \frac{4\pi c}{\ell^2} \int X(\mathbf{r}, \mathbf{r}_2, \Omega) C_D(\mathbf{r}_2, \mathbf{r}', \Omega) d\mathbf{r}_2 \\ &+ \left(\frac{4\pi c}{\ell^2} \right)^2 \int X(\mathbf{r}, \mathbf{r}_2, \Omega) C_D(\mathbf{r}_2, \mathbf{r}_3, \Omega) \\ &\times X(\mathbf{r}_3, \mathbf{r}_4, \Omega) C_D(\mathbf{r}_4, \mathbf{r}', \Omega) d\mathbf{r}_2 d\mathbf{r}_3 d\mathbf{r}_4 + \dots \end{aligned} \quad (\text{A.24})$$

Now let us perform integrations over \mathbf{r}_2 . We have to calculate an integral

$$I = \frac{4\pi c}{\ell^2} \int X(\mathbf{r}, \mathbf{r}_2, \Omega) C_D(\mathbf{r}_2, \mathbf{r}_3, \Omega) d\mathbf{r}_2, \quad (\text{A.25})$$

where $\mathbf{r}_3 = \mathbf{r}'$ for the first integral on the right-hand side of Eq. (A.24). To this end, we use Eq. (3.20) for $X(\mathbf{r}, \mathbf{r}_2, \Omega)$ and obtain

$$\begin{aligned} I &= \frac{-\ell^2 D_B}{2k^2} \int d\mathbf{r}_2 [\nabla_{\mathbf{r}} \cdot \Gamma_D(\mathbf{r}, \mathbf{r}_2, \Omega) \nabla_{\mathbf{r}_2} \delta(\mathbf{r} - \mathbf{r}_2)] C_D(\mathbf{r}_2, \mathbf{r}_3, \Omega) \\ &= \frac{-\ell^2 D_B}{2k^2} \nabla_{\mathbf{r}} \cdot [\Gamma_D(\mathbf{r}, \mathbf{r}, \Omega) \nabla_{\mathbf{r}}] C_D(\mathbf{r}, \mathbf{r}_3, \Omega), \end{aligned} \quad (\text{A.26})$$

where we integrated by parts. Replacing each integration over \mathbf{r}_2 by this result in Eq. (A.24), we obtain

$$\begin{aligned}
[-i\Omega - D_B \Delta_{\mathbf{r}}] C(\mathbf{r}, \mathbf{r}', \Omega) &= \delta(\mathbf{r} - \mathbf{r}') \\
&- \frac{\ell^2 D_B}{2k^2} \nabla_{\mathbf{r}} \cdot \Gamma_D(\mathbf{r}, \mathbf{r}, \Omega) \nabla_{\mathbf{r}} [C_D(\mathbf{r}, \mathbf{r}', \Omega) \\
&+ \frac{4\pi c}{\ell^2} \int C_D(\mathbf{r}, \mathbf{r}_3, \Omega) X(\mathbf{r}_3, \mathbf{r}_4, \Omega) C_D(\mathbf{r}_4, \mathbf{r}', \Omega) d\mathbf{r}_3 d\mathbf{r}_4 \\
&+ \left(\frac{4\pi c}{\ell^2}\right)^2 \int C_D(\mathbf{r}, \mathbf{r}_3, \Omega) X(\mathbf{r}_3, \mathbf{r}_4, \Omega) C_D(\mathbf{r}_4, \mathbf{r}_5, \Omega) \\
&\times X(\mathbf{r}_5, \mathbf{r}_6, \Omega) C_D(\mathbf{r}_6, \mathbf{r}', \Omega) d\mathbf{r}_3 d\mathbf{r}_4 d\mathbf{r}_5 d\mathbf{r}_6 + \dots] \quad (\text{A.27})
\end{aligned}$$

The infinite series in square brackets is nothing but the intensity Green's function $C(\mathbf{r}, \mathbf{r}', \Omega)$ as given by Eq. (3.21). Thus, Eq. (A.27) leads straightforwardly to Eq. (3.22).

A.4 Proportionality relation

We demonstrate here the proportionality between C_D and Γ_D in a finite medium. Calculations being similar to those of Sec. A.2, we only give the main ingredients of the proof. According to Eq. (3.7), at $|\mathbf{r} - \mathbf{r}'| \gg \ell$, $C_D(\mathbf{r}, \mathbf{r}', \Omega)$ is given by

$$C_D(\mathbf{r}, \mathbf{r}', \Omega) = \frac{4\pi}{c} \int d\mathbf{r}_1 d\mathbf{r}_2 \overline{G}(\mathbf{r}, \mathbf{r}_1) \overline{G}^*(\mathbf{r}, \mathbf{r}_1) \Gamma_D(\mathbf{r}_1, \mathbf{r}_2, \Omega) \overline{G}(\mathbf{r}_2, \mathbf{r}') \overline{G}^*(\mathbf{r}_2, \mathbf{r}'). \quad (\text{A.28})$$

Because $\overline{G}(\mathbf{r}, \mathbf{r}_1)$ is exponentially small for $|\mathbf{r} - \mathbf{r}_1| > \ell$, the main contribution to the integral comes from $|\mathbf{r} - \mathbf{r}_1|, |\mathbf{r}' - \mathbf{r}_2| < \ell$. This authorizes us to expand $\Gamma_D(\mathbf{r}_1, \mathbf{r}_2, \Omega)$ in series around $(\mathbf{r}, \mathbf{r}')$. This expansion has to be truncated to the same first order in $|\mathbf{r} - \mathbf{r}_1|$ and $|\mathbf{r}' - \mathbf{r}_2|$ as the expansion of Eq. (3.11):

$$\Gamma_D(\mathbf{r}_1, \mathbf{r}_2, \Omega) \simeq \Gamma_D(\mathbf{r}, \mathbf{r}', \Omega) + (\mathbf{r}_1 + \mathbf{r}_2 - \mathbf{r} - \mathbf{r}') \cdot \nabla_{\mathbf{r}} \Gamma_D(\mathbf{r}, \mathbf{r}', \Omega). \quad (\text{A.29})$$

We then substitute Eq. (A.29) into Eq. (A.28). The first term proportional to $\Gamma_D(\mathbf{r}, \mathbf{r}', \Omega)$ is the usual result obtained in the infinite medium. It equals $\ell^2/(4\pi c) \times \Gamma_D(\mathbf{r}, \mathbf{r}', \Omega)$. We hence obtain

$$C_D(\mathbf{r}, \mathbf{r}', \Omega) = \frac{\ell^2}{4\pi c} \Gamma_D(\mathbf{r}, \mathbf{r}', \Omega) \quad (\text{A.30})$$

$$\begin{aligned}
&+ \frac{4\pi}{c} \left[\int d\mathbf{r}_1 d\mathbf{r}_2 (\mathbf{r}_1 + \mathbf{r}_2 - \mathbf{r} - \mathbf{r}') |\overline{G}(\mathbf{r}, \mathbf{r}_1)|^2 |\overline{G}(\mathbf{r}_2, \mathbf{r}')|^2 \right] \\
&\cdot \nabla_{\mathbf{r}} \Gamma_D(\mathbf{r}, \mathbf{r}', \Omega). \quad (\text{A.31})
\end{aligned}$$

The integral on the right-hand side of Eq. (A.30) can be calculated exactly in the same way as \mathbf{H}_f^A , \mathbf{H}_f^B or \mathbf{H}_f^C in Sec. A.2, and it is easy to see that this integral is zero.

Average intensity and field correlation in a disordered
waveguide

B.1 Intensity Green's function

In this section, we solve the diffusion equation in a disordered waveguide of length L and cross-section A :

$$\left(\frac{\partial}{\partial t} - D_B \frac{\partial^2}{\partial z^2} \right) C_D(\mathbf{r}, \mathbf{R}, t) = \frac{1}{A} \delta(z - z_R) \delta(t), \quad (\text{B.1})$$

where z denotes the longitudinal coordinate of \mathbf{r} and z_R that of \mathbf{R} . We look for solutions of Eq. (B.1) in the form

$$C_D(\mathbf{r}, \mathbf{R}, t) = \sum_{n=0}^{\infty} A_n \Phi_n(z) f_n(t), \quad (\text{B.2})$$

where A_n , $\Phi_n(z)$ and $f_n(t)$ have to be determined. Due to the principle of causality, the time-dependent part $f_n(t)$ of Eq. (B.2) must be zero for $t < 0$. Substituting Eq. (B.2) into Eq. (B.1), we obtain:

$$\sum_{n=0}^{\infty} \left[A_n \Phi_n(z) \frac{df_n(t)}{dt} - D_B A_n \frac{d^2 \Phi_n(z)}{dz^2} f_n(t) \right] = \frac{1}{A} \delta(z - z_R) \delta(t). \quad (\text{B.3})$$

We now separate the time- and position-dependent variables in a standard way. For each term n of the sum, we obtain for $t > 0$

$$\frac{\left[\frac{df_n(t)}{dt} \right]}{f_n(t)} = \frac{D_B \left[\frac{d^2 \Phi_n(z)}{dz^2} \right]}{\Phi_n(z)} = -B_n, \quad (\text{B.4})$$

where B_n is a constant which has to be determined. B_n should be positive, otherwise an unphysical divergence of $f_n(t)$ for $t \rightarrow \infty$ would take place. Solving Eq. (B.4) for $f_n(t)$, we readily find $f_n(t) = \exp(-B_n t)$ for $t > 0$ (the choice of the prefactor before the exponential is arbitrary, so we choose it to be one).

We now assume Dirichlet boundary conditions for the solution (B.2):

$$C_D(\mathbf{r}, \mathbf{R}, t)|_{z=0} = C_D(\mathbf{r}, \mathbf{R}, t)|_{z=L} = 0. \quad (\text{B.5})$$

Therefore, $\Phi_n(0) = \Phi_n(L)$ for all n . Solving Eq. (B.4) for $\Phi_n(z)$ with these boundary conditions yields $B_n = k_n^2 D_B$, with $k_n = n\pi/L$, and

$$\Phi_n(z) = \sqrt{\frac{2}{L}} \sin(k_n z), \quad (\text{B.6})$$

where we have required that functions Φ_n are normalized. Using the expression of B_n , we obtain, for any time,

$$f_n(t) \propto \mathcal{H}(t) \exp\left(-n^2 \frac{t}{t_D}\right), \quad (\text{B.7})$$

where we have introduced the Thouless time $t_D = L^2 \pi^2 / D_B$ and the Heaviside function $\mathcal{H}(t)$. Our last task consists in calculating the constants A_n . This can be done by multiplying Eq. (B.3) by $\Phi_m(z)$, where m is some integer, and integrating over z from 0^- to L :

$$\begin{aligned} & \sum_{n=0}^{\infty} A_n \left[\int_0^L dz \Phi_m(z) \Phi_n(z) \int_{0^-}^{\infty} dt \frac{df_n(t)}{dt} - D_B \int_0^L dz \Phi_m(z) \frac{d^2 \Phi_n(z)}{dz^2} \int_{0^-}^{\infty} dt f_n(t) \right] \\ &= \frac{1}{A} \int_0^L \Phi_m(z) \delta(z - z_R) \int_{0^-}^{\infty} dt \delta(t). \end{aligned} \quad (\text{B.8})$$

The first integral over t of the left-hand side is zero, and the second is equal to $1/B_n$, such that Eq. (B.8) becomes

$$\sum_{n=0}^{\infty} -\frac{D_B}{B_n} A_n \int_0^L dz \Phi_m(z) \frac{d^2 \Phi_n(z)}{dz^2} = \frac{1}{A} \Phi_m(z_R). \quad (\text{B.9})$$

Making use of Eq. (B.6), we find that the integral over z is equal to $k_n^2 \delta_{mn}$, where δ_{mn} is the Kronecker symbol. This yields

$$A_n = \frac{1}{A} \Phi_n(z_R). \quad (\text{B.10})$$

Collecting Eqs. (B.7) and (B.10), we finally obtain

$$C_D(\mathbf{r}, \mathbf{R}, t) = \frac{1}{A} \sum_{n=1}^{\infty} \Phi_n(z) \Phi_n(z_R) \mathcal{H}(t) \exp\left(-n^2 \frac{t}{t_D}\right), \quad (\text{B.11})$$

which concludes the calculation.

B.2 Correlation of Green's functions

We now demonstrate Eq. (7.6) of Chapter 7. The average of the product of two amplitude Green's functions is given by

$$\overline{G(\mathbf{r}, \mathbf{R}, t)G^*(\mathbf{r}', \mathbf{R}', t')} = \int \frac{d\omega_1}{2\pi} \int \frac{d\omega_2}{2\pi} \overline{G(\mathbf{r}, \mathbf{R}, \omega_1)G^*(\mathbf{r}', \mathbf{R}', \omega_2)} \exp(-i\omega_1 t + i\omega_2 t') \quad (\text{B.12})$$

In the same spirit as in Sec. 6.2.3.1, we decompose Eq. (B.12) as

$$\begin{aligned} \overline{G(\mathbf{r}, \mathbf{R}, t)G^*(\mathbf{r}', \mathbf{R}', t')} &= \int d^3\mathbf{r}_1 \int d^3\mathbf{r}_2 \int \frac{d\omega_1}{2\pi} \int \frac{d\omega_2}{2\pi} \overline{G(\mathbf{r}_1, \mathbf{R}, \omega_1)\overline{G}(\mathbf{r}_1, \mathbf{R}', \omega_2)} \\ &\quad \times \Gamma_D(\mathbf{r}_2, \mathbf{r}_1, \omega_2, \omega_1) \overline{G}(\mathbf{r}, \mathbf{r}_2, \omega_1) \overline{G}^*(\mathbf{r}', \mathbf{r}_2, \omega_2) \\ &\quad \times \exp(-i\omega_1 t + i\omega_2 t') \end{aligned} \quad (\text{B.13})$$

where \mathbf{r}_1 and \mathbf{r}_2 denote, respectively, the first and last scattering events of the sum of ladder diagrams Γ_D . In Eq. (B.13), we have made explicit the frequency dependence of Γ_D . We now introduce new variables $\omega = (\omega_1 + \omega_2)/2$ and $\Omega = \omega_1 - \omega_2$, and assume $\Omega \ll \omega$, such that

$$\overline{G}(\mathbf{r}_1, \mathbf{R}, \omega_1) \simeq \overline{G}(\mathbf{r}_1, \mathbf{R}, \omega_2) \simeq \overline{G}(\mathbf{r}_1, \mathbf{R}, \omega), \quad (\text{B.14})$$

with a similar relation for other average amplitude Green's functions. We also have

$$\Gamma_D(\mathbf{r}_2, \mathbf{r}_1, \omega_2, \omega_1) = \Gamma_D\left(\mathbf{r}_2, \mathbf{r}_1, \omega - \frac{\Omega}{2}, \omega + \frac{\Omega}{2}\right). \quad (\text{B.15})$$

We then assume that Γ_D weakly varies with ω . We thus drop the ω dependence in Γ_D , and write

$$\Gamma_D\left(\mathbf{r}_2, \mathbf{r}_1, \omega - \frac{\Omega}{2}, \omega + \frac{\Omega}{2}\right) = \Gamma_D(\mathbf{r}_2, \mathbf{r}_1, \Omega). \quad (\text{B.16})$$

Besides, in the limit $\Omega \ll c/\ell$ and at large distances $|\mathbf{r} - \mathbf{R}| \gg \ell$, the spatial variations of $\Gamma_D(\mathbf{r}_2, \mathbf{r}_1, \Omega)$ are small on the scale of ℓ , and we have

$$\Gamma_D(\mathbf{r}_2, \mathbf{r}_1, \Omega) \simeq \Gamma_D(\mathbf{r}, \mathbf{R}, \Omega). \quad (\text{B.17})$$

Eq. (B.13) becomes

$$\begin{aligned} \overline{G(\mathbf{r}, \mathbf{R}, t)G^*(\mathbf{r}', \mathbf{R}', t')} &= \int d^3\mathbf{r}_1 \int d^3\mathbf{r}_2 \int \frac{d\omega}{2\pi} \int \frac{d\Omega}{2\pi} \overline{G}(\mathbf{r}_1, \mathbf{R}, \omega) \overline{G}(\mathbf{r}_1, \mathbf{R}', \omega) \\ &\quad \times \Gamma_D(\mathbf{r}, \mathbf{R}, \Omega) \overline{G}(\mathbf{r}_2, \mathbf{r}, \omega) \overline{G}^*(\mathbf{r}_2, \mathbf{r}', \omega) \\ &\quad \times \exp\left[-i\omega(t - t') - i\Omega\left(\frac{t + t'}{2}\right)\right]. \end{aligned} \quad (\text{B.18})$$

We now make use of $\Gamma_D(\mathbf{r}, \mathbf{R}, \Omega) = (4\pi c/\ell^2)C_D(\mathbf{r}, \mathbf{R}, \Omega)$, and perform the integrals over \mathbf{r}_1 and \mathbf{r}_2 . This yields

$$\begin{aligned} \overline{G(\mathbf{r}, \mathbf{R}, t)G^*(\mathbf{r}', \mathbf{R}', t')} &= \frac{c}{4\pi} f(\Delta r) f(\Delta R) \left\{ \int \frac{d\omega}{2\pi} \exp[-i\omega(t - t')] \right\} \\ &\quad \times \left\{ \int \frac{d\Omega}{2\pi} C_D(\mathbf{r}, \mathbf{R}, \Omega) \exp\left[-i\Omega\left(\frac{t + t'}{2}\right)\right] \right\}, \end{aligned} \quad (\text{B.19})$$

where $\Delta r = \mathbf{r} - \mathbf{r}'$, $\Delta R = \mathbf{R} - \mathbf{R}'$ and $f(x) = \text{sinc}(kx) \exp[-x/(2\ell)]$. The integral over ω is equal to $\delta(t - t')$, and that over Ω to $C_D(\mathbf{r}, \mathbf{R}, (t + t')/2)$. This leads to Eq. (7.6). Note that appearance of $\delta(t - t')$ in Eq. (B.19) is due to our hypothesis that $\overline{G(\mathbf{r}, \mathbf{R}, \omega_1)G^*(\mathbf{r}', \mathbf{R}', \omega_2)}$ depends on $\Omega = \omega_2 - \omega_1$ but not on $\omega = (\omega_1 + \omega_2)/2$.

Gross-Pitaevskii equation

In this appendix we propose a derivation of Gross-Pitaevskii equations (8.5) and (8.6) of the main text from the Hartree ansatz (8.3).

C.1 Energy functional

The first step consists in evaluating the mean energy of the condensate $\mathcal{E} = \langle \Theta | \hat{H} | \Theta \rangle$, where the N-particle wave function $|\Theta\rangle$ is given by the Hartree ansatz (8.3). The N-particle Hamiltonian reads

$$\hat{H} = \sum_{i=1}^N \left[\frac{\hat{p}_i^2}{2m} + V_{\text{ext}}(\mathbf{r}_i) \right] + \sum_{i<j} \hat{U}(\mathbf{r}_i - \mathbf{r}_j), \quad (\text{C.1})$$

where \hat{p}_i is the momentum operator of atom i , V_{ext} is an external potential and $\hat{U}(\mathbf{r}_i - \mathbf{r}_j)$ is the two-particle interaction potential¹. The precise form of this potential is of no importance if we remind that we work within the framework of the dilute approximation $n^{-1/3} \gg a_s$, where a_s is the scattering length of the potential U . From the point of view of scattering theory, we are therefore free to choose the position dependence of U , provided that its scattering length is equal to the scattering length of the “true potential”. We make the simplest choice and write

$$\hat{U}(\mathbf{r}_i - \mathbf{r}_j) = U_0 \delta(\mathbf{r}_i - \mathbf{r}_j). \quad (\text{C.2})$$

The mean energy then reads

$$\mathcal{E} = \sum_{i=1}^N \left[\frac{1}{2m} \langle \Theta | \hat{p}_i^2 | \Theta \rangle + V_{\text{ext}}(\mathbf{r}_i) \right] + \frac{1}{2} \sum_{i \neq j} U_0 \delta(\mathbf{r}_i - \mathbf{r}_j), \quad (\text{C.3})$$

¹For clarity, in this appendix we omit hats of position operators.

where the normalization of Θ is assumed. We now make use of the Hartree ansatz $|\Theta\rangle = \prod_{i=1}^N |\phi\rangle$ and write

$$\sum_{i=1}^N \frac{1}{2m} \langle \Theta | \hat{p}_i^2 | \Theta \rangle = \sum_{i=1}^N \int d^3\mathbf{r} \frac{\hbar^2}{2m} |\nabla_{\mathbf{r}}\phi(\mathbf{r})|^2 = N \int d^3\mathbf{r} \frac{\hbar^2}{2m} |\nabla_{\mathbf{r}}\phi(\mathbf{r})|^2, \quad (\text{C.4})$$

$$\begin{aligned} \sum_{i=1}^N V_{\text{ext}}(\mathbf{r}_i) &= \sum_{i=1}^N \int d^3\mathbf{r} \delta(\mathbf{r} - \mathbf{r}_i) V_{\text{ext}}(\mathbf{r}) = \sum_{i=1}^N \int d^3\mathbf{r} |\phi(\mathbf{r})|^2 V_{\text{ext}}(\mathbf{r}) \\ &= N \int d^3\mathbf{r} |\phi(\mathbf{r})|^2 V_{\text{ext}}(\mathbf{r}), \end{aligned} \quad (\text{C.5})$$

and

$$\begin{aligned} \frac{1}{2} \sum_{i \neq j} U_0 \delta(\mathbf{r}_i - \mathbf{r}_j) &= \frac{U_0}{2} \sum_{i \neq j} \int d^3\mathbf{r} d^3\mathbf{r}' \delta(\mathbf{r} - \mathbf{r}_i) \delta(\mathbf{r}' - \mathbf{r}_j) \delta(\mathbf{r} - \mathbf{r}') \\ &= \frac{U_0}{2} \sum_{i \neq j} \int d^3\mathbf{r} d^3\mathbf{r}' |\phi(\mathbf{r})|^2 |\phi(\mathbf{r}')|^2 \delta(\mathbf{r} - \mathbf{r}') \\ &= \frac{U_0}{2} N(N-1) \int d^3\mathbf{r} |\phi(\mathbf{r})|^4. \end{aligned} \quad (\text{C.6})$$

Then Eq. (C.3) can be rewritten as

$$\mathcal{E} = N \int d^3\mathbf{r} \left[\frac{\hbar^2}{2m} |\nabla_{\mathbf{r}}\phi(\mathbf{r})|^2 + |\phi(\mathbf{r})|^2 V_{\text{ext}}(\mathbf{r}) + \frac{U_0}{2} N(N-1) |\phi(\mathbf{r})|^4 \right]. \quad (\text{C.7})$$

We now introduce the wave function of the condensate $\psi = \sqrt{N}\phi$ defined in Sec. 8.1.2, and assume that $N \gg 1$, such that $N-1 \simeq N$. This yields

$$\mathcal{E} = \int d^3\mathbf{r} \left[\frac{\hbar^2}{2m} |\nabla_{\mathbf{r}}\psi(\mathbf{r})|^2 + |\psi(\mathbf{r})|^2 V_{\text{ext}}(\mathbf{r}) + \frac{U_0}{2} |\psi(\mathbf{r})|^4 \right]. \quad (\text{C.8})$$

The mean energy \mathcal{E} is sometimes called the ‘‘energy functional of the system’’. To be consistent with literature, we denote $g_0 = U_0$ (in the main text this quantity is referred to as the ‘‘interaction parameter’’). From scattering theory, the scattering length a_s is given (in the Born approximation) by $a_s = mg_0/(4\pi\hbar^2)$. Hence, $g_0 = 4\pi\hbar^2 a_s/m$ [16].

C.2 Gross-Pitaevskii equation

We now come back to our main task which is the derivation of Eqs. (8.5) and (8.6). Stationary Gross-Pitaevskii equation (8.5) is obtained by imposing the stationarity of the grand canonical energy

$$\Phi = \mathcal{E} - \mu \int d^3\mathbf{r} |\psi(\mathbf{r})|^2, \quad (\text{C.9})$$

where $\mu = \partial\mathcal{E}/\partial N$ is the chemical potential. The stationarity condition reads

$$\delta\Phi = 0. \quad (\text{C.10})$$

From Eq. (C.8), the grand canonical energy reads

$$\Phi = \int d^3\mathbf{r} \left[\frac{\hbar^2}{2m} |\nabla_{\mathbf{r}}\psi(\mathbf{r})|^2 + |\psi(\mathbf{r})|^2 V_{\text{ext}}(\mathbf{r}) + \frac{U_0}{2} |\psi(\mathbf{r})|^4 - \mu |\psi(\mathbf{r})|^2 \right]. \quad (\text{C.11})$$

Functional derivation of this formula yields

$$\frac{\delta\Phi}{\delta\psi^*} = \int d^3\mathbf{r} \left[-\frac{\hbar^2}{2m} \nabla_{\mathbf{r}}^2 + V_{\text{ext}}(\mathbf{r}) + g_0 |\psi(\mathbf{r})|^2 - \mu |\psi(\mathbf{r})|^2 \right] \psi(\mathbf{r}). \quad (\text{C.12})$$

The integral of the right-hand side is identically zero when the stationary Gross-Pitaevskii equation (8.5) is satisfied, which concludes the derivation of the latter.

Let us now consider the general dynamic situation, when the wave function of the condensate depends on time. The reasoning of Sec. C.1 is still valid with $\psi(\mathbf{r})$ replaced by $\psi(\mathbf{r}, t)$. We define the action $\mathcal{S} = \langle \Theta | \hat{\mathcal{S}} | \Theta \rangle$, where

$$\hat{\mathcal{S}} = \int dt (i\hbar\partial_t - \hat{H}). \quad (\text{C.13})$$

Dynamic Gross-Pitaevskii equation (8.6) follows from the principle of stationary action

$$\delta\mathcal{S} = 0. \quad (\text{C.14})$$

Inserting Eq. (C.8) into Eq. (C.14), we obtain

$$\mathcal{S} = \int d^3\mathbf{r} dt \left[i\hbar\partial_t\psi(\mathbf{r}, t) + \frac{\hbar^2}{2m} |\nabla_{\mathbf{r}}\psi(\mathbf{r}, t)|^2 - |\psi(\mathbf{r}, t)|^2 V_{\text{ext}}(\mathbf{r}) - \frac{g_0}{2} |\psi(\mathbf{r}, t)|^4 \right]. \quad (\text{C.15})$$

Functional derivation of this formula gives

$$\frac{\delta\mathcal{S}}{\delta\psi^*} = \int d^3\mathbf{r} dt \left[i\hbar\partial_t + \frac{\hbar^2}{2m} \nabla_{\mathbf{r}}^2 - V_{\text{ext}}(\mathbf{r}) - g_0 |\psi(\mathbf{r}, t)|^2 \right] \psi(\mathbf{r}, t). \quad (\text{C.16})$$

The integral of the right-hand side is identically zero when the dynamic Gross-Pitaevskii (8.6) equation is satisfied.

APPENDIX D

Density profile of a Bose-Einstein condensate

In this Appendix we present a derivation of the following formula for the atomic density of a condensate expanding in a random potential:

$$\bar{n}^{(0)}(\mathbf{r}, t) = \int \frac{d^d \mathbf{k}}{(2\pi)^d} |\phi_0(\mathbf{k})|^2 C_{\epsilon_k}(\mathbf{r}, t). \quad (\text{D.1})$$

Here $\epsilon_k = \hbar^2 k^2 / 2m$, $C_\epsilon(\mathbf{r}, t)$ is the diffusion propagator, and $|\phi_0(\mathbf{k})|^2$ is the initial momentum distribution of the condensate given by Eq. (8.18). This formula leads to Eq. (9.9) in the case of a quasi one-dimensional waveguide and to Eq (10.8) in the case of the three-dimensional unbounded space.

The starting point of the derivation is Eq. (9.8) of chapter 9:

$$\bar{n}(\mathbf{r}, t) = \int \frac{d\epsilon_1}{2\pi} \frac{d\epsilon_2}{2\pi} \int d^3 \mathbf{r}_1 d^3 \mathbf{r}_2 \overline{G_{\epsilon_1}(\mathbf{r}, \mathbf{r}_1) G_{\epsilon_2}^*(\mathbf{r}, \mathbf{r}_2)} \phi_0(\mathbf{r}_1) \phi_0^*(\mathbf{r}_2) e^{-i(\epsilon_1 - \epsilon_2)t/\hbar},$$

where G_ϵ is the Green's function of the Gross-Pitaevskii equation (10.1). We make a change of variables $\Delta \mathbf{r} = \mathbf{r}_1 - \mathbf{r}_2$ and $\mathbf{R} = (\mathbf{r}_1 + \mathbf{r}_2)/2$ for positions, and $\Omega = \epsilon_1 - \epsilon_2$ and $\epsilon = (\epsilon_1 + \epsilon_2)/2$ for energies. From the diagram of Fig. 9.4, for $\Omega \ll \epsilon$ and $|\mathbf{R}| \gg \ell$, the averaged product of two Green's functions is given by

$$\overline{G_{\epsilon_1}(\mathbf{r}, \mathbf{r}_1) G_{\epsilon_2}^*(\mathbf{r}, \mathbf{r}_2)} = \overline{G_{\epsilon_1}(\mathbf{r}, \mathbf{R}) G_{\epsilon_2}^*(\mathbf{r}, \mathbf{R})} \frac{\sin(k_\epsilon \Delta r)}{k_\epsilon \Delta r} e^{-\Delta r/2\ell}, \quad (\text{D.2})$$

where $k_\epsilon = 2m\epsilon/\hbar^2$ and

$$\overline{G_{\epsilon_1}(\mathbf{r}, \mathbf{R}) G_{\epsilon_2}^*(\mathbf{r}, \mathbf{R})} = 2\pi\nu_0(\epsilon) C_\epsilon(\mathbf{r}, \mathbf{R}, \Omega), \quad (\text{D.3})$$

with $\nu_0(\epsilon)$ the density of states. Eq. (D.2) can be rewritten as

$$\begin{aligned} \bar{n}(\mathbf{r}, t) &= \int \frac{d\epsilon}{2\pi} \frac{d\Omega}{2\pi} \int d^3 \mathbf{R} d^3 \Delta \mathbf{r} 2\pi\nu_0(\epsilon) C_\epsilon(\mathbf{r}, \mathbf{R}, \Omega) \frac{\sin(k_\epsilon \Delta r)}{k_\epsilon \Delta r} e^{-\Delta r/2\ell} \times \\ &\quad \times \phi_0\left(\mathbf{R} + \frac{\Delta \mathbf{r}}{2}\right) \phi_0^*\left(\mathbf{R} - \frac{\Delta \mathbf{r}}{2}\right) e^{-i\Omega t/\hbar}. \end{aligned} \quad (\text{D.4})$$

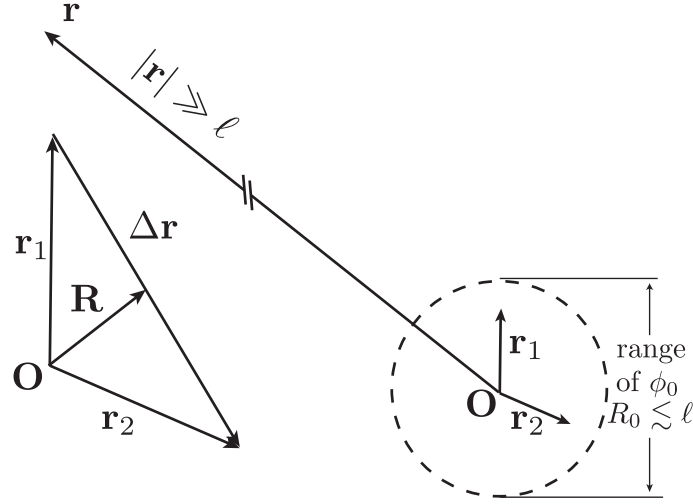


Figure D.1: Sketch illustrating the position vectors used in the appendix: \mathbf{r}_1 , \mathbf{r}_2 , $\mathbf{R} = (\mathbf{r}_1 + \mathbf{r}_2)/2$ and $\Delta\mathbf{r} = \mathbf{r}_1 - \mathbf{r}_2$. The atomic density is evaluated in \mathbf{r} , such that $|\mathbf{r}| \gg \ell$. The dashed circle indicates the range R_0 of the initial wave function ϕ_0 .

The range R_0 of the wave function ϕ_0 is assumed to be of the order of or smaller than the mean free path ℓ (see Eq. (8.20) and Fig. D.1), such that we can write

$$C_\epsilon(\mathbf{r}, \mathbf{R}, \Omega) \simeq C_\epsilon(\mathbf{r}, \mathbf{0}, \Omega). \quad (\text{D.5})$$

For simplicity, we write $C_\epsilon(\mathbf{r}, \Omega) = C_\epsilon(\mathbf{r}, \mathbf{0}, \Omega)$ and introduce

$$n_0(\mathbf{R}, \mathbf{k}) = \int d^3\Delta\mathbf{r} \phi_0\left(\mathbf{R} + \frac{\Delta\mathbf{r}}{2}\right) \phi_0^*\left(\mathbf{R} - \frac{\Delta\mathbf{r}}{2}\right). \quad (\text{D.6})$$

Eq. (D.4) then becomes

$$\begin{aligned} \bar{n}(\mathbf{r}, t) = & \int \frac{d\epsilon}{2\pi} \frac{d\Omega}{2\pi} \int \frac{d^3\mathbf{k}}{(2\pi)^3} \int d^3\mathbf{R} d^3\Delta\mathbf{r} 2\pi\nu_0(\epsilon) C_\epsilon(\mathbf{r}, \Omega) \frac{\sin(k_\epsilon \Delta r)}{k_\epsilon \Delta r} e^{-\Delta r/2\ell} \times \\ & \times n_0(\mathbf{R}, \mathbf{k}) e^{-i\Omega t/\hbar + i\mathbf{k}\cdot\Delta\mathbf{r}}. \end{aligned} \quad (\text{D.7})$$

The integral over Ω yields

$$\int \frac{d\Omega}{2\pi} C_\epsilon(\mathbf{r}, \Omega) e^{-i\Omega t/\hbar} = C_\epsilon(\mathbf{r}, t) \quad (\text{D.8})$$

and the integral over $\Delta\mathbf{r}$ reads

$$\int d^3\Delta\mathbf{r} \frac{\sin(k_\epsilon \Delta r)}{k_\epsilon \Delta r} e^{-\Delta r/2\ell} e^{i\mathbf{k}\cdot\Delta\mathbf{r}} = \frac{-1}{\pi\nu_0(\epsilon)} \text{Im} [\overline{G}_\epsilon(\mathbf{k})]. \quad (\text{D.9})$$

Finally, the integral over \mathbf{R} gives the momentum distribution of the condensate:

$$\int d^3\mathbf{R} n_0(\mathbf{R}, \mathbf{k}) = |\phi_0(\mathbf{k})|^2. \quad (\text{D.10})$$

We thus obtain

$$\bar{n}(\mathbf{r}, t) = -2 \int \frac{d\epsilon}{2\pi} \int \frac{d^3\mathbf{k}}{(2\pi)^3} C_\epsilon(\mathbf{r}, t) \text{Im} [\overline{G}_\epsilon(\mathbf{k})] |\phi_0(\mathbf{k})|^2. \quad (\text{D.11})$$

The last step consists in approximating $\text{Im} [\overline{G}_\epsilon(\mathbf{k})]$ by $-\pi\delta(\epsilon - \epsilon_{\mathbf{k}})$, which is valid provided that disorder is weak (this is the case in the three chapters on BECs in this thesis). This yields Eq. (D.1).

APPENDIX E

Nonlinear correction to the atomic density

In this appendix we present the main lines of derivation of Eq. (10.23) from Eq. (10.22). The first step consists in transforming both integrals over \mathbf{k} and \mathbf{k}' into integrals over energies ϵ and ϵ' by making use of $\epsilon = \hbar^2 k^2/2m$ and $\epsilon' = \hbar^2 k'^2/2m$. Writing explicitly the diffusion propagators, Eq. (10.22) can be represented as

$$\begin{aligned}
\overline{\Delta n}(\mathbf{r}, t) = & 2\text{Re} \left\{ \frac{g_0 J}{(2\pi)^9} \frac{v_\mu^2}{\nu_0 \hbar \ell^2} \left(\frac{m}{\hbar^2} \right)^3 \int_0^\infty r'^2 dr' \int_0^\pi \sin(\theta) d\theta \right. \\
& \times \int_0^\infty d\epsilon \int_0^\infty d\epsilon' \int_{-2\epsilon}^{2\epsilon} d\Omega \int_{-2\epsilon'}^{2\epsilon'} d\Omega' \sqrt{\epsilon\epsilon'} |\phi(\epsilon)|^2 |\phi(\epsilon')|^2 \\
& \times \exp \left[-|\mathbf{r} - \mathbf{r}'| \sqrt{\frac{-i\Omega}{\hbar D_{\epsilon+\Omega'/2}}} - r' \left(\sqrt{\frac{-i\Omega'}{\hbar D_{\epsilon'}}} + \sqrt{\frac{-i(\Omega - \Omega')}{\hbar D_\epsilon}} \right) \right] \\
& \left. \times \frac{\exp(-i\Omega t/\hbar)}{r'^2 |\mathbf{r} - \mathbf{r}'| D_{\epsilon+\Omega'/2} D_{\epsilon'} D_\epsilon} \right\}. \tag{E.1}
\end{aligned}$$

Energy distributions $|\phi(\epsilon)|^2$ and $|\phi(\epsilon')|^2$ are deduced from momenta distributions $|\phi(\mathbf{k})|^2$ and $|\phi(\mathbf{k}')|^2$ (we keep the same notation ϕ for clarity). We have, for example,

$$|\phi(\epsilon)|^2 = \frac{15\pi^2 N}{(\sqrt{2}k_\mu)^3} \left(1 - \frac{\epsilon}{2\mu} \right) \mathcal{H} \left(1 - \frac{\epsilon}{2\mu} \right), \tag{E.2}$$

with \mathcal{H} the Heaviside step function. The prefactor in Eq. (E.2) has been obtained by requiring conservation of the total number of atoms $N = \int d^3\mathbf{k} |\phi(\mathbf{k})|^2 / (2\pi)^3$. The integral over θ is readily performed:

$$\int_0^\pi \sin(\theta) d\theta \frac{e^{-|\mathbf{r}-\mathbf{r}'|x}}{|\mathbf{r} - \mathbf{r}'|} = \frac{1}{x r r'} \left[e^{-x|r-r'|} - e^{-x(r+r')} \right], \tag{E.3}$$

where $x = \sqrt{\frac{-i\Omega}{\hbar D_{\epsilon+\Omega'/2}}}$. Eq. (E.1) then reduces to:

$$\begin{aligned} \overline{\Delta n}(\mathbf{r}, t) &= 2\text{Re} \left\{ \frac{g_0 J}{(2\pi)^9} \frac{v_\mu^2}{\nu_0 \hbar \ell^2} \left(\frac{m}{\hbar^2} \right)^3 \int_\Lambda \frac{dr'}{r'} \int_0^\infty d\epsilon \int_0^\infty d\epsilon' \int_{-2\epsilon}^{2\epsilon} d\Omega \int_{-2\epsilon'}^{2\epsilon'} d\Omega' \right. \\ &\quad \times \sqrt{\frac{\hbar D_{\epsilon+\Omega'/2}}{-i\Omega}} \sqrt{\epsilon\epsilon'} |\phi(\epsilon)|^2 |\phi(\epsilon')|^2 \exp \left[-r' \left(\sqrt{\frac{-i\Omega'}{\hbar D_{\epsilon'}}} + \sqrt{\frac{-i(\Omega - \Omega')}{\hbar D_\epsilon}} \right) \right] \\ &\quad \times \left[\exp \left(-|r - r'| \sqrt{\frac{-i\Omega}{\hbar D_{\epsilon+\Omega'/2}}} \right) - \exp \left(-(r + r') \sqrt{\frac{-i\Omega}{\hbar D_{\epsilon+\Omega'/2}}} \right) \right] \\ &\quad \left. \times \frac{\exp(-i\Omega t/\hbar)}{r D_{\epsilon+\Omega'/2} D_{\epsilon'} D_\epsilon} \right\}, \end{aligned} \quad (\text{E.4})$$

where we have introduced a lower cutoff $\Lambda \sim \ell$ in the integral over r' . This cutoff is needed because of the breakdown of diffusion theory at small length scales. The next step consists in calculating the integral over r' . Before doing so, it is convenient to introduce new dimensionless variables $u = \Omega t/2\hbar$, $v = \Omega' t/2\hbar$, $p = \epsilon t/\hbar$, $q = \epsilon' t/\hbar$, $\tau = k_\mu \ell t/(\ell/v_\mu)$, $\rho = (r/\ell) \sqrt{3k_\mu \ell/\sqrt{2}}$, $\rho' = (r'/\ell) \sqrt{3k_\mu \ell/\sqrt{2}/\tau^{1/4}}$ and $\Lambda' = (\Lambda/\ell) \sqrt{3k_\mu \ell/\sqrt{2}/\tau^{1/4}}$. Using $D_\epsilon = (\ell/3) \sqrt{2\epsilon/m}$, we obtain

$$\begin{aligned} \overline{\Delta n}(\mathbf{r}, t) &= \text{Re} \left\{ -iC \int_{\Lambda'}^\infty \frac{d\rho'}{\rho'} \int_0^\tau dp \int_0^\tau dq \int_{-p}^p du \int_{-q}^q dv \frac{1}{\tau^{7/2}} \frac{\tau^{1/4}}{\rho} \right. \\ &\quad \times \sqrt{\frac{\sqrt{p+v}}{-2iu}} \left(1 - \frac{p}{\tau}\right) \left(1 - \frac{q}{\tau}\right) \exp \left[-\rho' \left(\sqrt{\frac{-2iv}{\sqrt{q}}} + \sqrt{\frac{-2i(u-v)}{\sqrt{p}}} \right) \right] \\ &\quad \times \left[\exp \left(-\left| \frac{\rho}{\tau^{1/4}} - \rho' \right| \sqrt{\frac{-2iu}{\sqrt{p+v}}} \right) - \exp \left(-\left(\frac{\rho}{\tau^{1/4}} + \rho' \right) \sqrt{\frac{-2iu}{\sqrt{p+v}}} \right) \right] \\ &\quad \left. \times \frac{\exp(-2iu)}{\sqrt{p+v}} \right\}, \end{aligned} \quad (\text{E.5})$$

with the prefactor $C \simeq (g_0 m N^2 k_\mu \ell)/(\hbar^2 \ell^4) \simeq (a_s N^2 k_\mu \ell)/\ell^4$. We can now perform the integral over ρ' . In the limit $\rho \ll \tau^{1/4}$, which corresponds to long times $t \gg t_2$ (t_2 is defined in the main text), this integral is

$$\begin{aligned} &\int_{\Lambda'}^\infty \frac{d\rho'}{\rho'} \left[\exp \left(-\left| \frac{\rho}{\tau^{1/4}} - \rho' \right| \sqrt{\frac{-2iu}{\sqrt{p+v}}} \right) - \exp \left(-\left(\frac{\rho}{\tau^{1/4}} + \rho' \right) \sqrt{\frac{-2iu}{\sqrt{p+v}}} \right) \right] \\ &\quad \times \exp \left[-\rho' \left(\sqrt{\frac{-2iv}{\sqrt{q}}} + \sqrt{\frac{-2i(u-v)}{\sqrt{p}}} \right) \right] \\ &\simeq 2 \left(\frac{\rho}{\tau^{1/4}} - \Lambda' \right) \sqrt{\frac{-2iu}{\sqrt{p+v}}} \simeq 2 \frac{\rho}{\tau^{1/4}} \sqrt{\frac{-2iu}{\sqrt{p+v}}}, \end{aligned} \quad (\text{E.6})$$

where the last equality results from $\rho/\tau^{1/4} \gg \Lambda'$. Inserting Eq. (E.6) into Eq. (E.5) we obtain

$$\overline{\Delta n}(\mathbf{r}, t) = 2\text{Re} \left[-i \frac{C}{\tau^{7/2}} \int_0^\tau dp \int_0^\tau dq \int_{-p}^p du \int_{-q}^q dv \frac{\exp(-2iu)}{\sqrt{p+v}} \right]. \quad (\text{E.7})$$

The four remaining integrals can be readily performed. We finally obtain:

$$\overline{\Delta n}(\mathbf{r}, t) \simeq \frac{-C}{\tau^{3/2}} = -\frac{a_s N^2}{\ell \sqrt{k_\mu \ell}} \frac{1}{(D_\mu t)^{3/2}}, \quad (\text{E.8})$$

which is Eq. (10.23) of the main text.

Bibliography

- [1] G. Maret and P. E. Wolf, *Multiple light scattering from disordered media : the effect of brownian motion of scatterers*, Z. Phys. B. **65**, 409 (1987).
- [2] J. H. Page, M. L. Cowan, and D. A. Weitz, *Diffusing acoustic wave spectroscopy of fluidized suspensions*, Physica B : Condensed Matter **279**, 130 (2000).
- [3] J. L. Thomas and M. Fink, *Ultrasonic beam focusing through tissue inhomogeneities with a time-reversal mirror: application to transskull therapy*, IEEE Trans. Ultrason. Ferroelec. Freq. Contr. **43**, 5459 (1995).
- [4] D. S. Wiersma, *The physics and applications of random lasers*, Nature Phys. **4**, 359 (2008).
- [5] J. W. S. Rayleigh, *On the scattering of light by small particles*, Philos. Mag. **41**, 447 (1871).
- [6] J. D. Jackson, *Classical electrodynamics*, New York, Wiley (1975).
- [7] G. Mie, *Beitrage zur optik truber medien, speziell kolloidaler metallosungen*, Ann. Phys. (Leipzig) **25**, 377 (1908).
- [8] O. D. Khvolson, *Grundzüge einer mathematischen theorie der inneren diffusion des lichtes*, Bull. St. Petersburg Acad. Sci. **33**, 221 (1890).
- [9] A. Schuster, *Radiation through a foggy atmosphere*, Astophys. J **21**, 1 (1905).
- [10] S. Chandrasekhar, *Radiative transfer*, Dover, New York, (1960).
- [11] H. C. van de Hulst, *Multiple light scattering*, Vols. 1 and 2, Academic, New York, (1980).
- [12] P. W. Anderson, *Absence of diffusion in certain random lattices*, Phys. Rev. **109**, 1492 (1958).

-
- [13] P. Sheng, *Introduction to wave scattering, localization and mesoscopic phenomena*, 2nd edition, Springer-Verlag, Heidelberg, (2006).
- [14] B. A. van Tiggelen, *Diffuse waves in complex media*, edited by J. P. Fouque, Kluwer, Dordrecht, (1999).
- [15] R. del Rio, S. Jitomirskaya, Y. Last, and B. Simon, *What is localization?*, Phys. Rev. Lett. **75**, 117 (1995).
- [16] E. Akkermans and G. Montambaux, *Mesoscopic physics of electrons and photons*, Cambridge University Press, Cambridge, (2007).
- [17] M. C. W. van Rossum and Th. M. Nieuwenhuizen, *Multiple scattering of classical waves: microscopy, mesoscopy, and diffusion*, Rev. Mod. Phys. **71**, 313 (1999).
- [18] A. F. Ioffe and A. R. Regel, *Non-crystalline, amorphous and liquid electronic semiconductors*, Prog. Semicon. **4**, 237 (1960).
- [19] D. J. Thouless, *Electrons in disordered systems and the theory of localization*, Phys. Rep. **13**, 93 (1974).
- [20] N. F. Mott, *Conduction in glasses containing transition metal ions*, J. Non-Crystal. Solids **1**, 1 (1968).
- [21] S. John, *Electromagnetic absorption in a disordered medium near a photon mobility edge*, Phys. Rev. Lett. **53**, 2169 (1984).
- [22] P. W. Anderson, *The question of classical localization a theory of white paint?*, Philos. Mag. B, **52**, 505 (1985).
- [23] F. R. Allen and C. J. Adkins, *Electrical conduction in heavily doped germanium*, Philos. Mag. **26**, 1027 (1972).
- [24] For a review, see P. A. Lee and T. V. Ramakrishnan, *Disordered electronic systems*, Rev. Mod. Phys. **57**, 287 (1985).
- [25] P. E. Wolf and G. Maret, *Weak localization and coherent backscattering of photons in disordered media*, Phys. Rev. Lett. **55**, 2696 (1985).
- [26] M. P. van Albada and A. Lagendijk, *Observation of weak localization of light in a random medium*, Phys. Rev. Lett. **55**, 2692 (1985).
- [27] A. Z. Genack and N. Garcia, *Observations of the Anderson transition for electromagnetic radiation*, Phys. Rev. Lett. **66**, 2064 (1991).
- [28] P. Bartolini, A. Lagendijk, R. Righini, and D. S. Wiersma, *Localization of light in a disordered medium*, Nature **390**, 671 (1997).

-
- [29] F. J. P. Schuurmans, M. Megens, D. Vanmaekelbergh, and A. Lagendijk, *Light scattering near the localization transition in macroporous GaP networks*, Phys. Rev. Lett. **83**, 2183 (1999).
- [30] F. Scheffold, R. Lenke, R. Tweert, and G. Maret, *Localization or classical diffusion of light?*, Nature **398**, 206 (1999); D. S. Wiersma, J. Gómez Rivas, P. Bartolini, A. Lagendijk, and R. Righini, *Reply: Localization or classical diffusion of light?*, Nature **398**, 207 (1999).
- [31] A. A. Chabanov, M. Stoytchev, and A. Z. Genack, *Statistical signatures of photon localization*, Nature (London) **404**, 850 (2000).
- [32] M. Störzer, P. Gross, C. M. Aegerter, and G. Maret, *Observation of the critical regime near Anderson localization of light*, Phys. Rev. Lett. **96**, 063904 (2006).
- [33] S. E. Skipetrov and B. A. van Tiggelen, *Dynamics of Anderson localization in open 3D media*, Phys. Rev. Lett. **96**, 043902 (2006).
- [34] H. Hu, A. Strybulevych, J. H. Page, S. E. Skipetrov, and B. A. van Tiggelen, *Localization of ultrasound in a three-dimensional elastic network*, Nature Physics **4**, 945 (2008).
- [35] J. Billy, V. Josse, Z. Zuo, A. Bernard, B. Hambrecht, P. Lugan, D. Clément, L. Sanchez-Palencia, A. Aspect, and P. Bouyer, *Direct observation of Anderson localization of matter waves in a controlled disorder*, Nature **453**, 891 (2008).
- [36] J. Chabé, G. Lemarié, B. Grémaud, D. Delande, P. Szriftgiser, and J-C Garreau, *Experimental observation of the Anderson metal-insulator transition with atomic matter waves*, Phys. Rev. Lett. **101**, 255702 (2008).
- [37] G. Casati, I. Guarneri and D. L. Shepelyansky, *Anderson transition in a one-dimensional system with three incommensurate frequencies*, Phys. Rev. Lett. **62**, 345 (1989).
- [38] E. Abrahams, P. W. Anderson, D. C. Licciardello, and T. V. Ramakrishnan, *Scaling theory of localization: absence of quantum diffusion in two dimensions*, Phys. Rev. Lett. **42**, 673 (1979).
- [39] D. Vollhardt and P. Wölfle, *Diagrammatic, self-consistent treatment of the Anderson localization problem in $d \leq 2$ dimensions*, Phys. Rev. B **22**, 4666 (1980); *Selfconsistent theory of Anderson localization*, in *Electronic phase transitions*, Elsevier Science, Amsterdam (1992).
- [40] C. W. J. Beenakker, *Random-matrix theory of quantum transport*, Rev. Mod. Phys. **69**, 731 (1997).
- [41] O. N. Dorokhov, *Transmission coefficient and the localization length of an electron in N bound disordered chains*, Pisma Zh. Eksp. Teor. Fiz. **36**, 259 (1982) [JETP Lett. **36**, 318].

-
- [42] P. A. Mello, P. Pereyra, and N. Kumar, *Macroscopic approach to multichannel disordered conductors*, Ann. Phys. (N.Y.) **181**, 290 (1988).
- [43] H. Schomerus, K. J. H. van Bommel, and C. W. J. Beenakker, *Localization-induced coherent backscattering effect in wave dynamics*, Phys. Rev. E **63**, 026605 (2001).
- [44] K. B. Efetov, *Supersymmetry and theory of disordered metals*, Adv. Phys. **32**, 53 (1983); *Supersymmetry in disorder and chaos*, Cambridge University, Cambridge, (1997).
- [45] A. D. Mirlin, *Statistics of energy levels and eigenfunctions in disordered systems*, Phys. Rep. **326**, 259 (2000).
- [46] B. A. van Tiggelen, A. Lagendijk, and D. S. Wiersma, *Reflection and transmission of waves near the localization threshold* Phys. Rev. Lett. **84**, 4333 (2000).
- [47] S. E. Skipetrov and B. A. van Tiggelen, *Dynamics of weakly localized waves*, Phys. Rev. Lett. **92**, 113901 (2004).
- [48] Z. Q. Zhang, A. A. Chabanov, S. K. Cheung, C. H. Wong, and A. Z. Genack, *Dynamics of localized waves: pulsed microwave transmissions in quasi-one-dimensional media*, Phys. Rev. B **79**, 144203 (2009).
- [49] R. Berkovits and M. Kaveh, *Backscattering of light near the optical Anderson transition*, Phys. Rev. B **36**, 9322 (1987).
- [50] R. Berkovits and M. Kaveh, *Propagation of waves through a slab near the Anderson transition: a local scaling approach*, J. Phys.: Condens. Matter **2**, 307 (1990).
- [51] L. P. Gorkov, A. Larkin, and D. E. Khmel'nitskii, *Particle conductivity in a two-dimensional random potential*, JETP Lett. **30**, 228 (1979).
- [52] S. Hikami, *Anderson localization in a nonlinear σ -model representation*, Phys. Rev. B **24**, 2671 (1981).
- [53] X. J. Zhu, D. J. Pine, and D. A. Weitz, *Internal reflection of diffusive light in random media*, Phys. Rev. A **44**, 3948 (1991).
- [54] C. Tian, *Supersymmetric field theory of local light diffusion in semi-infinite media*, Phys. Rev. B **77**, 064205 (2008).
- [55] H. de Raedt, A. Lagendijk, and P. de Vries, *Transverse localization of light*, Phys. Rev. Lett. **62**, 47 (1989).
- [56] T. Schwarz, G. Bartal, Sh. Fishman, and M. Segev, *Transport and Anderson localization in disordered two-dimensional photonic lattices*, Nature **446**, 52 (2007).

-
- [57] A. A. Chabanov, Z. Q. Zhang, and A. Z. Genack, *Breakdown of diffusion in dynamics of extended waves in mesoscopic media*, Phys. Rev. Lett. **90**, 203903 (2003).
- [58] D. Vollhardt and P. Wölfle, *Scaling equations from a self-consistent theory of Anderson localization*, Phys. Rev. Lett. **48**, 699 (1982).
- [59] F. Wegner, *Localization, interaction, and transport phenomena* (Springer Series in Solid State Science **61**), ed B. Kramer, G. Bergmann and Y. Bruynseraede, Berlin, Springer, p. 99.
- [60] A. MacKinnon and B. Kramer, *The scaling theory of electrons in disordered solids: additional numerical results*, Z. Phys. B **53**, 1 (1983); J. Kroha, T. Kopp, and P. Wölfle, *Self-consistent theory of Anderson localization for the tight-binding model with site-diagonal disorder*, Phys. Rev. B **41**, 888 (1990); K. Slevin and T. Ohtsuki, *Corrections to scaling at the Anderson transition*, Phys. Rev. Lett. **82**, 382 (1999).
- [61] S. K. Cheung and Z. Q. Zhang, *Scaling behavior of classical wave transport in mesoscopic media at the localization transition*, Phys. Rev. B **72**, 235102 (2005).
- [62] N. Cherroret, S. E. Skipetrov, B. A. Van Tiggelen *Comment on "Scaling behavior of classical wave transport in mesoscopic media at the localization transition"*, Phys. Rev. B. **80**, 037101 (2009).
- [63] B. Kramer and A. MacKinnon, *Localization: theory and experiment*, Rep. Prog. Phys. **56**, 1469 (1993).
- [64] A. M. García-García, *Semiclassical theory of the Anderson transition*, Phys. Rev. Lett. **100**, 076404 (2008).
- [65] J. W. Goodman, *Speckle phenomena in optics*, Roberts Company & Publishers, NY, (2007).
- [66] R. Berkovits and S. Feng, *Correlations in coherent multiple scattering*, Phys. Rep. **238**, 135 (1994).
- [67] S. Feng, C. Kane, P. A. Lee, and A. D. Stone, *Correlations and fluctuations of coherent wave transmission through disordered media*, Phys. Rev. Lett. **61**, 834 (1988).
- [68] M. C. van Rossum, Th. M. Nieuwenhuizen, and R. Vlaming, *Optical conductance fluctuations: diagrammatic analysis in the Landauer approach and nonuniversal effects*, Phys. Rev. E **51**, 6158 (1995).
- [69] R. A. Webb, S. Washburn, C. P. Umbach, and R. B. Laibowitz, *Observation of h/e Aharonov-Bohm oscillations in normal-metal rings*, Phys. Rev. Lett. **54**, 2696 (1985).

-
- [70] J. C. Licini, D. J. Bishop, M. A. Kastner, and J. Melngailis, *Aperiodic magnetoresistance oscillations in narrow inversion layers in Si*, Phys. Rev. Lett. **55**, 2987 (1985).
- [71] W. J. Skocpol, P. M. Mankiewich, R. E. Howard, L. D. Jackel, D. M. Tennant, and A. D. Stone, *Universal conductance fluctuations in silicon inversion-layer nanostructures*, Phys. Rev. Lett. **56**, 2865 (1986).
- [72] S. B. Kaplan and A. Hartstein, *Universal conductance fluctuations in narrow Si accumulation layers*, Phys. Rev. Lett. **56**, 2403 (1986).
- [73] B. L. Altshuler, *Fluctuations in the extrinsic conductivity of disordered conductors*, JETP Lett. **41**, 648 (1985).
- [74] A. D. Stone, *Magnetoresistance fluctuations in mesoscopic wires and rings*, Phys. Rev. Lett. **54**, 2692 (1985).
- [75] P. A. Lee, and A. D. Stone, *Universal conductance fluctuations in metals*, Phys. Rev. Lett. **55**, 1622 (1985).
- [76] P. Sebbah, B. Hu, A. Z. Genack, R. Pnini, and B. Shapiro, *Spatial-field correlation: the building block of mesoscopic fluctuations*, Phys. Rev. Lett. **88**, 123901 (2002).
- [77] N. Trégourès, *Approche mésoscopique des ondes en milieu complexe : des micro-ondes aux ondes sismiques*, Ph. D. thesis, University of Grenoble 1 (2001).
- [78] A. A. Chabanov, N. P. Trégourès, B. A. van Tiggelen, and A. Z. Genack, *Mesoscopic correlation with polarization rotation of electromagnetic waves*, Phys. Rev. Lett. **92**, 173901 (2004).
- [79] F. Scheffold, W. Härtl, G. Maret, and E. Matijević, *Observation of long-range correlations in temporal intensity fluctuations of light*, Phys. Rev. B **56**, 10942 (1997).
- [80] F. Scheffold and G. Maret, *Universal conductance fluctuations of light*, Phys. Rev. Lett. **81**, 5800 (1998).
- [81] A. A. Chabanov, B. Hu and A. Z. Genack, *Dynamic correlation in wave propagation in random media*, Phys. Rev. Lett. **93** 123901 (2004).
- [82] S. E. Skipetrov, *Enhanced mesoscopic correlations in dynamic speckle patterns*, Phys. Rev. Lett. **93**, 233901 (2004).
- [83] S. K. Cheung, X. Zhang, Z. Q. Zhang, A. A. Chabanov, and A. Z. Genack, *Impact of weak localization in the time domain*, Phys. Rev. Lett. **92**, 173902 (2004).

-
- [84] G. Casati, G. Maspero, and D. L. Shepelyansky, *Relaxation process in a regime of quantum chaos*, Phys. Rev. E **56**, R6233 (1997); K. M. Frahm, *Quantum relaxation in open chaotic systems*, Phys. Rev. E **56** R6237 (1997).
- [85] D. V. Savin and V. V. Sokolov, *Quantum versus classical decay laws in open chaotic systems*, Phys. Rev. E **56**, 4911 (1997).
- [86] L. Fallani, C. Fort, and M. Inguscio, *Bose-Einstein condensates in disordered potentials*, Adv. At. Mol. Opt. Phys. **56**, 119 (2008).
- [87] J. E. Lye, L. Fallani, M. Modugno, D. S. Wiersma, C. Fort, and M. Inguscio, *Bose-Einstein condensate in a random potential*, Phys. Rev. Lett. **95**, 070401 (2005).
- [88] D. Clément, A. F. Varón, M. Hugbart, J. A. Retter, P. Bouyer, L. Sanchez-Palencia, D. M. Gangardt, G. V. Shlyapnikov, and A. Aspect, *Suppression of transport of an interacting elongated Bose-Einstein condensate in a random potential*, Phys. Rev. Lett. **95**, 170409 (2005).
- [89] C. Fort, L. Fallani, V. Guarrera, J. E. Lye, M. Modugno, D. S. Wiersma, and M. Inguscio, *Effect of optical disorder and single defects on the expansion of a Bose-Einstein condensate in a one-dimensional waveguide*, Phys. Rev. Lett. **95**, 170410 (2005).
- [90] G. Roati, C. D'Errico, L. Fallani, M. Fattori, C. Fort, M. Zaccanti, G. Modugno, M. Modugno, and M. Inguscio, *Anderson localization of a non-interacting Bose-Einstein condensate*, Nature **453**, 895 (2008).
- [91] B. Shapiro, *Expansion of a Bose-Einstein condensate in the presence of disorder*, Phys. Rev. Lett. **99**, 060602 (2007).
- [92] S. E. Skipetrov, A. Minguzzi, B. A. van Tiggelen, and B. Shapiro, *Anderson localization of a Bose-Einstein condensate in a 3D random potential*, Phys. Rev. Lett. **100**, 165301 (2008).
- [93] K. B. Davis, M. O. Mewes, M. R. Andrews, N. J. van Druten, D. S. Durfee, D. M. Kurn, and W. Ketterle, *Bose-Einstein condensation in a gas of sodium atoms*, Phys. Rev. Lett. **75**, 3969 (1995).
- [94] M. H. Anderson, J. R. Ensher, M. R. Matthews, C. E. Wiemann, and E. A. Cornell, *Observation of Bose-Einstein condensation in a dilute atomic vapor*, Science **269**, 198 (1995).
- [95] L. Pitaevskii and S. Stringari, *Bose-Einstein condensation*, Clarendon, Oxford, (2003).
- [96] L. Sanchez-Palencia, D. Clément, P. Lugan, P. Bouyer, G. V. Shlyapnikov, and A. Aspect, *Anderson localization of expanding Bose-Einstein condensates in random potentials*, Phys. Rev. Lett. **98**, 210401 (2007).

-
- [97] Yu. Kagan, E. L. Surkov, and G. V. Schlyapnikov, *Evolution of a Bose-condensed gas under variations of the confining potential*, Phys. Rev. A **54**, R1753 (1996).
- [98] Y. Castin and R. Dum, *Bose-Einstein condensates in time dependent traps*, Phys. Rev. Lett. **77**, 5315 (1996).
- [99] L. Fallani, J. E. Lye, V. Guarrera, C. Fort and M. Inguscio, *Ultracold atoms in a disordered crystal of light: towards a Bose glass*, Phys. Rev. Lett. **98**, 130404 (2007).
- [100] P. Henseler and B. Shapiro, *Density correlations in cold atomic gases: atomic speckles in the presence of disorder*, Phys. Rev. A **77**, 033624 (2008).
- [101] R. Kuhn, O. Sigwarth, C. Miniatura, D. Delande, and C. A. Müller, *Coherent matter wave transport in speckle potentials*, New. J. Phys. **9**, 161 (2007).
- [102] R. Pnini and B. Shapiro, *Fluctuations in transmission of waves through disordered slabs*, Phys. Rev. B **39**, 6986 (1989).
- [103] M. J. Stephen and G. Cwilich, *Intensity correlation functions and fluctuations in light scattered from a random medium*, Phys. Rev. Lett. **59**, 285 (1988).
- [104] S. Feng and P. A. Lee, *Mesoscopic conductors and correlations in laser speckle patterns*, Science **251**, 633 (1991).
- [105] D. B. Rogozkin and M. Yu. Cherkasov, *Long-range intensity correlations in wave reflection from a disordered medium*, Phys. Rev. B **51**, 12256 (1995).
- [106] A. S. Pikovsky and D. L. Shepelyansky, *Destruction of Anderson localization by a weak nonlinearity*, Phys. Rev. Lett. **100**, 094101 (2008).
- [107] S. Flach, D. O. Krimer, and Ch. Skokos, *Universal spreading of wave packets in disordered nonlinear systems*, Phys. Rev. Lett. **102**, 024101 (2009).
- [108] B. Spivak and A. Zyuzin, *Mesoscopic sensitivity of speckles in disordered nonlinear media to changes of the scattering potential*, Phys. Rev. Lett. **84**, 1970 (2000).
- [109] V. M. Agranovich and V. E. Kravtsov, *Nonlinear backscattering from opaque media*, Phys. Rev. B **43**, 13691 (1991).
- [110] A. Heiderich, R. Maynard and B. A. van Tiggelen, *Coherent backscattering in nonlinear media*, Opt. Commun. **115**, 392 (1995).
- [111] T. Wellens and B. Grémaud, *Observation of coherent backscattering “factor of three” in a numerical experiment*, J. Phys. B **39**, 4719 (2006).

List of publications

Most of the work presented in this thesis is also published in:

- N. Cherroret and S. E. Skipetrov, *Microscopic derivation of self-consistent equations of Anderson localization in a disordered medium of finite size*, Physical Review E **77**, 046608 (2008).
- N. Cherroret, S. E. Skipetrov, and B. A. van Tiggelen, *Transverse confinement of waves in 3D random media*, submitted to Phys. Rev. E (2009).
- N. Cherroret, A. Peña, A. A. Chabanov, and S. E. Skipetrov *Nonuniversal dynamic conductance fluctuations*, Phys. Rev. B **80**, 045118 (2009).
- N. Cherroret and S. E. Skipetrov, *Long-range correlations of density in a Bose-Einstein condensate expanding in a random potential*, Phys. Rev. Lett. **101**, 190406 (2008).
- N. Cherroret and S. E. Skipetrov, *Effect of interactions on the diffusive expansion of a Bose-Einstein condensate in a three-dimensional random potential*, Phys. Rev. A **79**, 063604 (2009).
- N. Cherroret, S. E. Skipetrov, and B. A. van Tiggelen, *Comment on ‘Scaling behavior of classical wave transport in mesoscopic media at the localization transition’*, Phys. Rev. B **80**, 037101 (2009).

And also:

- B. A. van Tiggelen, S. E. Skipetrov, N. Cherroret, and S. Kawka. *Self-consistent treatment of Anderson localization. An attempt to engineer with scaling theory*, ADVANCES IN NANOPHOTONICS II: International Summer School on Advances in Nanophotonics II. AIP Conference Proceedings **959**, 79 (2007).

- S. E. Skipetrov, N. Cherroret, and B. A. van Tiggelen, *Anderson Localization in Open Random Media*, in Photonic Metamaterials: From Random to Periodic, OSA Technical Digest (CD) (Optical Society of America, 2007), paper MB2.